Core-Based In-Situ Stress Estimation for Utah FORGE Well 16A(78)-32 using Triaxial Ultrasonic Velocity and Deformation Rate Analysis

Report documenting completion of Milestone 2.1.1 of Utah FORGE project 2439: A Multi-Component Approach to Characterizing In-Situ Stress at the U.S. DOE FORGE EGS Site: Laboratory, Modeling and Field Measurement

Andrew Bunger[a,b,*], Joshua Higgins[b,#], Yao Huang[a,$], Mark Kelley[c]

a Department of Civil and Environmental Engineering, University of Pittsburgh, Pittsburgh, PA, USA

b Department of Chemical and Petroleum Engineering, University of Pittsburgh, Pittsburgh, PA, USA

c Battelle Memorial Institute, Columbus, OH, USA

Now with Deloitte, Risk in Financial Advisory Department, Pittsburgh, PA, USA

$ Now with Los Alamos National Laboratory, Los Alamos, NM, USA

* Lead author: bunger@pitt.edu

Last Updated: 2 December 2022

Abstract

Core-based methods for in-situ stress estimation were applied using samples from 5 intervals within the Utah FORGE 16A(78)-32 well. At three of these locations, Triaxial Ultrasonic Velocity (TUV) tests were performed, resulting in experimentally-determined relationships between wave velocities and stresses. Non-monotonic increase in the velocity-stress relationships are inferred provide evidence of stress history and are therefore used to estimate in-situ stress magnitudes. Additionally, Deformation Rate Analysis (DRA) tests were run on core plugs from various orientations at each of the 5 sampling locations. These, too, provide evidence of stress history based on stress-strain behavior. A novel Weight of Evidence (WoE) method was developed as a means of synthesizing in-situ stress evidence from these two types of tests. Results indicate the minimum horizontal stress gradient ranges from 0.58 psi/ft to 0.69 psi/ft, with 4 of the 5 values between 0.66 psi/ft and 0.69 psi/ft. The vertical stress gradient ranges from 1.05 psi/ft to 1.12 psi/ft, with 4 of the 5 zones given results between 1.09 psi/ft and 1.12 psi/ft. The maximum horizontal stress gradient ranges from 0.98 psi/ft to 1.34 psi/ft, with 4 of the 5 zones falling between 0.98 psi/ft and 1.24 psi/ft. The stress regime thus appears to be on the edge between normal faulting and strike-slip

faulting, potentially flipping back and forth between the two regimes due to variability of rock properties, structures such as faults, and/or thermal anomalies. Only near the toe of the well does the regime appear to be clearly strike-slip with the best estimate of maximum stress gradient at 1.34 psi/ft. However, only a few meters away but in an apparently quite different composition and fabric of rock, the maximum stress gradient is 1.05 psi/ft. Additionally, the only unit that is very clearly in normal faulting regime is the Lower Granitoid, but it also has a unique fabric and lower stiffness compared to the others. The picture that emerges is of higher and lower stress zones in terms of the maximum horizontal stress. With that said, projecting the rate of increase of maximum stress for the lower stress zones implies that even these might become strike-slip below a depth of about 2700 m. Finally, although the confidence level is not very high, there is some evidence from the inclined core taken from the Gneiss near the toe of the well that the minimum horizontal stress orientation is dipping by 20 degrees or more from the horizontal. This could be indicative of the impact of nearby structure(s) and/or thermal anomalies. Such in-situ stress inclination could cause the hydraulic fracture orientation to deviate noticeably from vertical.

Task and Milestone Description

This report documents the task completion and technical accomplishments comprising achievement of Milestone 2.1.1, as per the project SOPO:

> **Milestone 2.1.1** – relationship between wave speed and stress established experimentally for 3-5 sample locations in 78B-32 (or a legacy well if project plans change and material is not available for 78B-32), with completion verified by generation of plots of 9 wave speed components varying with 3 stress components for each of the 3-5 intervals. Assumes 78B-32 core is available by August 2021.

The core availability and relevance was determined to be superior for 16A(78)-32, and therefore this milestone was completed on this well rather than the originally-planned well 78B-32. Otherwise, the milestone was completed in accordance with the SOPO *Task 2.1 – Characterize relationship between stress state and wave speed for Utah FORGE granite.*

As planned, the milestone completion entailed testing of samples from 5 intervals within the 16A(78)-32 well. At three of these locations, Triaxial Ultrasonic Velocity (TUV) tests were performed, resulting in experimentally-determined relationships between wave velocities and stresses. Striking variations in these relationships provide evidence of stress history and are therefore used to estimate in-situ stress magnitudes. Additionally, Deformation Rate Analysis (DRA) tests were run on core plugs from various orientations at each of the 5 sampling locations. These, too, provide evidence of stress history based on stress-strain behavior.

In the course of completing this milestone, a novel Weight of Evidence (WoE) method has been developed as a means of synthesizing in-situ stress data from multiple sources.

This report begins with a description of the TUV, DRA, and WoE methods that were used in completion of this milestone. After this, a succinct, enumerated summary of key findings is presented in which the evidence for in-situ stresses around well 16A(78)-32 are stated. Finally, the data for each of the 5 sampled sections are presented in a format that begins with a brief summary followed by a comprehensive data compendium.

Methods

Triaxial Ultrasonic Velocity (TUV)

Triaxial ultrasonic velocity (TUV) experiments entail measurement of acoustic velocities (p-wave, s-wave) under different combinations of true-triaxial stresses. For the 16A(78)-32 well, sample preparation consisted of cutting a 2.5 inches cubic sample from two locations in the granitoid and one in the gneiss (see details of these sampling locations in the results section). Samples were cut from the 4 inch parent core using a wet saw and then were precision ground to ensure flat, square, and parallel faces using a diamond-impregnated grinding wheel on a surface grinder.

True triaxial (i.e. all 3 axes were independently controlled) stress conditions were generated using a hydraulic piston-actuated loading cell, as shown in Figure 1. The ultrasound wave velocity measurements require a ½ inch diameter transducer on each face of the specimen. These transducers were accommodated by pockets in the loading platens (Figure 2). The contact pressure needed to assure coupling of the transducers with the rock was assured by firstly placing glucose between the transducer face and the rock, and secondly placing a rubber pad behind each transducer inside the pocketed platen that acted as a spring. When cut to the correct thickness, this pad was slightly compressed upon loading, ensuring a sufficient load holding the transducer in contact, but far less than the applied load to the rest of the specimen so that the transducer would not be damaged. Once assembled, the experimental apparatus applied loads in all three directions while also measuring wave velocities in all directions.

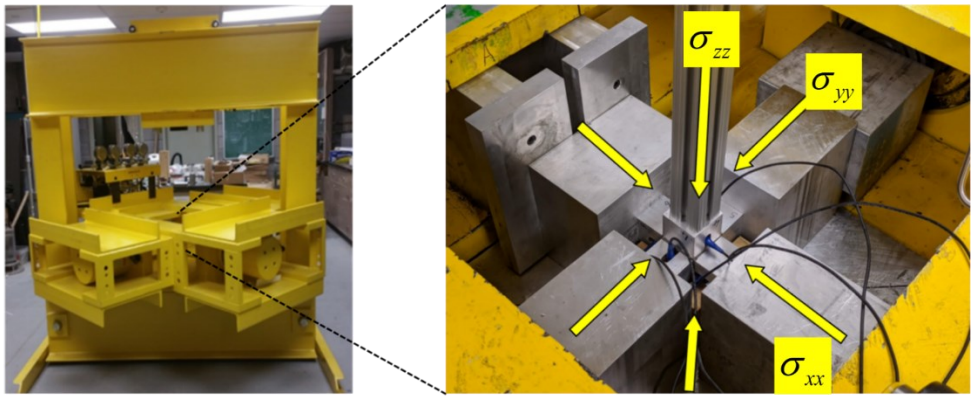

Figure 1: Experimental setup; a) Triaxial load frame; b) Rock specimen (with attached transducers that are inside the aluminum blocks) under loading. Vertical stress is denoted as σzz, and horizontal stress in two directions are σ_{yy} and σ_{xx}.

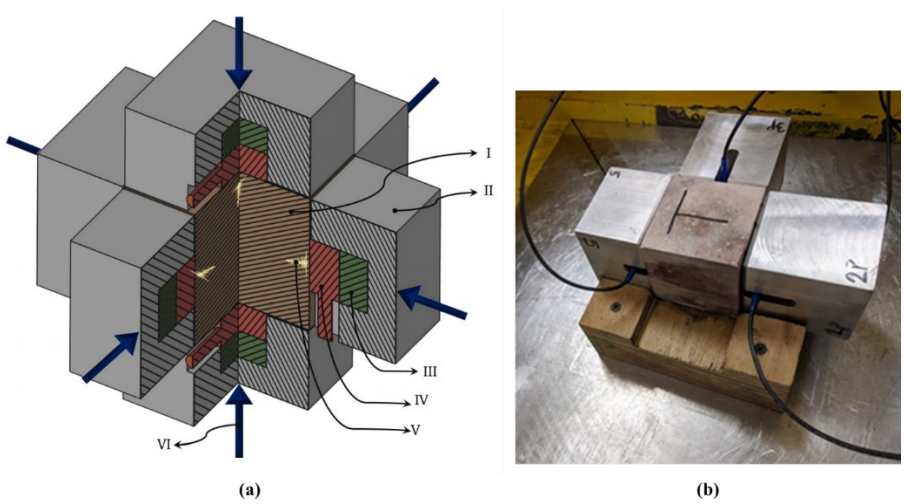

Figure 2: Specimen setup; a) A schematic with cross-sectional view of the rock sample, transducers, and aluminum blocks together. Numbers on the schematic is show the following: I) rock sample, II) aluminum block, III) rubber band, IV) transducer with cable attached, V) signal generated from the transducer, VI) the loading direction; b) Partially disassembled via of sample with transducers located inside the aluminum blocks before the rock is loaded in the triaxial-machine. Cables connected to the transducers are shown.

The ultrasound transducers were used as pulser-receiver pairs in each of three directions through the specimen. The transducers selected for this work were Olympus V153-RM, which are 0.5-inch contact transducers with central frequency of 1 MHz. These transducers are designed as shear wave transducers. However, because there is mode conversion at the boundary between the transducer and the specimen, both compressional (p-wave) and shear (s-wave) modes are produced. The p-wave, however, is much smaller in amplitude than the s-wave. This is helpful because it arrives first (having the higher velocity, as always), but quickly attenuates so there is a distinctive gap between the p- and s-wave arrivals in the waveforms (Figure 3). In this manner, a single pulse-receive test can obtain both p- and s-wave velocities. With that said, the s-wave velocity is not only dependent upon direction of propagation, but also on the polarity of the wave (direction of motion, which for an s-wave is perpendicular to the direction of propagation). So, to capture both fast and slow polarities, every experiment is run firstly with one set of s-wave polarities, and then it is re-run with all transducers rotated 90 degrees in order to obtain another, orthogonally-polarized s-wave velocity. For these transducers, the s-wave polarity is aligned with the sensor cable (Figure 2, and also see Figure 3), making it straightforward to ensure that the testing sequence measures p-wave, fast s-wave, and slow s-wave for all three directions through sample. The final data presented for the TUV experiments therefore consists of 9 wave velocities corresponding to each of the load combinations comprising the testing program for each specimen.

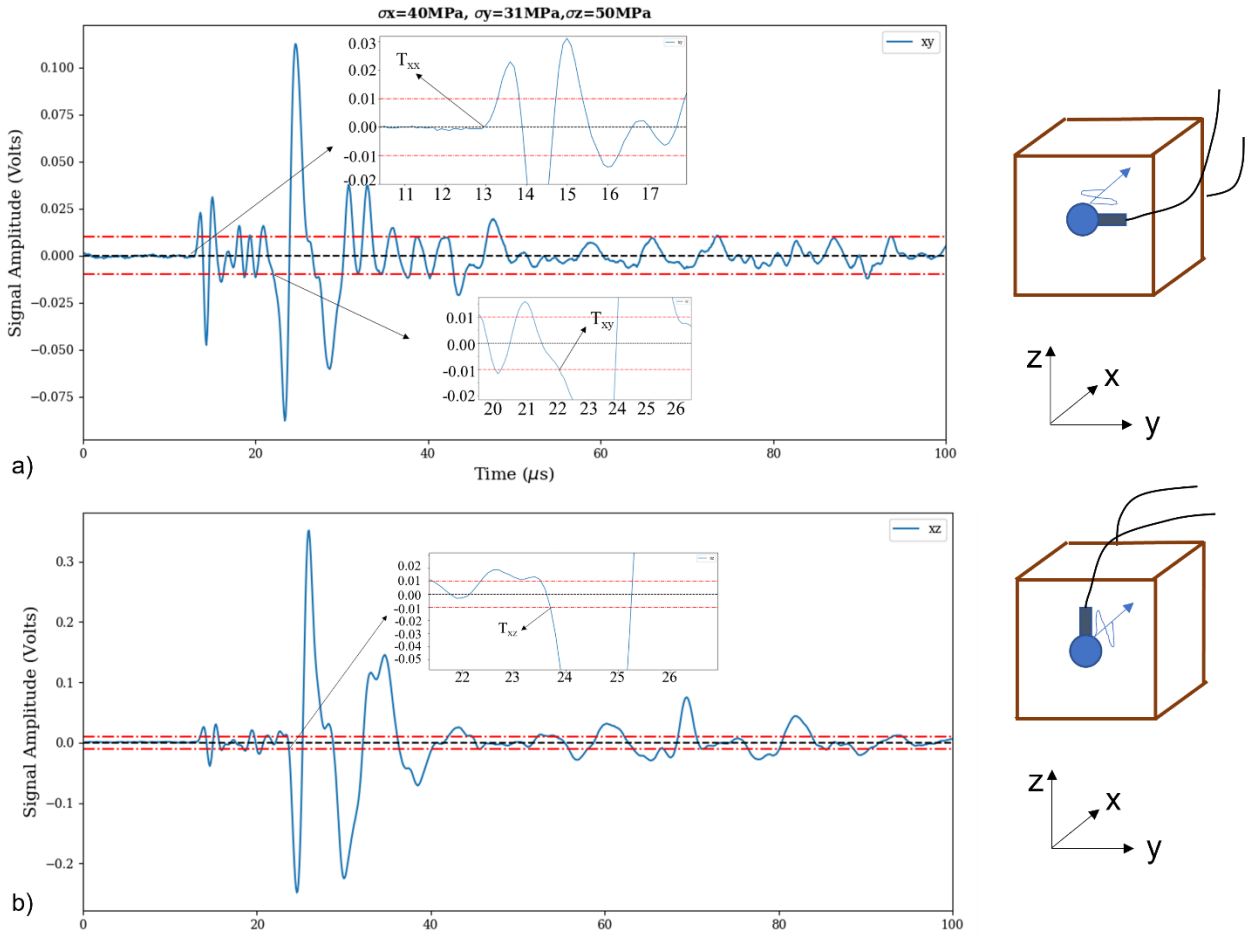

Figure 3: Example of waveforms from Lower Granitoid, x-direction. Waveforms result from two separate experiments with transducers oriented to capture the y-polarization (a) and z-polarization (b). Here the threshold used to pick the shear wave first arrivals is indicated and the later arrival time for the z-polarization indicates it is the slow shear wave. Sketches show sample and transducer orientation to illustrate propagation direction and shear wave polarity for each of these cases.

As an example, the 3 wave velocities for the x-direction of propagation are shown in Figure 4 for the Lower Granitoid. Here, as in all cases, the convention is used that the first subscript gives the direction of propagation and the second subscript gives the direction of particle motion associated with the wave. So, v_{xx} gives the p-wave velocity in the x-direction. Similarly, v_{xy} and v_{xz} give the s-wave velocities propagating in the x-direction with polarity in the y- and z-directions, respectively. Hence, for the x-direction of propagation, the y-polarity is clearly the fast shear wave and the z-polarity is clearly the slow shear wave. In this example, all three stresses are varied. However, because the normal stress in the x-direction, σ_{xx}, has the most substantial impact on velocities of waves propagating in the x-direction, the plots use this quantity for the x-axis. The scatter of the data is therefore indicative not of signal to noise issues, but rather of the sensitivity of the wave velocities to variation of the y- and z- components of the applied stresses. To aid in visualization, one "partial derivative" with respect to σ_{xx} is highlighted by coloring an outline around the symbols for points for which the y- and z- components of the stress are held constant and only σ_{xx} is varied. As will be discussed in the results to come, these examples clearly show correlation of wave velocities with stress including distinctive inflections in the slope and even non-monotonic behavior that can be taken as indicators of stress levels experiences in the past by this rock.

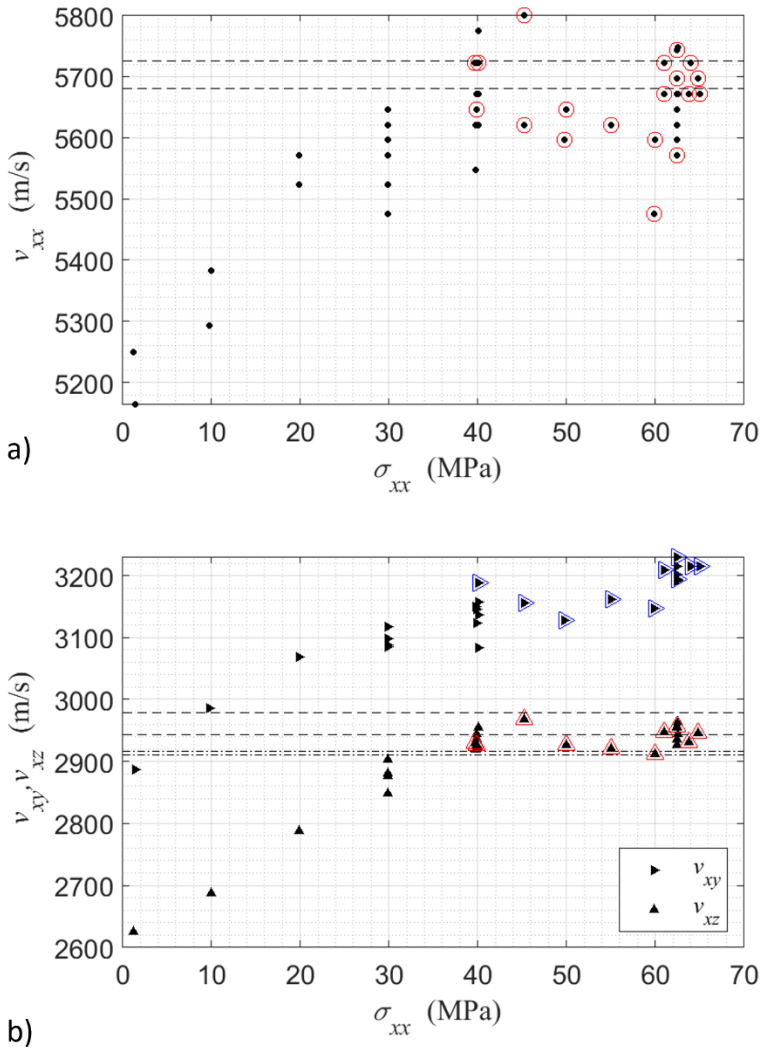

Figure 4: Example from Lower Granitoid, x-direction of wave propagation illustrating correlation of p-wave velocity (a) and fast and slow s-wave velocities (b) with normal stress in the x-direction. Note that all 3 stresses (x, y, and z) were varied, and the points with colored outlines indicate cases with similar y- and z-components of the stress and thus experimental partial derivatives with respect to σ_{xx}.

As an intermediate step to this final stress-dependent wave velocity data set, the full waveform data was collected for each transducer pair for every pulse-receive event. Once triggered, each channel recorded waveform data with the sampling rate is set as 10^7 Hz. With this waveform, as with any wave velocity survey, one of the most important steps was picking first arrivals. In this case, the decision was made to pick all first arrivals manually. Fewer load combinations were possible because of the time-intensive nature of this approach. However, the variation of ultrasonic velocities with stress were comprising total changes of about 10%, meaning that automated approaches with less precision would risk obfuscation of the phenomenon of interest.

The detailed approach to picking first arrivals is illustrated by way of Figure 3. First the p-wave arrival was picked. This arrival was automatically picked initially based on the signal crossing an amplitude threshold; this was what triggered the detection in the first place. However, to avoid spurious dependence of p-wave

arrival on the value of the threshold, the pick was modified manually to be at the initial upward inflection of the signal as it approaches the trigger threshold (Figure 3a, inset). Once the p-wave arrival was obtained, the s-wave arrival was determined by the crossing of the trailing, higher amplitude wave of a pre-set threshold that is kept consistent at 0.01 V throughout the testing (Figure 3, see insets). While one could project this apparent s-wave arrival back to where it crosses the time axis (zero voltage), in some cases the inevitable superposition of the tail of the p-wave with the arrival of the s-wave led to complicated waveforms that were not easily projected in this way. Hence, the most consistent approach was found to be a simple threshold crossing.

Deformation Rate Analysis (DRA)

Specimens were core-drilled as 30 mm diameter plugs from the parent sections of 4 inch diameter core from FORGE 16A(78)-32. One vertical and three horizonal core plugs were taken for each formation. The orientation for the horizontal plugs were measured relative to one another, however it should be noted that the parent core was not oriented and so the global orientation of the core plugs is not known.

After coring, the rough ends were removed with a diamond saw, and then the flat edges were ground using a diamond impregnated wheel on a surface grinder to ensure that the bases would be exactly parallel and flat. Note that all samples were room-dried based on unsealed storage since their retrieval and no effort was made either to thoroughly dry or to re-saturate the specimens. This is in contrast to the TUV experiments, where we recall the samples were re-saturated prior to testing. Water with soluble oil was used as a lubricant during coring and grinding.

For each specimen, the same procedure including setup, application of stress, and equipment was used. The first step entailed firstly loading the cylindrical core plug specimen in a sleeve which was then placed inside a Hoek-type triaxial (axisymmetric) compression cell (Figure 5). The Hoek cell was then placed in an INSTRON load frame that was used for application of the axial loading. During testing, the confining pressure in the cell is maintained at 15 MPa for the (shallower) Granitoid specimens, and it was maintained at 25 MPa for the (deeper) Gneiss specimens. The confining pressure was applied using an ISCO syringe pump. Load was measured by a load cell on the INSTRON load frame. The displacement was measured by three Linear Variable Differential Transformers (LVDTs) arranged every 120 degrees around the circumference and outside of the Hoek cell (Figure 5), and the cell pressure was measured by a pressure sensor in the ISCO pump. All tests were performed at room temperature.

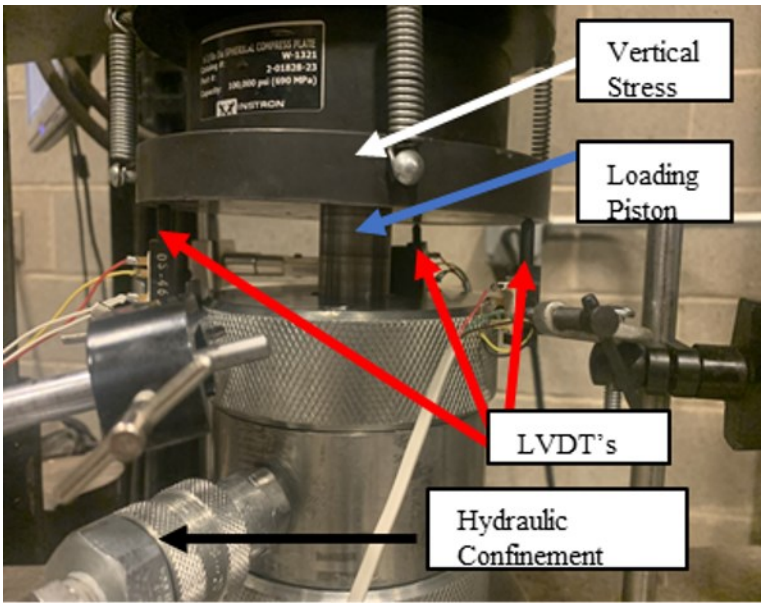

Figure 5: Hoek-type triaxial cell in load frame, showing also 3 LVDTs used for measuring vertical displacement.

The detailed loading sequence is as follows:

- Ramp the axial stress on the sample up to 0.100 MPa over a period of 1 minute.
- Ramp pressure from atmospheric up to 0.689 MPa (gauge pressure) on the confinement over a period of 1 minute.
- Increase axial stress and cell pressure in 5 MPa increments up to 15 MPa over a period of 25 min for Granitoid samples. Increase to 25 MPa over a period of 55 minutes for Gneiss samples.
- Loading and unloading phases begin now. First, ramp axial stress from the confining level up to 70 MPa for the Granitoid samples and 115 MPa for the Gneiss samples. The loading ramp is set to take 15 minutes.
- Reduce the axial stress from the maximum back to match the confining stress over a period of 15 minutes.
- Repeat the loading phase, raising axial stress to the maximum, again in 15 minutes.
- Reduce axial stress once more, ramping down to confining stress in 15 minutes.
- Relieve the confining stress gradually, over the course of 5 minutes.
- Relieve axial stress.

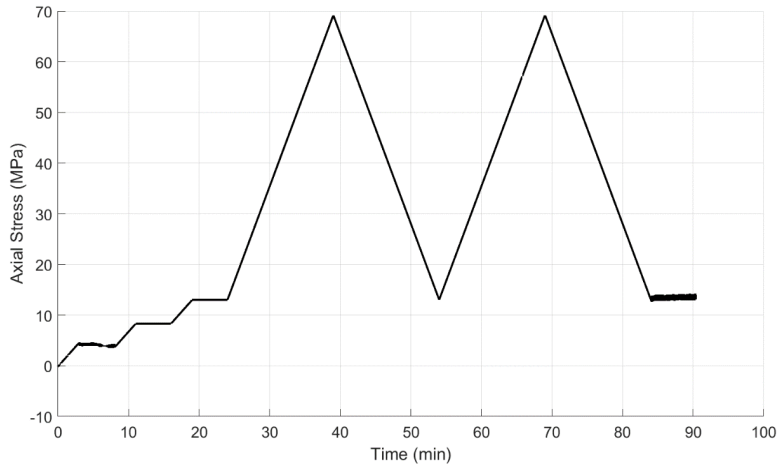

Figure 6: Example stress versus time plot showing the loading sequence for the Lower Granitoid, x-direction.

Specific stress versus time data is given for each sample in the Data Compendium. An example is shown in Figure 6, which gives a particular example for the x-direction from the Lower Granitoid. This loading sequence results in the displacements shown in Figure 7, which have been reduced by an amount estimated for deformation of 100mm of tool steel with E=210 GPa (comprising a lower bound on the platen deformation). There is a slight tilting of the platens evidenced by larger displacement on one LVDT compared to the other two.

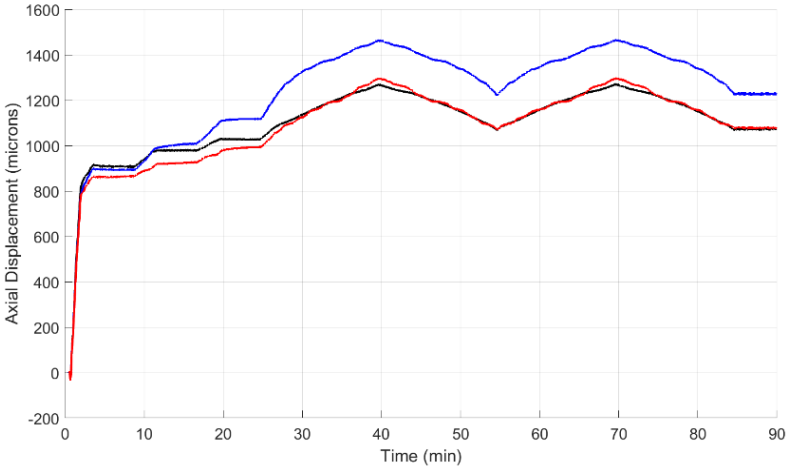

Figure 7: Displacements from 3 LVDTs placed at 120 degree increments around the specimen during the Load-Unload-Load-Unload cycle for an x-direction, Lower Granitoid sample.

Averaging and plotting stress versus strain relationships for the 2 load/unload cycles, setting zero strain at the beginning of the first load cycle, gives the result portrayed in Figure 8. In this example it is clear that the initial loading results in stiffening around 45 MPa. The first unloading and second loading curves track relatively closely to one another, and there is essentially zero hysteresis. This is a common behavior observed in the vast majority of tests. The permanent (or at least quasi-permanent) deformation from the first loading cycle causes the sample to stiffen and behavior more or less elastically in the subsequent

stages of the cycle. In these subsequent cycles, the slope of these curves is non-monotonic, with steepening (i.e. stiffening) at around 30 MPa, 39 MPa, and 57 MPa).

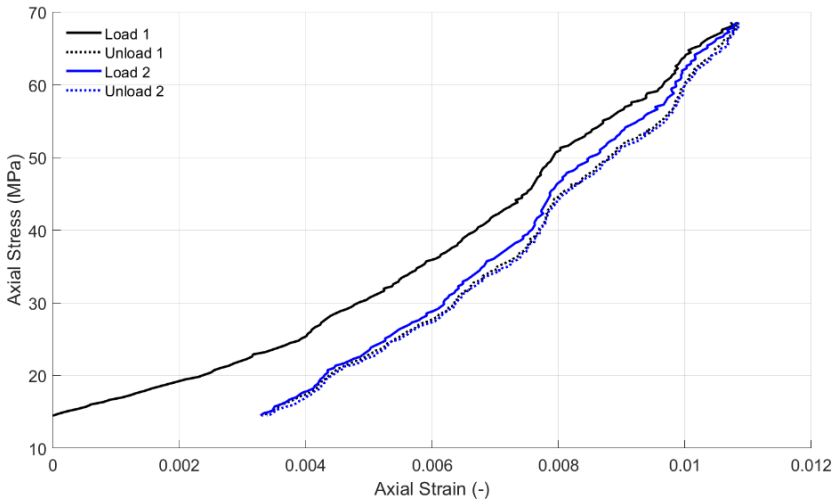

Figure 8: Stress-strain curves for an x-direction, Lower Granitoid sample.

In order to more clearly see the inflections, the instantaneous stiffness, i.e. the derivative ds/de based on Figure 8 is plotted as a function of axial stress. The result is shown for the x-direction, Lower Granitoid example in Figure 9a. The inflections observed in Figure 4 are once again reflected in this non-monotonic behavior of the stiffness. The stress levels are consistent after the first loading, which stiffens are larger values of the stress compared to subsequent cycles. However, when the instantaneous stiffness is plotted as a function of axial strain (Figure 9b), it is clear that the stiffness is strain dependent with remarkable consistency through load-unload cycles. This consistency is observed in a majority of DRA experiments, as presented in the Data Compendium.

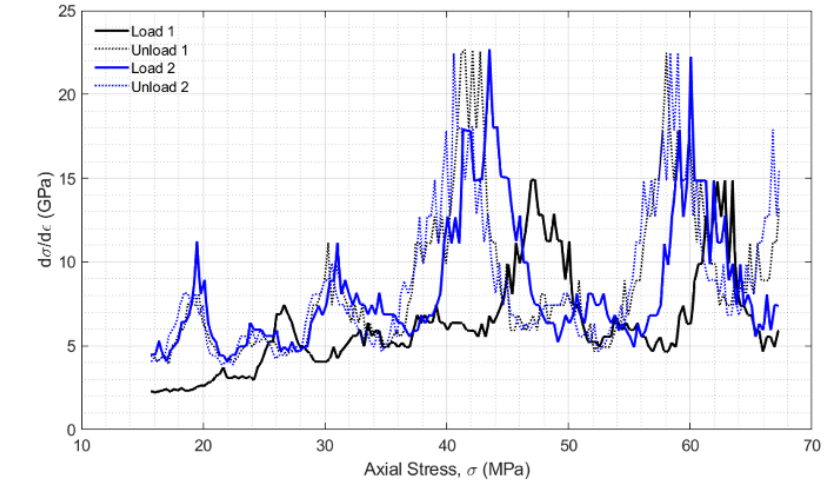

a)

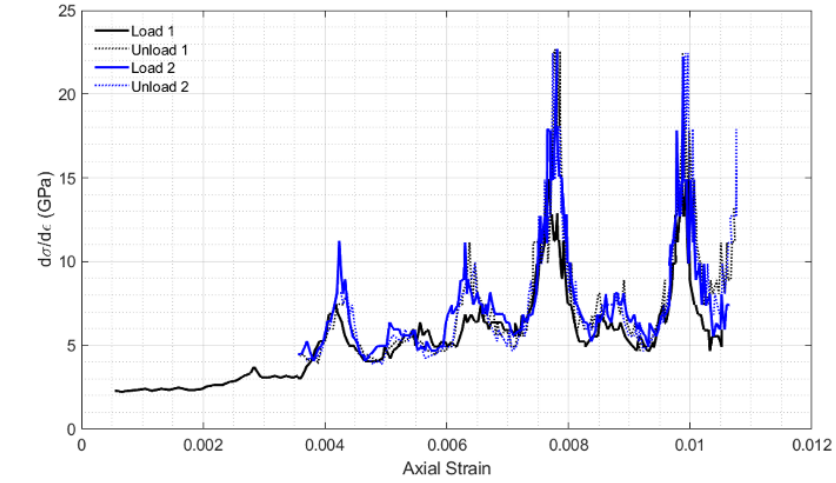

b)

Figure 9: Instantaneous stiffness as a function of a) axial stress, showing non-monotonic stiffening, and b) axial strain, showing consistency of stiffness as a function of strain. Example is presented here for x-direction in the lower Granitoid.

Besides observing stress-strain inflections, it is useful to examine the difference between the strain measurements for the load stages as a function of stress. This is the original, central step in the DRA method (Yamamoto et al. 1990, Dight 2006), where downward inflections are taken to be indicative of stress magnitudes experienced in the specimen's history. The result for the x-direction, Lower Granitoid example is shown in Figure 10, where we also plot the strain difference for the unload stages. With a focus primarily on the load stages, there are downward inflections at about 28, 39, 51, and 58 MPa.

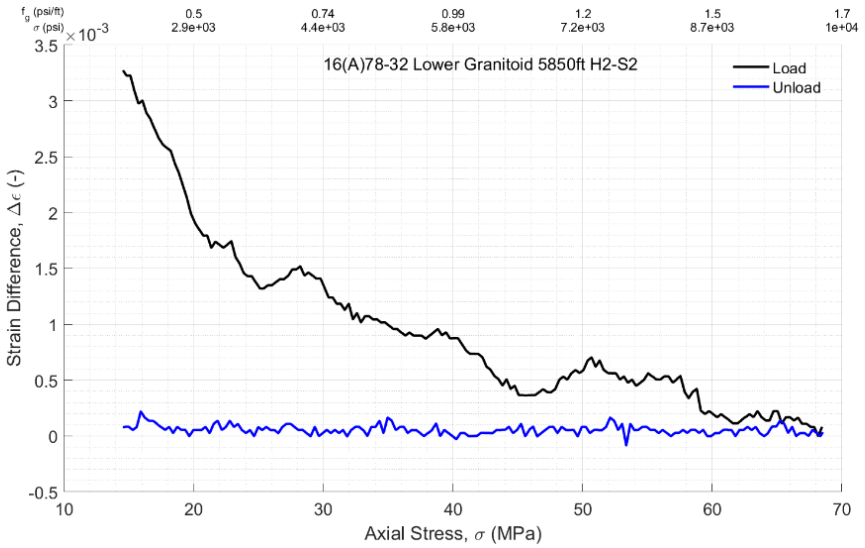

Figure 10: Strain difference between the first and second load stages, and first and second unload stages, as a function of axial stress for the example case from an x-direction, Lower Granitoid sample.

Weight of Evidence Integration

One of the challenges of both DRA and TUV approaches for stress estimation is they generate a multitude of lines of evidence regarding candidate values for in-situ stress magnitudes. Some of these evidences are very clear, with strong indications in the data. Others or more subtle. Some are consistently repeatable from one experiment to another, while others are less consistent. Some data clearly tie to in-situ stress magnitudes via a mechanical model, which others are not as clear in their relevance. Some of the data converge towards certain stress magnitudes, while others appear as outliers.

This challenge can become an opportunity if these various lines of evidence are incorporated in a consistent framework. To facilitate the necessary synthesis of data, a Weight of Evidence (WoE) approach is developed. While novel in the context of in-situ stress estimation, WoE approaches have a long history of use particularly in quantitative risk assessment (e.g. Weed 2005, Hardy et al. 2017), and including quantification of landslide risks in geotechnical engineering (Regmi et al. 2010). WoE approaches, in general, entail: 1) collecting all lines of evidence, 2) weighting the lines of evidence based on objective criteria, and 3) integrating the weight of evidence in order to ascertain the most strongly supported conclusions. In the present context, these three steps are carried out as described in the subsequent sections.

Collecting Lines of Evidence

The first step is to collect all lines of evidence from both TUV and DRA experiments. A line of evidence in this context can be:

1) A flattening or distinctive change in slope in a plot of one or more wave velocities versus the confining stress component applied in the direction of wave propagation from TUV experiments.
2) Flattening, slope changes, or convergence to sonic log velocities of elastic properties of the rock estimated from TUV experiments.
3) Clear inflections in stress-strain and strain difference versus stress curves for DRA tests.

4) Locations of distinctive upward inflections in the stiffness versus stress plots (Figure). Note these can sometimes reproduce the line of evidence from the stress-strain curve on which they are based, but this only serves to give more weight to inflections that are strong enough to be seen from the original curve, while more subtle inflections are accounted for but naturally receive less weight in the integration because they are only counted once.

Examples from the x-direction, Lower Granitoid are shown in Figure 11, with arrows indicating individual lines of evidence that can be collected from these data.

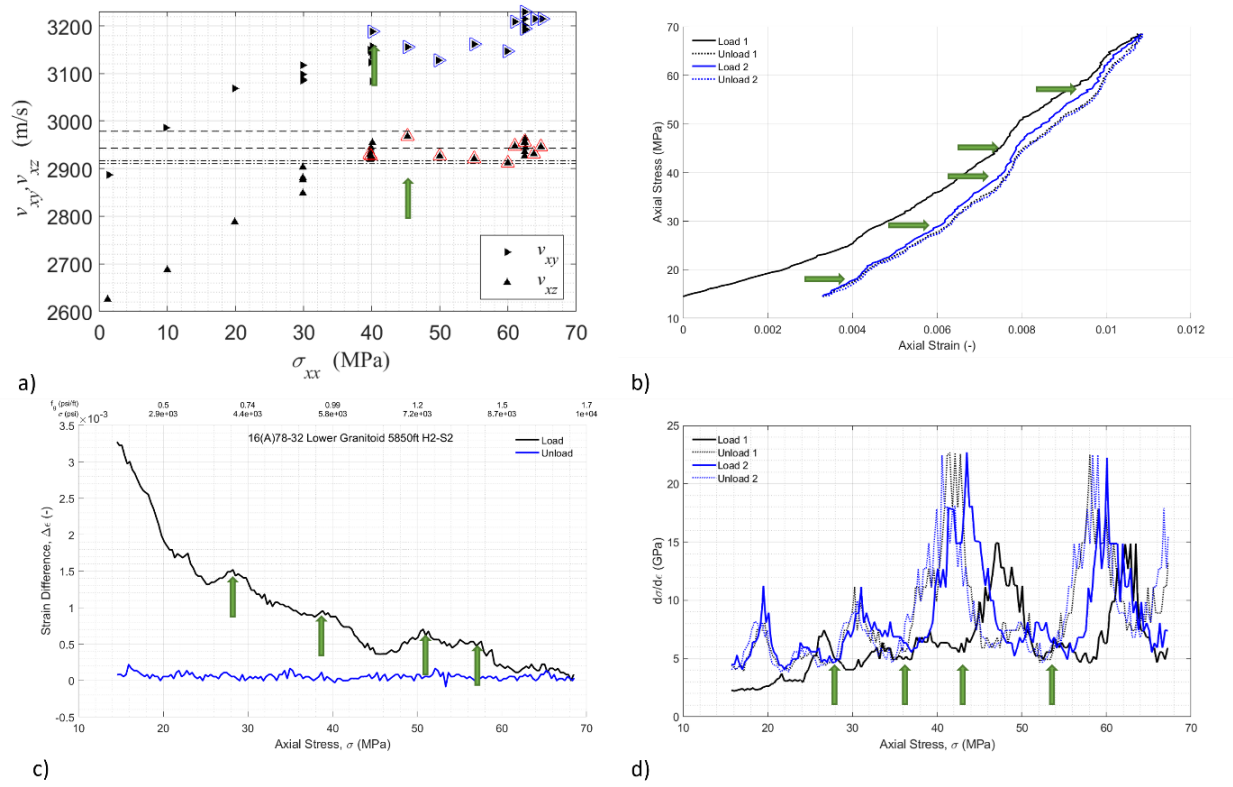

Figure 11: Lines of evidence, indicated here by green arrows, for both TUV (a) and DRA (b,c,d) data. This example uses previously-presented plots for x-direction, Lower Granitoid.

Assigning Weights

Classically, WoE approaches assign weights based on three criteria: 1) Relevance, 2) Reliability, and 3) Consistency. For rock mechanics applications, we add a fourth criterion, which is representivity. This provides a natural way to account for whether a line of evidence comes from a more "typical" section of the core (or well, in case of log-based applications). On the other hand, if evidence comes from an atypical section (i.e. the only intact section of an otherwise rubblized core or the only section with breakouts in an otherwise in-gage borehole), it will be assigned a lower score for representivity. The scoring rubric for these categories for the current application is given by

Table 1.

Table 1: Scoring rubric for assigning weight to lines of evidence from DRA and TUV experiments.

Criterion	High	Medium	Low	Base
Relevance (V)	Directly tied to mechanics by a formal model (3 pts)	Sound intuitive consistency with mechanics (2 pts)	Possible though somewhat unclear intuitive consistency with mechanics (1 pt)	No viable consistency with physical theory or intuition (0 pts)
Reliability (L)	Clear result, excellent signal to noise ratio (S/N) (3 pts)	Clean test, no large evidence of platen tilt (2 pts)	Visible pattern but with low S/N ratio (1 pt)	No visible patterns (0 pts)
Consistency (C)	Results experimentally replicated in this study (3 pts)	Consistent with similar tests in this study (1.5 pts)	Not contradicting results from other studies (0.5 pts)	Senseless outlier (0 pts)
Representivity (R)	Graded from 0 to 1 based on proportion of parent core appearing to be similar to the section sampled for the experiments			

Integrating

Once scores are assigned to each line of evidence per

Table 1, the cumulative Weight of Evidence is tallied by the following algorithm:

1) Divide the applied stress domain into bins, so that the width of the bins is commensurate with the precision of the measurements. Here the inflection points comprising the lines of evidence are recorded to the neared whole value of MPa, and so the bins are taken with widths of 3 MPa.
2) For the i^{th} bin, carry out a summation over all N_i lines of evidence that fall in that bin to get the cumulative weight of evidence for that bin, W_i, as

$$W_i = \sum_{j=1}^{N_i} \left(\frac{V}{V_{max}} \times \frac{L}{L_{max}} \times \frac{C}{C_{max}} \times \frac{R}{R_{max}} \right) \quad \text{Eq. 1}$$

Here V is relevance, L is reliability, C is consistency, and R is representivity. The maximum score, per

Table 1, comprising R_{max} is one, while the other three maximum scores are three.

Note there are other ways one could integrate, for example by using summation of the weights rather than the product. However, by using the product, assignment of zero points for any category naturally leads to a particular line of evidence being neglected. Additionally, the product approach gives a weight of one to a perfect line of evidence. Therefore, upon integration, the Weight of Evidence for a particular bin is naturally normalized to a perfect score, meaning that a bin with a cumulative weight of 3, while potentially containing many more than 3 lines of evidence, they are equivalent to 3 perfect lines of evidence in terms of relevance, reliability, consistency, and representivity.

Summary of Key Findings

Synthesis of DRA and TUV experiments run on 3 sections in the Granitoid and 2 sections from the Gneiss core from Utah FORGE well 16A(78)-32 leads to the following key findings:

1) Minimum horizontal stress gradient ranges from 0.58 psi/ft to 0.69 psi/ft, but with 4 of the 5 values between 0.66 psi/ft and 0.69 psi/ft (Table 2). Hence the minimum horizontal stress is potentially correlated to depth in a rather simple way (Figure 12).

Table 2: Summary of minimum horizonal stress estimates, including two options, where the first is considered most consistent with the data and the second is a viable alternative interpretation. The Young's modulus and Poisson's ratio are taken from the TUV experiments at stress levels near the estimated in-situ stresses. For Middle Granitoid and Lower Gneiss there are no TUV experiments, and so the elastic properties are taken from the nearby formations immediately above. Implied tectonic strain is estimated using Eq. (2).

			Minimum Horiz. Stress				Young's	Poisson's	Implied Tectonic Strain	
Formation	Vert Depth	Vert Depth	Option 1	Option 2	Gradient 1	Gradient 2	Modulus	Ratio	Option 1	Option 2
	(ft)	(m)	(MPa)	(MPa)	(psi/ft)	(psi/ft)	(GPa)		(microstr)	(microstr)
Upper Gran	5474	1669	25	30	0.66	0.79	76	0.24	159	224
Mid Gran	5488	1673	22	19	0.58	0.50	76	0.24	115	75
Lower Gran	5846	1782	27	24	0.67	0.60	60	0.32	97	47
Upper Gn	8548	2606	40	49	0.68	0.83	75	0.23	278	398
Lower Gn	8557	2609	41	47	0.69	0.80	75	0.23	300	380

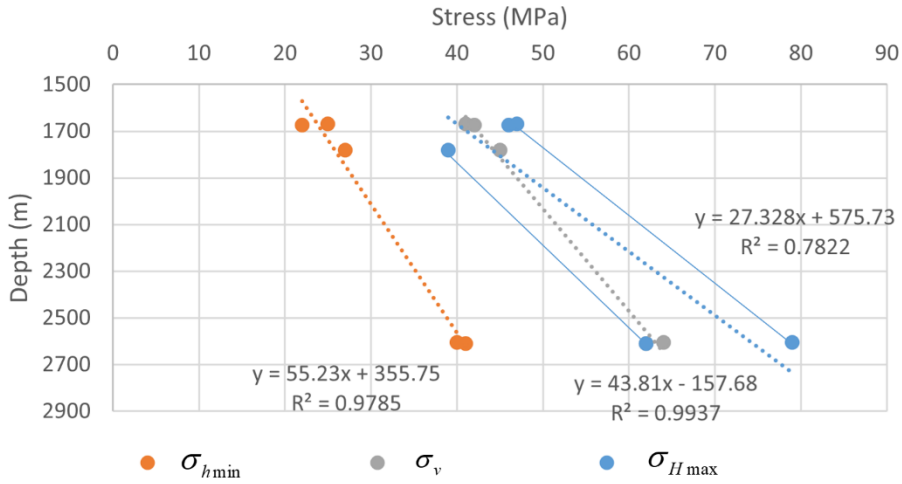

Figure 12: Plot of best estimates for minimum horizontal, vertical, and maximum horizontal stresses as functions of depth, along with best fit linear relationships. Additional light blue lines indicate individual trends of low and high estimates of maximum horizontal stress.

2) Vertical stress correlates rather simply with depth, as shown in Table 3 and Figure 12. The implied vertical stress gradient ranges from 1.05 psi/ft to 1.12 psi/ft, with 4 of the 5 results between 1.09 psi/ft and 1.12 psi/ft (and 1.05 psi/ft coming from a location where there was no TUV data and hence is based on a less comprehensive data set).

Table 3: Summary of vertical stress estimated from TUV and DRA experiments. There are also other stresses levels that generated enough evidence to bear mentioning; these are denoted "Other Stresses".

			Vertical Stress		Other Stresses					
Formation	Vert Depth	Vert Depth	Option 1	Gradient 1	Other A	Gradient A	Other B	Gradient B	Other C	Gradient C
	(ft)	(m)	(MPa)	(psi/ft)	(MPa)	(psi/ft)	(MPa)	(psi/ft)	(MPa)	(psi/ft)
Upper Gran	5474	1669	41	1.09	20	0.53	56	1.48	62	1.64
Mid Gran	5488	1673	42	1.11	19	0.50	55	1.45	61	1.61
Lower Gran	5846	1782	45	1.12	-	-	57	1.41	-	-
Upper Gn	8548	2606	64	1.09	30	0.51	85	1.44	94	1.59
Lower Gn	8557	2609	62	1.05	29	0.49	86	1.46	95	1.61

3) Maximum horizontal stress gradient is ranging from 0.97 psi/ft to 1.34 psi/ft (Table 4). Hence, the stress regime appears to be right on the edge between normal faulting and strike-slip faulting, potentially flipping back and forth between the two regimes due to variability of rock properties, structures such as faults, and other contributors to stress variation. Only in the Upper Gneiss, which is near the toe of the well, does the regime appear to be clearly strike-slip with the best estimate of maximum stress gradient at 1.34 psi/ft. Although there is an overall trend, there does not appear to be a simple linear relationship between maximum stress and depth (Figure 12). With that said, it is worth noting that even if the lower estimates are adopted, the slope of the maximum horizontal stress suggests that a normal faulting regime, if it indeed exists at shallower depths, is replaced by strike slip below about 2700 m TVD.

Table 4: Summary of maximum horizonal stress estimates, including two options, where the first is considered most consistent with the data and the second is a viable alternative interpretation. The Young's modulus and Poisson's ratio are taken from the TUV experiments at stress levels near the estimated in-situ stresses. For Middle Granitoid and Lower Gneiss there are no TUV experiments, and so the elastic properties are taken from the nearby formations immediately above. Implied tectonic strain is estimated using Eq. (2).

			Maximum Horiz. Stress				Young's	Poisson's	Implied Tectonic Strain	
Formation	Vert Depth	Vert Depth	Option 1	Option 2	Gradient 1	Gradient 2	Modulus	Ratio	Option 1	Option 2
	(ft)	(m)	(MPa)	(MPa)	(psi/ft)	(psi/ft)	(GPa)		(microstr)	(microstr)
Upper Gran	5474	1669	47	41	1.24	1.09	68	0.28	457	368
Mid Gran	5488	1673	46	34	1.22	0.90	68	0.28	436	260
Lower Gran	5846	1782	39	-	0.97	-	61	0.32	292	-
Upper Gn	8548	2606	79	49	1.34	0.83	57	0.27	971	444
Lower Gn	8557	2609	62	77	1.05	1.30	57	0.27	685	949

4) The Lower Granitoid contrasts with other formations in that it has lower Young's modulus, higher Poisson's ratio, and apparently lower maximum horizontal stress. It is the only formation clearly showing normal faulting stress regime. It has a unique needle-like fabric with the maximum stress direction roughly parallel to the needle orientation.
5) All five locations show an additional larger stress consistent with a gradient of 1.41-1.48 psi/ft. Four of the five locations show yet another larger stress consistent with a gradient of 1.59-1.64 psi/ft. The only location without lines of evidence associated with this highest stress is the Lower Granitoid, which also has an apparently smaller value of interpreted maximum horizontal stress.

It is unclear the origin of these higher stress rock behaviors, although is seems sensible they could be associated with stress conditions at other points in the rocks stress history. Perhaps they imply requiring the rock experienced higher compression in the past, and since that time it has not experienced temperatures that invoke annealing so that stress history is forgotten.

6) All cases except the Lower Granitoid also have a lower stress that consistently generates an apparent impact on data, especially from DRA tests. These all imply a similar stress gradient, between 0.49-0.53 psi/ft.
7) There is some evidence from the inclined core taken from the Gneiss near the toe of the well that the minimum horizontal stress orientation could be dipping by 20 degrees or more from the horizontal. This is possible evidence of impact of nearby structure(s) and/or thermal anomalies, and could cause the hydraulic fracture orientation to deviate noticeably from vertical.
8) The foliation in the Gneiss appears to be oriented so that maximum horizontal stress is acting across the foliation. This could potentially be useful for estimating parent core orientation for other parts of 16A(78)-32 and/or for other core taken from the Gneiss formation.
9) The implied minimum tectonic strain is estimated by Eq. (1), makes use laboratory determined values of dynamic Young's modulus and Poisson's ratio, and ranges from 100-300 microstrain (Table 2). Similarly, the maximum tectonic strain ranges from 300-1000 microstrain (Table 4). However, what is most interesting is that the ratio of the inferred minimum to maximum horizontal tectonic strain remains very close to 3 (Table 5). Even with an apparently different stress regime between the Upper and Lower Granitoid formations, the ratio of implied tectonic strain is almost the same.
10) With the exception of the Lower Granitoid (which is different from the others in a variety of ways) and the Lower Gneiss (which has no TUV data and so is more difficult to interpret), the other 3 formations indicate a ratio of maximum horizontal to minimum horizontal stress that is about 2.0 (ranging from 1.88-2.09, see Table 5). Even with these other formations, the range only increases to 1.44-2.09. Hence, an overall rough interpretation is that the maximum horizontal stress is tracking with a magnitude around twice the magnitude of the minimum horizontal stress.

Table 5: Summary of the ratios of maximum horizontal to minimum horizontal stress (sH/sh) and the ratios of calculated estimate of maximum horizontal tectonic strain to minimum horizontal tectonic strain (eH/eh).

Formation	Vert Depth (ft)	Vert Depth (m)	sH/sh	eH/eh
Upper Gran	5474	1669	1.88	2.88
Mid Gran	5488	1673	2.09	3.80
Lower Gran	5846	1782	1.44	3.01
Upper Gn	8548	2606	1.98	3.49
Lower Gn	8557	2609	1.51	2.29

Note that the preceding values of tectonic strain are computed, following an approach used for DRA interpretation by Higgins et al. (2022), using a classical geomechanical stress model for a region subjected to uniform tectonic strain is considered (after e.g. Dolinar, 2003). That is

$$\sigma_{hmin} = \frac{\nu}{1-\nu}\sigma_v + Ee_{tect,min}$$
$$\sigma_{h\max} = \frac{\nu}{1-\nu}\sigma_v + Ee_{tect,\max} \qquad \text{Eq. 2}$$

Here $e_{tect,max}$ and $e_{tect,min}$ are the maximum and minimum tectonic strains to which each layer is subjected. Hence, the second term on the right-hand sides give the tectonic component of the stress and depends upon Young's Modulus, *E*. The first term on the right-hand side gives the part that is related to restriction of lateral strain and that is induced by the overburden stress σ_v. It is a function of Poisson's ratio, ν.

These relationships, then, depend upon elastic properties. When necessary, the dynamic values are used owing to the fact that in many cases the static values approach dynamic values when confining is near expected in-situ levels and the loading system deformation is appropriately compensated for in the calculations. However, to do this properly, one would need to use orthorhombic elasticity. But, such a level of rigor is not commensurate with the isotropic rock model underlying Eq. (2). Characterizing orthorhombic elastic properties and using these in an orthorhombic tectonic stress model is therefore left to future work. Instead, we use an approach of converting wave velocities to elastic moduli in each direction independently, as if the rock were isotropic. This gives the nominal dynamic moduli, henceforth called "pseudo-isotropic" moduli, as (e.g. Economides and Nolte 2000)

$$G = \rho_b v_s^2, \qquad \nu = \frac{2v_s^2 - v_p^2}{2\left(v_s^2 - v_p^2\right)}, \qquad E = 2G\left(1+\nu\right), \qquad K = \frac{2G(1+\nu)}{3(1-2\nu)}$$

Eq. 3

Here *G*, ν, *E*, and *K* are the shear modulus, Poisson's ratio, Young's modulus, and bulk modulus, respectively. They are expressed in terms of experimentally-determined values of shear and compressional wavespeed, v_s and v_p, respectively. The relationships also use the bulk density of the rock, ρ_b.

Upper Granitoid

Summary

The 16A(78)-32 Upper Granitoid samples are from 5474' MD (1669m). The TVD is the same as the MD because the well is vertical to this point. There are flattened crystals in a nearly horizontal orientation with a slight additional elongation subparallel to the y-direction (Figure 13). The vertical z-direction is clearly across, essentially perpendicular, to the fabric.

Figure 13: Upper Granitoid sample preparation for TUV sample (cube) with DRA samples (cylinders), showing x, y, z axes on TUV sample and with cylinders laying in approximate directional correspondence to TUV sample. The TUV sample was cut from the core section in the upper right, and the slight elongation of crystals in y-direction can be seen from the top of the core.

The main observations begin with alignment of the minimum horizontal stress, which appears to be closer to the x-direction compared to the y-direction. The evidence comes from the single rollover points in the shear wave velocities, which indicate that shear waves with an x-direction of travel are reaching a maximum value at around 22 MPa (~0.6 psi/ft) compared to the y-direction where the maximum shear wave velocity is reached around 40 MPa (~1.05 psi/ft). This can be seen by contrasting Figure 14a and b. Note that highlighted points with colored overmarkings in this type of figure indicate results where two of the three applied stresses are fixed while the stress that is plotted on the x-axis is varied, hence experimentally taking a "partial derivative". Note that this orientation is sub-perpendicular to the direction of horizontal crystal elongation and is sub-parallel to the slower direction of wave propagation.

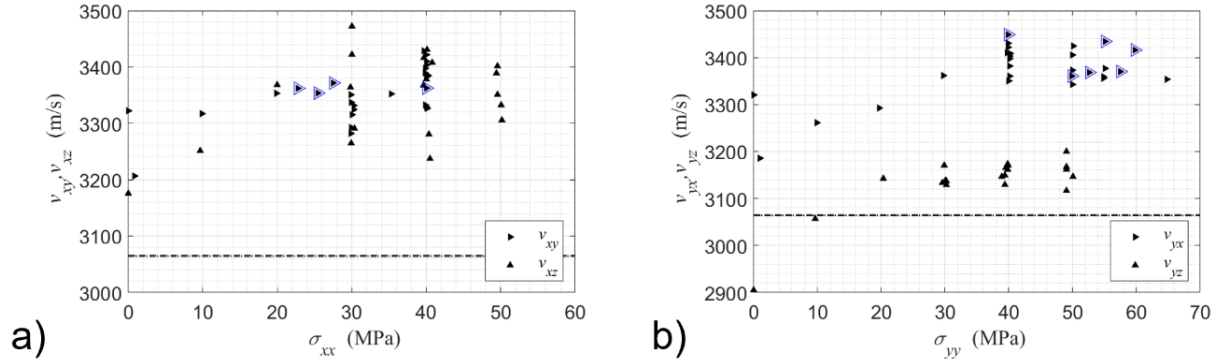

Figure 14: Shear wave velocities versus normal stress applied in the direction of wave propagation for a) x-direction, and b) y-direction. Highlighted points with colored overmarkings in this type of figure indicate results where two of the three applied stresses are fixed while the stress that is plotted on the x-axis is varied, hence experimentally taking a "partial derivative". The dashed lines give a reference to the measured shear wave velocity from well-logging, which was obtained for waves propagating in the slower vertical (z-) direction.

Secondly, the various inflection points from both TUV and DRA approaches amass the most evidence for a minimum stress that is somewhere between 25-30 MPa (0.65-0.8 psi/ft), as indicated by Figure 15. While this range is relatively large, it is proposed that misalignment of the x- and y-axes with the actual orientations of the in-situ stresses relative to the parent core will lead to inflection points that give upper bounds on the minimum stress. Combined with the observation that TUV data suggests lower values of minimum stress (previous point), the best estimate is taken as s_{hmin}~25 MPa (~0.66 psi/ft).

Thirdly, the weight of evidence from both DRA and TUV highlights two additional stress levels where multiple lines of evidence are converging. These are 41 MPa (~1.08 psi/ft) and 47 MPa (~ 1.25 psi/ft). It is difficult to say whether one of these should be attributed to the vertical stress and the other to the maximum horizontal stress. Ongoing efforts in rock physics modeling of DRA and TUV experiments are expected to provide much more clarity. However, if 1.08 psi/ft is taken as a more likely value for overburden gradient, then perhaps at this point the best estimate of maximum horizontal stress gradient is 1.25 psi/ft. Note also that misalignment of the x- and y-directions will lead to underestimates of maximum horizontal stress. So it is unlikely that 1.08 psi/ft is appearing because of an overestimate of a maximum horizontal stress that is somewhat lower.

Finally, it is observed that there are some additional inflections giving several lines of evidence around 63 MPa (~1.65 psi/ft). The origin of these responses remains unknown but, again, can be expected to be clarified by application of a micromechanical rock physics model (being developed now) to the interpretation.

To summarize:

1) **Minimum horizontal stress** is aligned roughly perpendicular to horizontal needle-like fabric (which is also the slow wavespeed direction) and with magnitude around 25 MPa (~0.66 psi/ft).
2) **Maximum horizontal stress** is aligned roughly parallel to horizontal needle-like fabric which also means it is roughly parallel with the maximum horizontal wavespeed direction. Two candidates for its value are 41 MPa and 47 MPa, corresponding to 1.08 psi/ft and 1.25 psi/ft, respectively. If

1.08 psi/ft is taken as vertical stress, then the remaining 1.25 psi/ft is attributable as an estimate of the maximum horizontal stress.

3) **Vertical stress** is likely around 41 MPa at this location, corresponding to an overburden stress gradient of 1.08 psi/ft. However, if 1.08 psi/ft is the maximum horizontal stress, then a very large overburden stress gradient of 1.25 psi/ft would be inferred and would need to be explained (perhaps based on paleostress conditions).

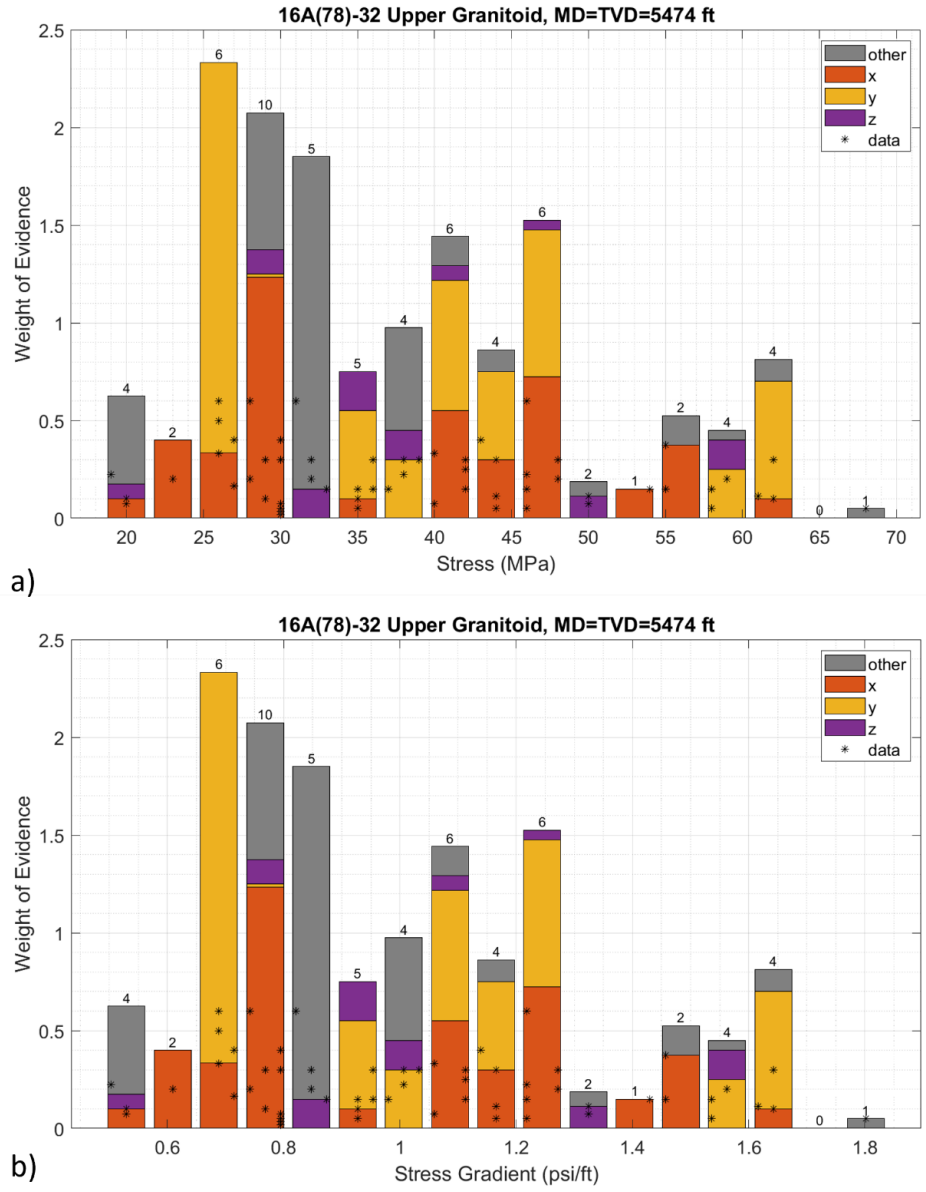

Figure 15: Integrated weight of evidence from TUV and DRA tests versus a) applied stress (axial stress in DRA experiments and normal stress in direction of propagation in TUV tests), b) corresponding implied stress gradient. The stars indicate individual data points, noting some lie directly on top of one another. The number at the top of each bar is the total lines of evidence in that bin. The bars are color coded to indicate the orientation of the sample giving the line(s) of evidence leading to that part of the bar.

X-Direction: Compendium

The 16A Upper Granitoid samples are from around 5474 MD and the same TVD because well is vertical to this point. There are elongated crystals in nearly horizontal orientation. Unlike in the Lower Granitoid, the TUV sample was cut oblique to the needle-like plates. However, the x-direction is more across than parallel to the needles and y-direction is more parallel than across. The vertical z-direction is clearly across, essentially perpendicular, to the fabric. One would therefore expect the x-direction in the Upper Granitoid to be more like the y-direction in the Lower Granitoid, and vice-versa.

Running the TUV experiments, we find

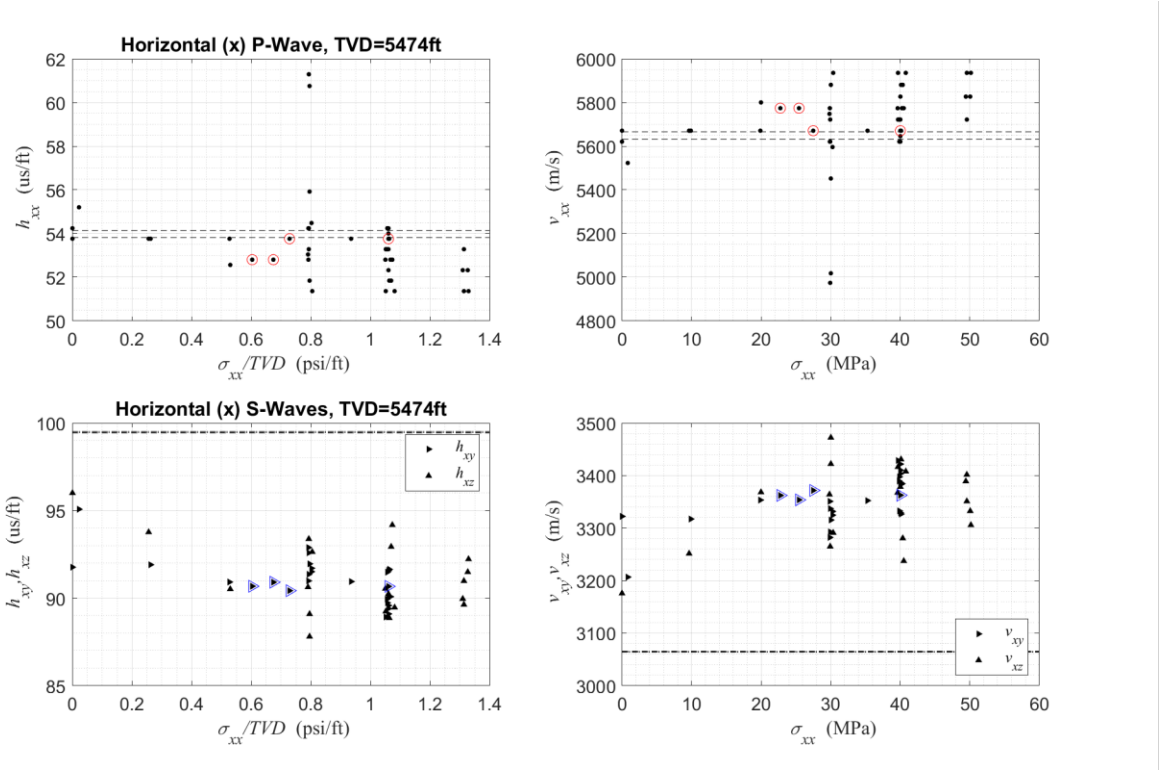

Here we see that wavespeed inflects between 20-30 MPa, possibly suggesting that the x-direction normal stress is returning to a value near in-situ conditions when stress is going through this range. Without using orthorhombic framework, just converting to elastic moduli as if isotropic gives the nominal dynamic moduli as (e.g. Economides and Nolte 2000)

$$G = \rho_b v_s^2, \qquad \nu = \frac{2v_s^2 - v_p^2}{2\left(v_s^2 - v_p^2\right)}, \qquad E = 2G\left(1+\nu\right), \qquad K = \frac{2G(1+\nu)}{3(1-2\nu)}$$

Here G, ν, E, and K are the shear modulus, Poisson's ratio, Young's modulus, and bulk modulus, respectively. They are expressed in terms of experimentally-determined values of shear and compressional wavespeed, v_s and v_p, respectively. The relationships also use the bulk density of the rock, ρ_b, measured for these formations as

Lower granitoid: 2.6699 g/cm^3
Upper granitoid: 2.6255 g/cm^3
Upper Gneiss: 2.8205 g/cm^3
Untested Lower Gneiss: 2.6977 g/cm^3

Obviously, this is not the correct approach for an orthorhombic material. However, the complexity of the method increases significantly because of the need to measure first arrivals for waves propagating at 45 degrees (or some other oblique angle) relative to the fast/medium/slow principal axes of the material. Such effort is not warranted in this case because we are interested in observing the general trend of these quantities, specifically how that trend inflects as a function of applied stress. By Eq. 3 we obtain

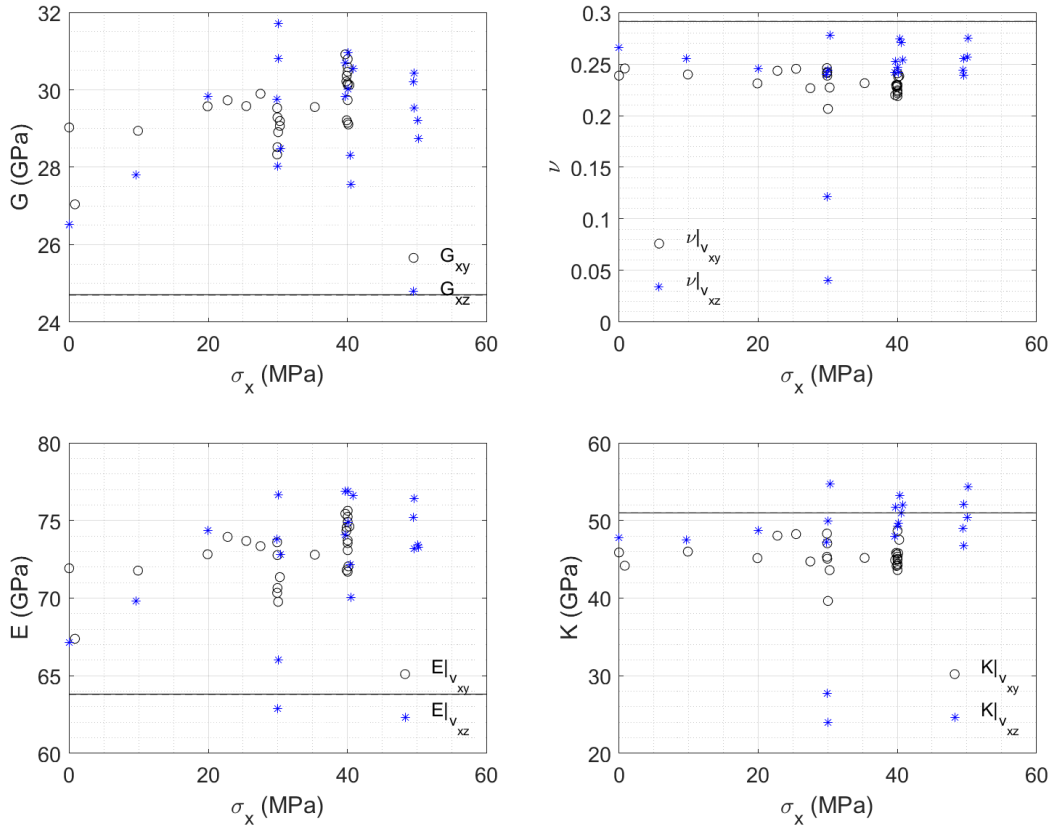

While none of the DRA and TUV axes are perfectly aligned with one another, H3 is the best to compare with the x-direction, as it is only 7 degrees differently aligned. There are two samples in this direction, which will be presented together. The sample dimensions and an image of the sample are as follows. Notice the visible infilled cracks (i.e. veins) oblique to the core axis. These are more pronounced in the shorter H3-2 specimen.

H3-1 H3-2

Dimensions		**Dimensions**	
height (mm):	42.49	height (mm):	36.44
width (mm):	32.03	width (mm):	31.95
Angle retrieved (degrees):	46.9	**Angle retrieved (degrees):**	46.9

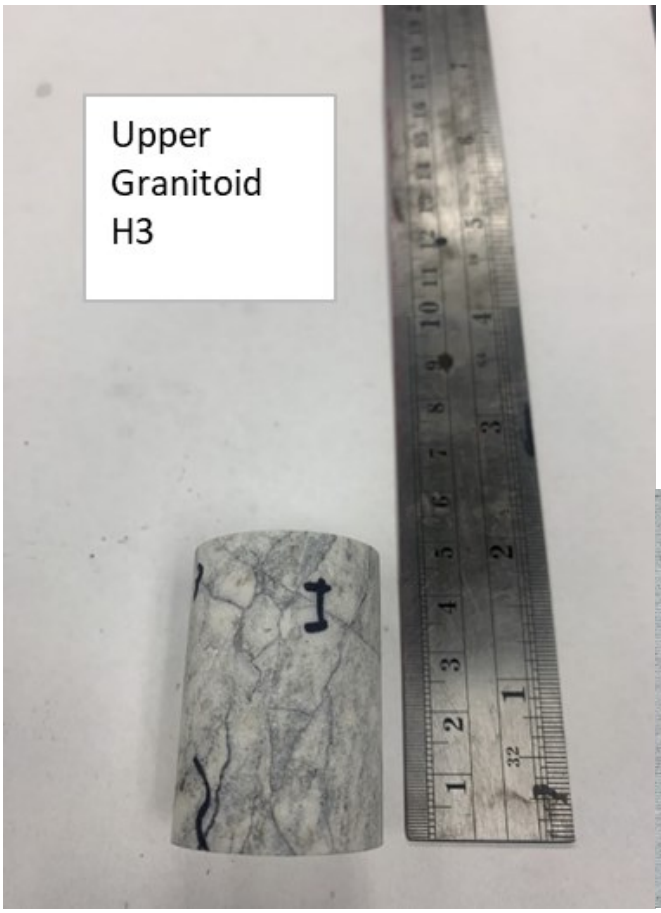

DRA experiments are run with the loading sequence (as with all cases to follow, H3-1 is presented immediately followed by H3-2)

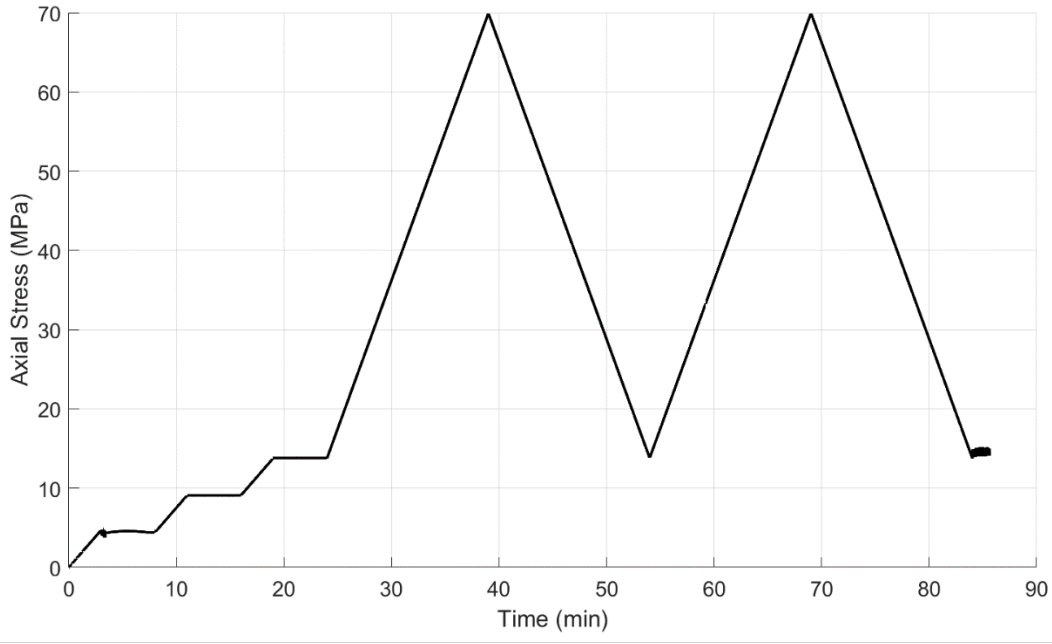

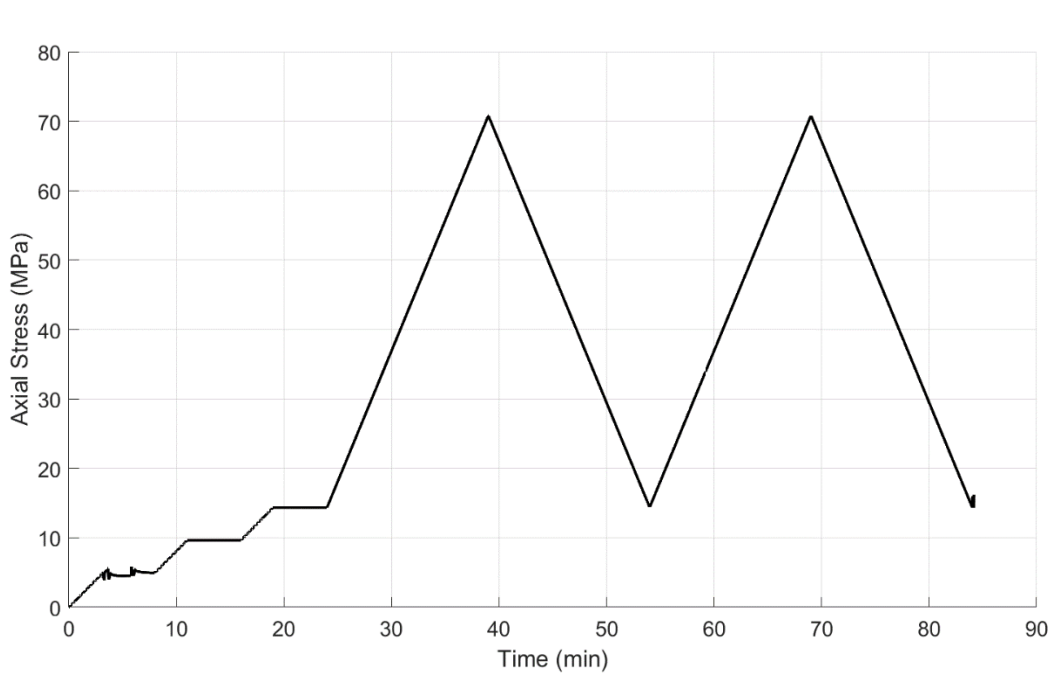

This loading results in the following displacements, which have been reduced by an amount estimated for deformation of 100 mm of tool steel with E=210 GPa (comprising a lower bound on the platen deformation). This gives

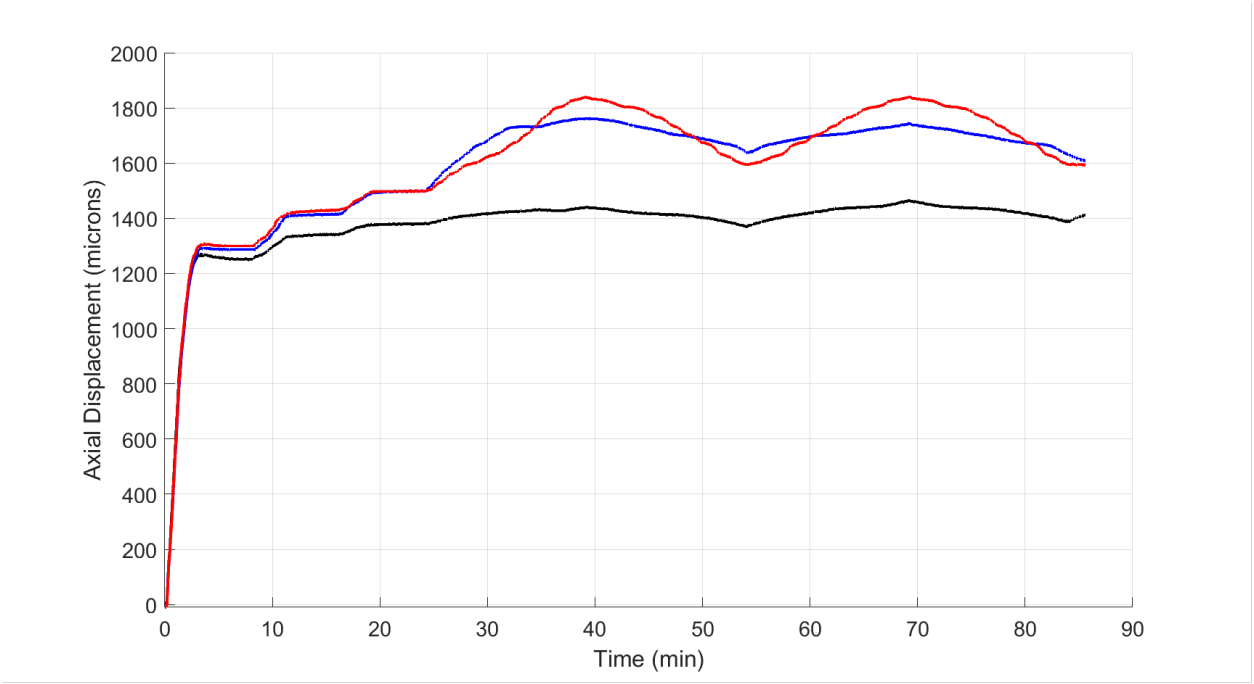

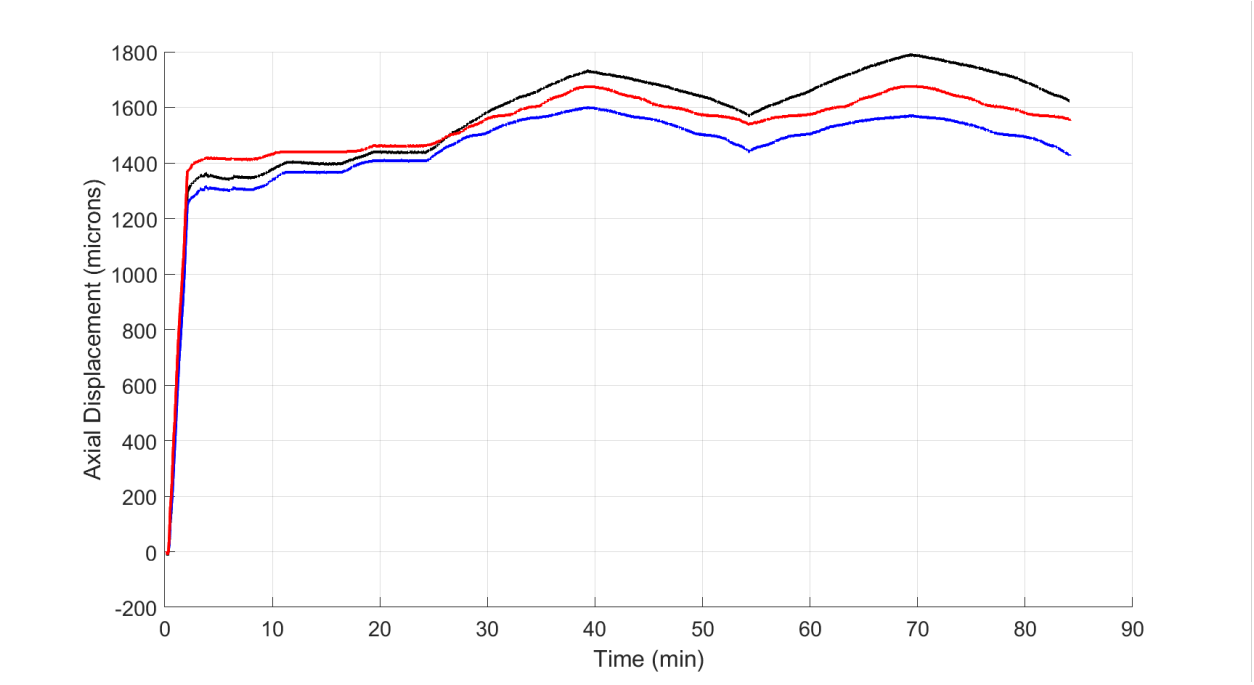

Observe that the first load cycle involved a small amount of tilting of the platens. It is possible this was caused by a slightly larger preponderance of inclined veins in the first sample compared to the second.

Averaging and plotting stress versus strain relationships for the 2 load/unload cycles, setting zero strain at the beginning of the first load cycle, gives

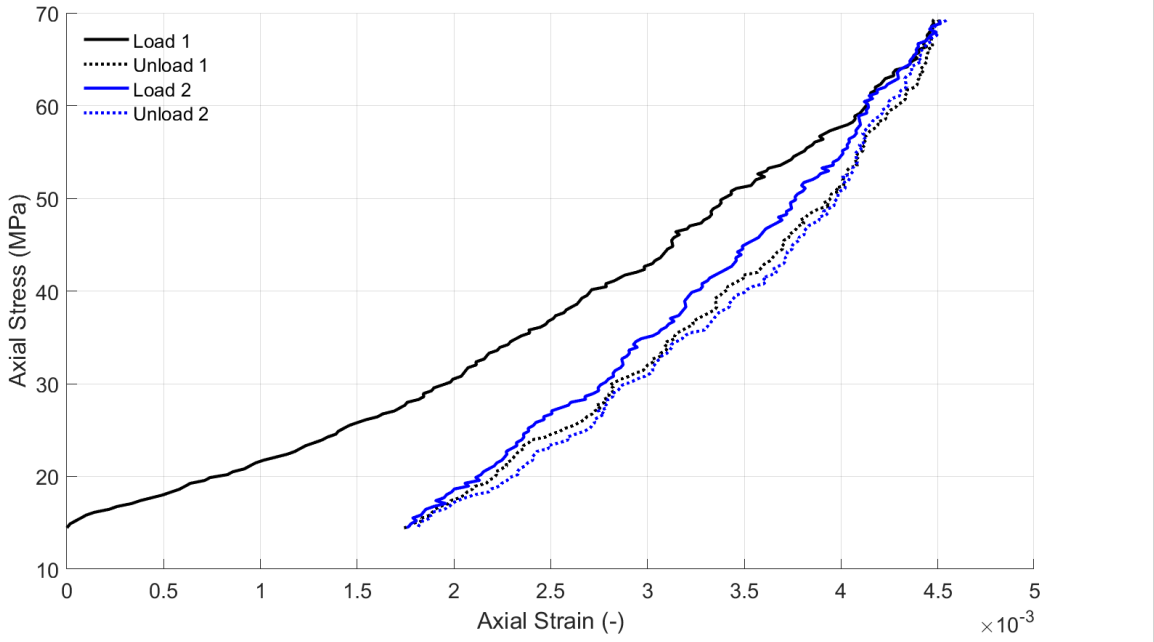

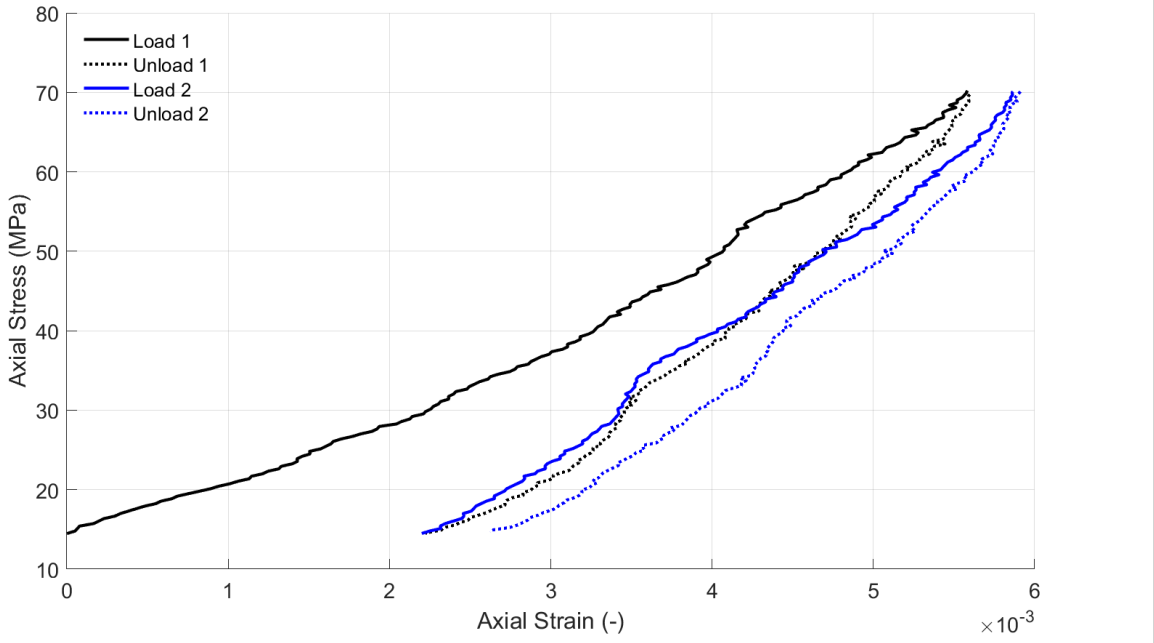

Both cases clearly stiffening between 25-30 MPa, and maybe again between 40-50 MPa. Note that in the second case there is some hysteresis indicative of plastic strain on the order of 0.0003. Recall (see the sample photos earlier in this section) that the veining was more pronounced in the H3-2 sample, which could have been accounting for the greater plastic strain. In the first case there is almost no apparent plastic strain except for that encountered in the first loading and which was almost perfectly compensated by change in the stiffness so that the strain in the second loading converges with the strain from the first loading at around 58 MPa. The corresponding difference between the strain measurements for the load/unload stages is given by

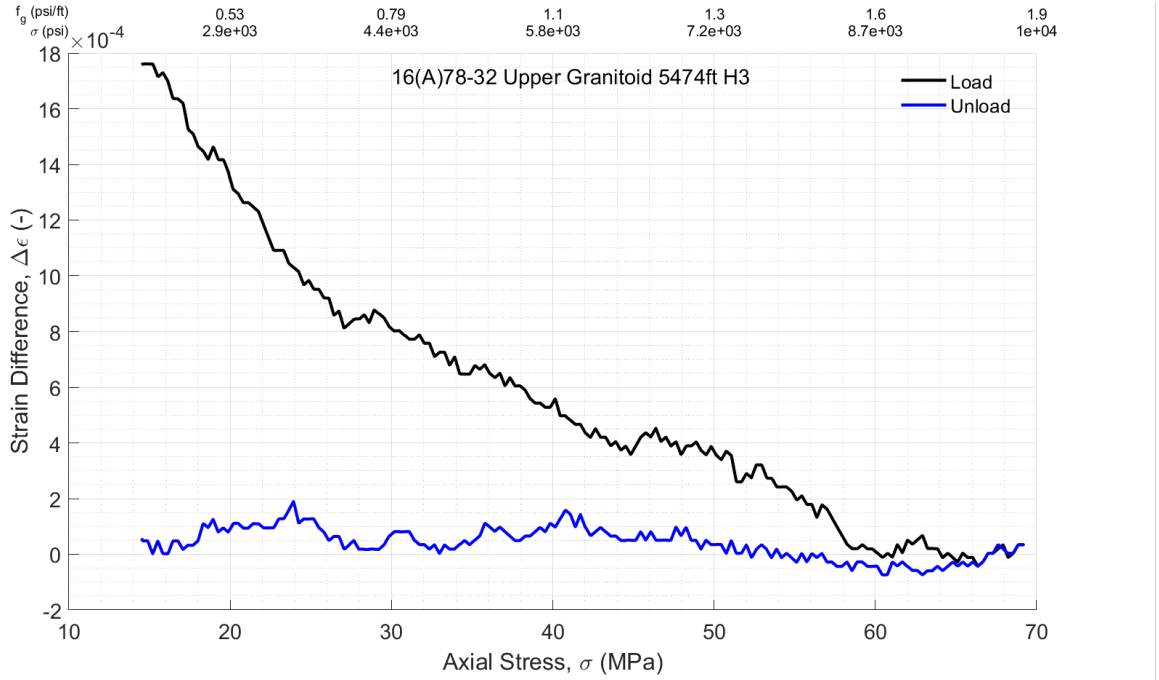

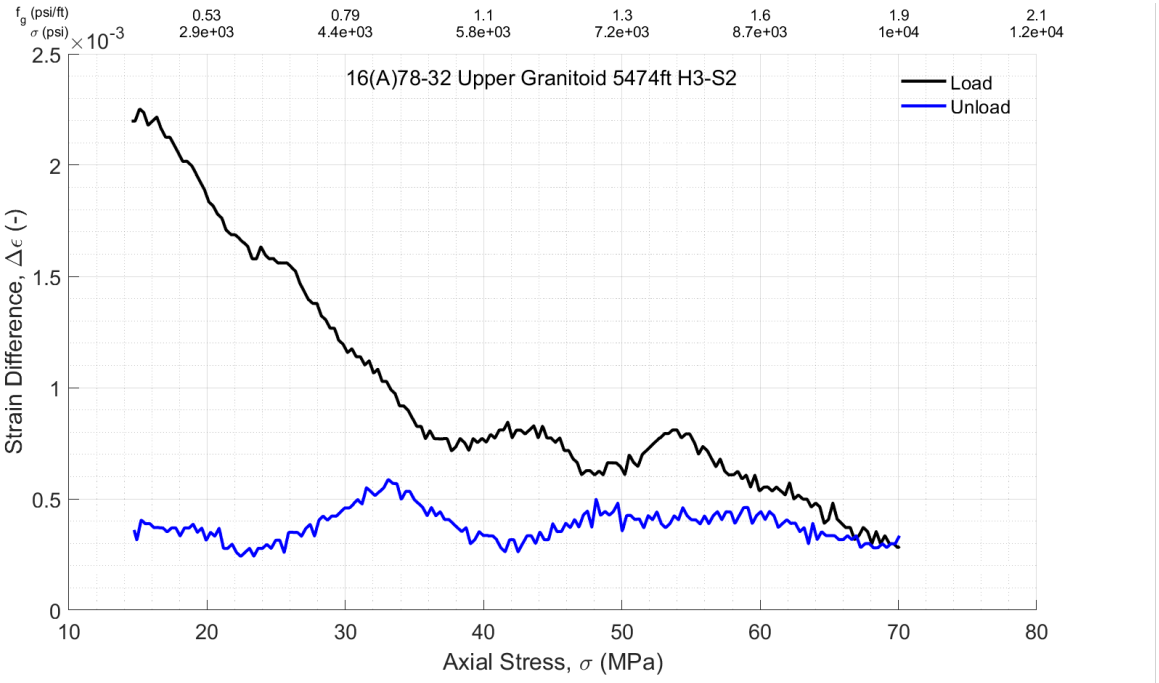

Next, we examine the instantaneous stiffness through the load/unload cycles and plot it firstly as a function of stress. For reference, and not necessarily because there should be agreement but just because it provides context, the value of Young's modulus from the well log is plotted here (note, however, that it is measured based on wavespeeds in vertical direction). We also show the nominal values of dynamic Young's modulus based on the TUV experiments presented earlier. This gives

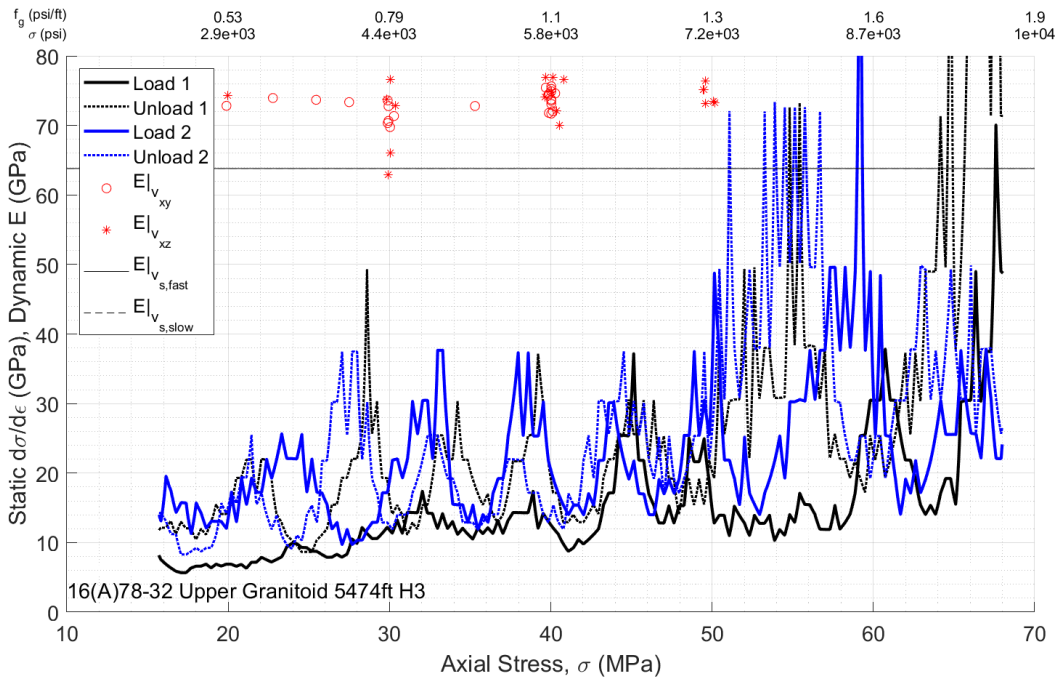

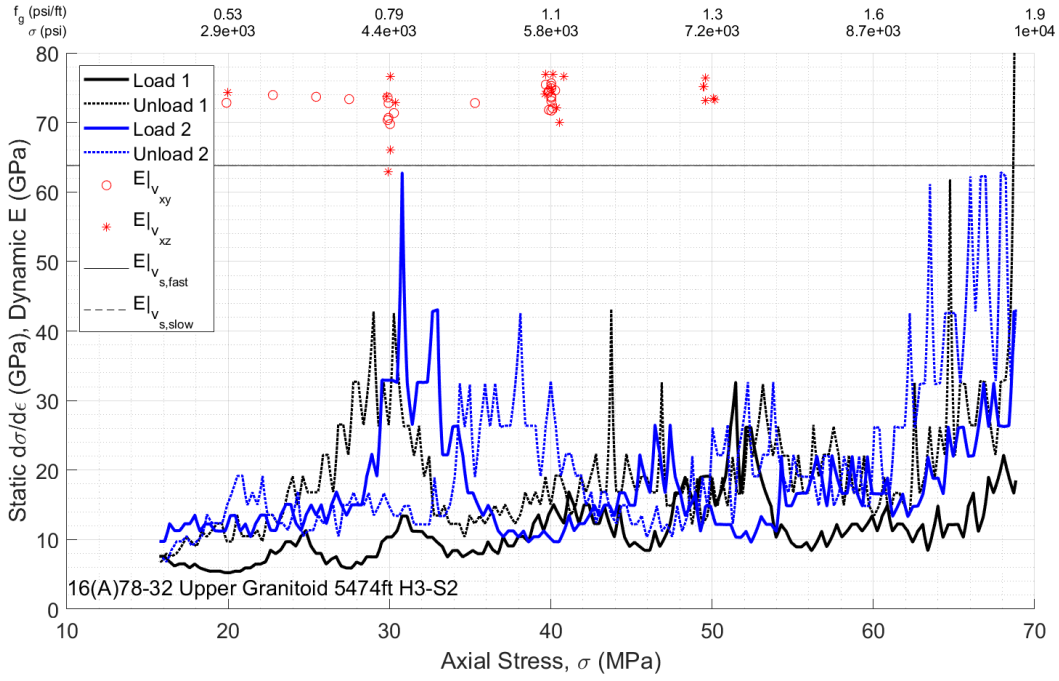

While there are multiple stiffening/softening ranges, the most striking and consistent is occurring between 25-30 MPa, as expected based on the change in slope observable in the stress-strain curves. We can also see that the impact of stress on static stiffness is much larger than its relative impact on dynamically-determined Young's modulus. Interestingly, if we plot this stiffness versus strain, the stiffening and softening are always happening at the same level of strain, viz.

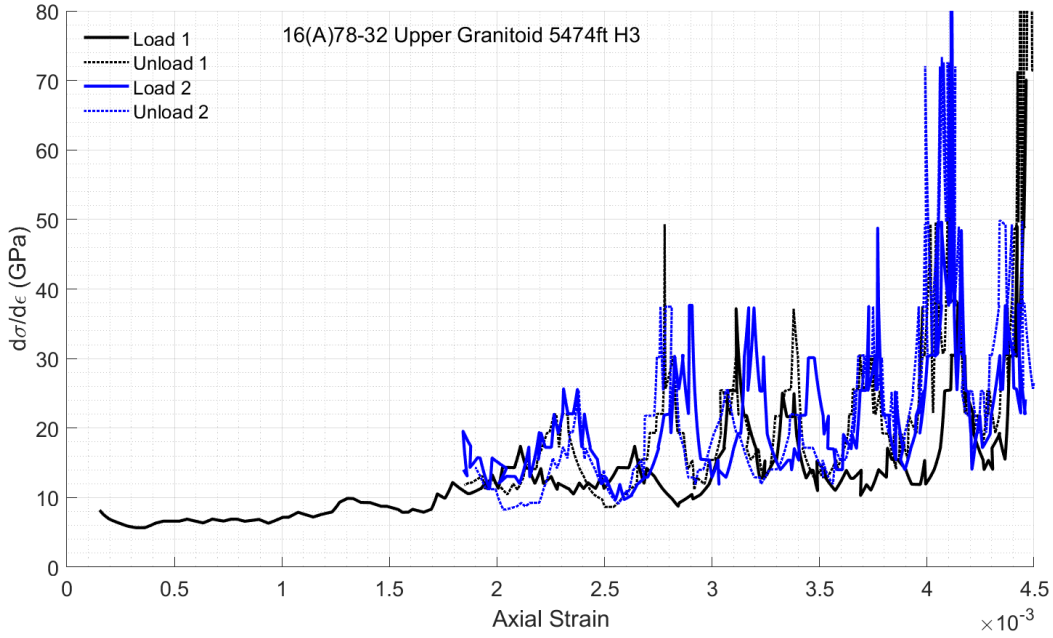

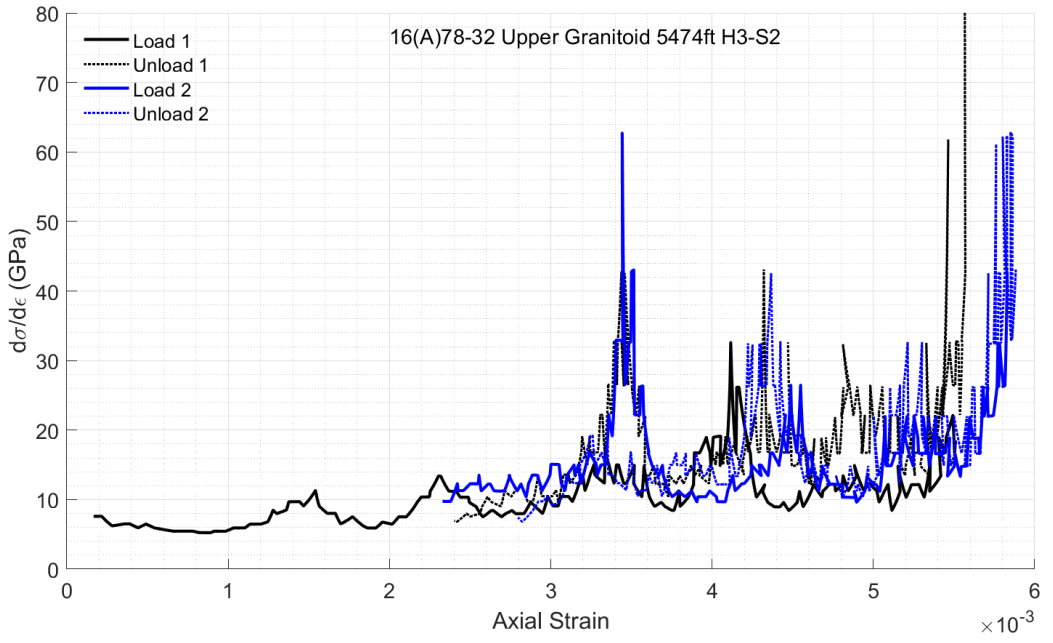

Y-Direction: Compendium

The 16A Upper Granitoid samples are from around 5474 MD and the same TVD because well is vertical to this point. There are elongated crystals in nearly horizontal orientation. Unlike in the Lower Granitoid, the TUV sample was cut oblique to the needle-like plates. However, the x-direction is more across than parallel to the needles and y-direction is more parallel than across. The vertical z-direction is clearly across, essentially perpendicular, to the fabric. One would therefore expect the y-direction in the Upper Granitoid to be more like the x-direction in the Lower Granitoid, and vice-versa.

Running the TUV experiments, we find there is an observed rolling over of wavespeed, especially v_{yx}, around 40 MPa, as indicated by

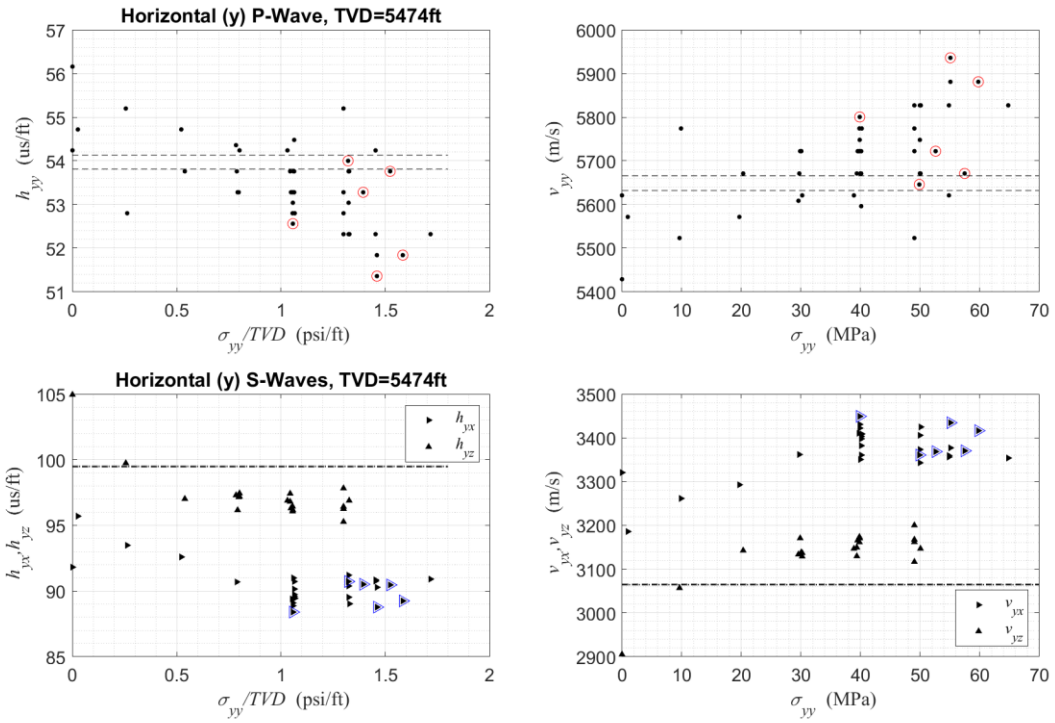

Without using orthorhombic framework, just converting to elastic moduli as if isotropic gives the nominal dynamic moduli using Eq. 3 gives

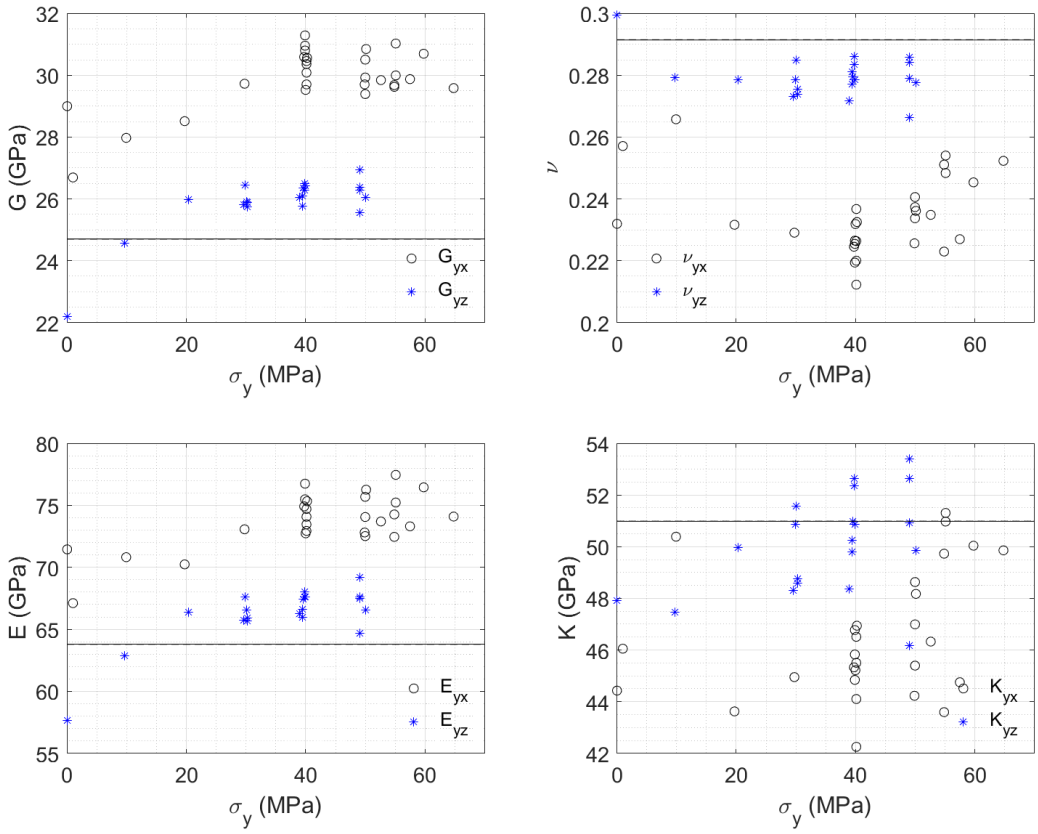

Note that the vertical polarizations lead to closer agreement with the well logs (shows in solid and dashed lines). This makes sense if the p-waves are nearly the same (which they are) and the velocity tensor is symmetric so that v_{yz}=v_{zy} (because v_{zx} and v_{zy} are what we get from the fast and slow shear in the well log).

The DRA samples in the H2 direction are best to compare with the y-direction, as they are the closest in orientation. Specifically, H2 is 19 degrees differently aligned compared to the y-axis of the TUV sample. There are two samples in this direction, which will be presented together. Notice a few visible infilled cracks (i.e. veins) that are oblique to the core axis. Generally, though, there are fewer of these than in the H3 samples used to approximate the x-direction. The geometry of the specimens and images are as follows:

H2-1 H2-2

Dimensions		**Dimensions**	
height (mm):	40.94	height (mm):	36.72
width (mm):	31.99	width (mm):	31.99
Angle retrieved (degrees):	291.3	**Angle retrieved (degrees):**	291.3

The DRA loading sequence is given for the two tests as

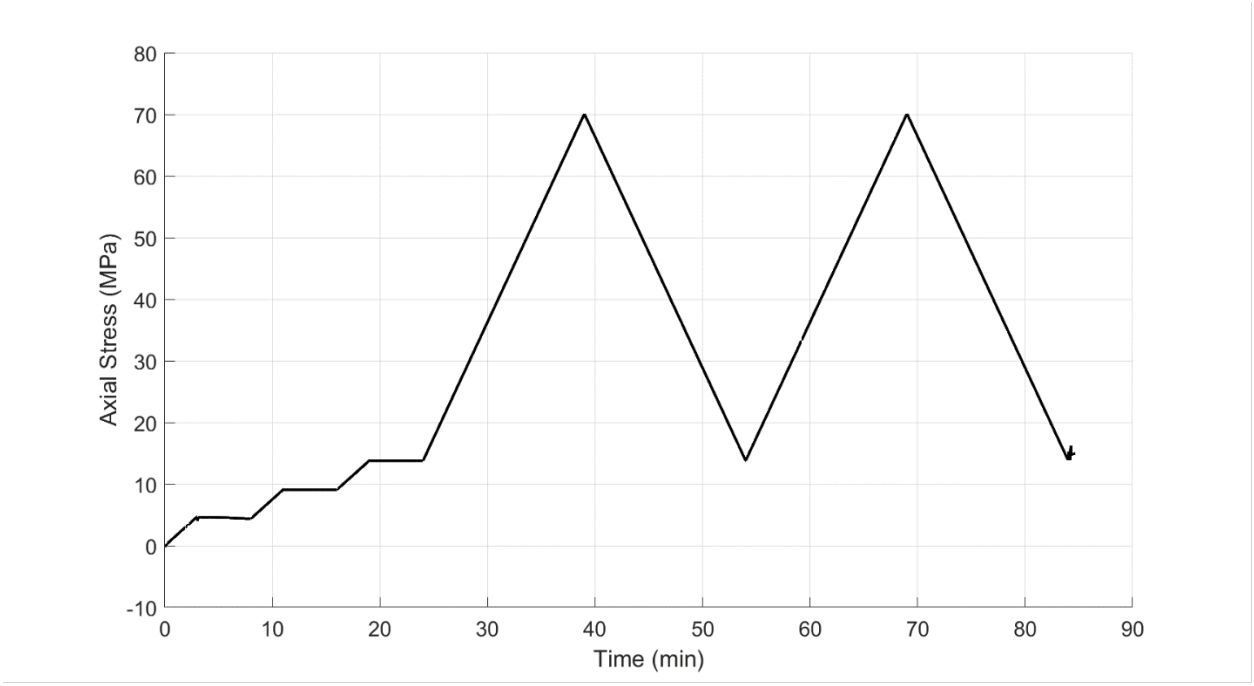

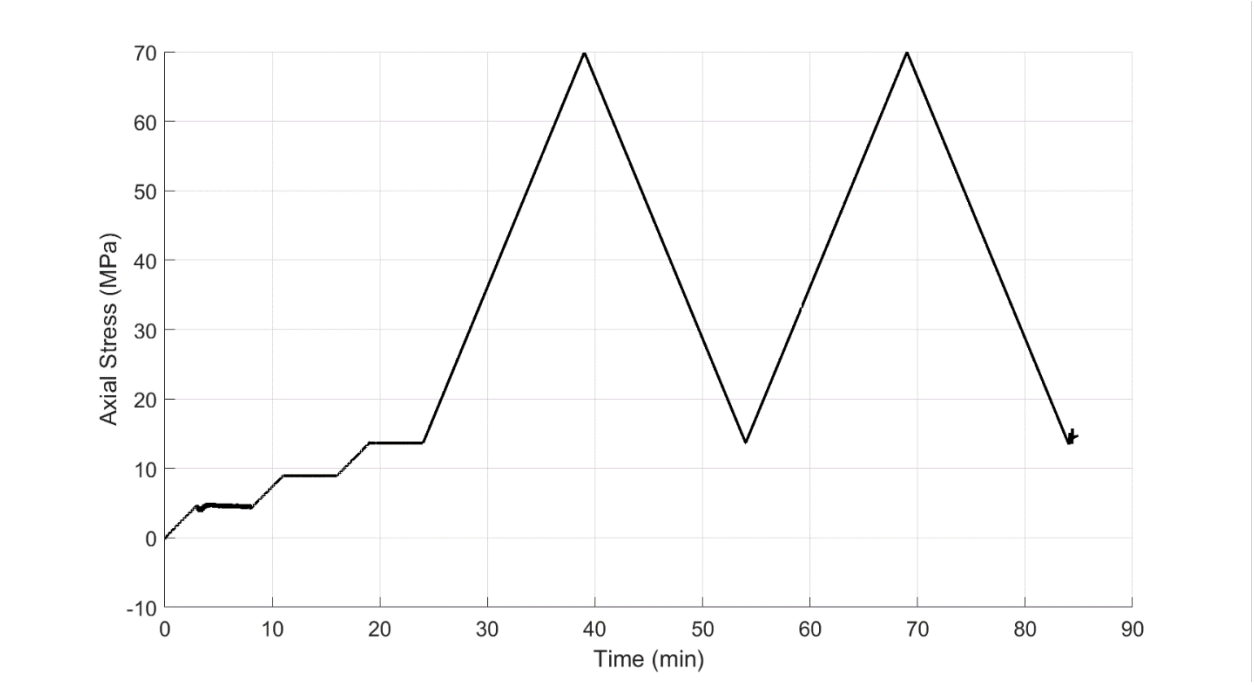

This results in the following displacements, which have been reduced by an amount estimated for deformation of 100mm of tool steel with E=210 GPa (comprising a lower bound on the platen deformation). This gives

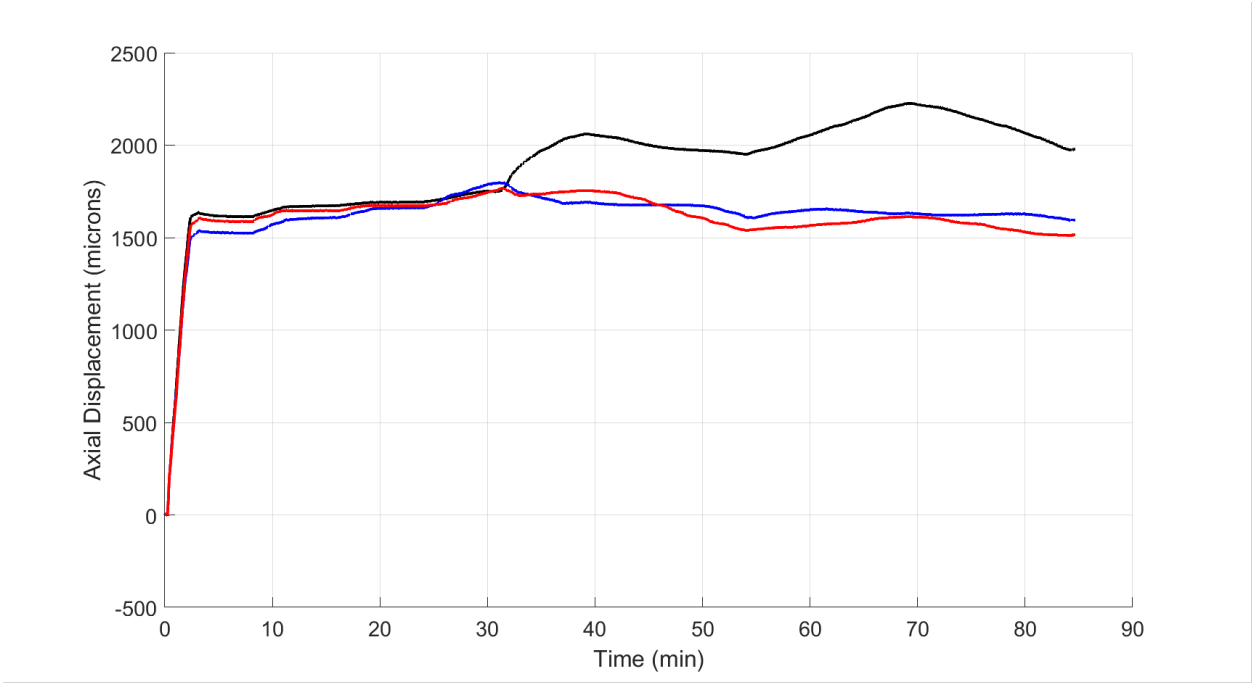

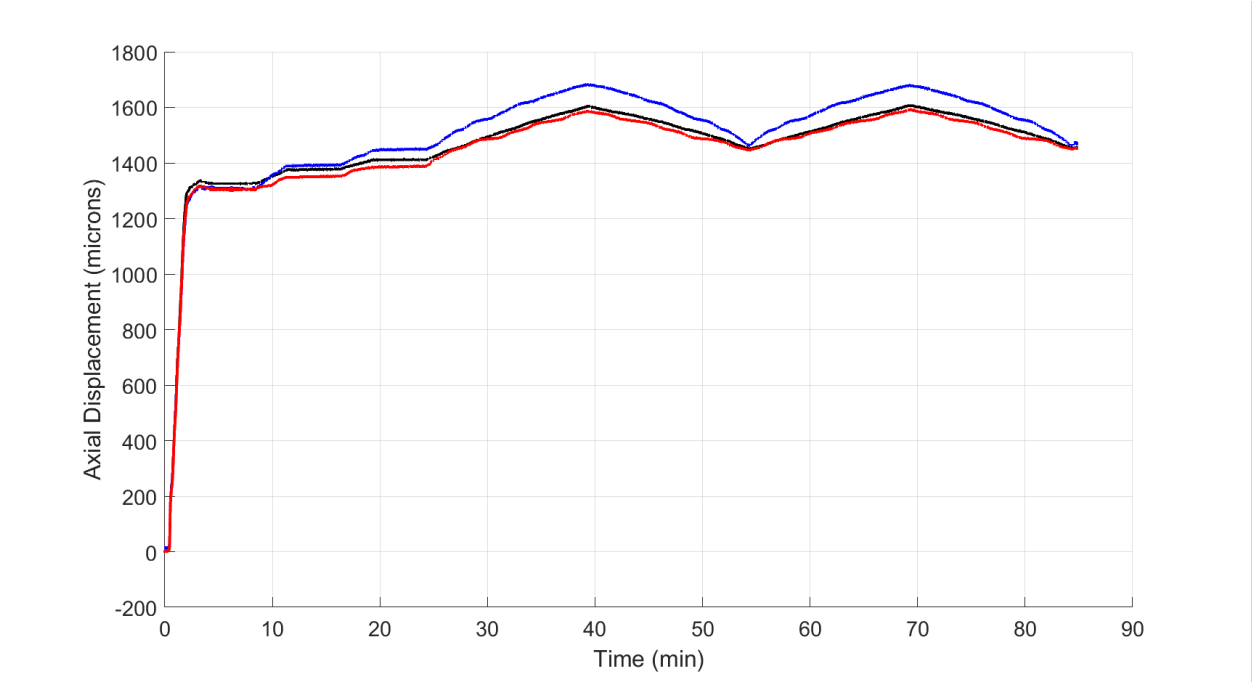

Observe that the first load cycle involved significant tilting of the top platen. Test 1 is probably less reliable as a result of this in comparison to test 2, where the displacements indicate almost the same values for all 3 LVDTs.

Averaging and plotting stress versus strain relationships for the 2 load/unload cycles, setting zero strain at the beginning of the first load cycle, gives

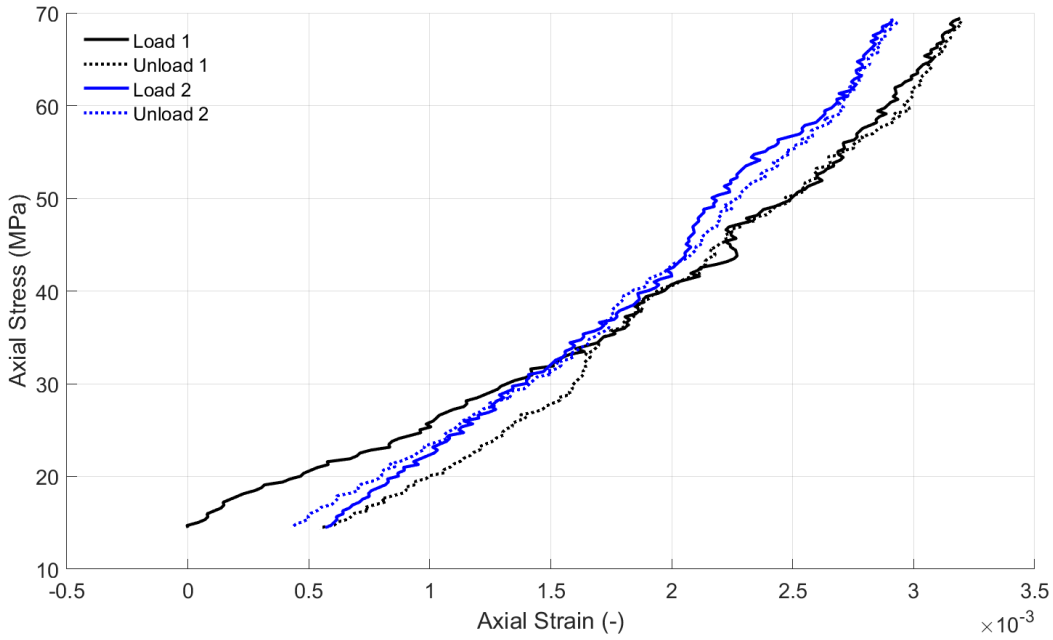

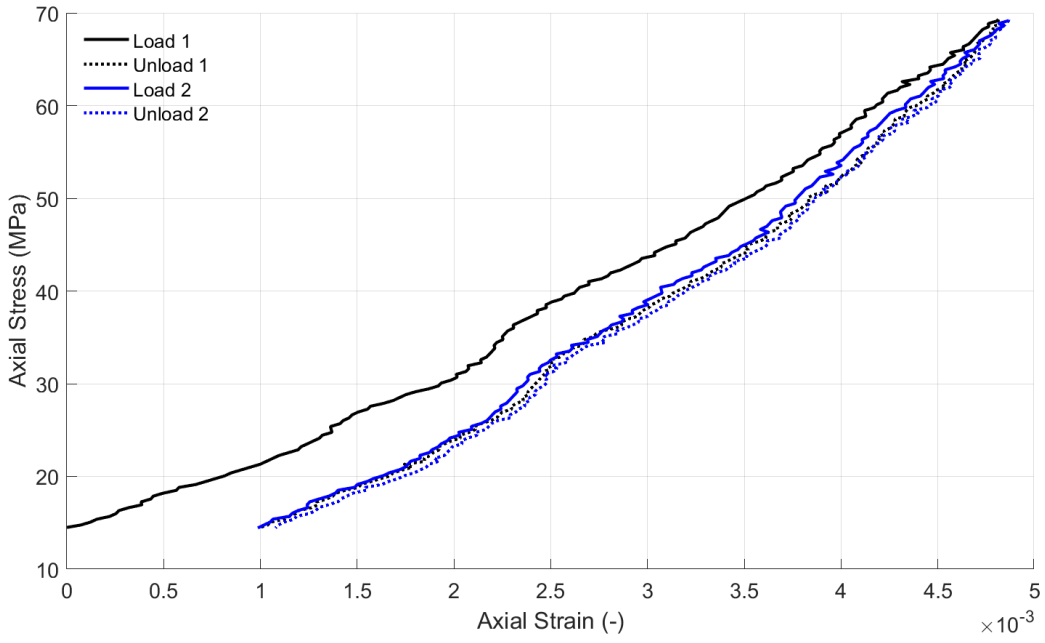

The stress-strain curve for the first test is unexpected, with second loading showing lower strain at the same stress compared to the first. This could be due to the tilting and hence the test is, again, probably not as reliable as test 2. In test 2, there is stiffening observed between 25-30 MPa and again between 45-50 MPa. In this second case, there is almost no hysteresis, just an initial loading that induces some apparent grain locking, after which the load and unload cycles almost precisely follow one another. The difference between the strain measurements for the load/unload stages is given by

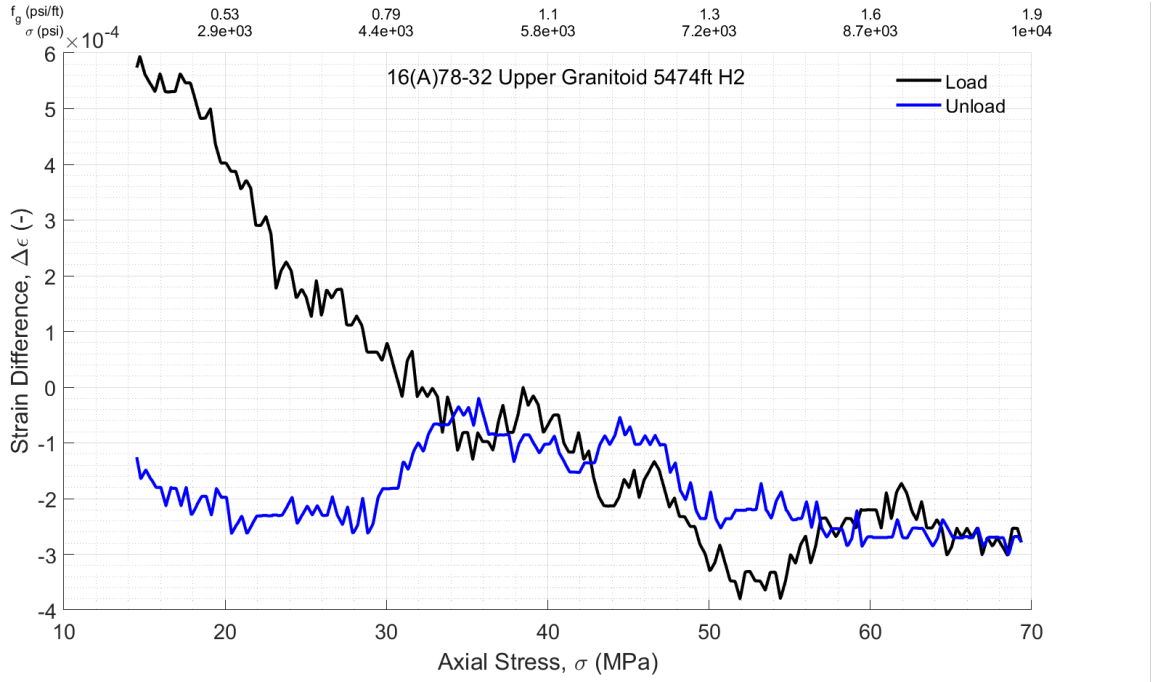

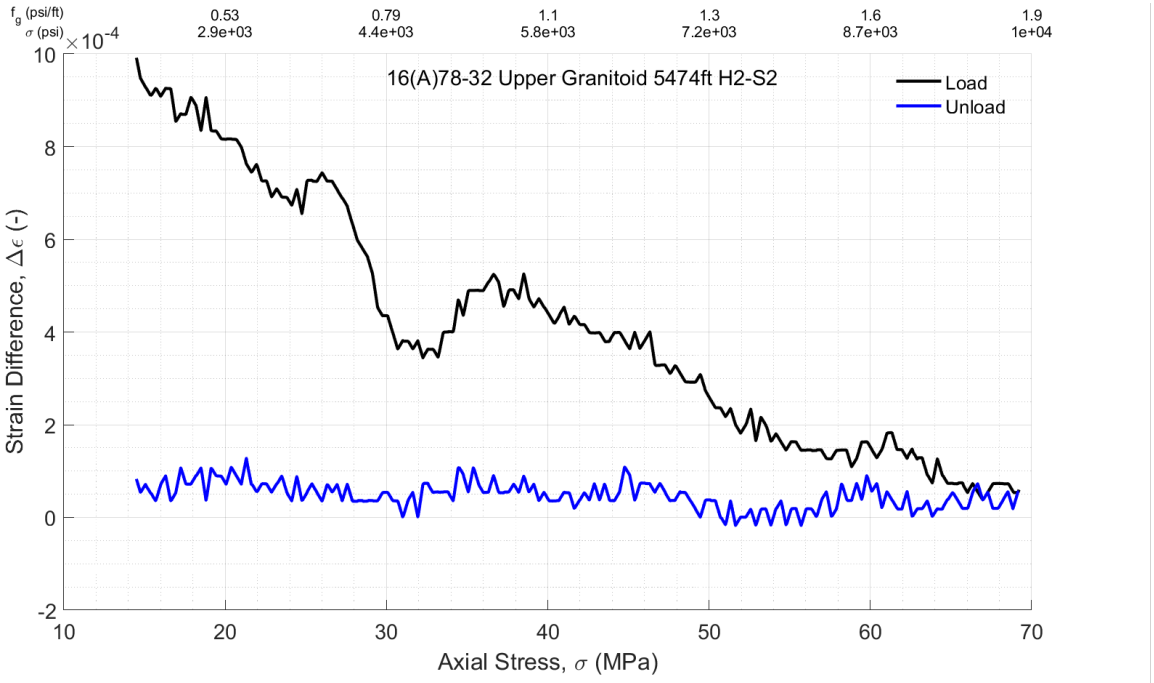

Something definitely appears to be causing an inflection around 28 MPa. There is a possible change of slope in the mid 30s and a very subtle change in the mid-40s. A final change occurs around 62 MPa.

Next, we examine the instantaneous stiffness through the load/unload cycles and plot it firstly as a function of stress. For reference, and not necessarily because there should be agreement but just because it provides context, the value of Young's modulus from the well log is plotted here (note, however, that it

is measured based on wavespeeds in vertical direction). We also show the nominal values of dynamic Young's modulus based on the TUV experiments presented earlier. This gives

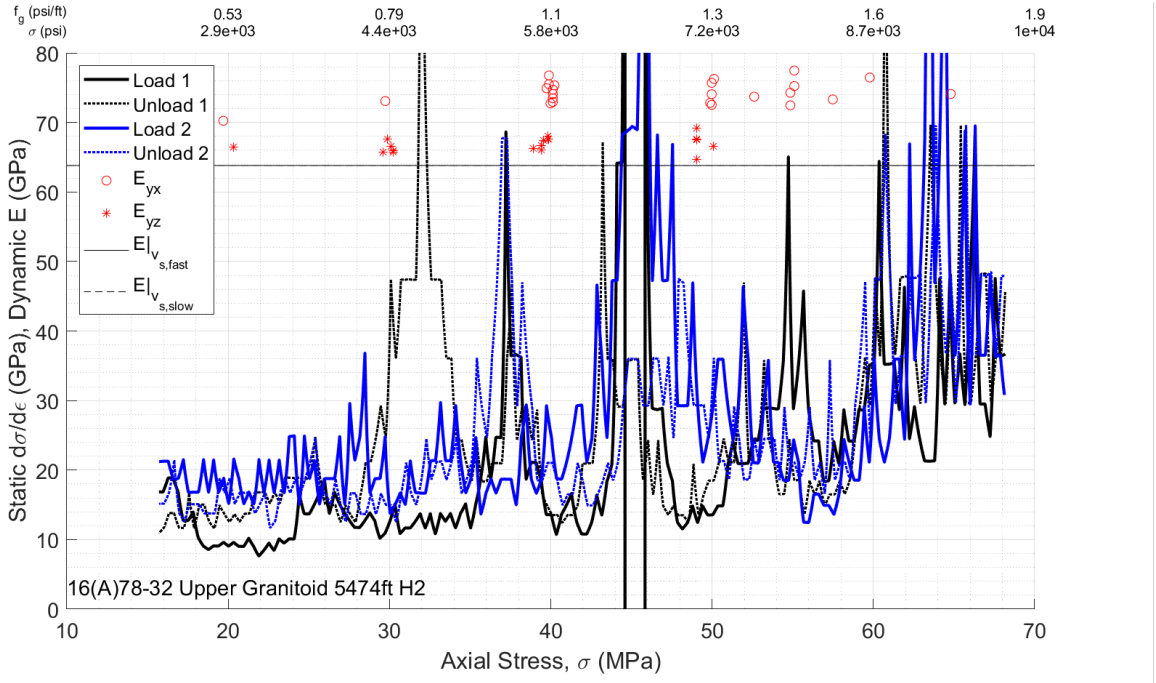

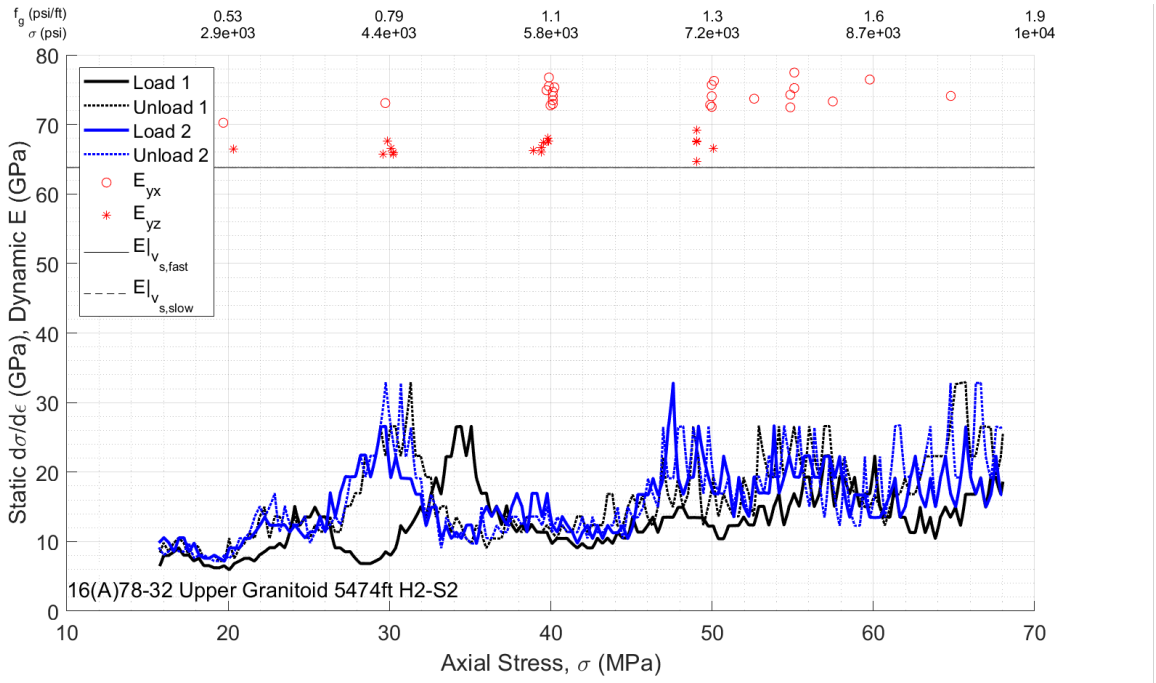

Here we have clear evidence of stiffening at around 26 MPa. There is also something around 34 MPa on the first loading. Interesting that the first loading has some softening right at the stress where there is stiffening in the second loading. A clear additional stiffening is consistently occurring at around 45 MPa.

Once again, if we plot this stiffness versus strain, the stiffening and softening are always happening at the same level of strain (at least in the more reliable second case), viz.

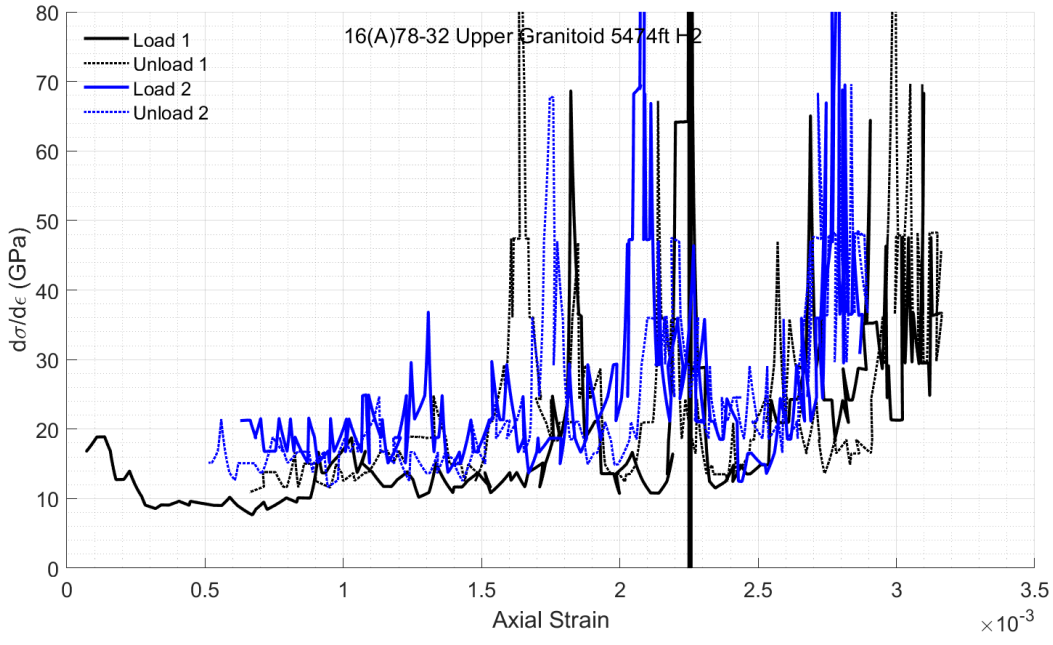

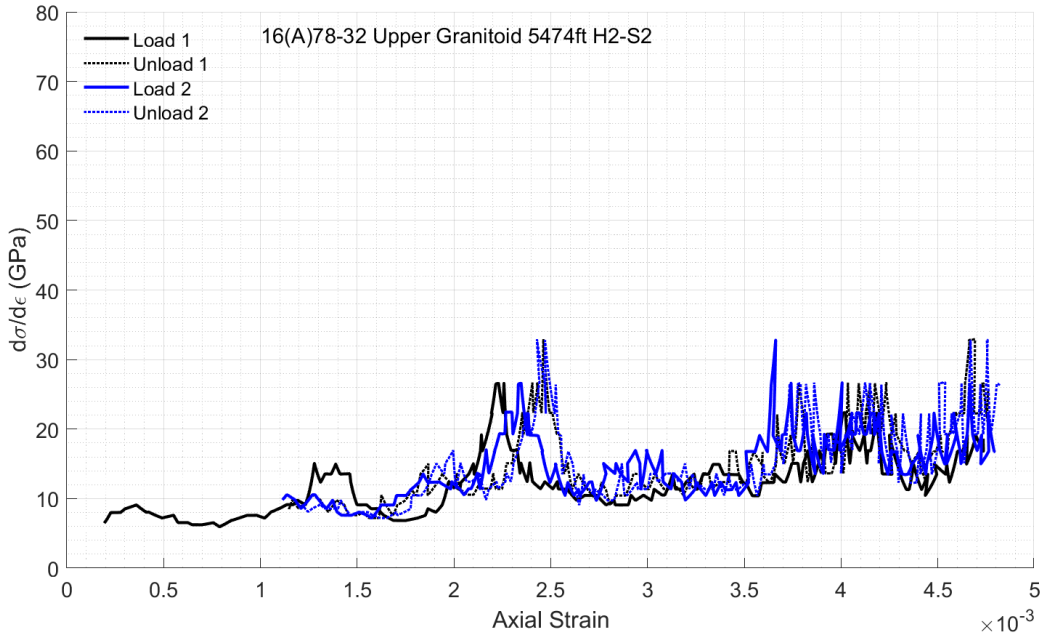

H1-Direction: Compendium

The H1 direction is not well-aligned with either x- or y- on the TUV samples. Hence one would expect any estimates of minimum stress to be upper estimates and of maximum stress to be lower estimates. In the following it is found that there are a couple of clear stiffening zones around 32 MPa and 42 MPa

Details of the H1 specimens are as follows, noting it is 52 degrees from H3 and almost exactly 45 degrees from the x-axis direction in the TUV experiments.

H1-1 H1-2

Dimensions		**Dimensions**	
height (mm):	36.47	height (mm):	34.86
width (mm):	31.94	width (mm):	31.79
Angle retrieved (degrees):	354.5	**Angle retrieved (degrees):**	354.5

DRA experiments are run with the loading sequence

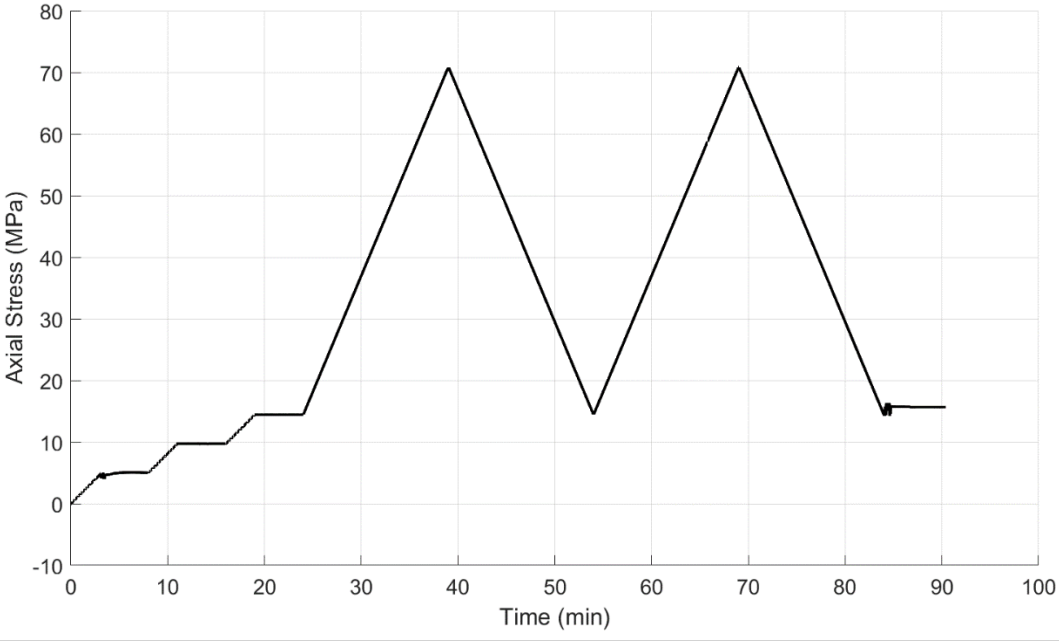

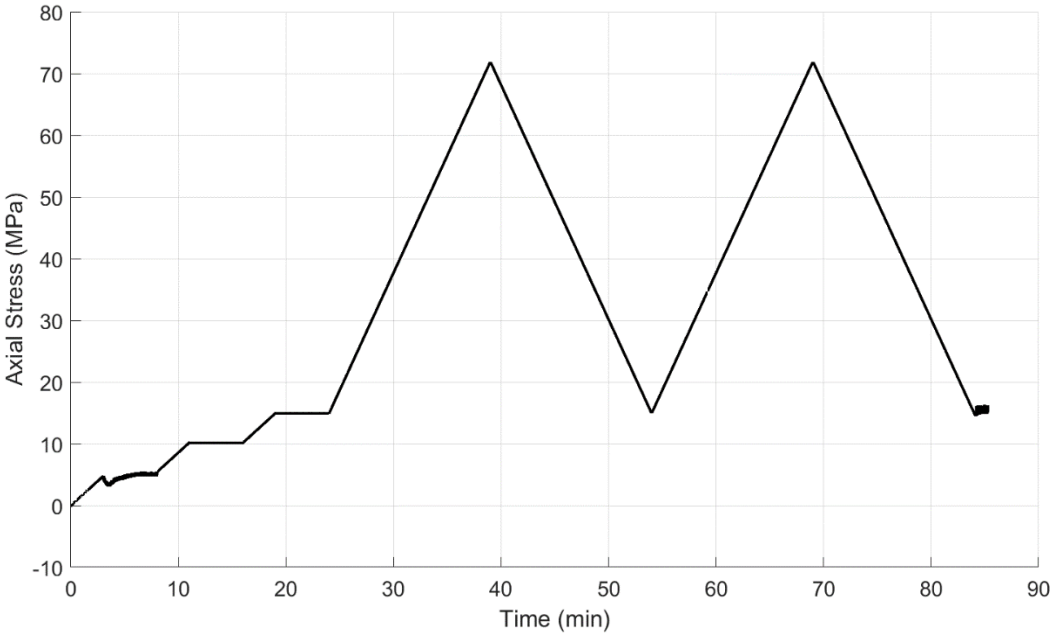

This results in the following displacements, which have been reduced by an amount estimated for deformation of 100mm of tool steel with E=210 GPa (comprising a lower bound on the platen deformation). This gives

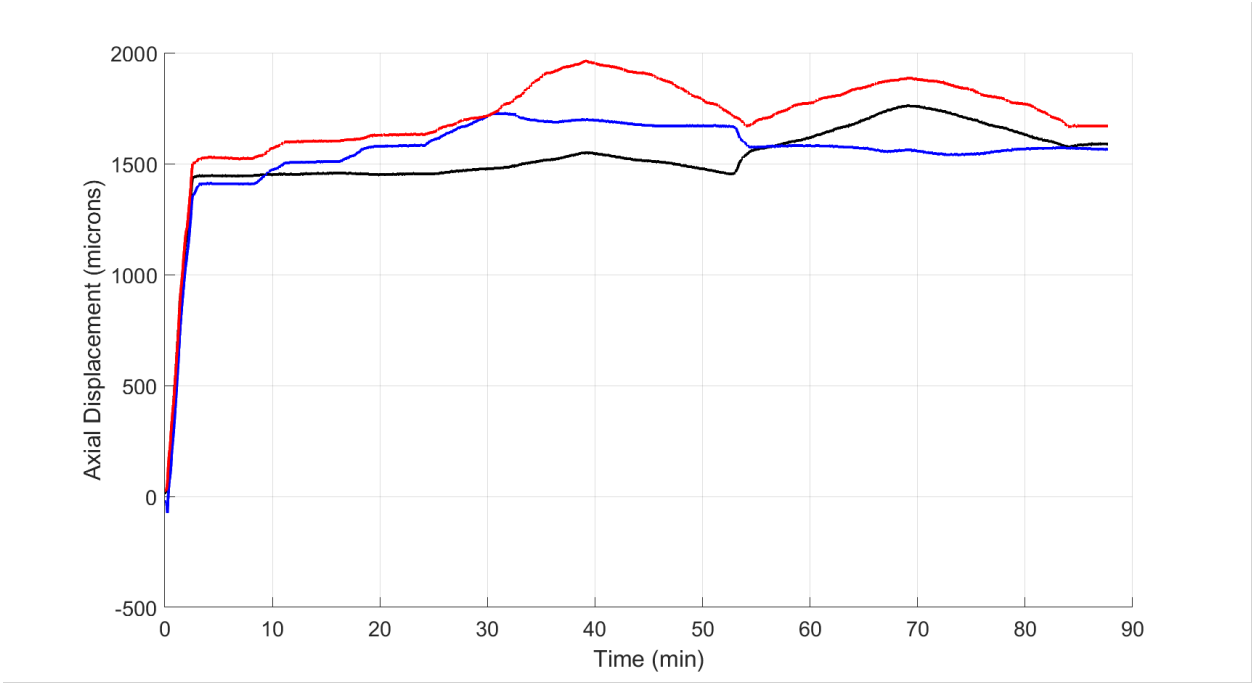

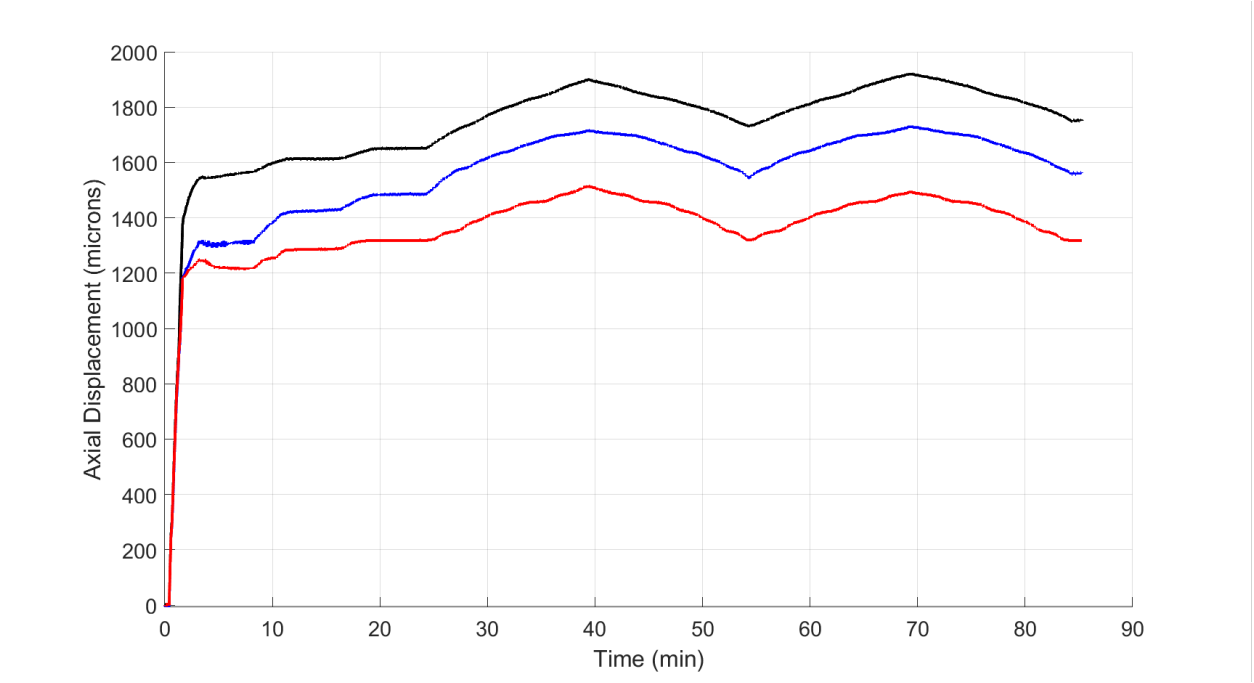

While there is a slight asymmetry in the response of the second case, it appears to be much higher quality than the first, which appears to have some significant platen tilting and resulting inconsistency between the LVDTs. Averaging and plotting stress versus strain relationships for the 2 load/unload cycles, setting zero strain at the beginning of the first load cycle, gives

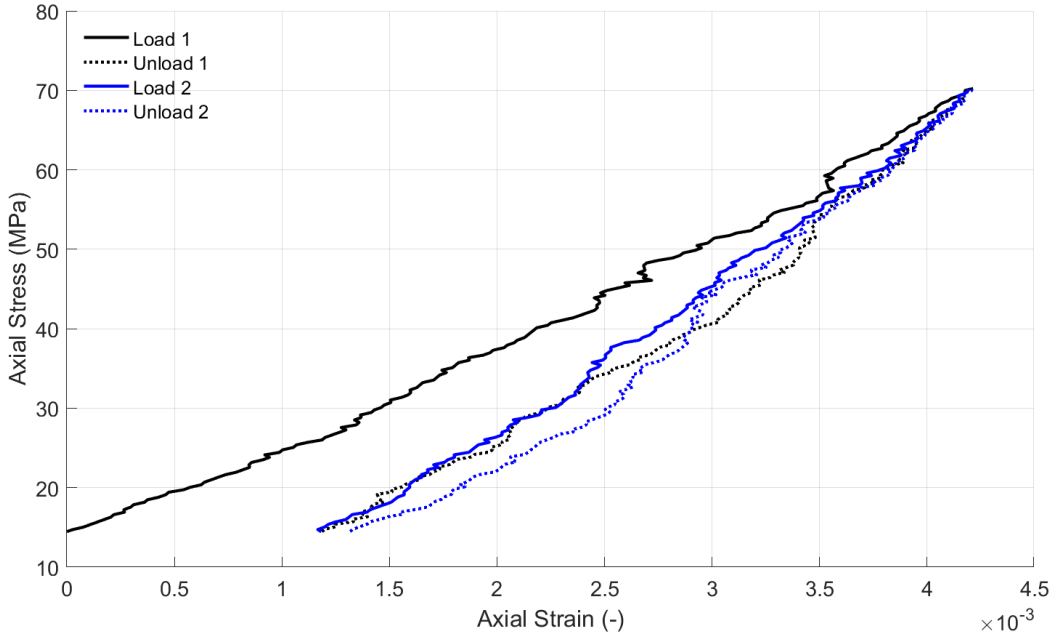

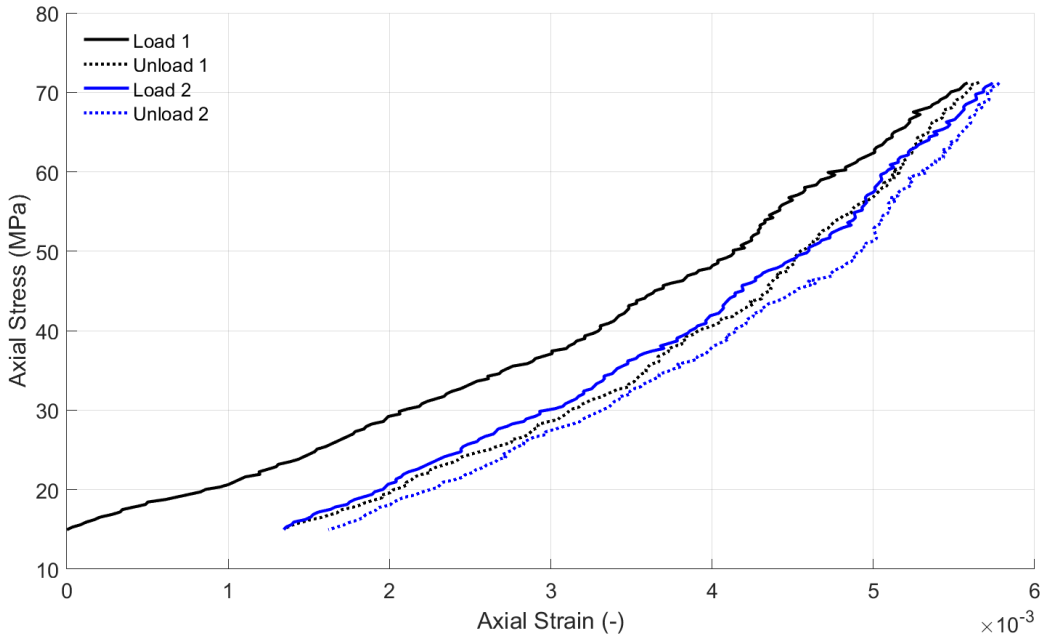

While there is some evidence of a lower reliability test for case 1, there is a consistent picture tween the two tests of stiffening around 30 MPa and maybe also around 39 MPa. The second test also shows stiffening around 54 MPa. The difference between the strain measurements for the load/unload stages is given by

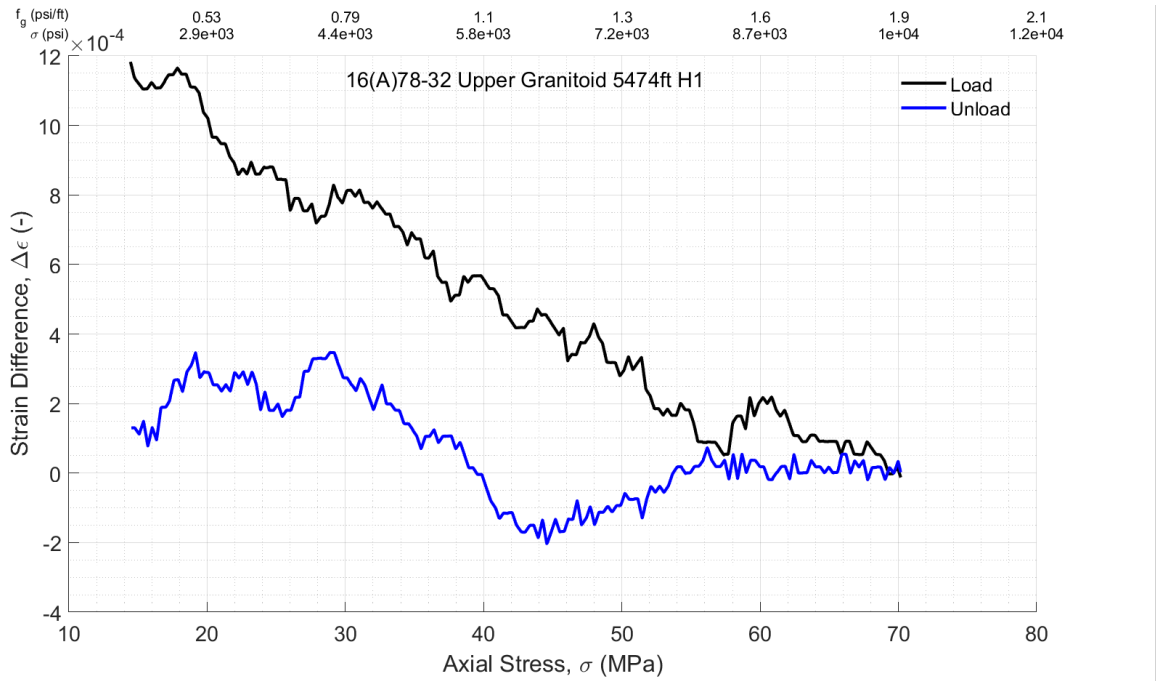

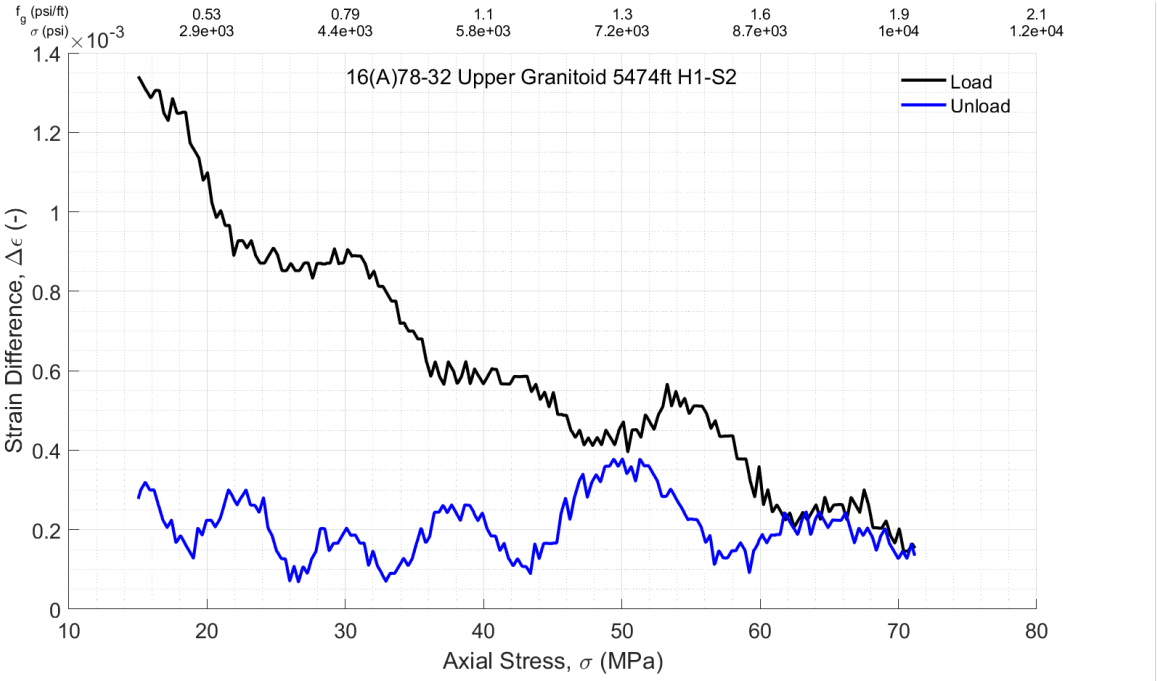

Both show a clear drop in strain difference around 32 MPa. Second test shows additional drops at 44 MPa and 55 MPa.

Once again, we examine the instantaneous stiffness through the load/unload cycles and plot it firstly as a function of stress. For reference, and not necessarily because there should be agreement but just because it provides context, the value of Young's modulus from the well log is plotted here (note, however, that it is measured based on wavespeeds in vertical direction). We also show the nominal values of dynamic

Young's modulus based on the TUV experiments presented earlier noting that y-direction values are given for comparison purposes. This gives

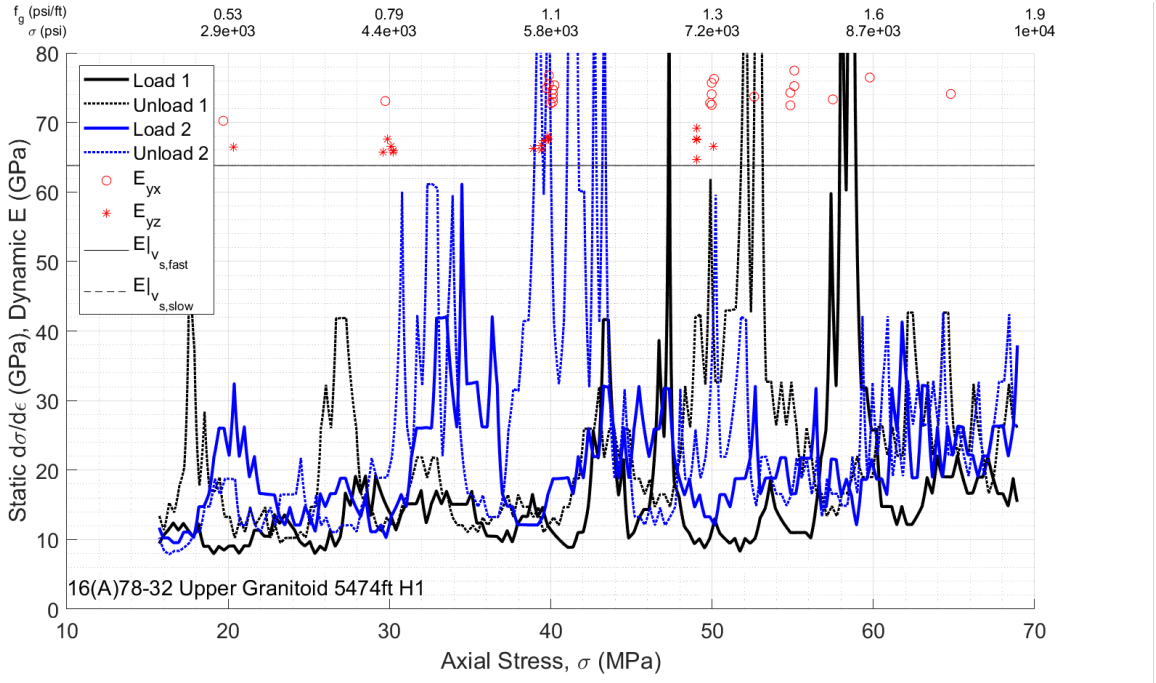

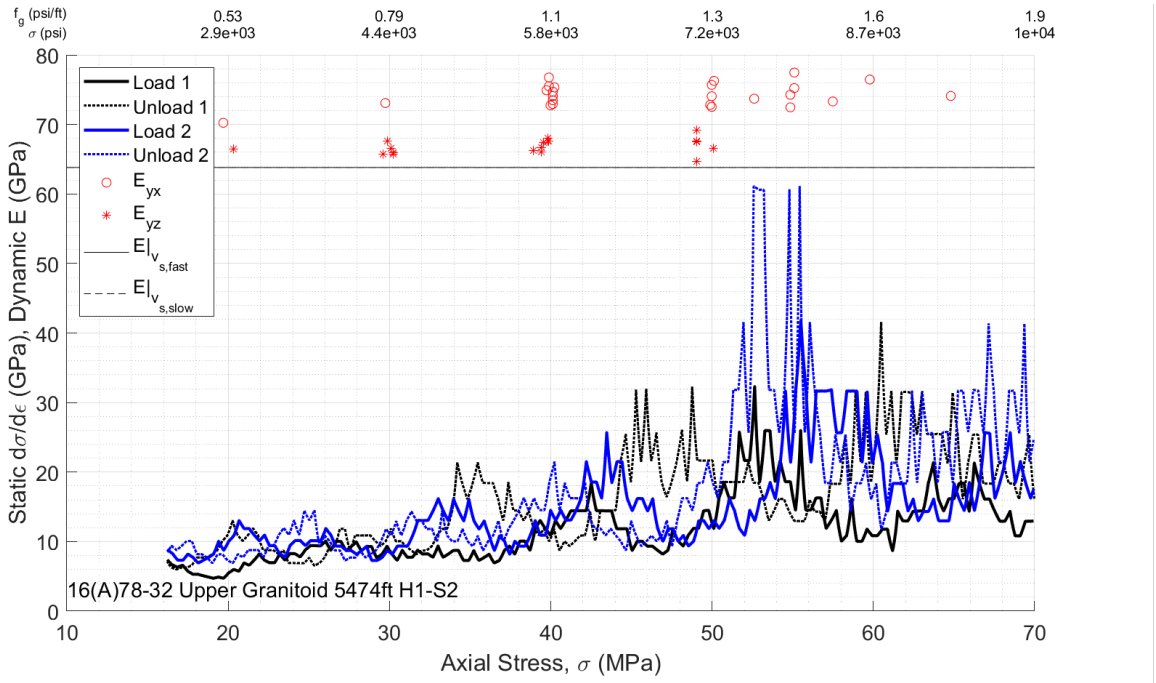

Not quite as clean as some other cases, but still second loading in first test clearly stiffens around 32 and 42 MPa. in both cases. It is a bit subtle, through, which could be indicative of a case inclined at around 45 degrees to the principal axes associated with in-situ stresses. Even when plotted versus strain, the consistency of the inflections is not as strong as in the H3 and H2 DRA cases (x- and y- directions), viz.

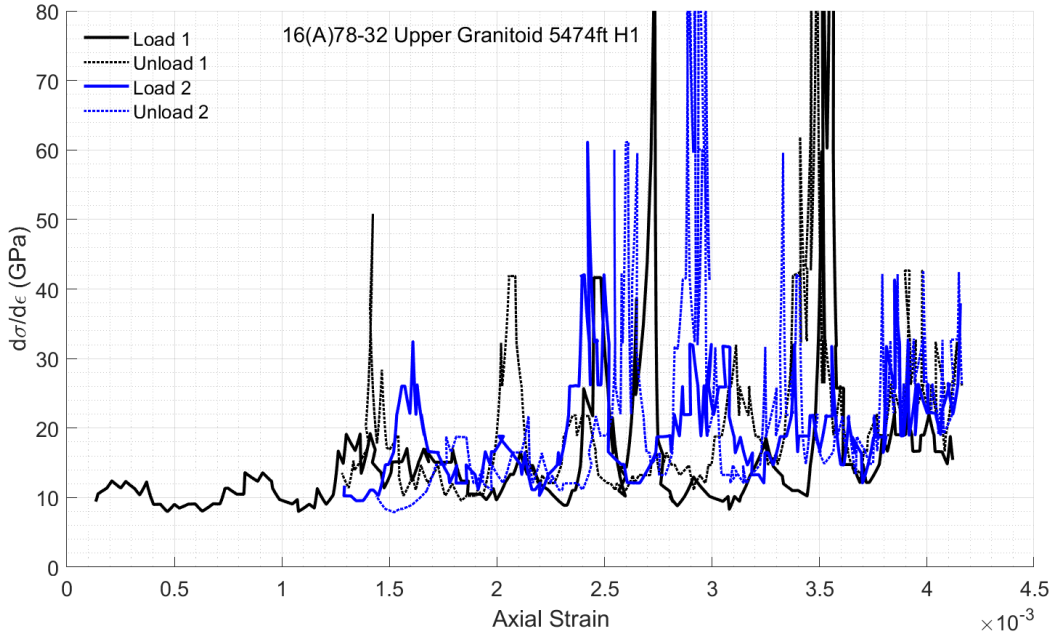

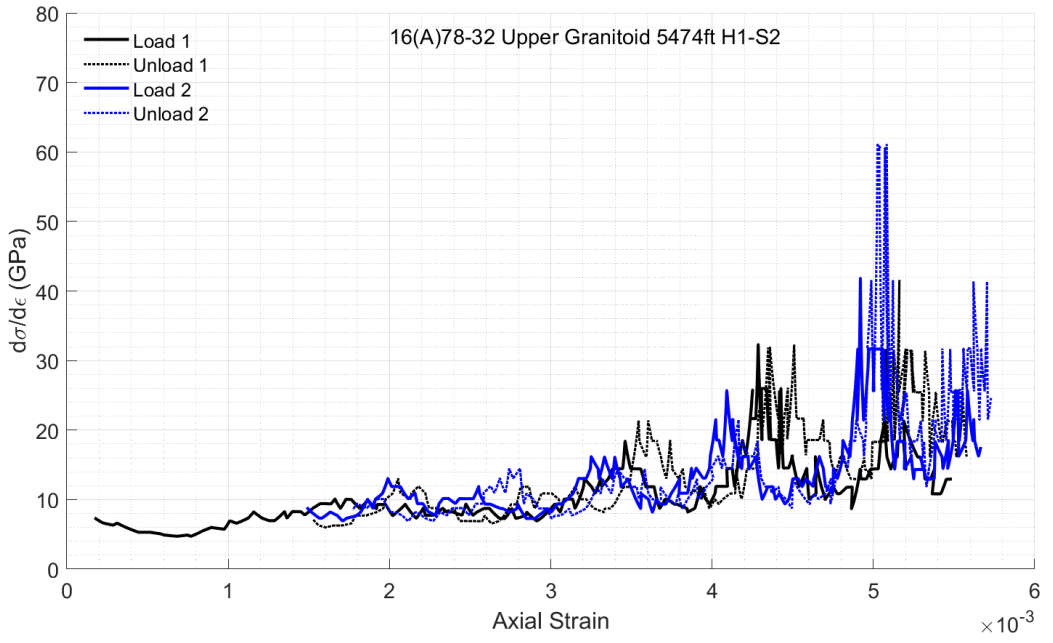

Z-Direction: Compendium

The vertical z-direction is clearly across, essentially perpendicular, to the fabric. Running the TUV experiments for the vertical (z-) direction, we find

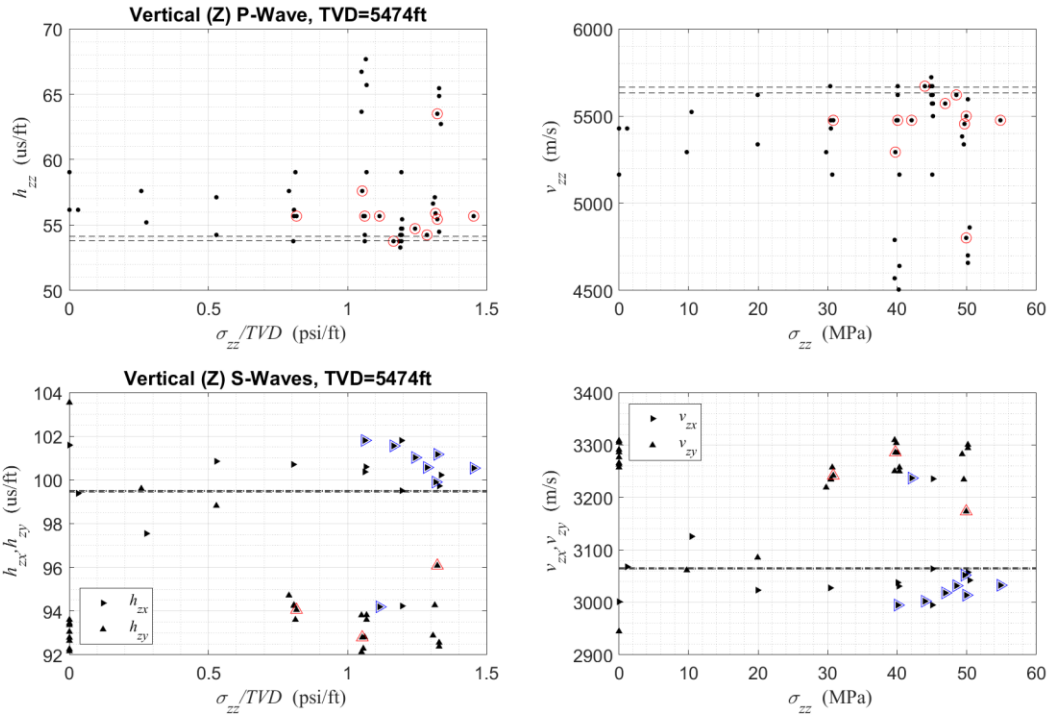

There is potentially a rolling over of shear wave speed in the low 40 MPa range (maybe ~42 MPa), but the evidence is not as strong as for the horizontal directions. Then, using Eq. 3 the nominal, quasi-isotropic elastic moduli are given by

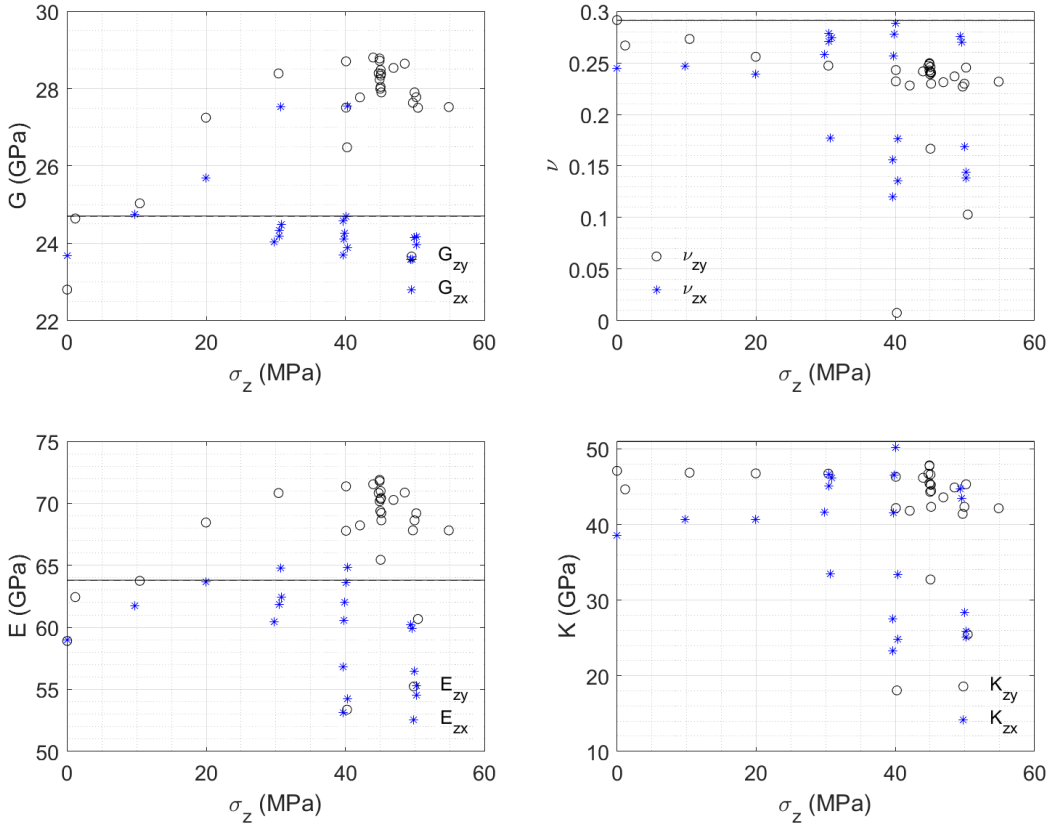

The vertical waves lead to agreement with the well logs (shows in solid and dashed lines). This makes sense because this is the direction of propagation for the sonic logging tool. But, there is also a cluster with totally different properties, most strikingly, a very different Poisson's ratio. This is most likely caused by specifics of waveform changes that may have caused errors in picking the first arrivals.

From the DRA on the V core, which is oriented vertically and hence perpendicular to the fabric:

Dimensions	
height (mm):	33.59
width (mm):	32.00

The z-direction for TUV is vertical, so there is a 0 degree misalignment between the H1 core and the y-direction of the TUV. DRA experiments are run with the loading sequence

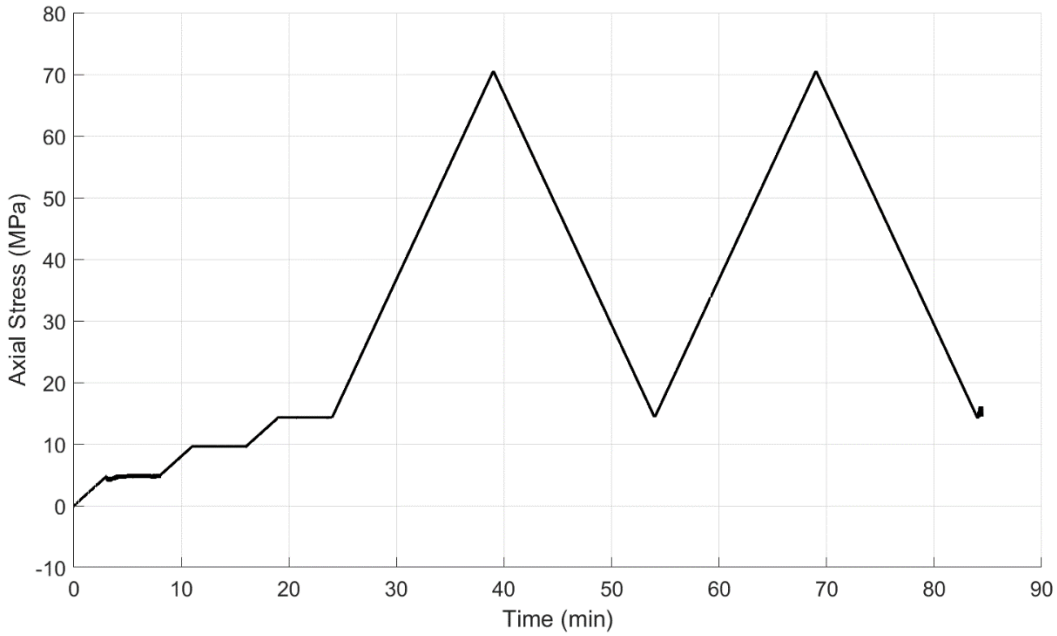

This results in the following displacements, which have been reduced by an amount estimated for deformation of 100mm of tool steel with E=210 GPa (comprising a lower bound on the platen deformation). This gives

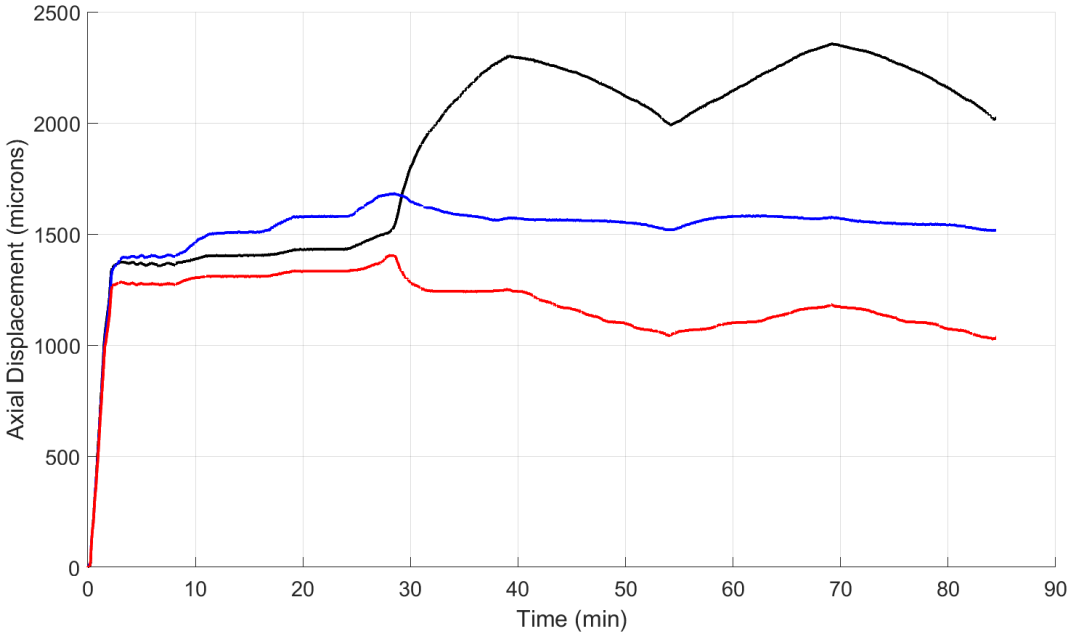

The 3 LVDTs have very different readings, indicating that the deformation was not very symmetric and hence the test is probably of relatively low reliability. Averaging and plotting stress versus strain relationships for the 2 load/unload cycles, setting zero strain at the beginning of the first load cycle, gives

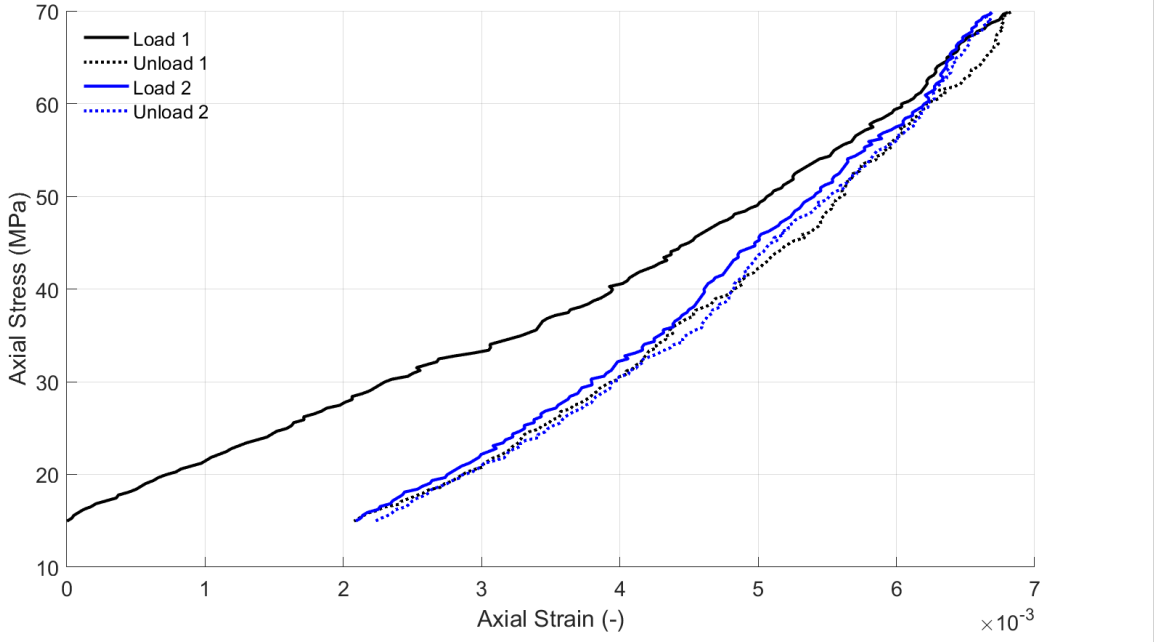

There appears to be stiffening around 38-40 MPa. The difference between the strain measurements for the load/unload stages is given by

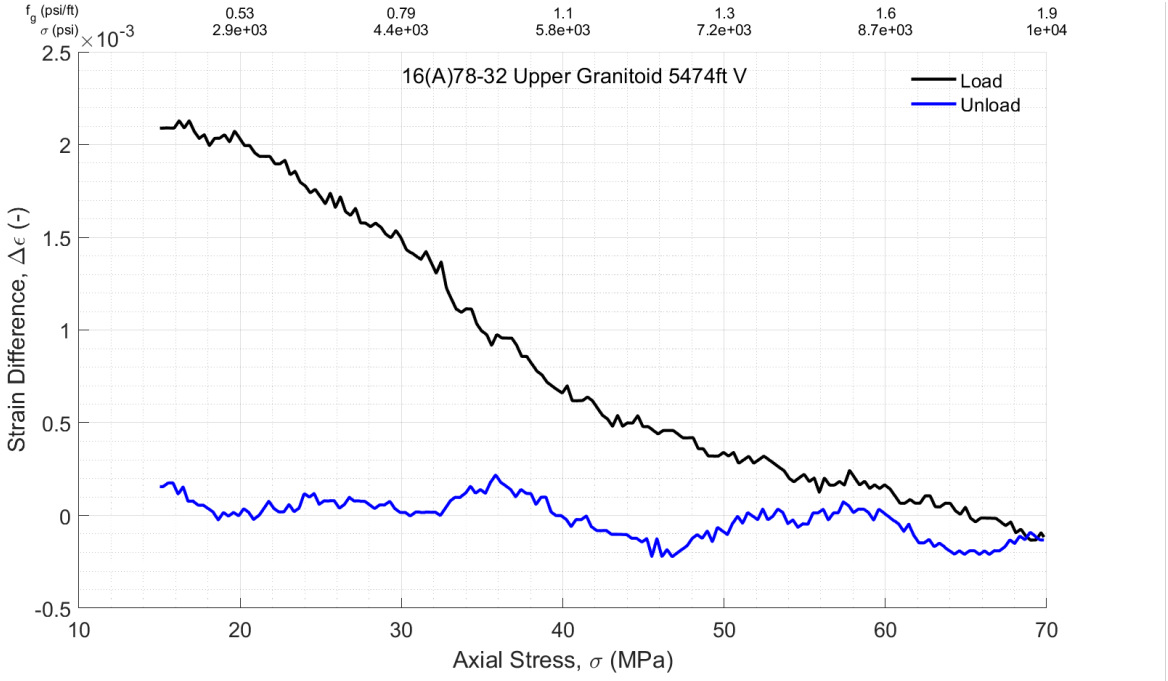

Here the main drop is around 32 MPa. There are few other discernable inflections, probably because of the apparent asymmetry of the deformation of the specimen. Bringing DRA and TUV stiffnesses together (by taking derivative of stress with respect to strain for DRA curves) gives

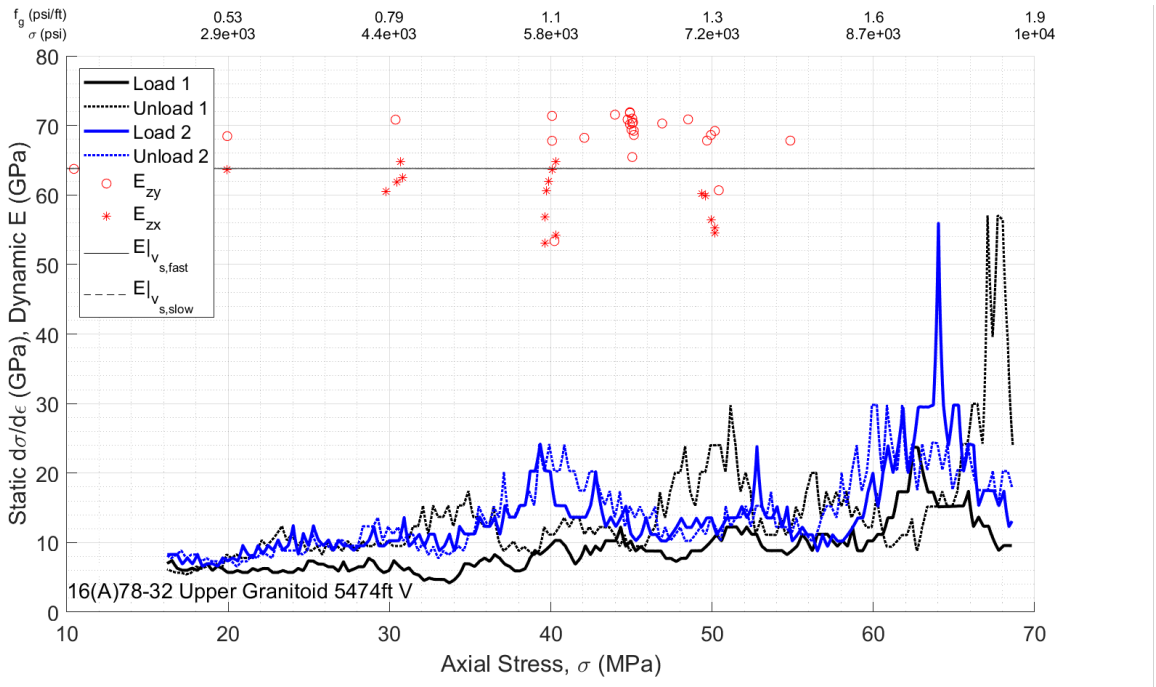

Once again there is some stiffening around 35-40 MPa. As usual, we can make a similar plot (though DRA only) but putting strain on the x-axis:

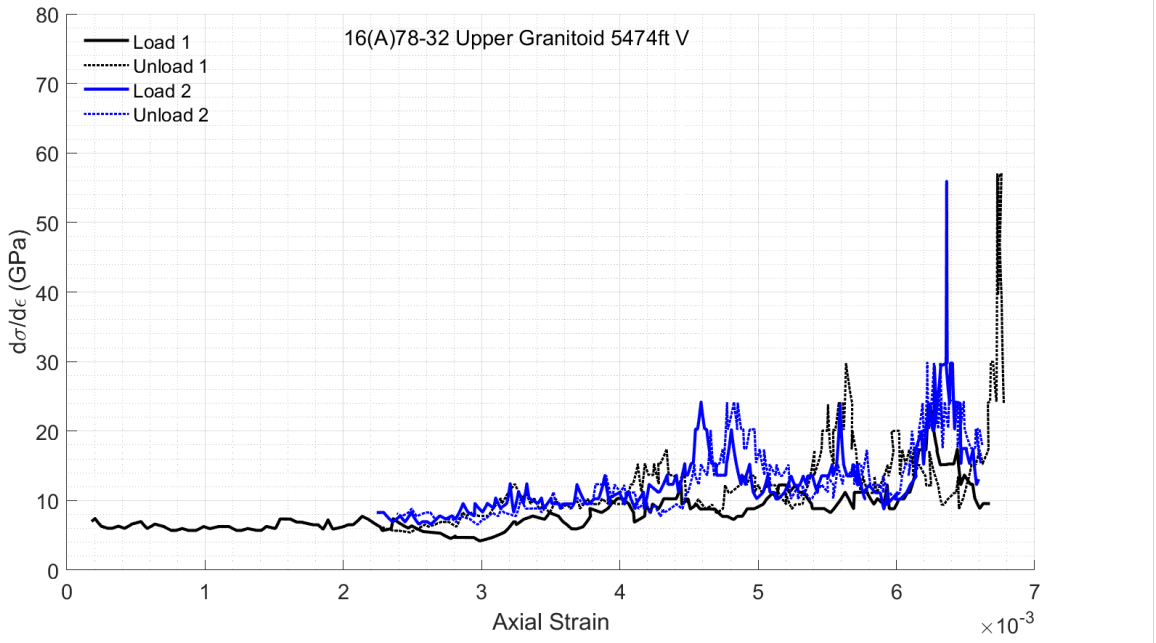

Although a bit more subtle compared to x- and y-directions, there are clear bumps at around strain values of 0.0045, 0.0055, and 0.006.

Lines of Evidence

A summary of the lines of evidence obtained from these experiments is given by:

Series	LoE	s1_val	s1_V	s1_L	s1_C	s1_R	s2_val	s2_V	s2_L	s2_C	s2_R	s3_val	s3_V	s3_L	s3_C	s3_R	s4_val	s4_V	s4_L	s4_C	s4_R	s5_val	s5_V	s5_L	s5_C	s5_R
UpGr_x	vxy	23	2	2	1.5	0.9	0	0	0	0	0.9	0	0	0	0	0.9	0	0	0	0	0.9	0	0	0	0	0.9
UpGr_x	Exy	23	2	2	1.5	0.9	0	0	0	0	0.9	0	0	0	0	0.9	0	0	0	0	0.9	0	0	0	0	0.9
UpGr_x	Exz	30	1	1	1	0.9	0	0	0	0	0.9	0	0	0	0	0.9	0	0	0	0	0.9	0	0	0	0	0.9
UpGr_x	s_e	28	2	3	3	0.9	42	1.5	2.5	2	0.9	55	1.5	2.5	3	0.9	0	0	0	0	0.9	0	0	0	0	0.9
UpGr_x	De	29	2	3	1.5	0.9	46	1.5	1.5	3	0.9	0	0	0	0	0.9	0	0	0	0	0.9	0	0	0	0	0.9
UpGr_x	De	26	2	2.5	2	0.9	44	1.5	2	3	0.9	54	1.5	3	1	0.9	0	0	0	0	0.9	0	0	0	0	0.9
UpGr_x	ds_de	20	2	1	1.5	0.9	29	2	1	1.5	0.9	35	2	1	1.5	0.9	42	2	3	1.5	0.9	48	2	3	1.5	0.9
UpGr_x	ds_de	28	2	2	1.5	0.9	48	2	2	1.5	0.9	62	2	1	1.5	0.9	0	0	0	0	0.9	0	0	0	0	0.9
UpGr_y	vyx	40	2	2	2.5	0.9	0	0	0	0	0.9	0	0	0	0	0.9	0	0	0	0	0.9	0	0	0	0	0.9
UpGr_y	vyz	30	1	1	0.5	0.9	0	0	0	0	0.9	0	0	0	0	0.9	0	0	0	0	0.9	0	0	0	0	0.9
UpGr_y	Eyx	40	2	2	2.5	0.9	0	0	0	0	0.9	0	0	0	0	0.9	0	0	0	0	0.9	0	0	0	0	0.9
UpGr_y	s_e	44	1	1	1.5	0.9	58	1	1	1.5	0.9	0	0	0	0	0.9	0	0	0	0	0.9	0	0	0	0	0.9
UpGr_y	s_e	26	2	2	2.5	0.9	46	1.5	1.5	2	0.9	0	0	0	0	0.9	0	0	0	0	0.9	0	0	0	0	0.9
UpGr_y	De	27	2	2	3	0.9	39	1.5	2	3	0.9	62	1.5	2	3	0.9	0	0	0	0	0.9	0	0	0	0	0.9
UpGr_y	De	26	2	2.5	3	0.9	36	1.5	2	3	0.9	62	1.5	2	3	0.9	0	0	0	0	0.9	0	0	0	0	0.9
UpGr_y	ds_de	27	2	1	2.5	0.9	35	2	1.5	1.5	0.9	43	2	2	3	0.9	59	2	2	1.5	0.9	0	0	0	0	0.9
UpGr_y	ds_de	26	2	3	3	0.9	46	2	3	3	0.9	0	0	0	0	0.9	0	0	0	0	0.9	0	0	0	0	0.9
UpGr_H1	s_e	30	2	1.5	3	0.9	38	1.5	1.5	3	0.9	0	0	0	0	0.9	0	0	0	0	0.9	0	0	0	0	0.9
UpGr_H1	s_e	30	2	2	3	0.9	38	1.5	2	3	0.9	0	0	0	0	0.9	0	0	0	0	0.9	0	0	0	0	0.9
UpGr_H1	De	31	2	3	3	0.9	61	1.5	1.5	1.5	0.9	0	0	0	0	0.9	0	0	0	0	0.9	0	0	0	0	0.9
UpGr_H1	De	31	2	3	3	0.9	44	1.5	1.5	1.5	0.9	55	1.5	2	1.5	0.9	68	1	1	1.5	0.9	0	0	0	0	0.9
UpGr_H1	ds_de	19	1.5	1.5	3	0.9	32	2	1.5	3	0.9	42	1.5	2	1.5	0.9	58	1	1	1.5	0.9	0	0	0	0	0.9
UpGr_H1	ds_de	19	1.5	1.5	3	0.9	32	2	1	3	0.9	50	1.5	1	1.5	0.9	0	0	0	0	0.9	0	0	0	0	0.9
UpGr_z	vzx	40	1.5	1	1.5	0.9	0	0	0	0	0.9	0	0	0	0	0.9	0	0	0	0	0.9	0	0	0	0	0.9
UpGr_z	vzy	30	1.5	1	1.5	0.9	50	1.5	1.5	1.5	0.9	0	0	0	0	0.9	0	0	0	0	0.9	0	0	0	0	0.9
UpGr_z	Ezx	30	1.5	1	1	0.9	0	0	0	0	0.9	0	0	0	0	0.9	0	0	0	0	0.9	0	0	0	0	0.9
UpGr_z	Ezy	35	1.5	1	1	0.9	0	0	0	0	0.9	0	0	0	0	0.9	0	0	0	0	0.9	0	0	0	0	0.9
UpGr_z	s_e	37	2	1.5	1.5	0.9	0	0	0	0	0.9	0	0	0	0	0.9	0	0	0	0	0.9	0	0	0	0	0.9
UpGr_z	De	20	1.5	1.5	1	0.9	33	1.5	2	1.5	0.9	0	0	0	0	0.9	0	0	0	0	0.9	0	0	0	0	0.9
UpGr_z	ds_de	36	1.5	2	1.5	0.9	46	1.5	1	1	0.9	58	1.5	2	1.5	0.9	0	0	0	0	0.9	0	0	0	0	0.9

To note:

- Each series is named with the direction after an underscore (column 1).
- The source of the line of evidence (LoE) is given in column 2, where v is velocity, E is Young's modulus, s_e is stress-strain curve, De is the change in strain curve, and ds_de is the instantaneous stiffness curve. Subscripts indicate direction of propagation followed by polarity, as usual, such that for example vxy indicates a shear wave velocity propagating in x-direction with y-polarity.
- All stress values (i.e. s1_val, s2_val) are given in MPa.
- Each source can give multiple lines of evidence, thus the table is set up to accept up to 5 lines of evidence for each source. Zeros are filled into the table where there are no additional lines of evidence.
- The weight assigned according to the prescribed rubric is given after an underscore, where V indicates relevance, L indicates reliability, C indicates consistency, and R indicated representivity. All values of representivity are set at 0.9 because there is insufficient data to determine exactly how representative the sample is of the surrounding formation.

Middle Granitoid

Summary

The 16A(78)-32 Middle Granitoid samples are from around 5488' MD (1800 m). The TVD is the same as the MD because the well is vertical to this point. This is 14 ft (4.6 m) below Upper Granitoid and around 360 ft (118 m) above the Lower Granitoid. It has large grains and slight horizontal foliation and also slight elongation. This elongation is similar to Upper Granitoid and for consistency is set as subparallel to the y-

direction (Figure 16). Hence all 3 DRA directions are oblique to the nominal x- and y- directions. The vertical z-direction is clearly across, essentially perpendicular, to the fabric.

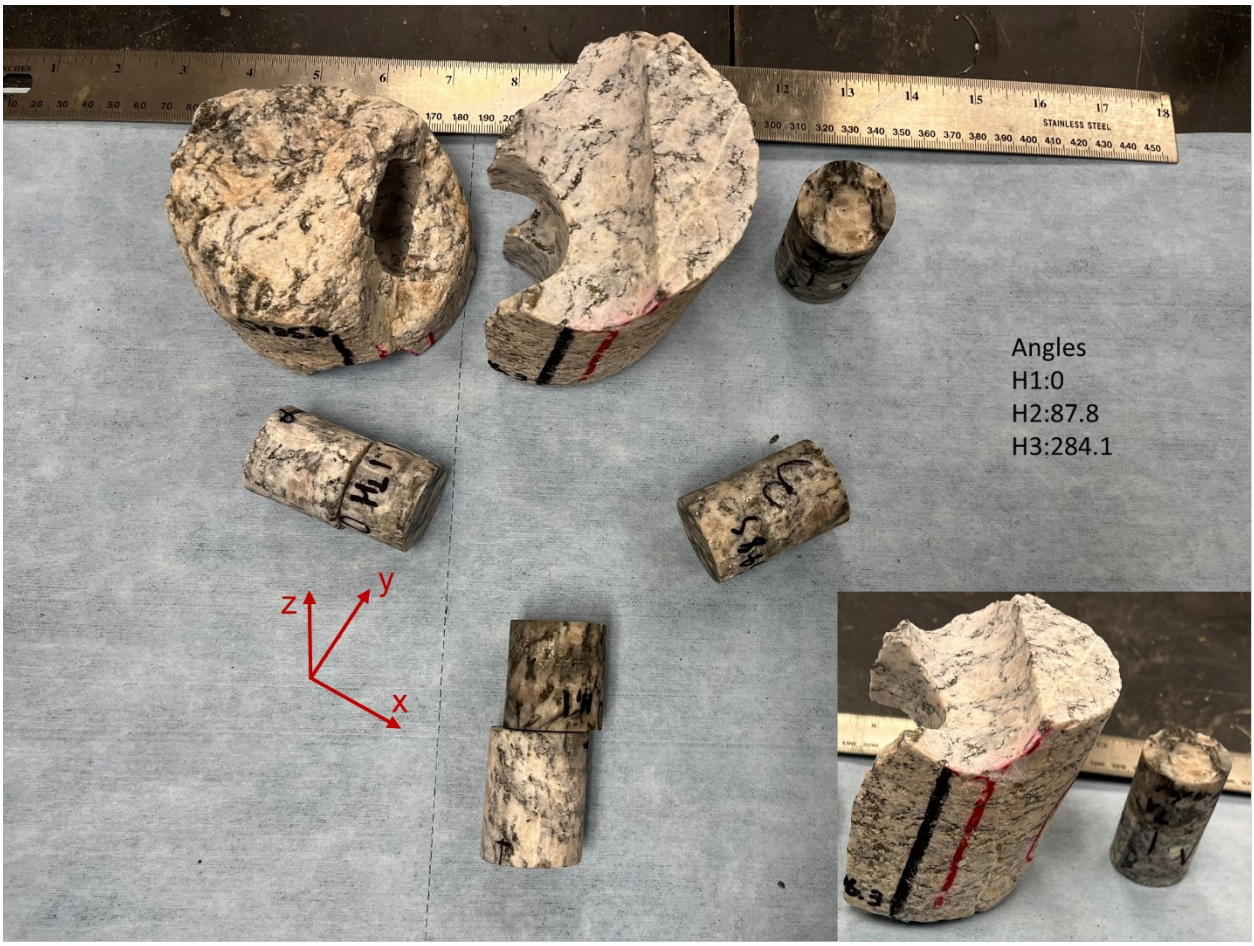

Figure 16: Parent core for Middle Granitoid with DRA samples (cylinders), showing x, y, z axes and with cylinders laying in approximate directional correspondence to TUV sample. The inset changes viewpoint to better show slight horizontal foliation.

The oblique orientation of all DRA axes to the fabric and the lack of TUV data make it impossible to orient principal stresses for this core. However, there are several stress magnitudes that have concentrated weight of evidence (Figure 17) that bear discussion. Firstly, the lowest cluster of lines of evidence are centered around 22 MPa (~0.58 psi/ft). These could be upper estimates due to misalignment of the cores, and hence it is possible that the minimum stress estimate could be as low as 19 MPa (~0.5 psi/ft). Note, however, a collection of lines of evidence that would imply a minimum stress gradient of 0.6 psi/ft, which would be more consistent with result from the nearby Upper Granitoid.

The second concentration of evidence occurs around 34 MPa (~0.9 psi/ft). Interpreting this as maximum horizontal stress would provide consistency with the Lower Granitoid, but would not be consistent with observation in the nearby Upper Granitoid. Bear in mind, though, that the absence of TUV data here in the Middle Granitoid renders evidence from this section as weaker compared to the Upper and Lower Granitoid, where TUV data is available.

The next concentration of evidence is centered at 46 MPa (~1.22 psi/ft). This would be considerably higher than the vertical stress gradient of 1.08 psi/ft obtained from the nearby Upper Granitoid, and it is very

close to the best estimate of maximum horizontal stress gradient from that formation (which was 1.25 psi/ft). Note that the stiffening at around 46-47 MPa is, in the details, one of the strongest signals in the data from the horizontal core (in the H3 core, see Data Compendium). Furthermore, in the details of the tests on Vertical core plugs, there is evidence of stiffening and changes in strain difference behavior that is closer to 41-43 MPa (~1.10-1.15 psi/ft, which would be more consistent with expected vertical stress and would indicate that in this case, the vertical and maximum horizontal stress are probably very close in magnitude.

Finally, there are a few lines of evidence at higher stresses of 55 MPa (~1.45 psi/ft) and 61 MPa (~1.62 psi/ft). Both of these are observed in other formations as well, again raising a question as to their origin. If such high present-day stresses are out of the question, then perhaps they are reflective of conditions experienced by the rock during its history.

To summarize:

1) **Minimum horizontal stress** is not well-constrained, but the best guess is probably around 23 MPa (~0.60 psi/ft).
2) **Maximum horizontal stress** could be associated with to two candidates, one at around 34 MPa (~0.90 psi/ft) and the other at around 46 MPa (~1.22 psi/ft). The former would be consistent with the (considerably deeper) Lower Granitoid, while the latter would be consistent with the nearby Upper Granitoid. The strongest signal from any horizontal core in this section supports the higher value of 46 MPa (~1.22 psi/ft).
3) **Vertical stress** is around 42 MPa (~1.13 psi/ft), although this is based on just a couple of the clearest lines of evidence from vertical core plugs and is difficult to constrain in detail due to the lack of TUV data and the possible closeness in magnitude between vertical and maximum horizontal stress.

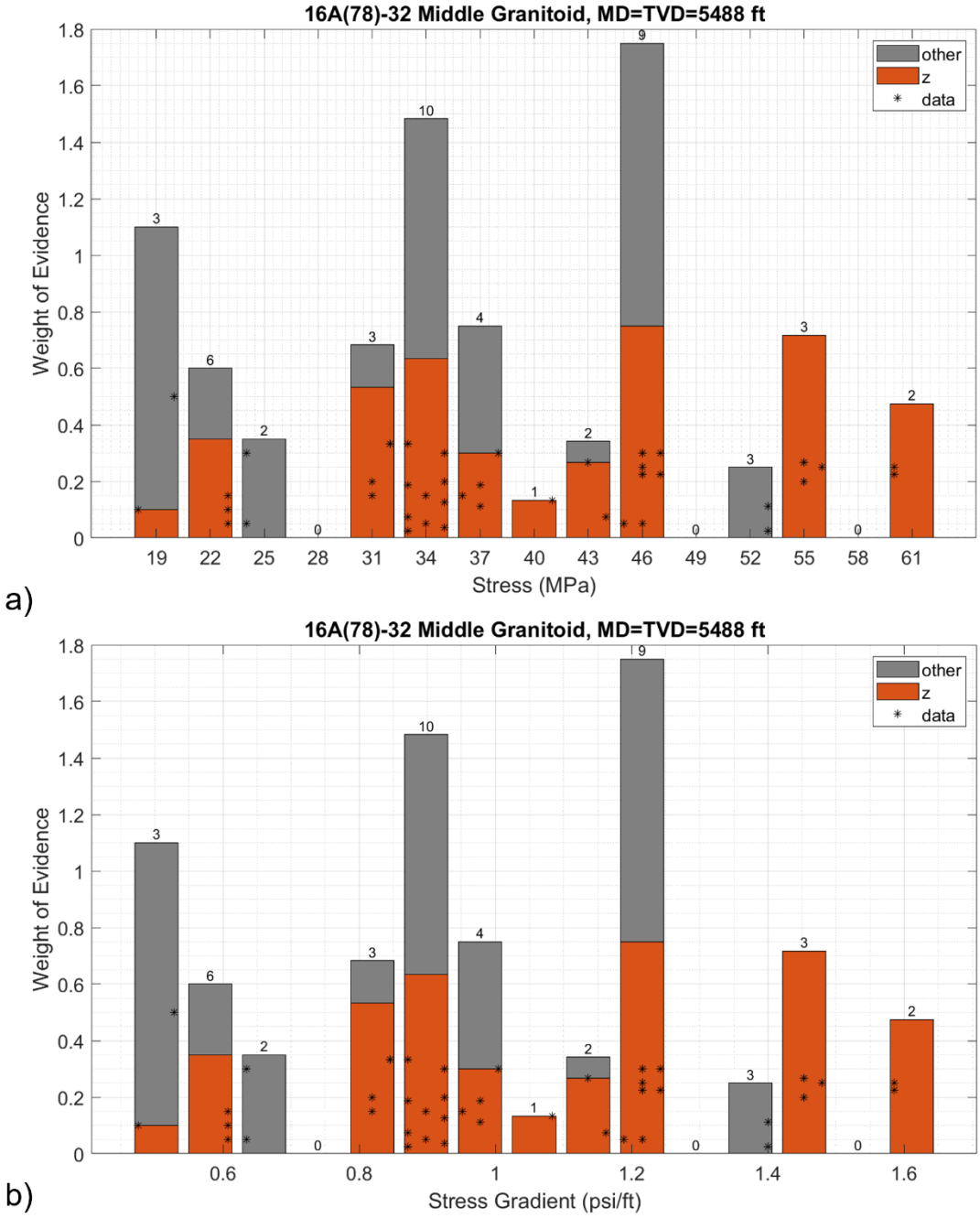

Figure 17: Integrated weight of evidence from DRA tests versus a) applied axial stress for the DRA experiments, b) corresponding implied stress gradient. The stars indicate individual data points, noting some lie directly on top of one another. The number at the top of each bar is the total lines of evidence in that bin. The bars are color coded to indicate the orientation of the sample giving the line(s) of evidence leading to that part of the bar.

H1-Direction: Compendium

The H1 direction generated two samples:

H1-1

Dimensions	
height (mm):	39.54
width (mm):	32.00
Angle retrieved (degrees):	0

H1-2

Dimensions	
height (mm):	33.76
width (mm):	31.94
Angle retrieved (degrees):	0

DRA experiments are run with the loading sequence (in all cases to come, showing H1-1 followed by H1-2). Also note that in cases with wavespeeds, these are coming from the nearby Upper Granitoid in all figures to come.

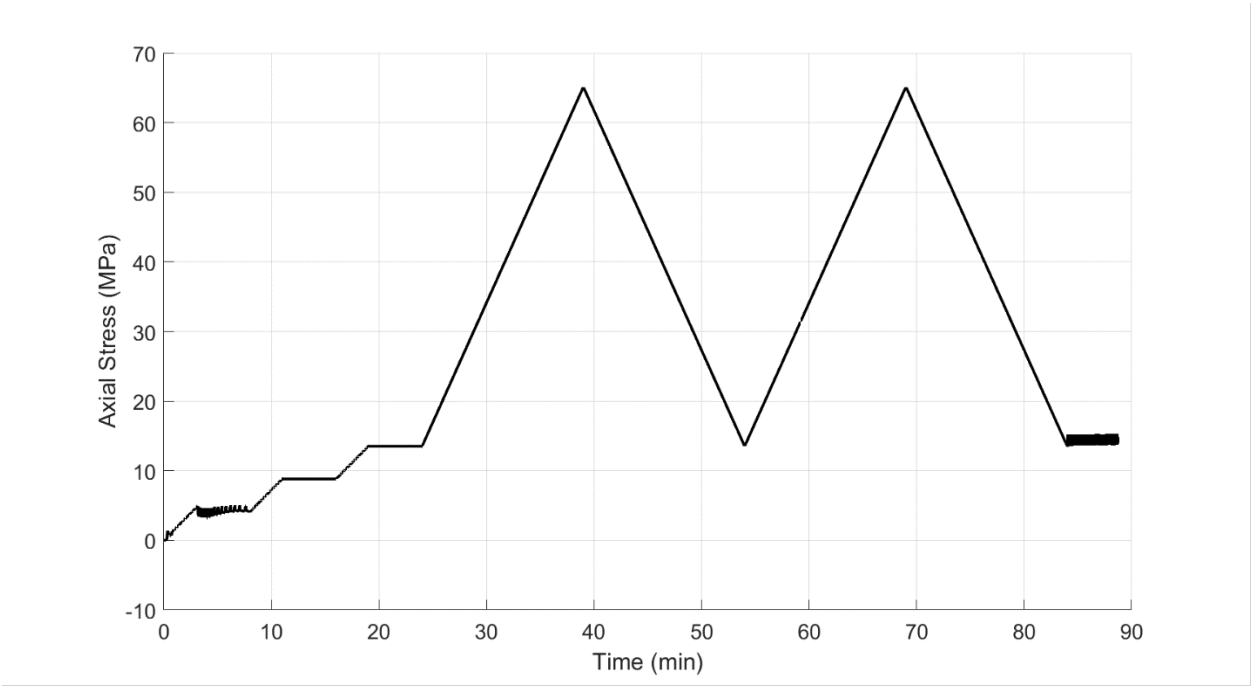

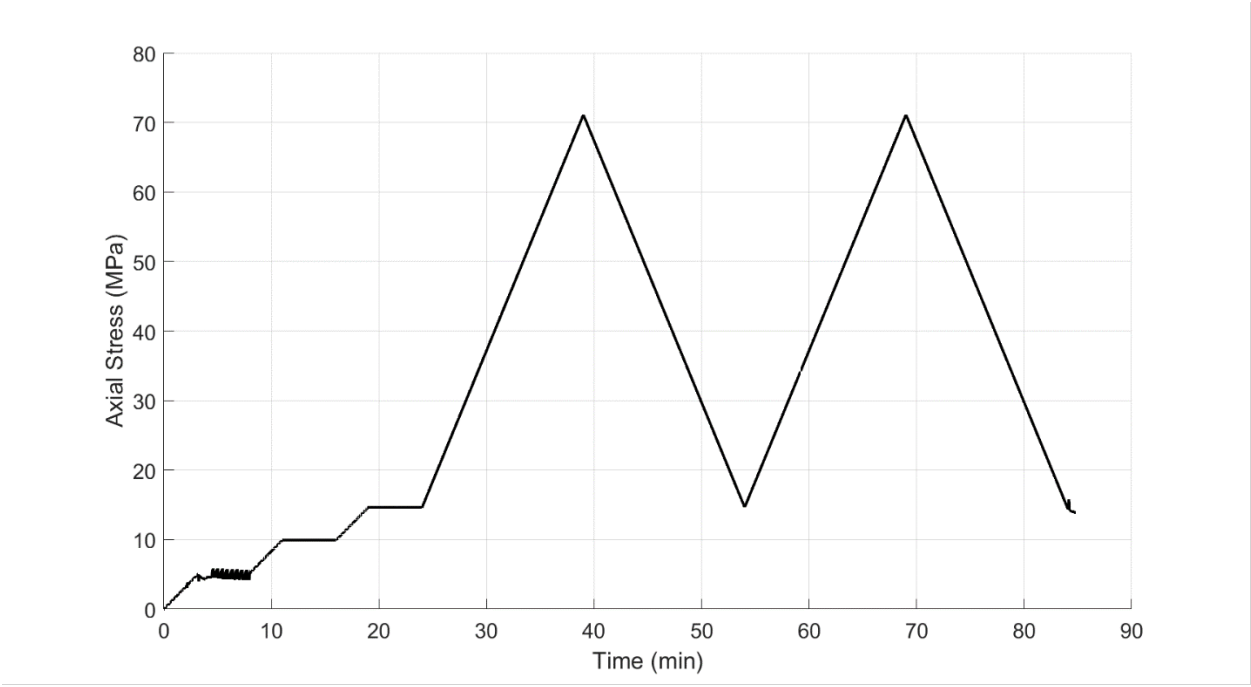

This results in the following displacements, which have been reduced by an amount estimated for deformation of 110mm of tool steel with E=210 GPa (comprising a lower bound on the platen deformation). This gives

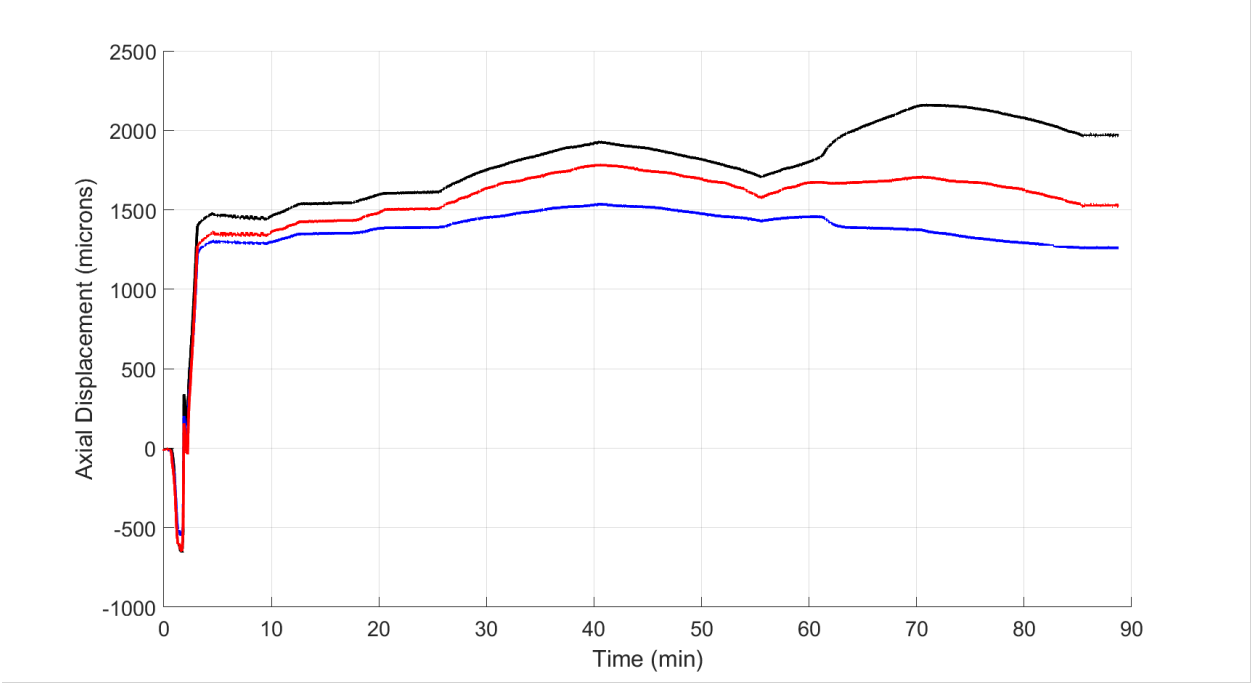

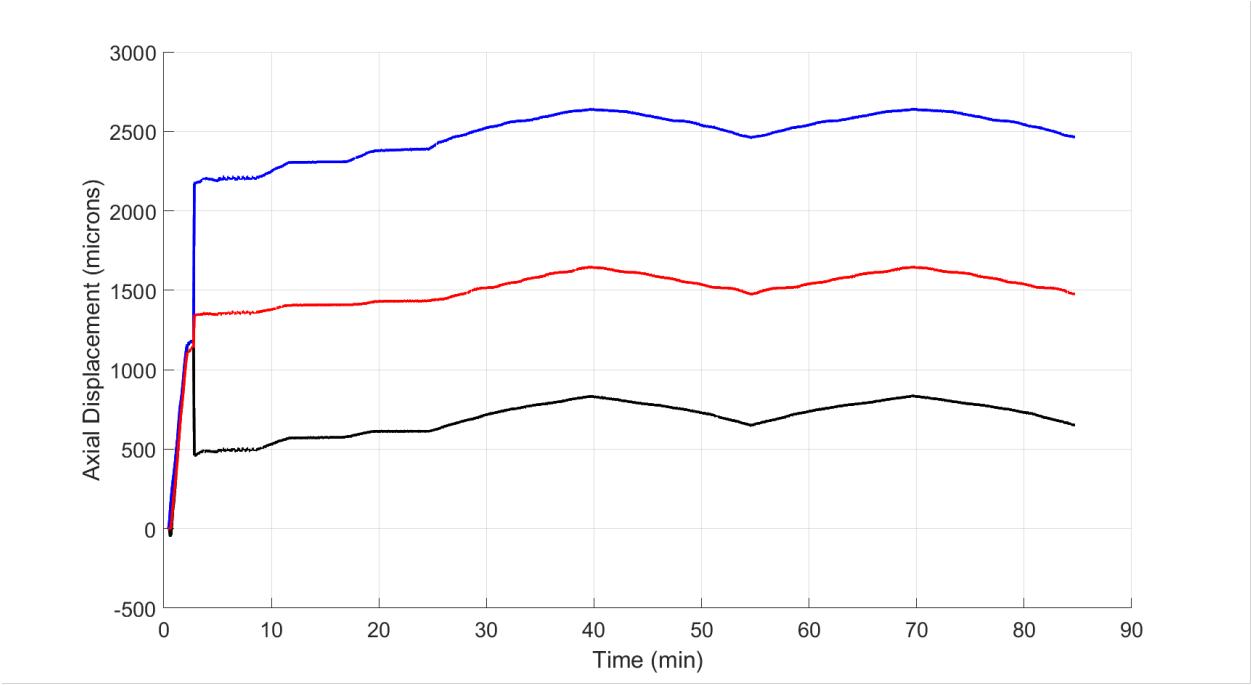

Observe that the second load cycle involved some tilting of the platens. Unclear at this point if it is local settling of platen to specimen or if there is a directional bias to the plastic deformation.

Averaging and plotting stress versus strain relationships for the 2 load/unload cycles, setting zero strain at the beginning of the first load cycle, gives

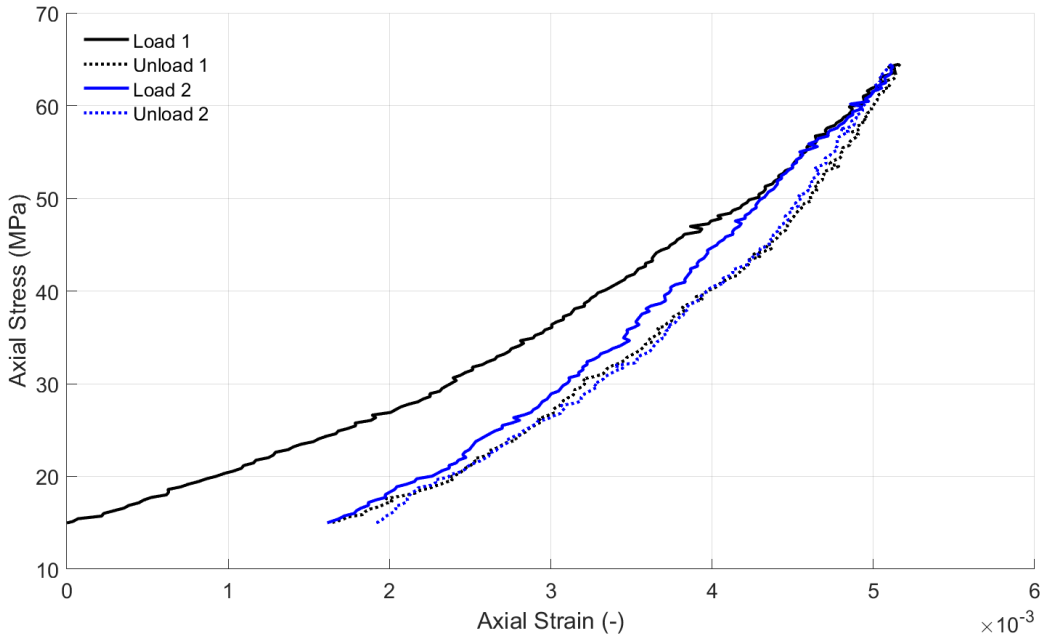

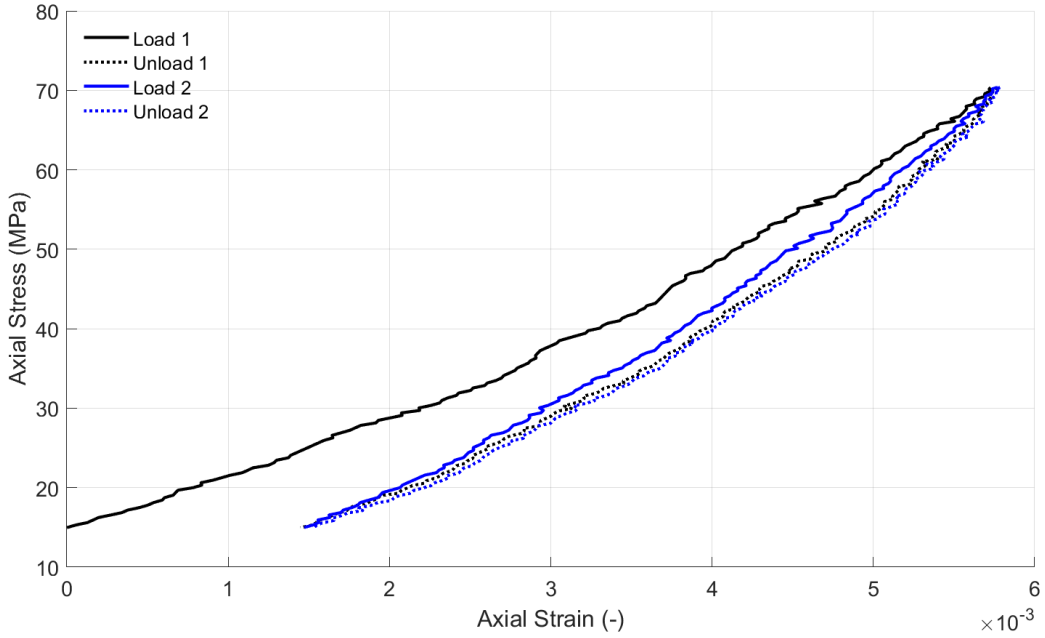

Both cases have very subtle indications of stiffening compared to other zones, possibly because all DRA directions were oblique to fabic (and possibly hence also to principal stresses and/or predominant microcracks impacting dependence of wavespeed on stress).

The difference between the strain measurements for the load/unload stages is given by

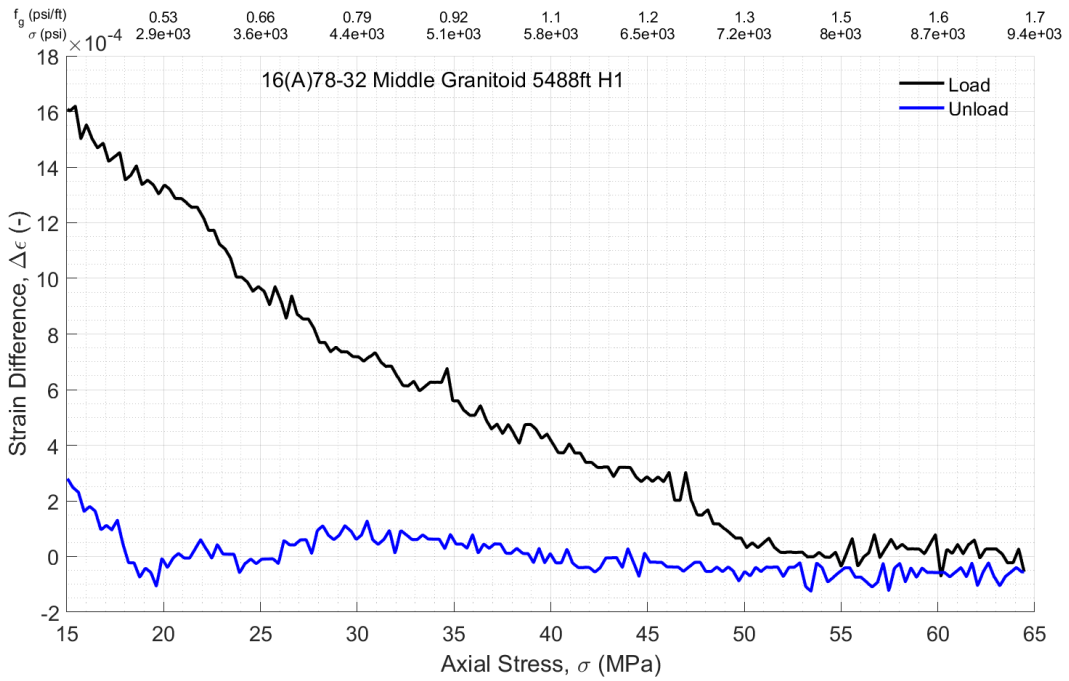

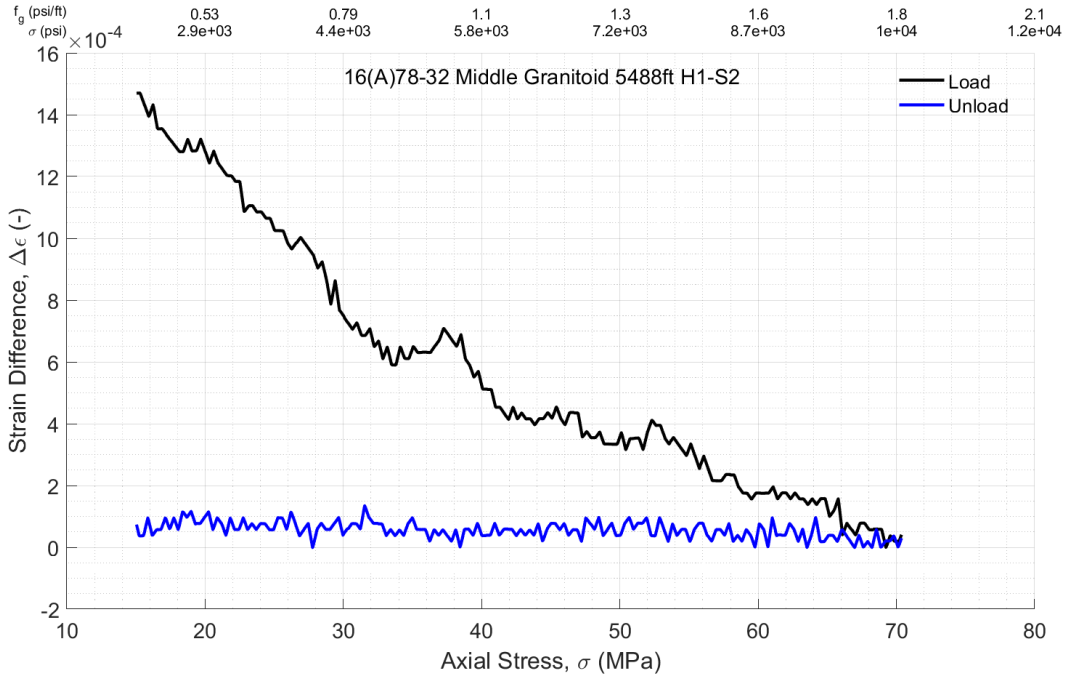

In the second test, one can observe a strong inflection at around 38 MPa.

Taking the derivative of stress with respect to strain for DRA curves gives

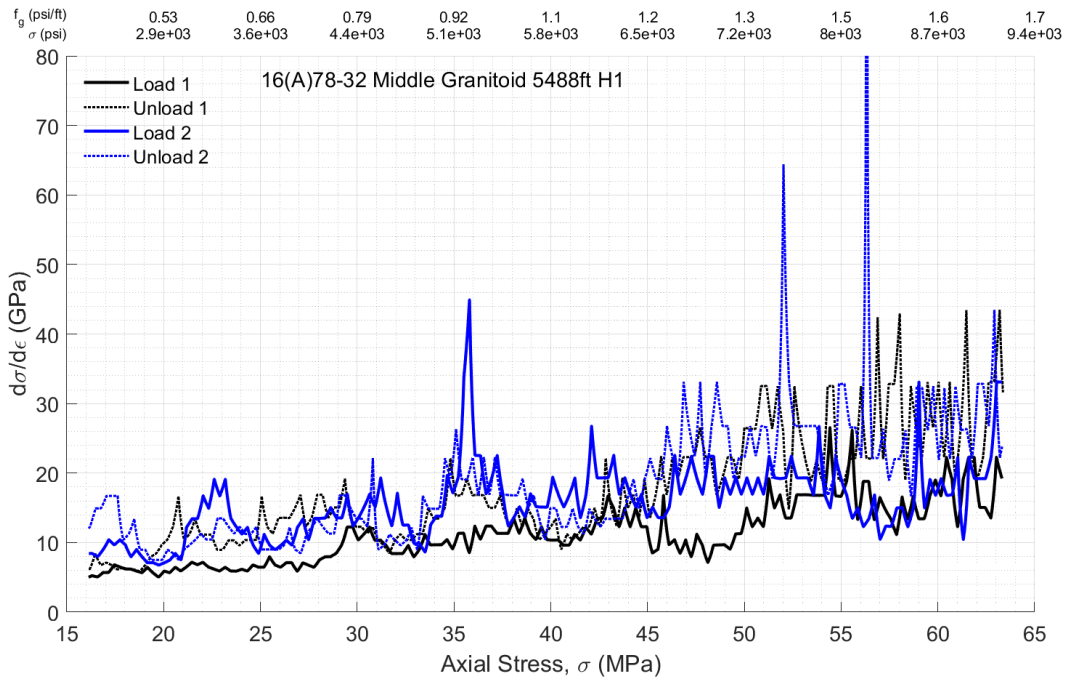

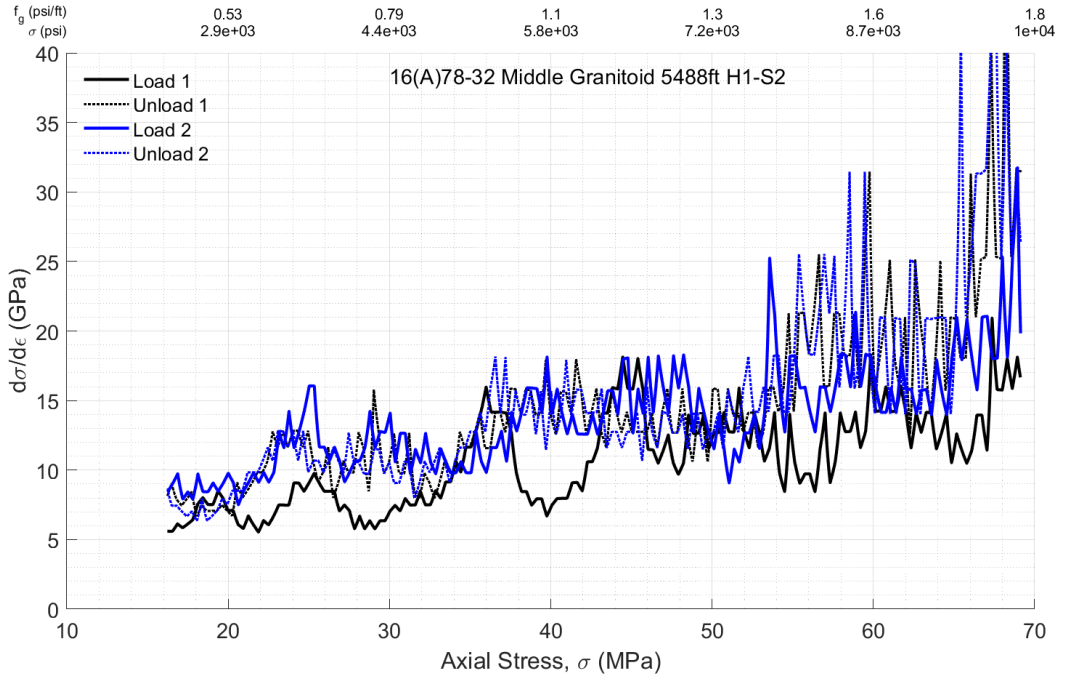

As expected based on observation of the stress-strain curves, the stiffening behavior is subtle.

Additionally, we can make a similar plot (though DRA only) but putting strain on the x-axis:

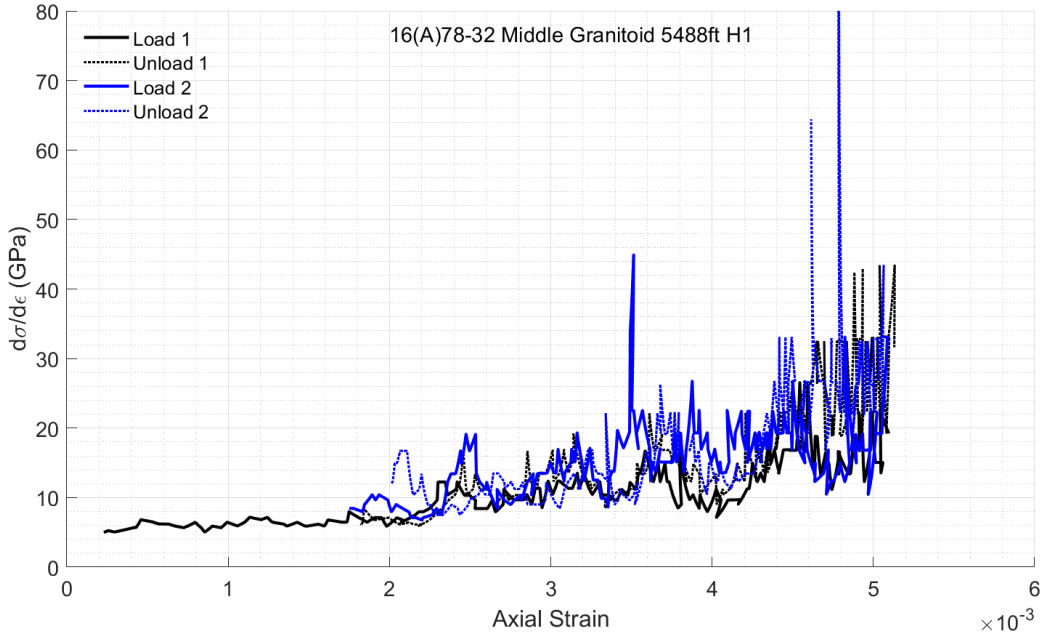

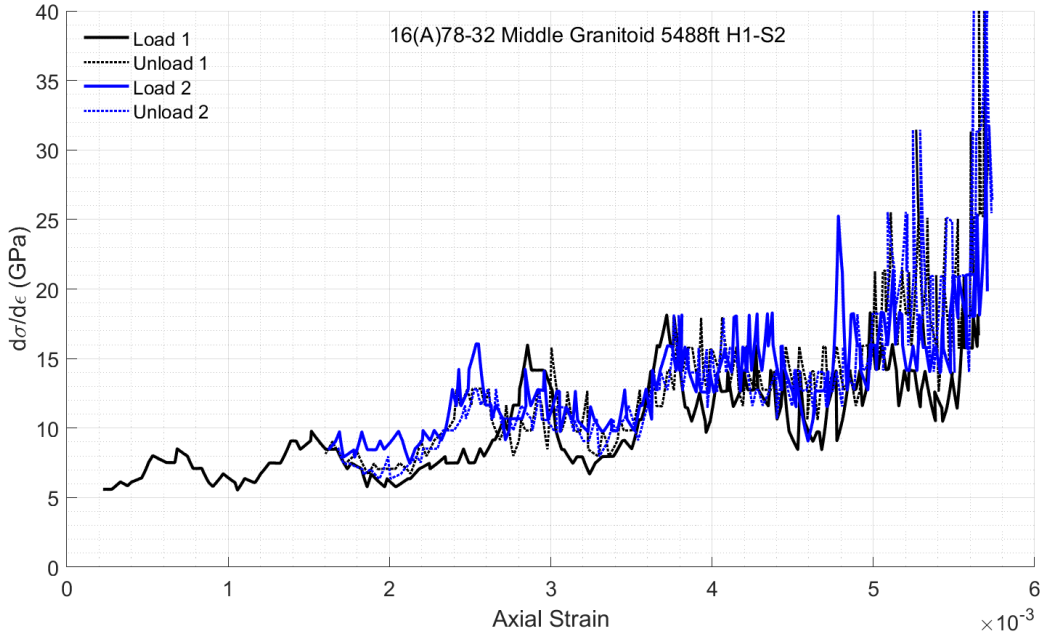

H2-Direction: Compendium

One sample is available in this orientation.

Dimensions	
height (mm):	22.58
width (mm):	32.02
Angle retrieved (degrees):	87.8

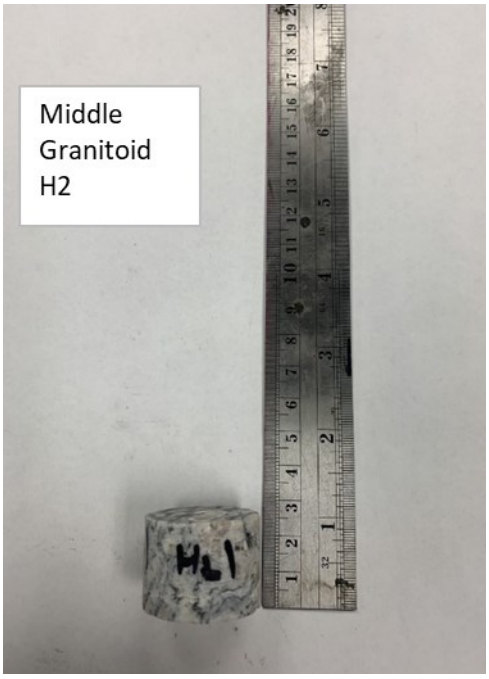

DRA experiments are run with the loading sequence that follows. Also note that in cases with wavespeeds, these are coming from the nearby Upper Granitoid in all figures to come.

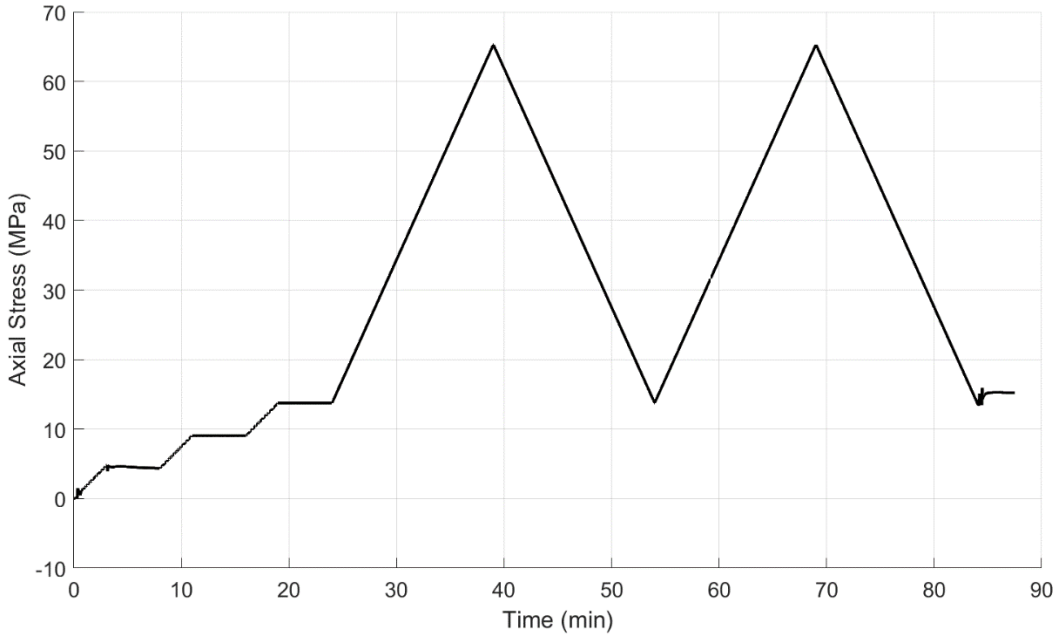

This results in the following displacements, which have been reduced by an amount estimated for deformation of 100mm of tool steel with E=210 GPa (comprising a lower bound on the platen deformation). This gives

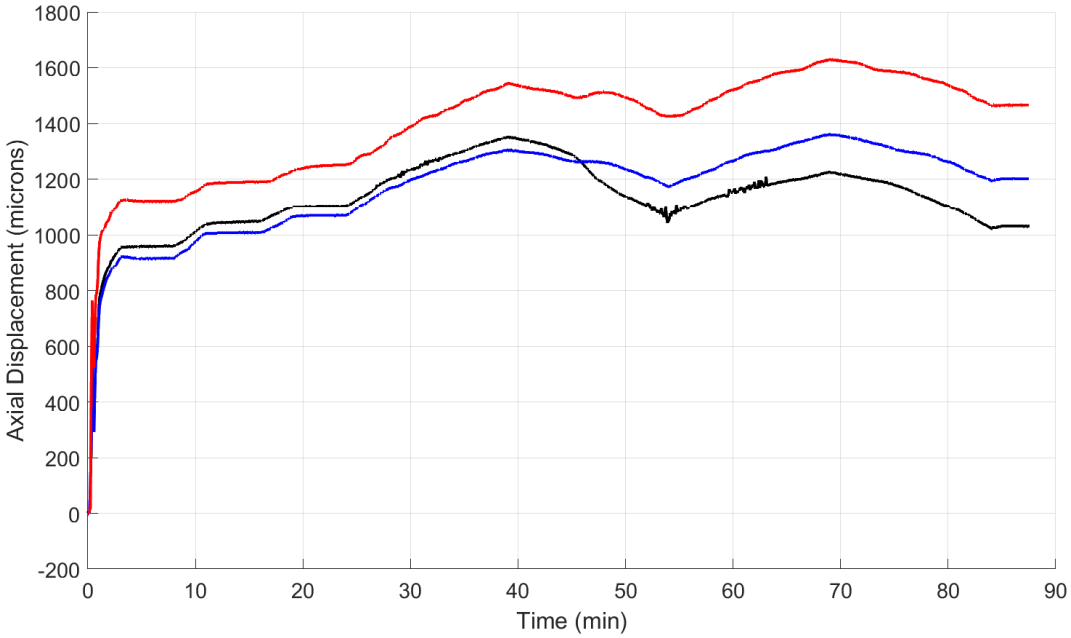

One of the LVDT's experiences very different behavior on the first unloading. Could be impacted by a pre-existing fracture or other meso-scale structure in the specimen.

Averaging and plotting stress versus strain relationships for the 2 load/unload cycles, setting zero strain at the beginning of the first load cycle, gives

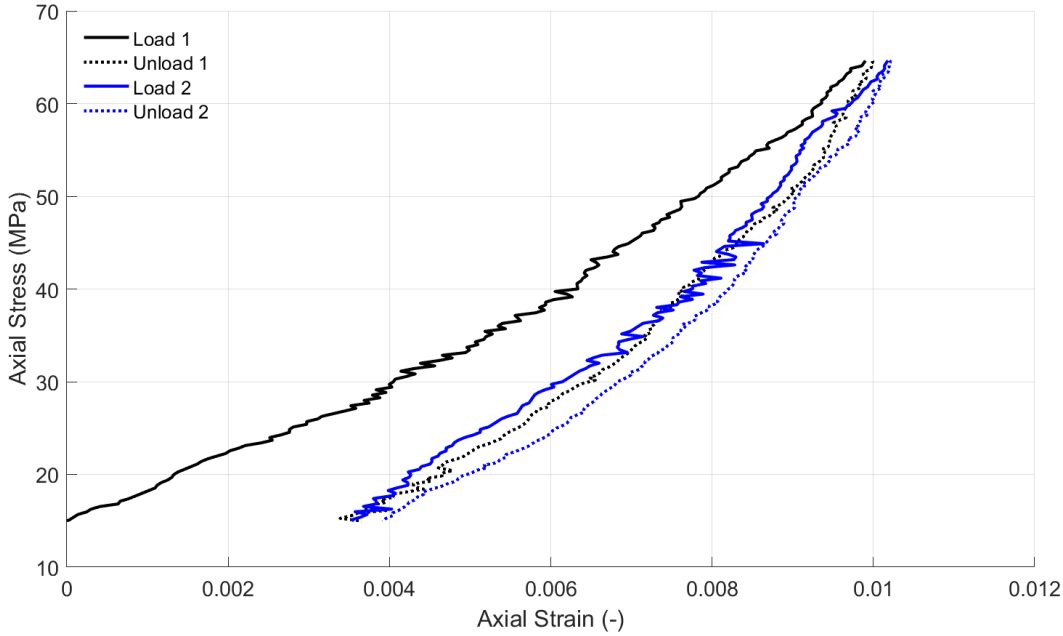

There is not very much stiffening observable here. The difference between the strain measurements for the load/unload stages is given by

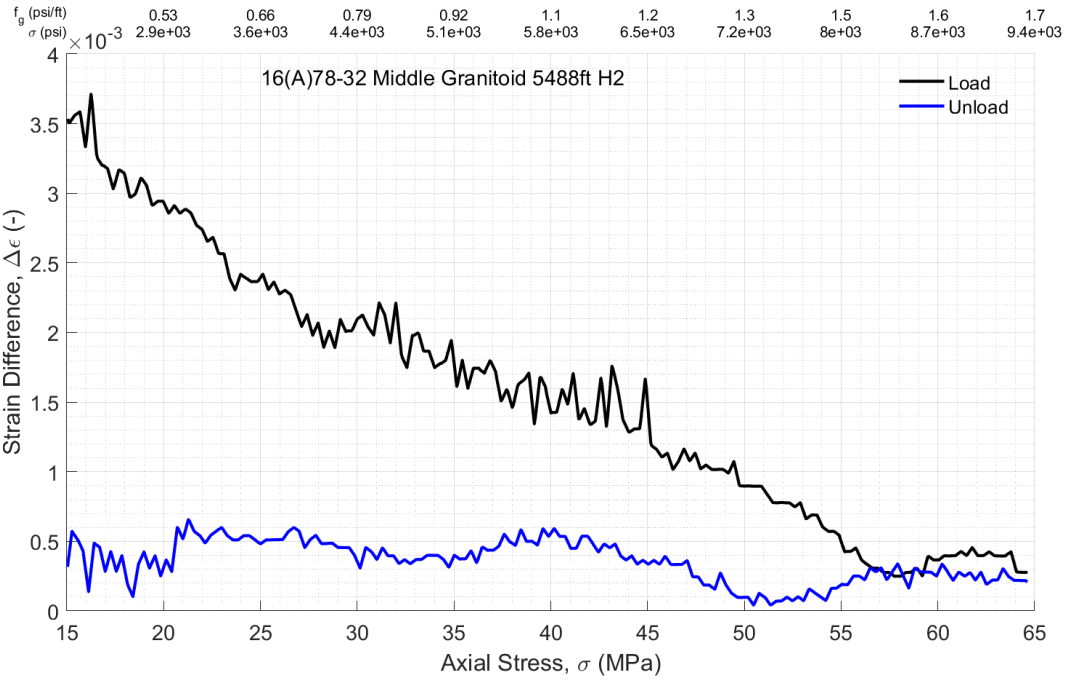

Here also there are subtle inflections, at best.

Taking the derivative of stress with respect to strain for DRA curves gives

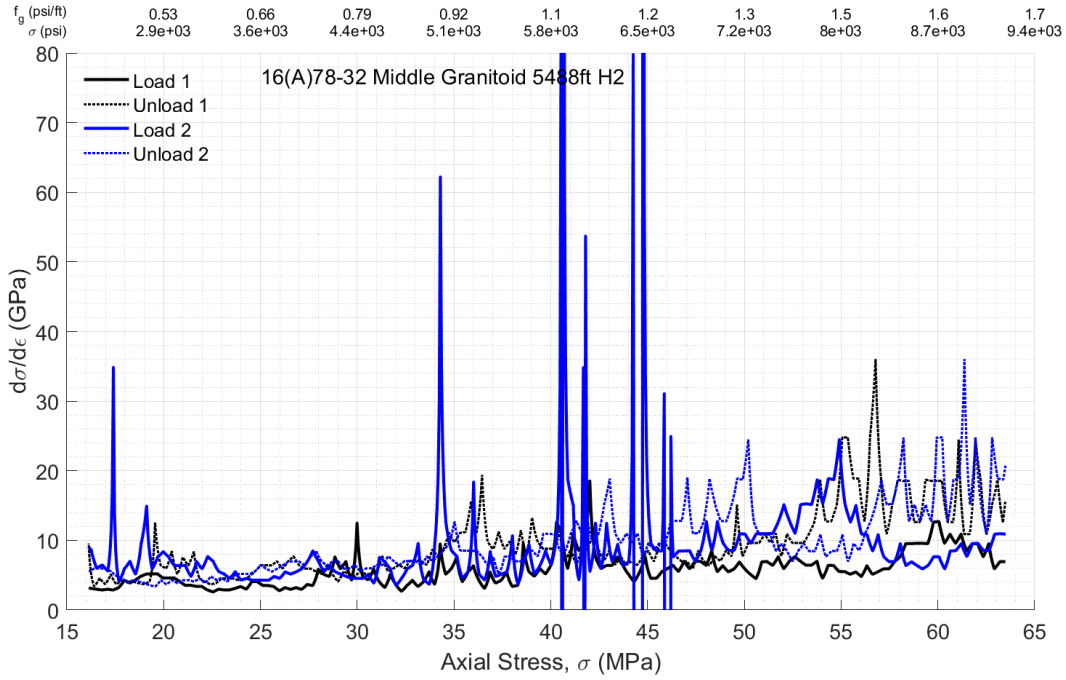

As anticipated from the stress-strain curves, there is subtle nonmonotonicity in the stiffness.

Additionally, we can make a similar plot (though DRA only) but putting strain on the x-axis:

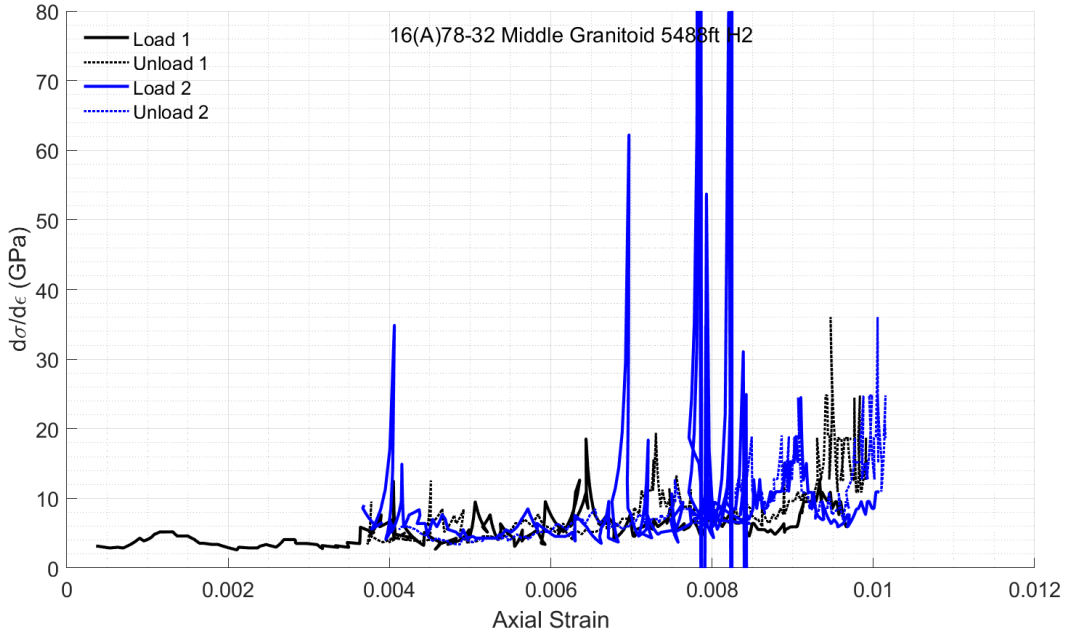

H3-Direction: Compendium

As a summary, unlike the other two horizontal directions, the H3 appears to have a pretty distinctive stiffening at around 29 MPa which is around 0.76 psi/ft, and then again but just in the unloading curves at around 43 MPa (1.15 psi/ft). This could be sensible with the platyness of the fabric that would be reflective of interplay between a horizontal and vertical stress, primarily. The results are obtained from a single DRA sample:

Dimensions	
height (mm):	49.53
width (mm):	31.99
Angle retrieved (degrees):	284.1

DRA experiments are run with the loading sequence

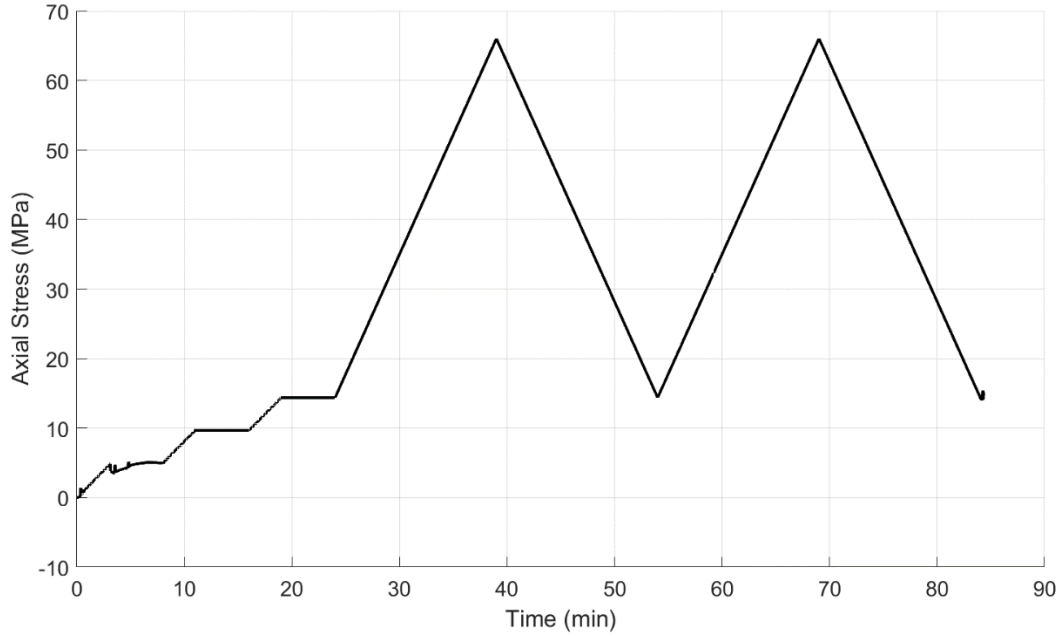

This results in the following displacements, which have been reduced by an amount estimated for deformation of 100mm of tool steel with E=210 GPa (comprising a lower bound on the platen deformation). This gives

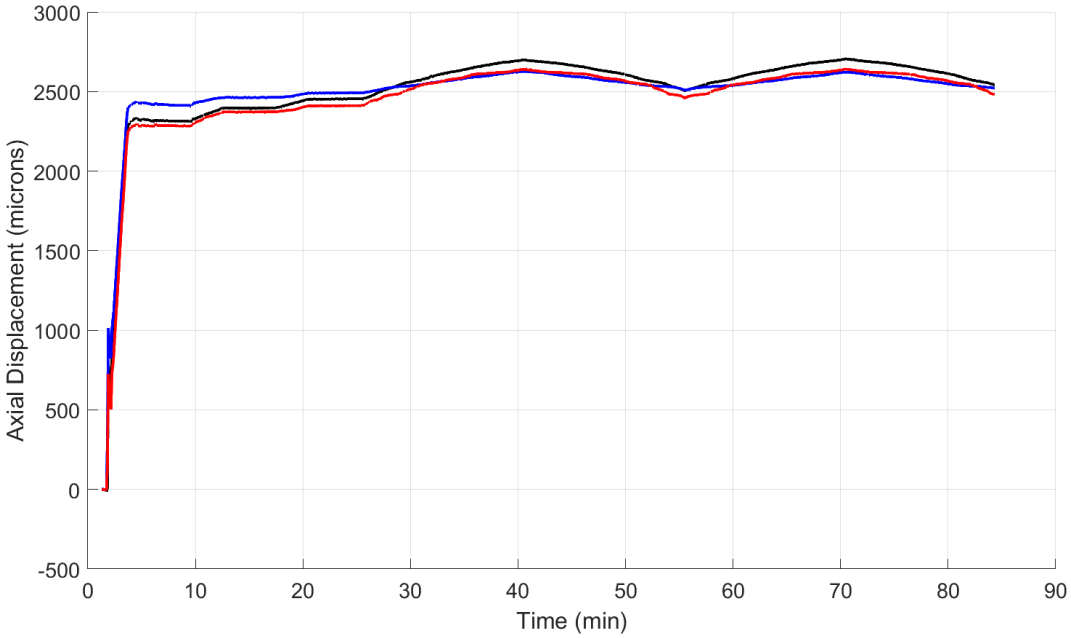

The LVDTs are very close together indicating almost no platen tilting. Averaging and plotting stress versus strain relationships for the 2 load/unload cycles, setting zero strain at the beginning of the first load cycle, gives

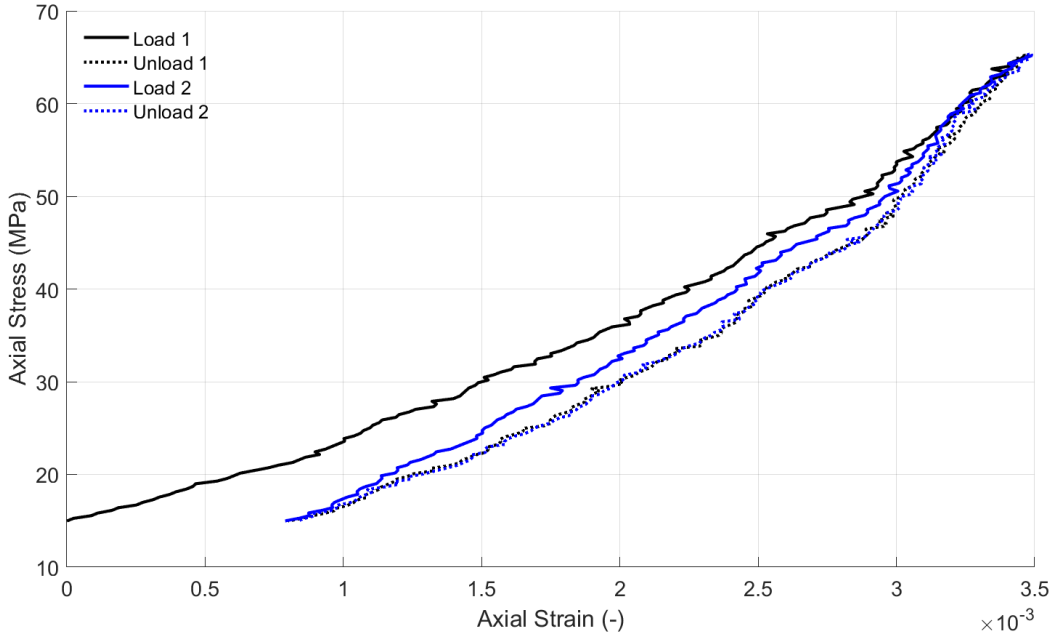

There are a couple of clear stiffening regions, namely around 50 MPa on first loading and then around 45 MPa and 35 MPa during unloading cycles.

The difference between the strain measurements for the load/unload stages is given by

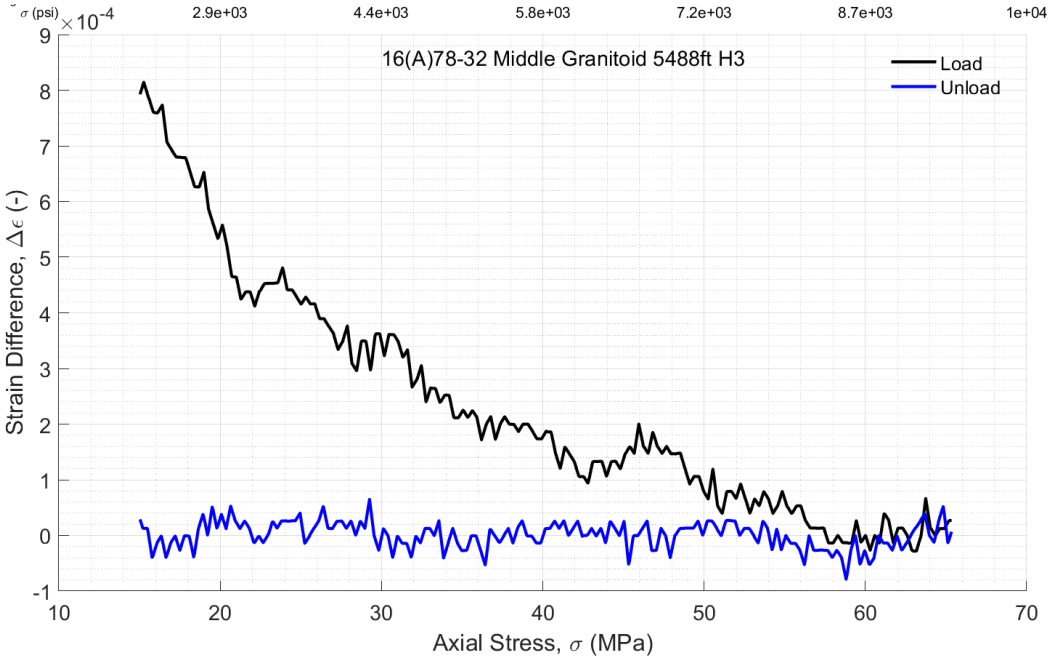

There is a striking drop around 24 MPa, but note there are others at 32 MPa and a more striking one around 46 MPa.

Taking the derivative of stress with respect to strain for DRA curves gives

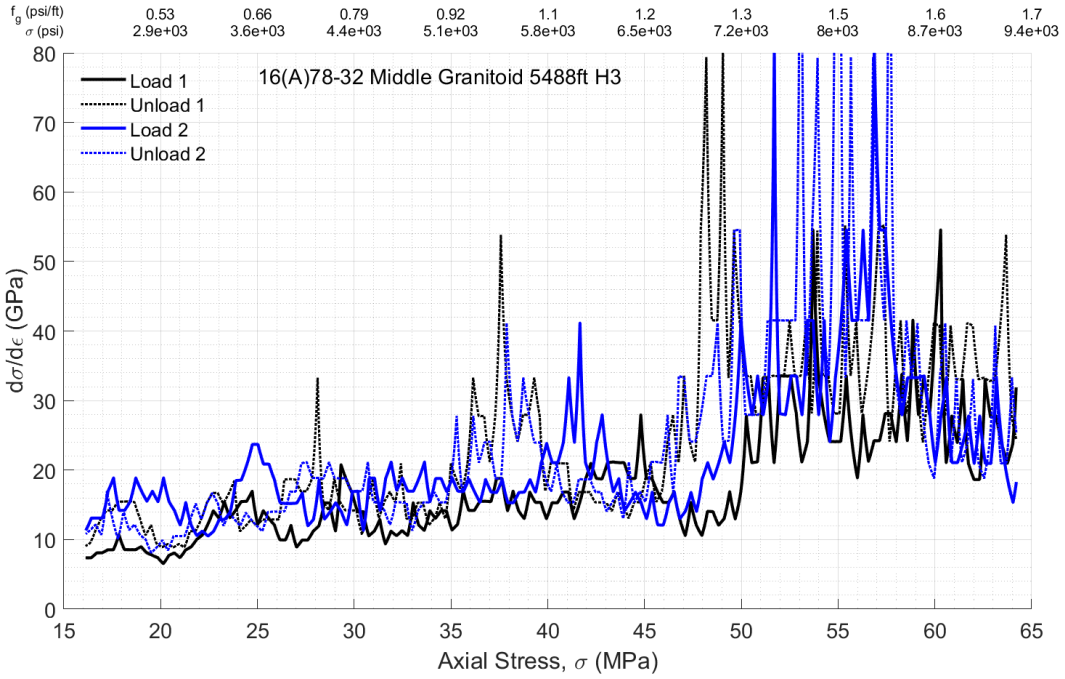

Most striking stiffening is around 47 MPa.

Additionally, we can make a similar plot (though DRA only) but putting strain on the x-axis:

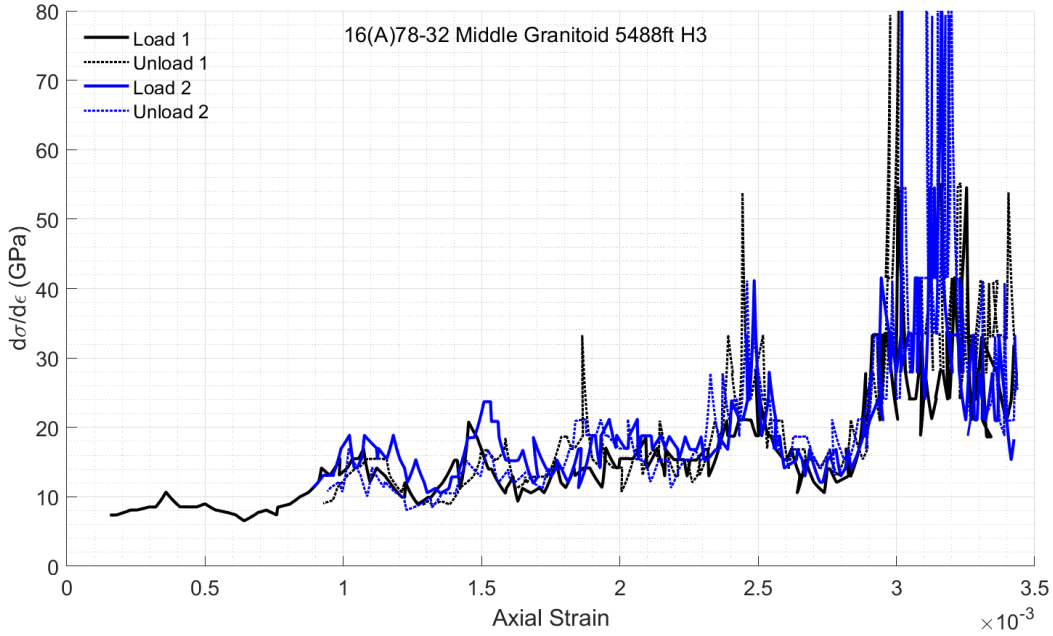

There is a significant level of consistency in two stiffening regions. The lower one maps to around 35 MPa and the upper one to around 47 MPa from the plots above where stiffness is plotted with respect to stress.

Z-Direction: Compendium

As a summary, there is some observable stiffening at around 1.1 psi/ft, as would be expected for vertical direction. There is also something around 0.80 psi/ft, which can be explained as related to minimum horizontal stress. The results are obtained from two DRA tests on core plugs which are vertically oriented vertically and hence perpendicular to the fabric:

V-1

Dimensions	
height (mm):	28.05
width (mm):	31.96
Angle retrieved (degrees):	NA

V-2

Dimensions	
height (mm):	24.1
width (mm):	32.00
Angle retrieved (degrees):	NA

DRA experiments are run with the loading sequence

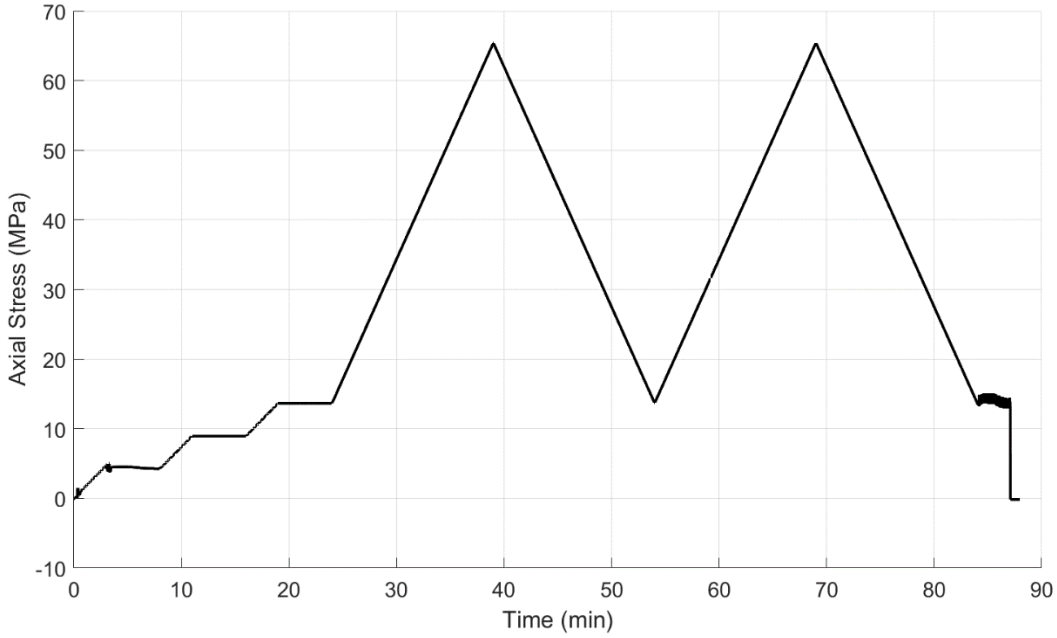

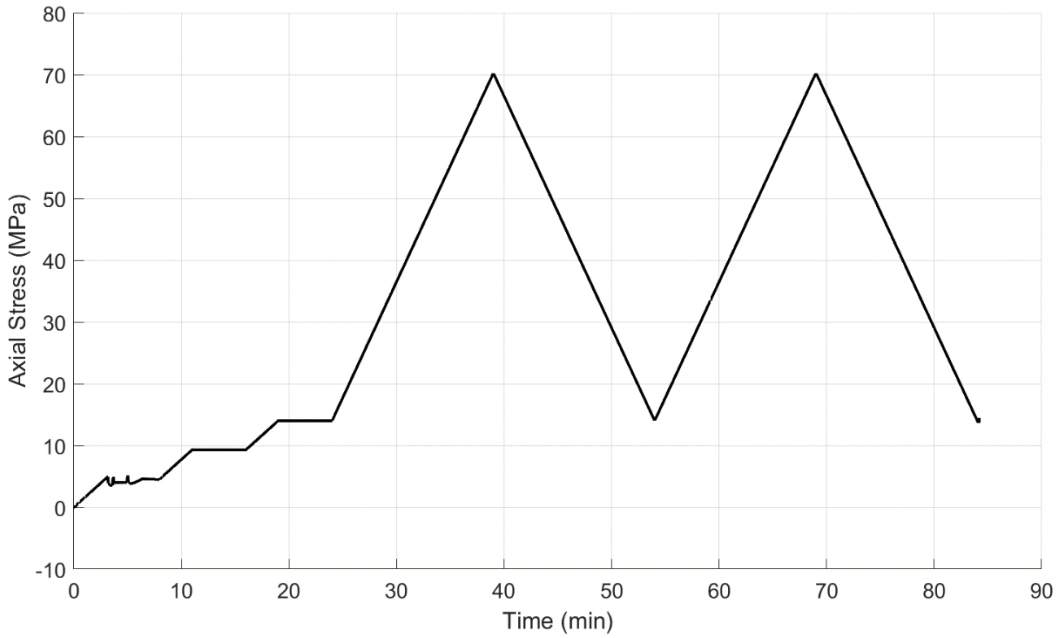

This results in the following displacements, which have been reduced by an amount estimated for deformation of 100mm of tool steel with E=210 GPa (comprising a lower bound on the platen deformation). This gives

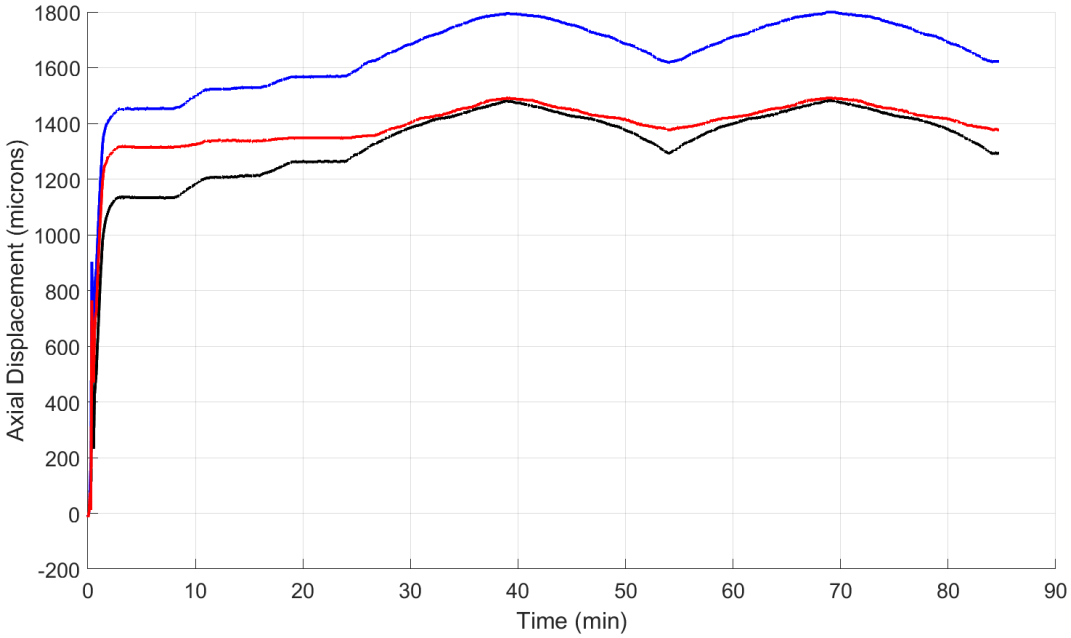

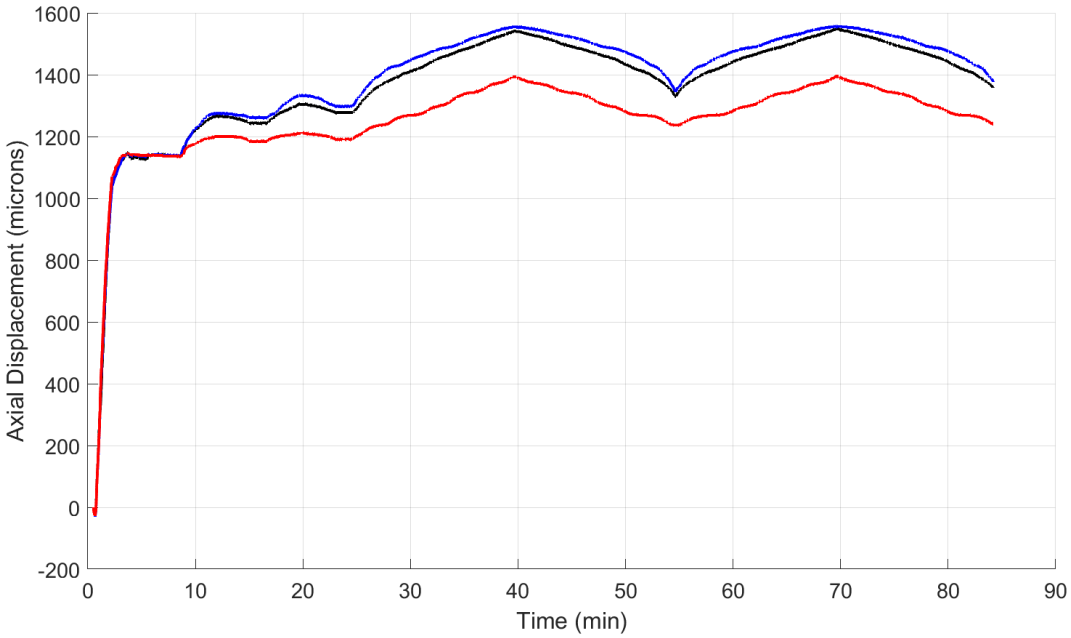

Slight platen tilting for both tests, although more for test 1 than test 2. Averaging and plotting stress versus strain relationships for the 2 load/unload cycles, setting zero strain at the beginning of the first load cycle, gives

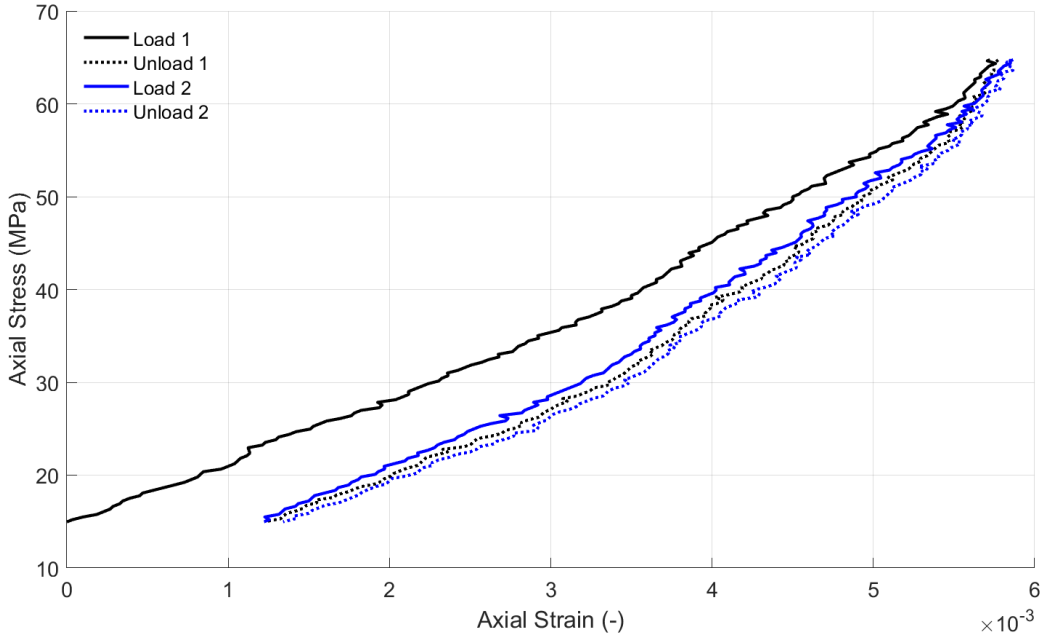

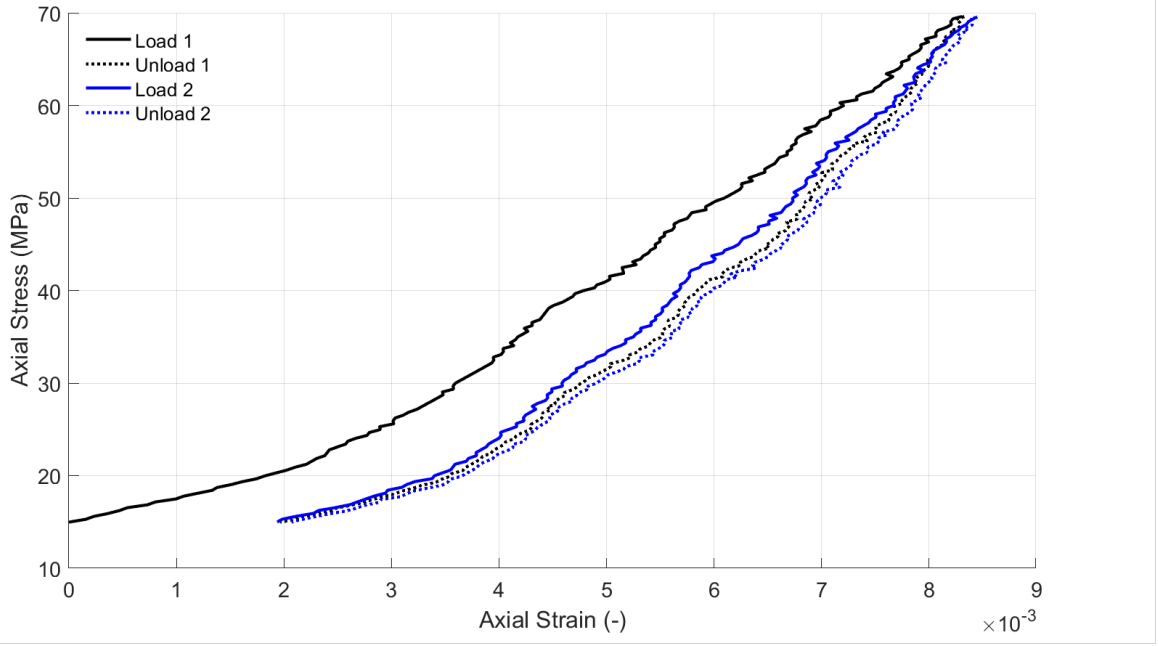

Stiffening is clearest in the second test around 35 MPa and again around 44 MPa.

The difference between the strain measurements for the load/unload stages is given by

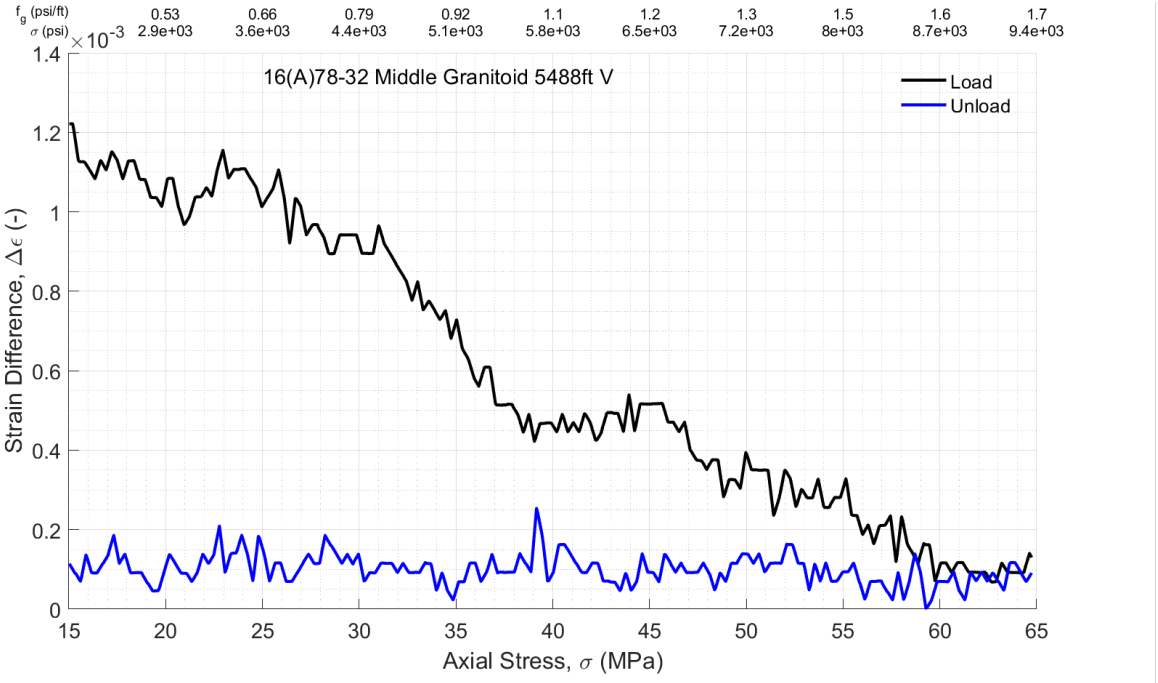

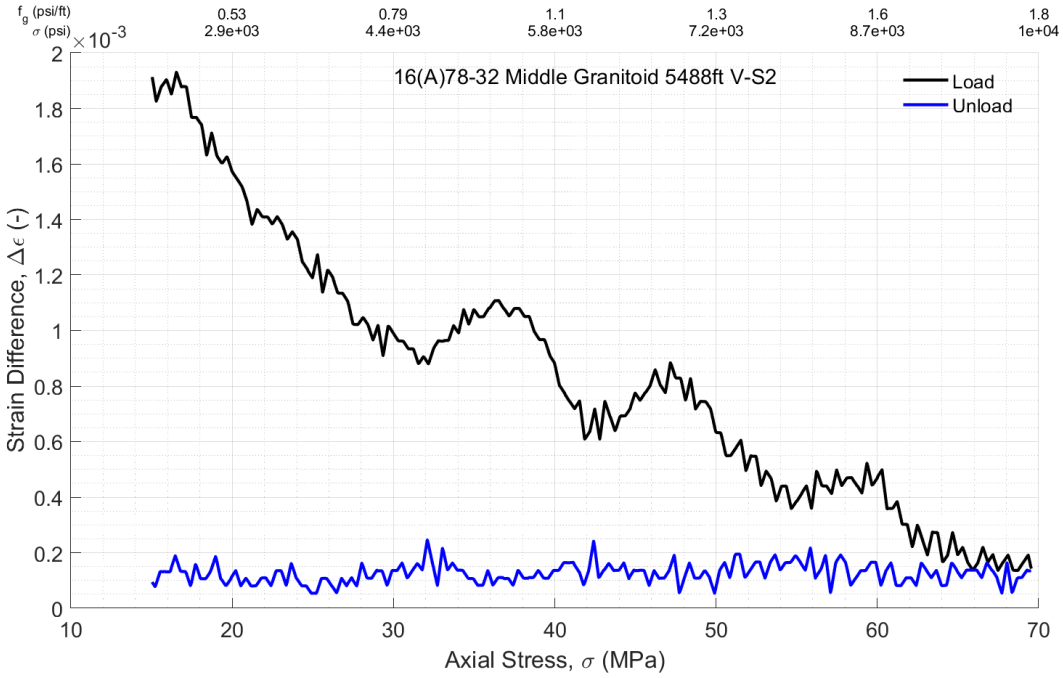

There are clear downward inflection in both cases, especially around 45-47 MPa. Taking the derivative of stress with respect to strain for DRA curves gives

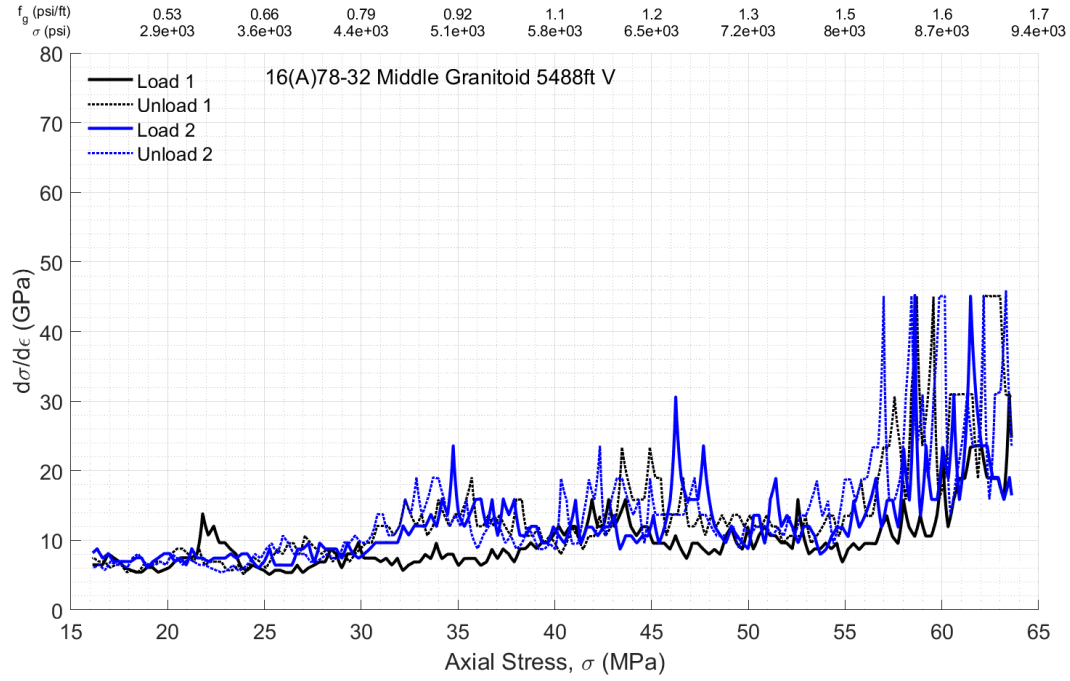

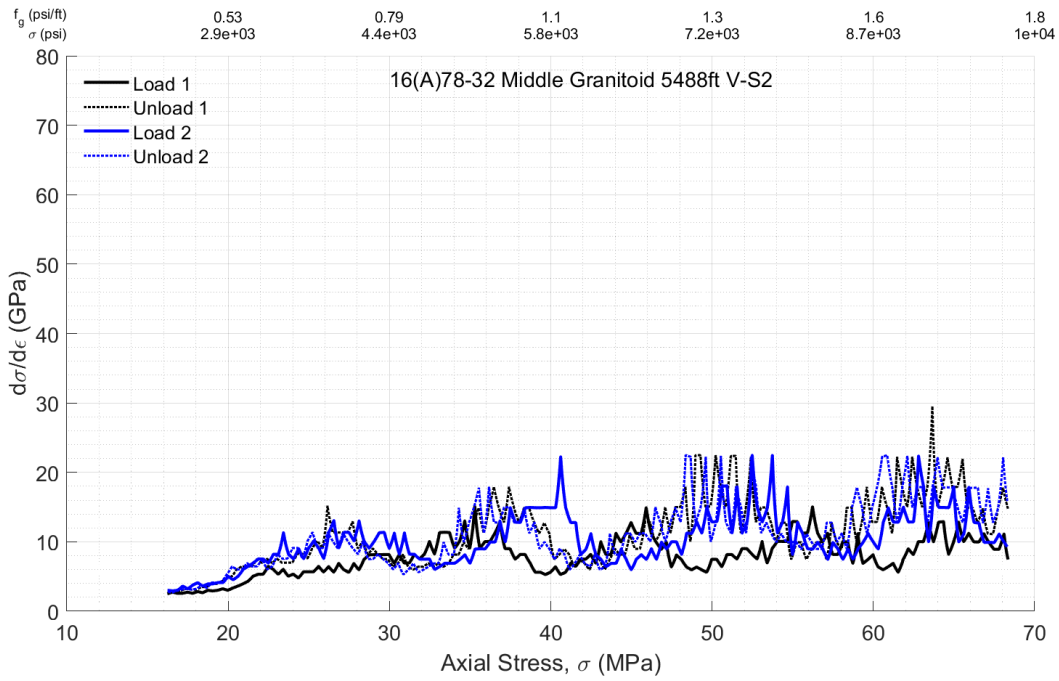

Additionally, we can make a similar plot (though DRA only) but putting strain on the x-axis:

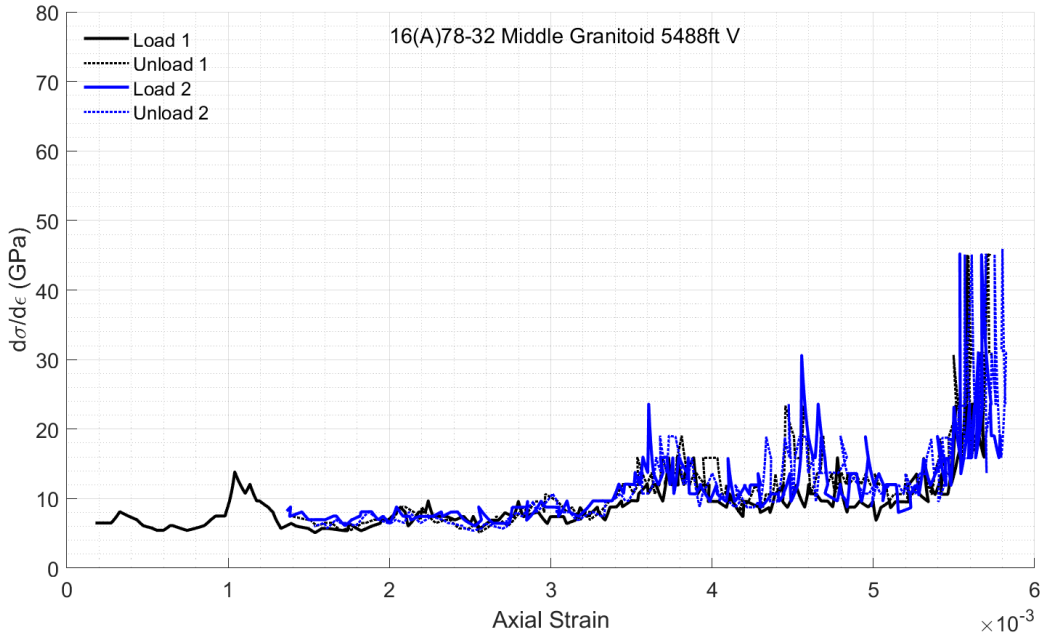

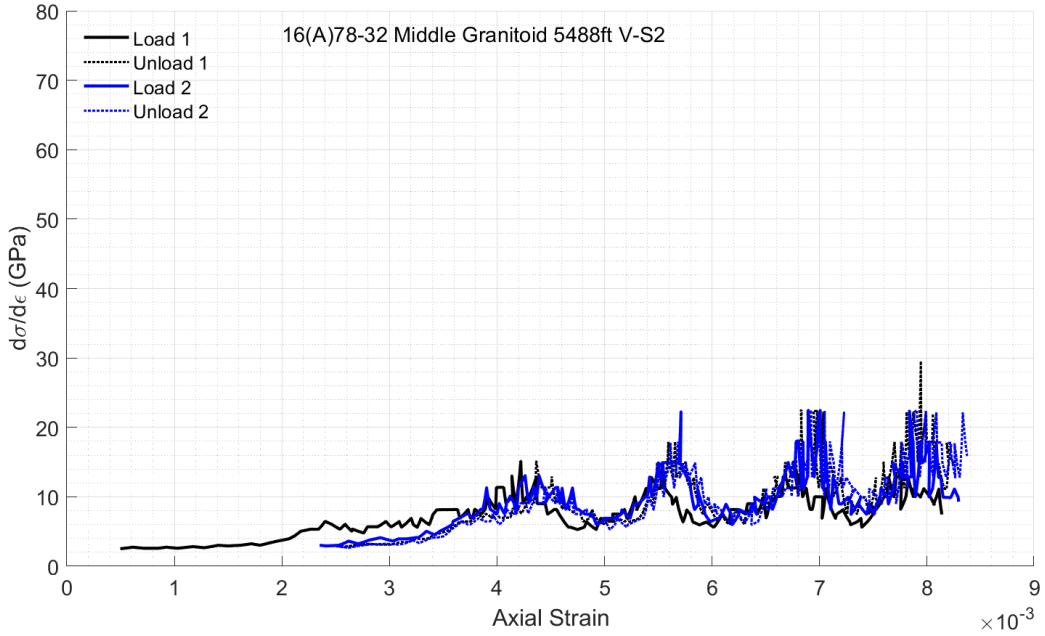

Lines of Evidence

A summary of the lines of evidence obtained from these experiments is given by:

Series	LoE	s1_val	s1_V	s1_L	s1_C	s1_R	s2_val	s2_V	s2_L	s2_C	s2_R	s3_val	s3_V	s3_L	s3_C	s3_R	s4_val	s4_V	s4_L	s4_C	s4_R	s5_val	s5_V	s5_L	s5_C	s5_R
LrGn_H1	s_e	33	1.5	0.5	1	0.9	45	1.5	1	1	0.9	0	0	0	0	0.9	0	0	0	0	0.9	0	0	0	0	0.9
LrGn_H1	s_e	0	0	0	0	0.9	0	0	0	0	0.9	0	0	0	0	0.9	0	0	0	0	0.9	0	0	0	0	0.9
LrGn_H1	De	23	2	1	1.5	0.9	35	1.5	0.5	1.5	0.9	44	1.5	1	1.5	0.9	0	0	0	0	0.9	0	0	0	0	0.9
LrGn_H1	De	38	2	3	1.5	0.9	46	1.5	0.5	2	0.9	53	1.5	1.5	1.5	0.9	0	0	0	0	0.9	0	0	0	0	0.9
LrGn_H1	ds_de	20	2	2.5	3	0.9	33	1.5	1.5	2.5	0.9	0	0	0	0	0.9	0	0	0	0	0.9	0	0	0	0	0.9
LrGn_H1	ds_de	20	2	2.5	3	0.9	35	1.5	1	2.5	0.9	53	1.5	1.5	1.5	0.9	0	0	0	0	0.9	0	0	0	0	0.9
LrGn_H2	s_e	33	1.5	1	1.5	0.9	0	0	0	0	0.9	0	0	0	0	0.9	0	0	0	0	0.9	0	0	0	0	0.9
LrGn_H2	De	23	2	1	1.5	0.9	34	2	1.5	1.5	0.9	45	2	0.5	1.5	0.9	0	0	0	0	0.9	0	0	0	0	0.9
LrGn_H2	ds_de	34	2	0.5	1.5	0.9	53	1.5	0.5	1	0.9	0	0	0	0	0.9	0	0	0	0	0.9	0	0	0	0	0.9
LrGn_H3	s_e	36	2	1.5	1.5	0.9	46	2	3	1.5	0.9	23	2	0.5	1.5	0.9	0	0	0	0	0.9	0	0	0	0	0.9
LrGn_H3	De	24	2	3	1.5	0.9	31	2	1.5	1.5	0.9	46	2	2.5	1.5	0.9	0	0	0	0	0.9	0	0	0	0	0.9
LrGn_H3	ds_de	35	2	2	1.5	0.9	47	2	3	1.5	0.9	24	2	0.5	1.5	0.9	0	0	0	0	0.9	0	0	0	0	0.9
LrGn_V	s_e	31	2	1.5	2	0.9	55	2	2	2	0.9	0	0	0	0	0.9	0	0	0	0	0.9	0	0	0	0	0.9
LrGn_V	s_e	35	2	3	1.5	0.9	47	2	3	1.5	0.9	60	2	2.5	1.5	0.9	23	2	1	1.5	0.9	0	0	0	0	0.9
LrGn_V	De	23	2	1.5	1.5	0.9	37	1.5	1.5	1.5	0.9	46	1.5	3	1.5	0.9	0	0	0	0	0.9	0	0	0	0	0.9
LrGn_V	De	18	2	1	1.5	0.9	37	1.5	2.5	1.5	0.9	47	1.5	3	1.5	0.9	60	1.5	3	1.5	0.9	0	0	0	0	0.9
LrGn_V	ds_de	32	2	2	2.5	0.9	41	2	1	2	0.9	55	2	2	1.5	0.9	0	0	0	0	0.9	0	0	0	0	0.9
LrGn_V	ds_de	23	2	1	1.5	0.9	43	2	2	2	0.9	56	2	2.5	1.5	0.9	33	2	2	2.5	0.9	0	0	0	0	0.9

To note:

- Each series is named with the direction after an underscore (column 1).
- The source of the line of evidence (LoE) is given in column 2, where v is velocity, E is Young's modulus, s_e is stress-strain curve, De is the change in strain curve, and ds_de is the instantaneous stiffness curve. Subscripts indicate direction of propagation followed by polarity, as usual, such that for example vxy indicates a shear wave velocity propagating in x-direction with y-polarity.
- All stress values (i.e. s1_val, s2_val) are given in MPa.
- Each source can give multiple lines of evidence, thus the table is set up to accept up to 5 lines of evidence for each source. Zeros are filled into the table where there are no additional lines of evidence.

- The weight assigned according to the prescribed rubric is given after an underscore, where V indicates relevance, L indicates reliability, C indicates consistency, and R indicated representivity. All values of representivity are set at 0.9 because there is insufficient data to determine exactly how representative the sample is of the surrounding formation.

Lower Granitoid

Summary

The 16A(78)-32 Lower Granitoid samples are from 5846'-5850' MD (1782.3-1783.5 m) and the same TVD because well is vertical to this point. There are needle-like crystals in a roughly horizontal orientation and the x-direction on the TUV sample is nearly aligned with these (Figure 18). The vertical z-direction is clearly across, essentially perpendicular, to the fabric.

Figure 18: Lower Granitoid sample preparation for TUV sample (cube) with DRA samples (cylinders), showing x, y, z axes on TUV sample and with cylinders laying in approximate directional correspondence to TUV sample. The TUV sample was cut from the core section in the top of the image and the needle-like crystal elongation that is subparallel to the x-axis of the TUV sample is visible in both the TUV sample and the parent cores.

The main observations begin with alignment of the minimum horizontal stress, which appears to be closer to the y-direction compared to the x-direction. The evidence comes from the rollover points in the shear wave velocities, which indicate that shear waves with the y-direction of travel are reaching a maximum value at around 30 MPa (~0.75 psi/ft) compared to the x-direction where the maximum shear wave velocity is reached around 40 MPa (~1.0 psi/ft) for the x (horizontal) polarization and 45 MPa (~1.12 psi/ft)

for the z (vertical polarization). This can be seen by contrasting Figure 19a and b. Hence the inferred minimum stress orientation is sub-perpendicular to the direction of horizontal crystal elongation and is sub-parallel to the slower direction of wave propagation. A similar alignment maximum stress with the direction of crystal alignment and the direction of fastest wavespeed was observed for the Upper Granitoid.

Secondly, the various inflection points from both TUV and DRA approaches amass the most evidence for a minimum stress that is somewhere between 24-33 MPa (0.60-0.82 psi/ft), as indicated by Figure 20. While this range is relatively large, it is proposed that misalignment of the x- and y-axes with the actual orientations of the in-situ stresses relative to the parent core will lead to inflection points that give upper bounds on the minimum stress. Combined with the observation that much of the evidence at the higher end of the range is from somewhat misaligned DRA core and putting emphasis on data from the x-direction most, a best guess is s_{hmin}~27 MPa (~0.67 psi/ft).

Thirdly, the weight of evidence from both DRA and TUV highlights two additional stress levels where multiple lines of evidence are converging. These are 39 MPa (~0.97 psi/ft) and 45 MPa (~ 1.10 psi/ft). Because the peak at 0.98 psi/ft is almost certainly too low to be attributed to overburden, but it is clearly distinct from the lines of evidence comprising the upper end of the minimum principal stress estimates, it is most likely that the maximum principal stress at this location is 39 MPa, implying a maximum principal stress gradient of 0.97 psi/ft. The lines of evidence point to a gradient of 1.10 psi/ft are likely arising from the vertical stress, which is corroborated by the fact that they are coming most substantially from vertical (z-direction) tests (purple color in Figure 20).

Finally, it is observed that there are some additional inflections giving several lines of evidence around 57 MPa (~1.42 psi/ft). The origin of these responses remains unknown but, again, can be expected to be clarified by application of a micromechanical rock physics model (being developed now) to the interpretation.

To summarize:

1) **Minimum horizontal stress** aligned roughly perpendicular to horizontal needle-like fabric (which is also the slow wavespeed direction) and with magnitude around 27 MPa (~0.67 psi/ft).
2) **Maximum horizontal stress** is aligned roughly parallel to horizontal needle-like fabric which also means it is roughly parallel with the maximum horizontal wavespeed direction. It's most likely value of 39 MPa, which gives a maximum horizontal stress gradient of 0.98 psi/ft.
3) **Vertical stress** is likely around 45 MPa at this location, corresponding to an overburden stress gradient of 1.10 psi/ft.

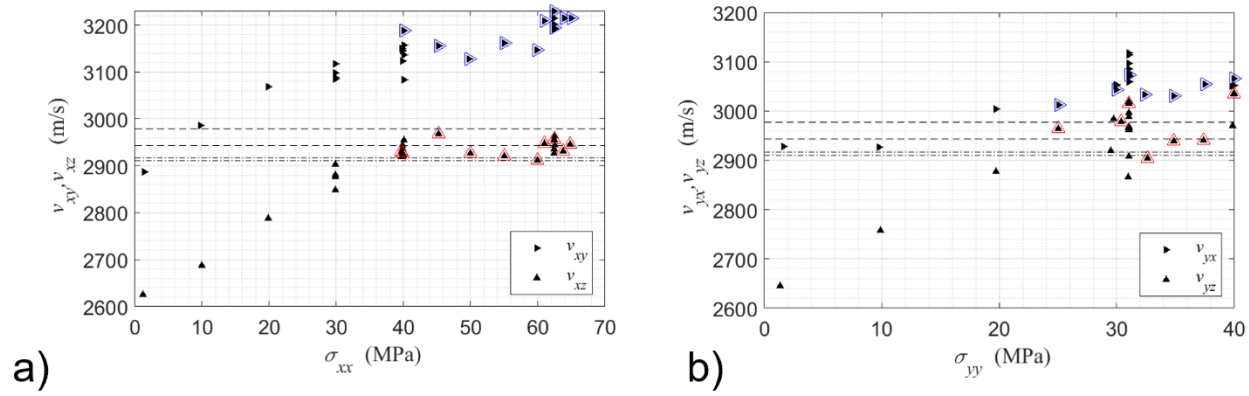

Figure 19: Shear wave velocities versus normal stress applied in the direction of wave propagation for a) x-direction, and b) y-direction. Highlighted points with colored overmarkings in this type of figure indicate results where two of the three applied stresses are fixed while the stress that is plotted on the x-axis is varied, hence experimentally taking a "partial derivative". The dashed lines give a reference to the measured shear wave velocity from well-logging, which was obtained for waves propagating in the slower vertical (z-) direction.

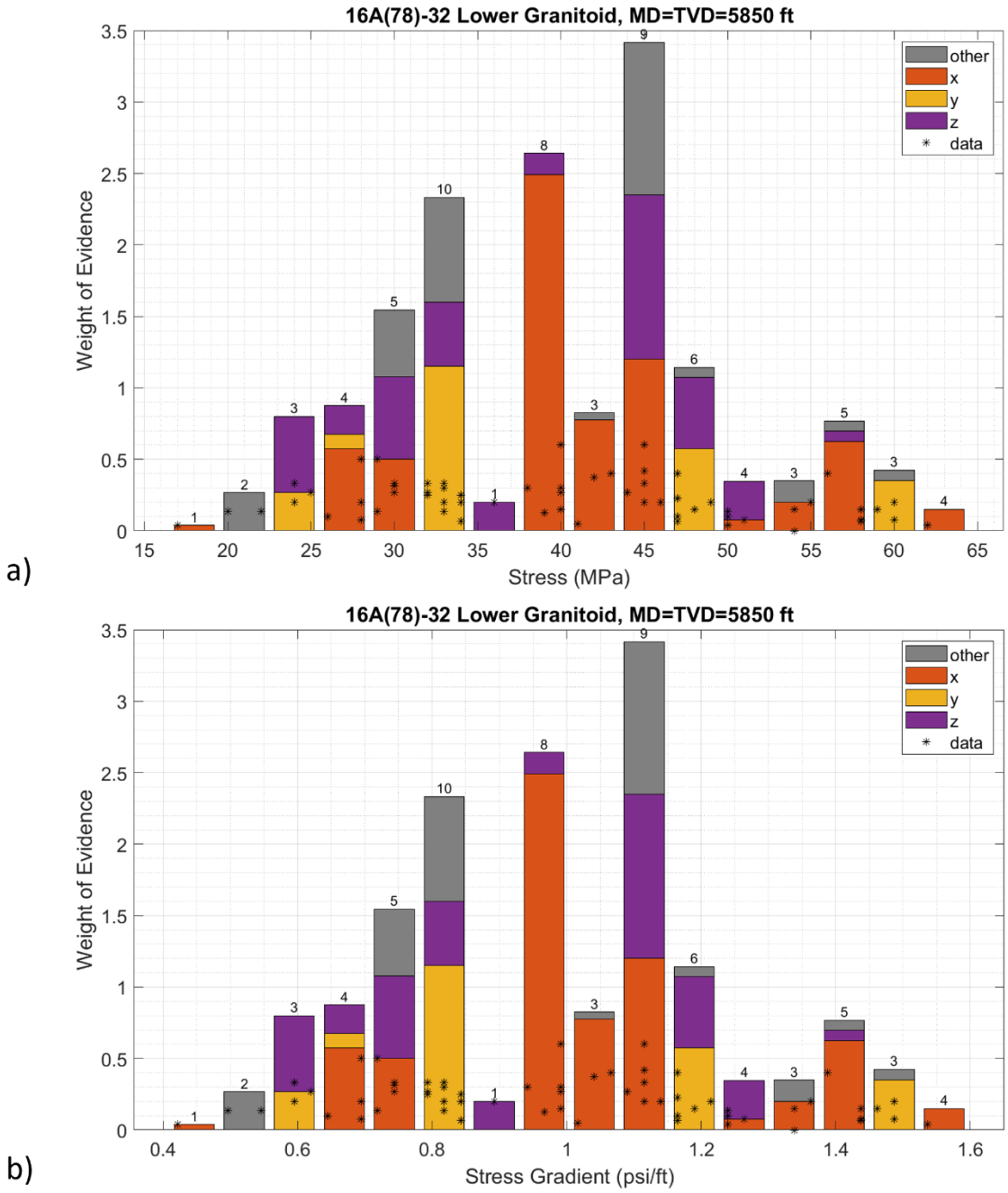

Figure 20: Integrated weight of evidence from TUV and DRA tests versus a) applied stress (axial stress in DRA experiments and normal stress in direction of propagation in TUV tests), b) corresponding implied stress gradient. The stars indicate individual data points, noting some lie directly on top of one another. The number at the top of each bar is the total lines of evidence in that bin. The bars are color coded to indicate the orientation of the sample giving the line(s) of evidence leading to that part of the bar.

X-Direction: Compendium

The 16A Lower Granitoid samples are from 5848-5850 MD and the same TVD because well is vertical to this point. There are needle-like crystals in nearly horizontal orientation and x-direction on the TUV sample is nearly aligned with these.

Running the TUV experiments, we find

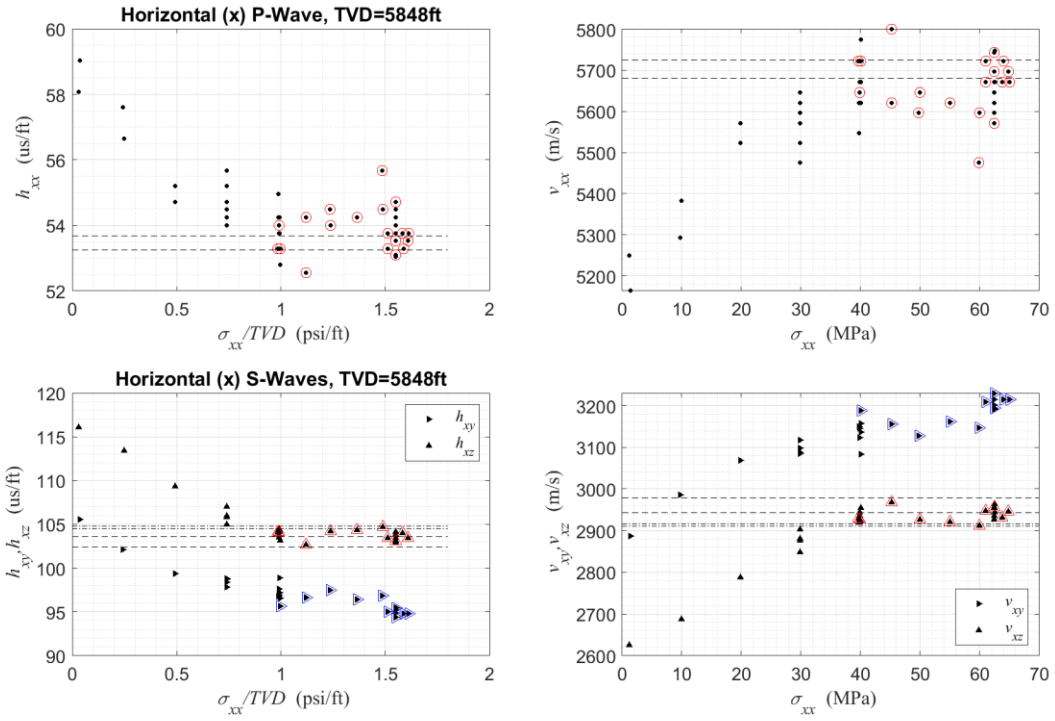

Using Eq. (1), we can estimate the quasi-isotropic elastic moduli as

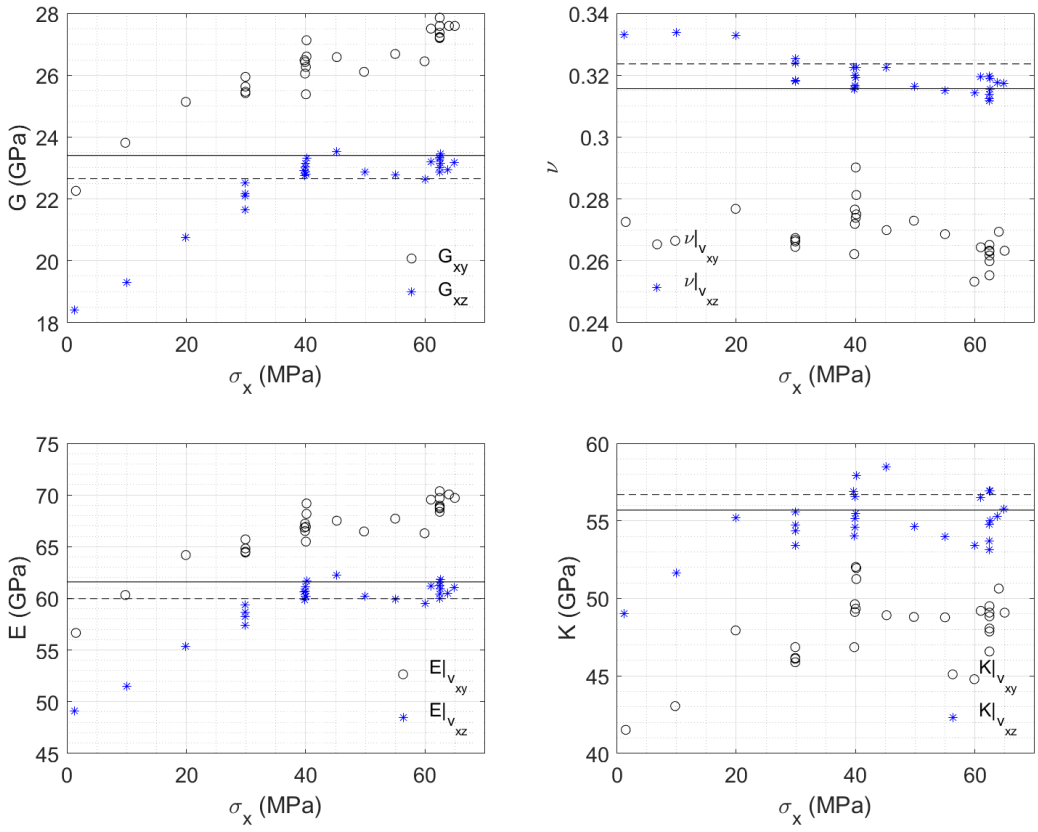

Note that the vertical polarizations lead to agreement with the well logs (shows in solid and dashed lines). This makes sense if the p-waves are nearly the same (which they are) and the velocity tensor is symmetric so that $v_{xz}=v_{zx}$ (because v_{zx} and v_{zy} are what we get from the fast and slow shear in the well log).

From the DRA on the H2 core, which is oriented at 291 degrees to the reference core axes. This is about 21 degrees misaligned relative to the x-axis of the TUV sample, but it is the closest to be chosen for comparison. Note that because of this misalignment, we expect DRA may overestimate the minimum stress. To establish repeatability, the H2 core plug was cut in half (prior to any testing) so that a repeat could be established on exactly the same material, location, and orientation. The sample geometry and sample photo are as follows:

Dimensions	
height (mm):	37.36
width (mm):	31.99
Angle retrieved (degrees):	291.3

Dimensions	
height (mm):	23.62
width (mm):	32.02
Angle retrieved (degrees):	291.3

Again, we restate that the x-direction for TUV is as 90 and 270 degrees, so there is a 21 degree misalignment between the H2 core and the x-direction of the TUV. Still, H2 is the closest to having the same orientation. DRA experiments are run with the loading sequence

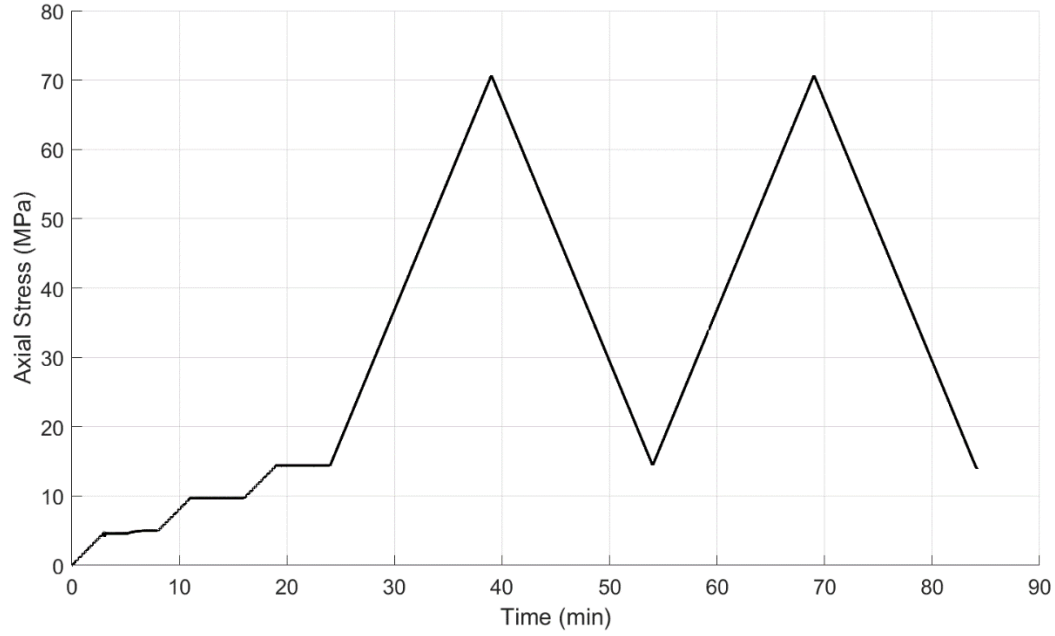

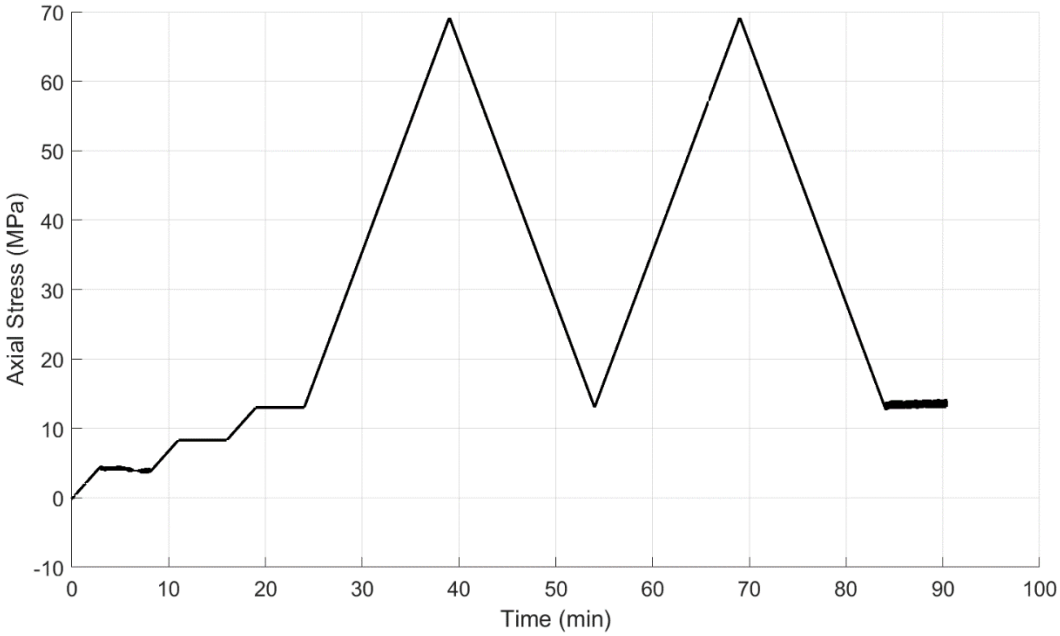

This results in the following displacements, which have been reduced by an amount estimated for deformation of 100mm of tool steel with E=210 GPa (comprising a lower bound on the platen deformation). In the second case, sample is shorter, so take 115mm of tool steel. This gives

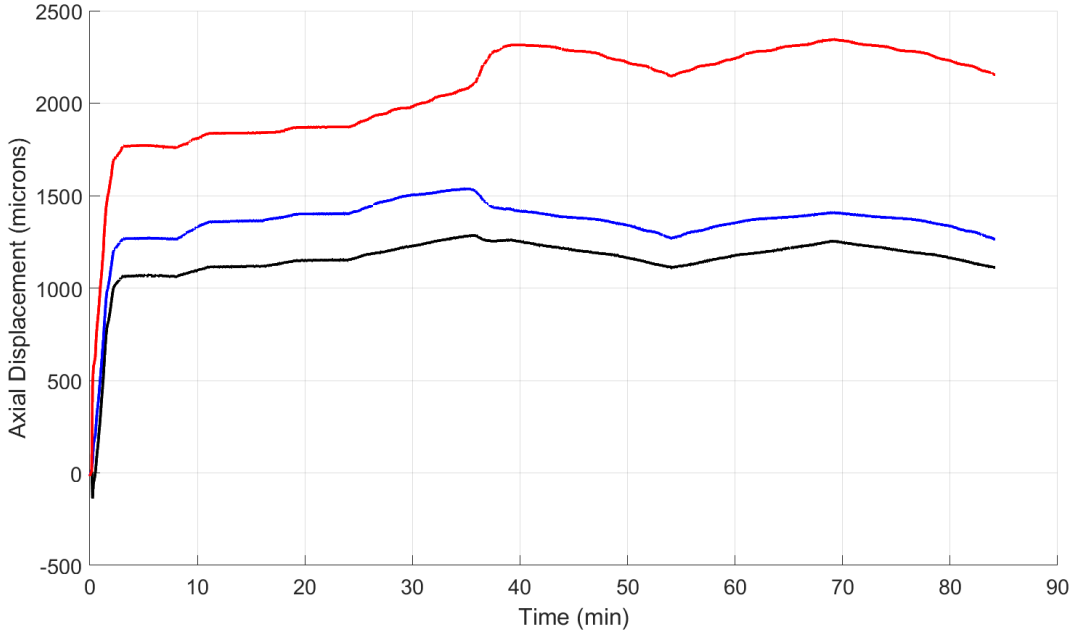

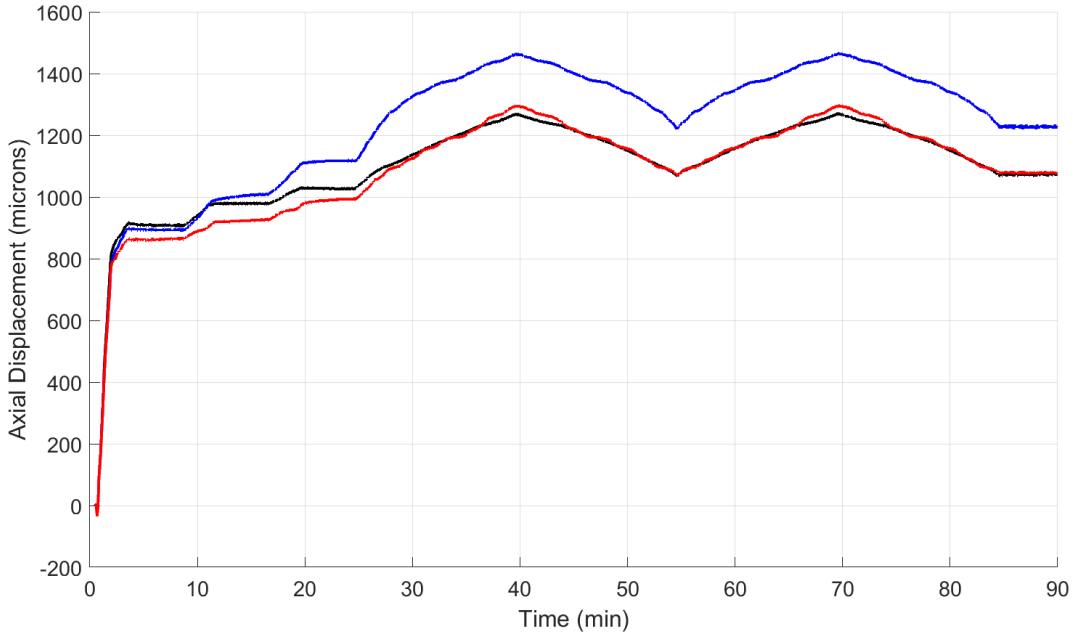

Observe that the first load cycle involved some tilting of the platens. Unclear at this point if it is local settling of platen to specimen or if there is a directional bias to the plastic deformation. Remember, the sample is inclined by about 20 degrees to the needle-like crystals.

Averaging and plotting stress versus strain relationships for the 2 load/unload cycles, setting zero strain at the beginning of the first load cycle, gives

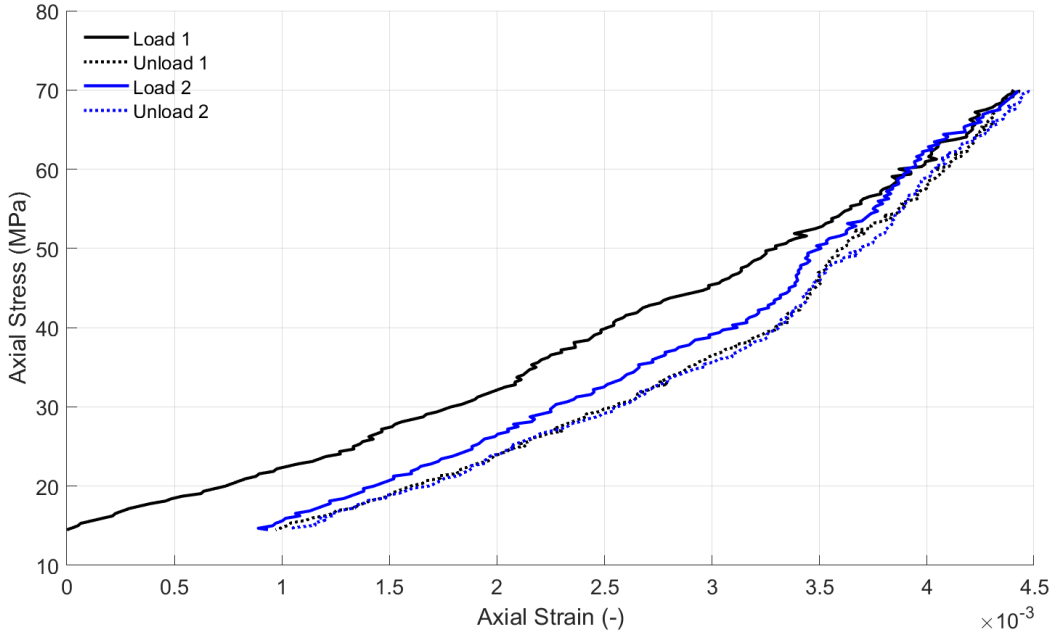

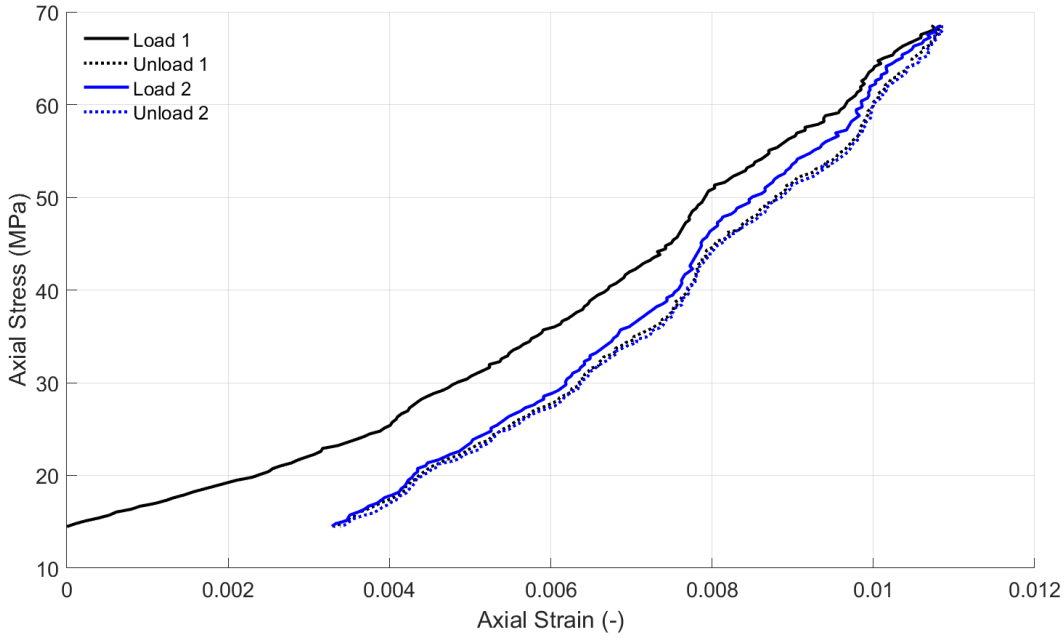

The difference between the strain measurements for the load/unload stages is given by

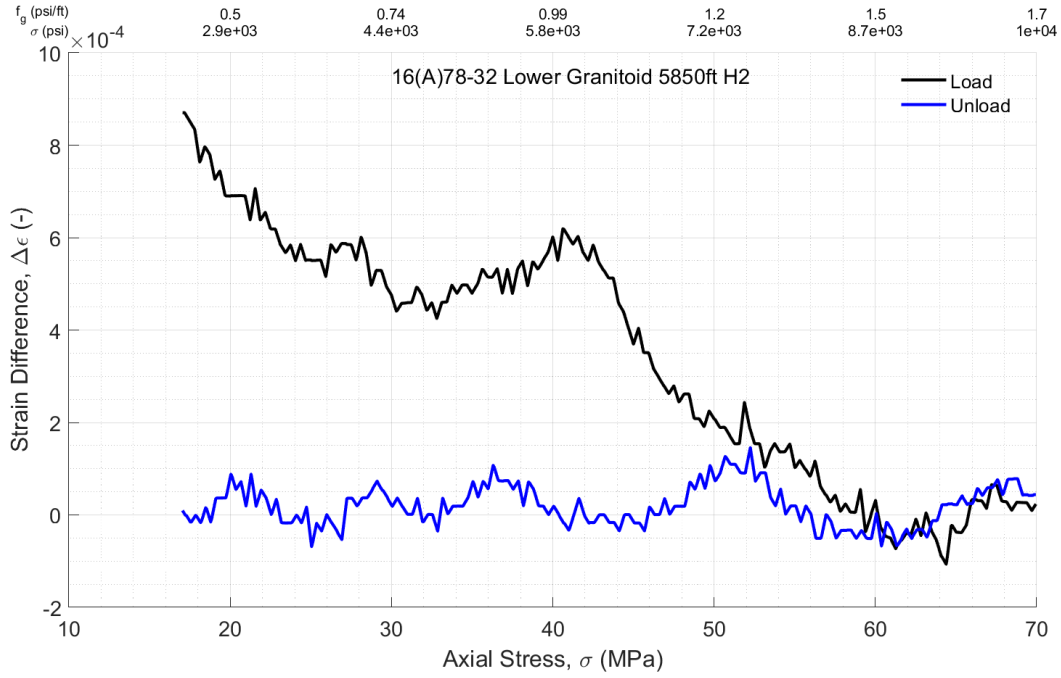

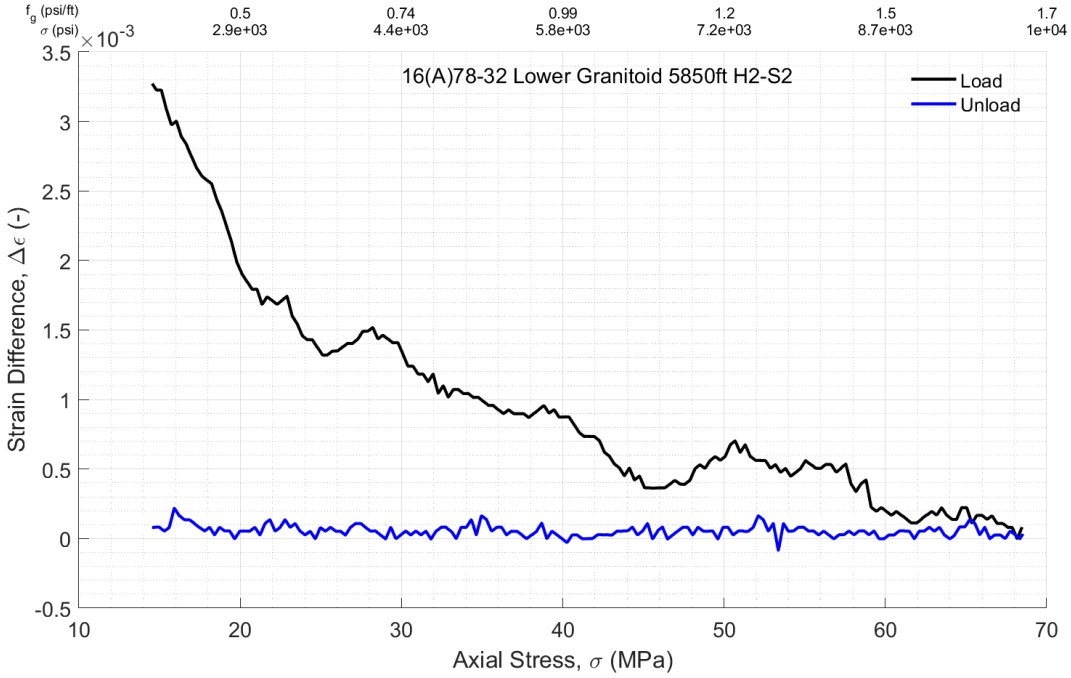

One can observe:

1) Upon the first load/unload cycle, it would interpreted that the hysteresis loop implies plastic strain around 0.001.
2) However, upon reloading, the stiffness of the material is almost exactly compensating the amount of plastic strain, so that by the end of the reloading, the stress-strain curves from the first and second loadings are nearly identical once the stress reaches about 60 MPa.
3) Both unloading curves are nearly identical.

4) At around 42 MPa of axial stress on the second loading, the specimen abruptly stiffens, bringing the curve much closer to the first loading and causing a sudden downward deflection of the strain difference.
5) The stiffening is non-monotonic. The sample stiffens in the mid-40 MPa range, then softens again, and then stiffens again. Similar non-monotonic behavior at similar stresses can be seen in the plot of dynamic E versus stress.

Bringing DRA and TUV stiffnesses together (by taking derivative of stress with respect to strain for DRA curves) gives

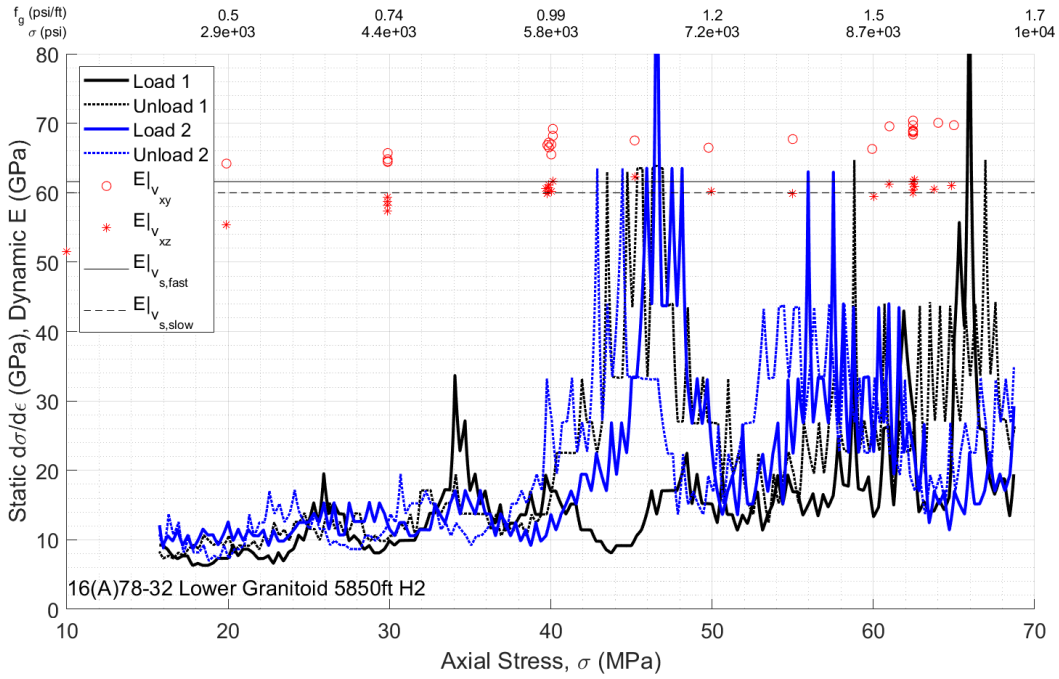

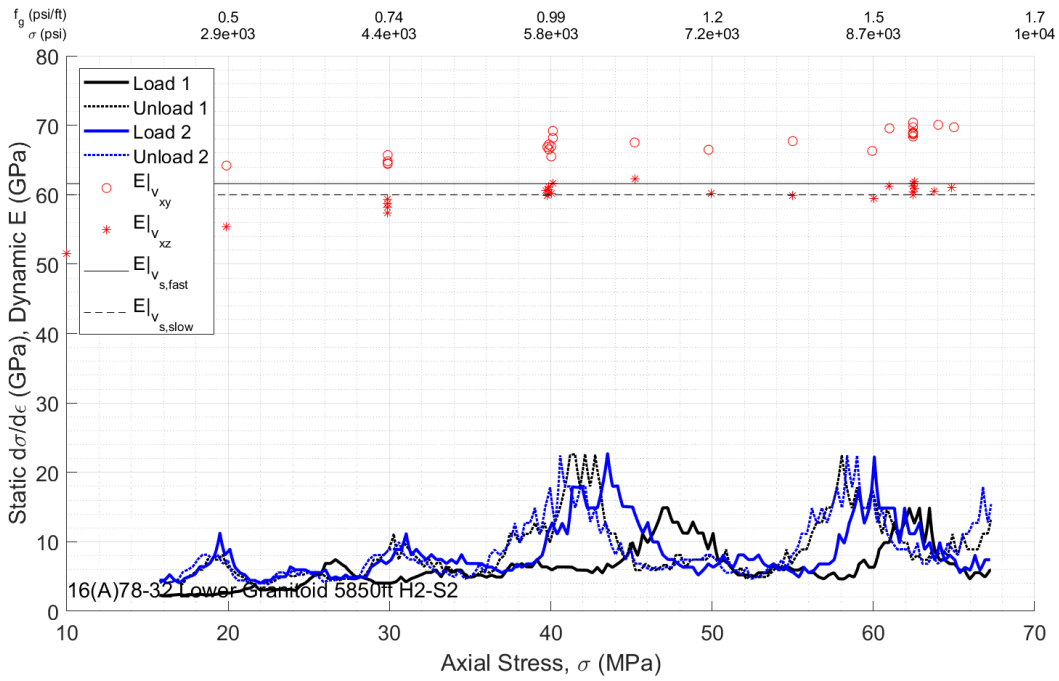

Here we observe:

1) Upon first loading, any computed value of stiffness would be well below the maximum stiffness obtained in unloading and second re-loading, and also well below dynamic values.
2) In the range of 42-48 MPa, both unloadings and the second re-loading give the same stiffness, which peaks at nearly 60 GPa (could be a bit higher if the lower bound on platen deformation is appreciably too small). The peak approaches the dynamic values from the lab and, as discussed above, the lab dynamic values are consistent with the well log values from this location in 16A.
3) After softening again, the static stiffnesses level out in the around of 30-40 GPa. The dynamic values of E also level out in this range of stresses, but at values much above the static values.
4) There is a small shift of unloading to lower stresses, which could indicate there is some time dependence (viscoelasticity) in the material response.

Additionally, we can make a similar plot (though DRA only) but putting strain on the x-axis:

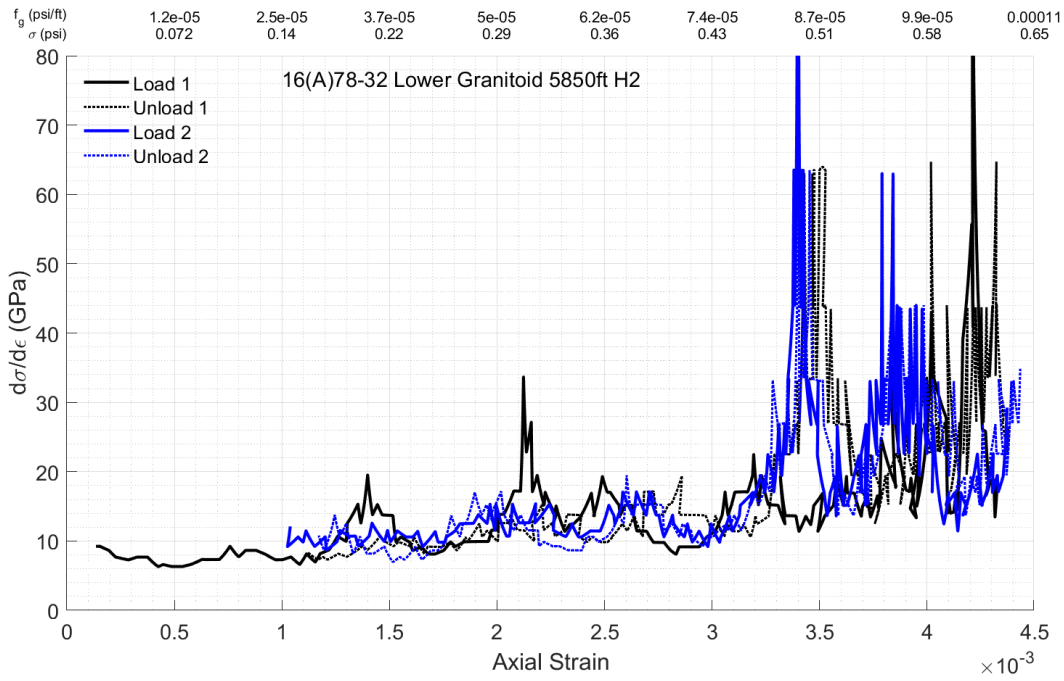

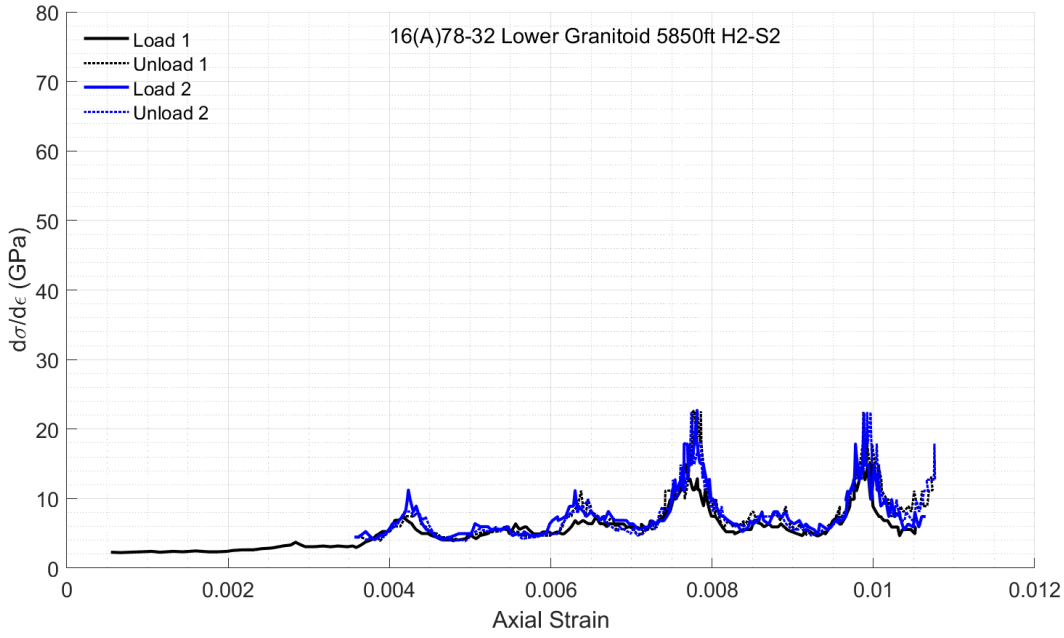

It looks like there is potentially a certain strain where the sample is stiffest, although in this case the stiffening does not appear on the first loading.

Y-Direction: Compendium

The 16A Lower Granitoid samples are from 5848-5850 MD and the same TVD because well is vertical to this point. There are needle-like crystals in nearly horizontal orientation and y-direction on the TUV sample is nearly perpendicular to these.

Running the TUV experiments, we find

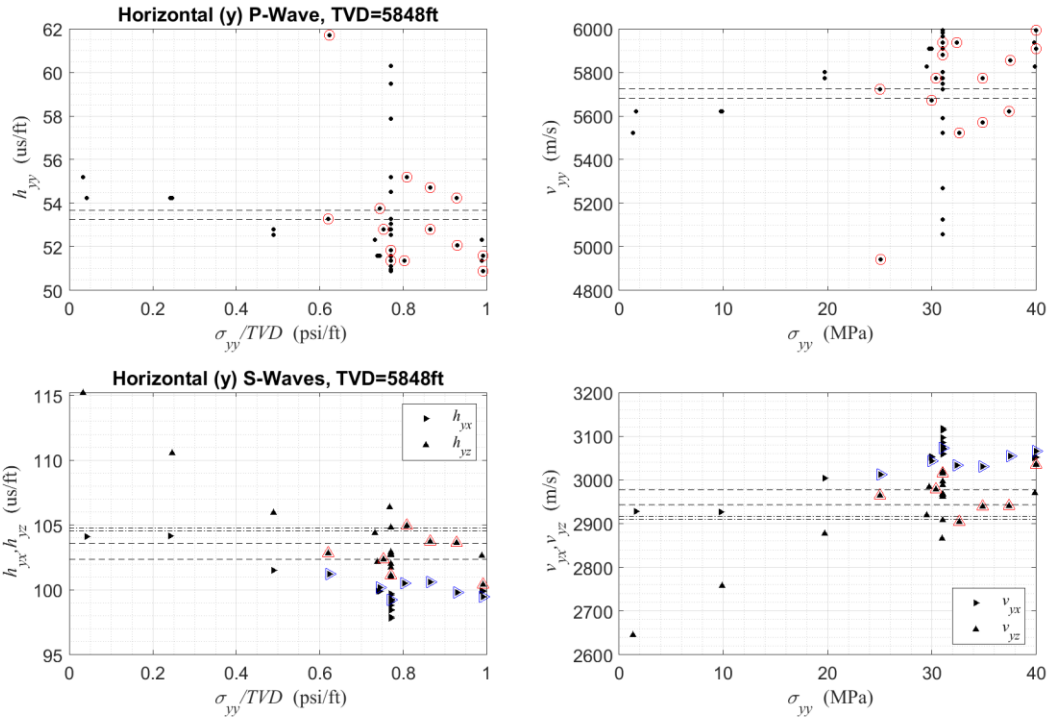

By Eq. (1), the quasi-isotropic elastic moduli are

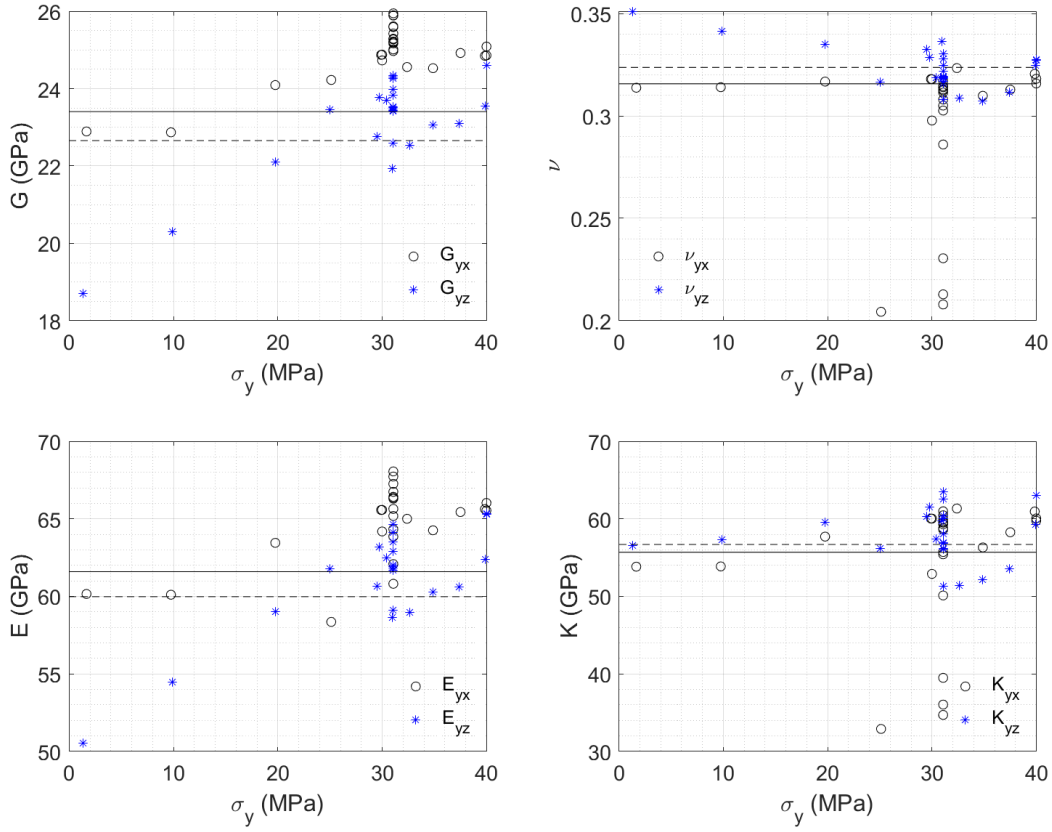

Again the vertical polarizations lead to agreement with the well logs (shows in solid and dashed lines). This makes sense if the p-waves are nearly the same (which they are) and the velocity tensor is symmetric so that v_{yz}=v_{zy} (because v_{zx} and v_{zy} are what we get from the fast and slow shear in the well log).

From the DRA on the H1 core, which is oriented at 0 degrees to the chosen axes. Have to check this, but it seems it is more directly aligned relative to the internal fabric, rather than having the 20 degree offset that was in H2.

Dimensions	
height (mm):	38.37
width (mm):	32.07
Angle retrieved (degrees):	0

The y-direction for TUV is 0 degrees, so there is a 0 degree misalignment between the H1 core and the y-direction of the TUV. DRA experiments are run with the loading sequence

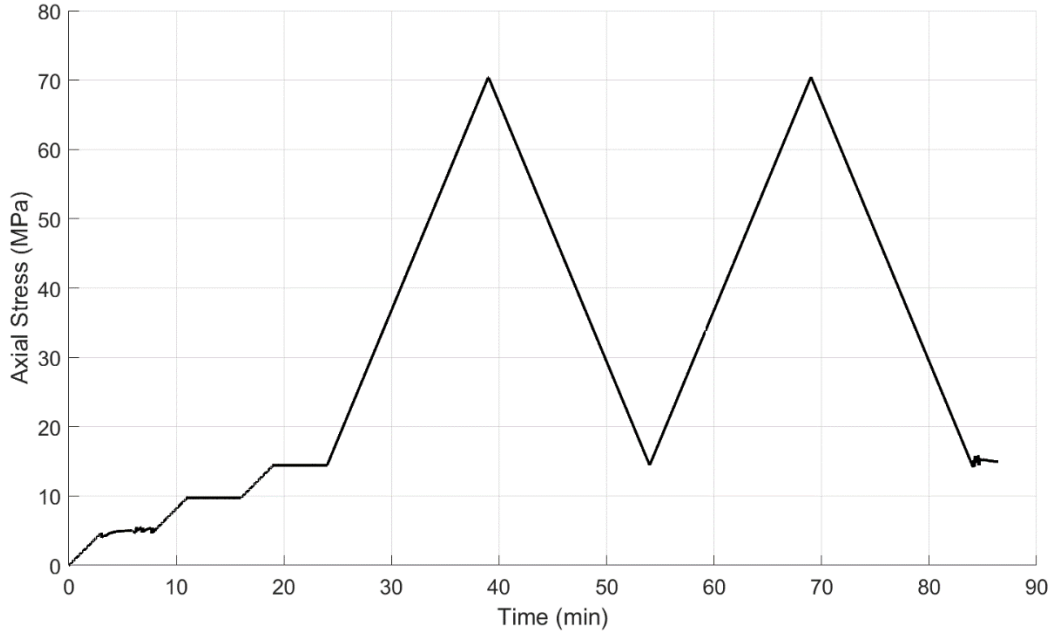

This results in the following displacements, which have been reduced by an amount estimated for deformation of 100mm of tool steel with E=210 GPa (comprising a lower bound on the platen deformation). This gives

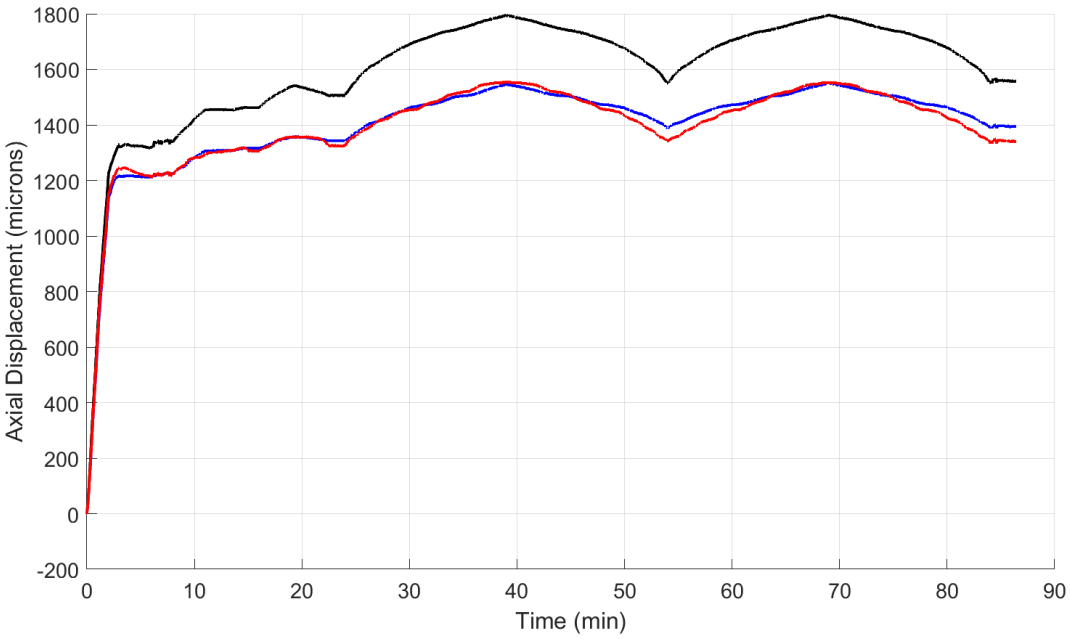

Averaging and plotting stress versus strain relationships for the 2 load/unload cycles, setting zero strain at the beginning of the first load cycle, gives

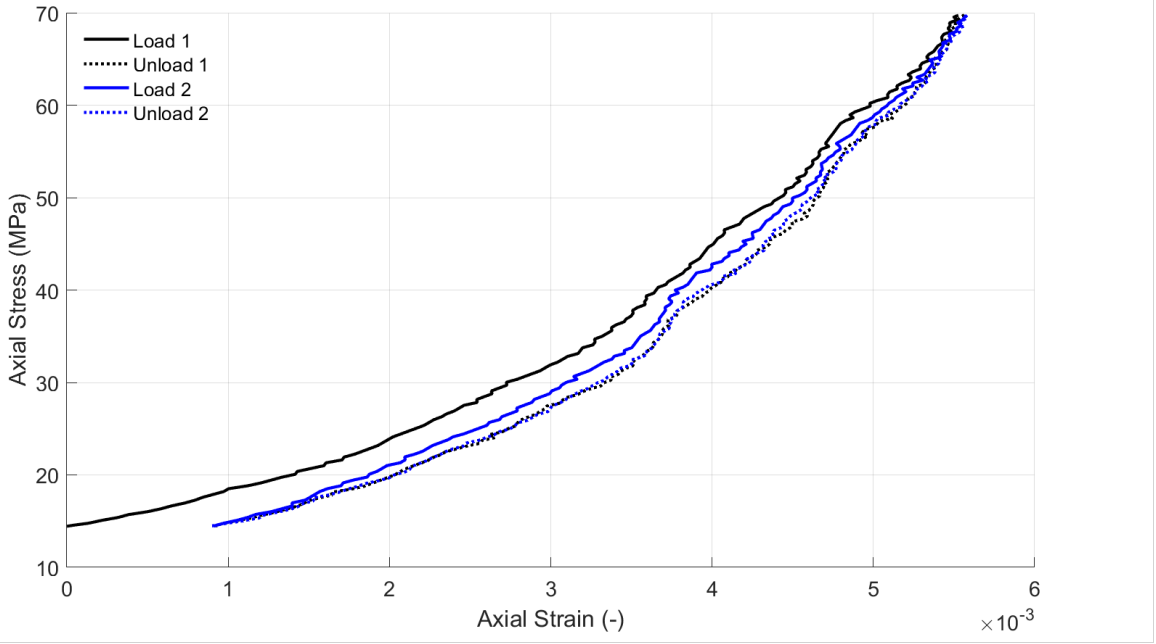

The difference between the strain measurements for the load/unload stages is given by

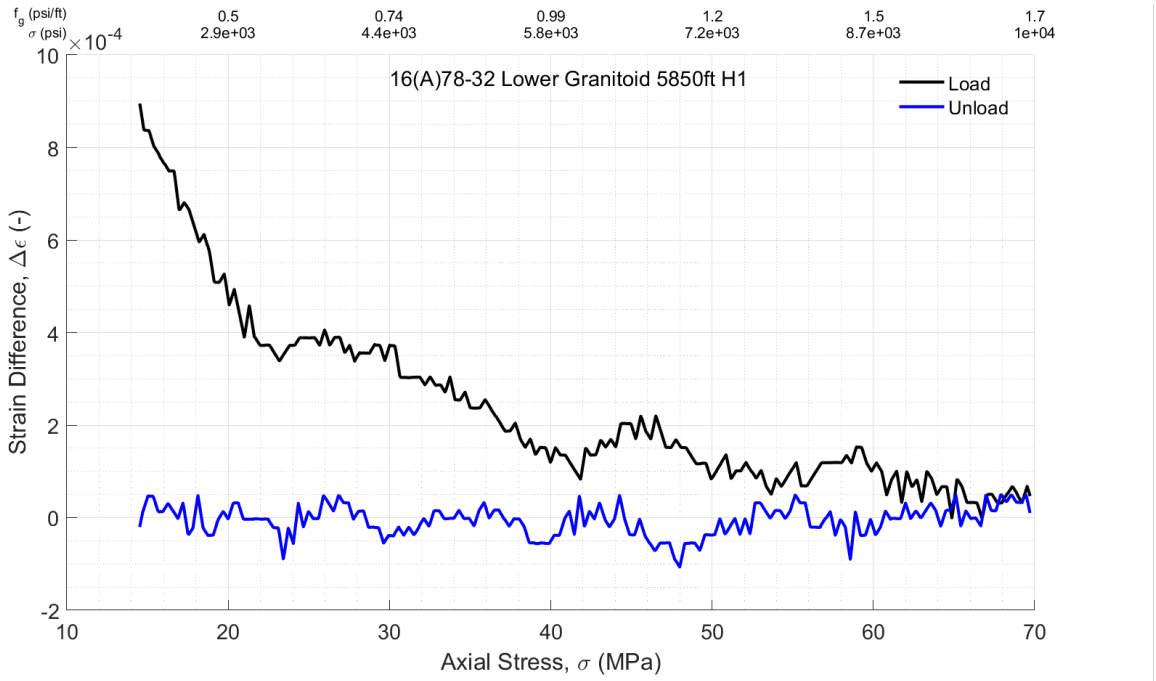

One can observe:

1) Upon the first load/unload cycle, it would interpreted that the hysteresis loop implies plastic strain around 0.001. This is basically the same as H2.
2) However, upon reloading, the stiffness of the material is almost exactly compensating the amount of plastic strain, so that by the end of the reloading, the stress-strain curves from the first and

second loadings are nearly identical once the stress reaches about 60 MPa. This is also very similar to H2.

3) Both unloading curves are nearly identical. Also very similar to H2.
4) At around 32 MPa of axial stress on the second loading, the specimen abruptly stiffens, bringing the curve much closer to the first loading and causing a sudden downward deflection of the strain difference. This is a lower stress compared to 42 MPa for H2 sample.
5) The stiffening is non-monotonic. The sample stiffens in the ~50 MPa range, then softens again, and then stiffens again. Similar non-monotonic behavior at similar stresses can be seen in the wavespeeds, though not as clearly due to the stress combinations used in this direction. Clearest is if one takes the fixed x- and z- stress cases with the velocity v_{yx}.

Bringing DRA and TUV stiffnesses together (by taking derivative of stress with respect to strain for DRA curves) gives

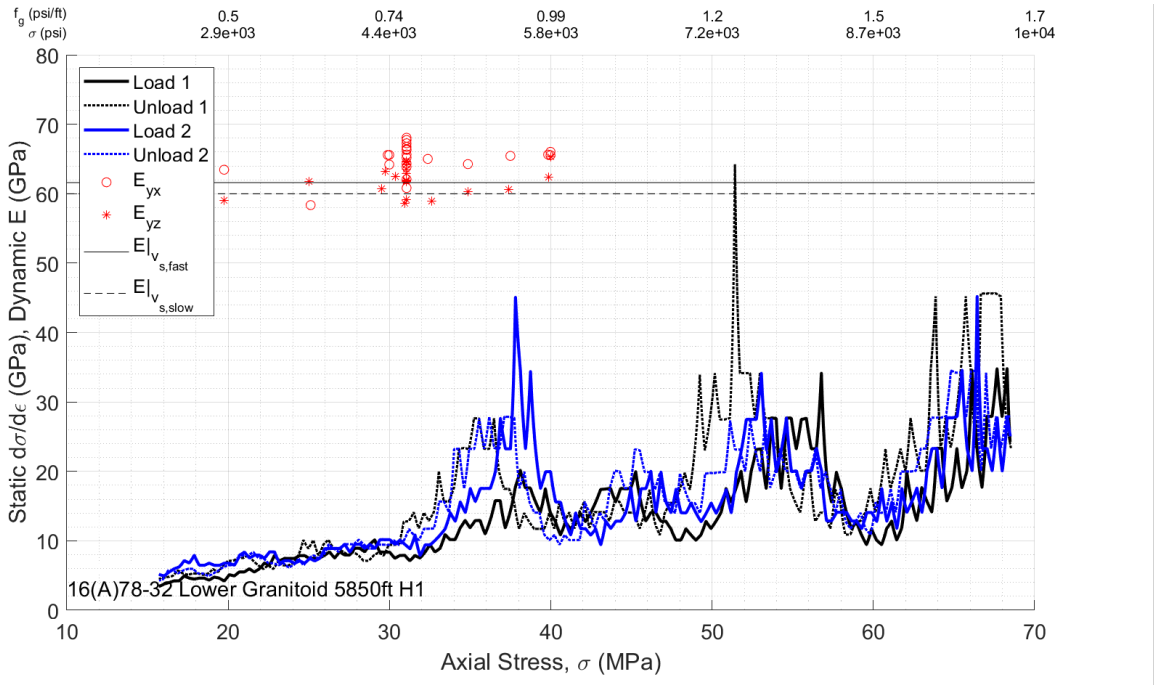

Here we observe:

1) Upon first loading, any computed value of stiffness would be well below the maximum stiffness obtained in unloading and second re-loading, and also well below dynamic values.
2) In the range of 32-40 MPa, both unloadings and the second re-loading give the same stiffness, which peaks at around 25 GPa (could be a bit higher if the lower bound on platen deformation is appreciably too small). The peak approaches the estimated static (if those can be trusted) for the well log from this location in 16A.
3) After softening again, the static stiffnesses increase and then decrease again between 50-58 MPa.
4) There is a small shift of unloading to lower stresses, which could indicate there is some time dependence (viscoelasticity) in the material response.

Additionally, we can make a similar plot (though DRA only) but putting strain on the x-axis:

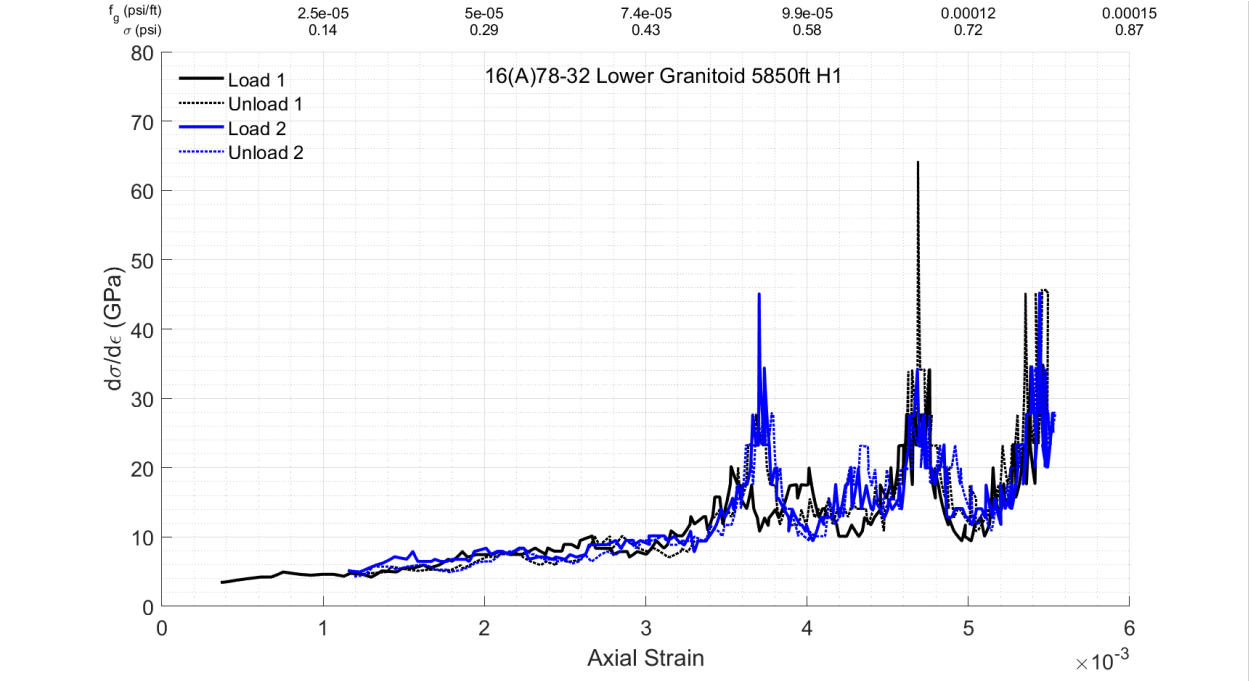

It looks like there is potentially a certain strain (actually two distinct strains) where the sample is stiffest. The strain is actually similar to strain at which the second stiffening occurred in the H2-1 sample. The second stiffening is much more distinct.

The H1 core was not long enough to make two samples for testing.

H3-Direction: Compendium

The H3 core plug for DRA is oblique to the TUV testing axes and to the needle-like fabric. Specifically, the DRA H3 core is oriented at 53 degrees to the chosen axes. Hence it is 53 degrees from H1 and around 58 degrees from H2, with H1 and H2 at 111 degrees from one another (with H3 in between them). It appears to be about 30-40 degrees from aligned with the fabric, which makes sense if H1 is misaligned to the fabric by around 20 degrees (to the other side). There are actually two core, and here the results will be shown with H3-1 first then H3-2.

H3-1

Dimensions	
height (mm):	38.72
width (mm):	32.04
Angle retrieved (degrees):	53.4

H3-2

Dimensions	
height (mm):	41.76
width (mm):	32.04
Angle retrieved (degrees):	53.4

DRA experiments are run with the loading sequence

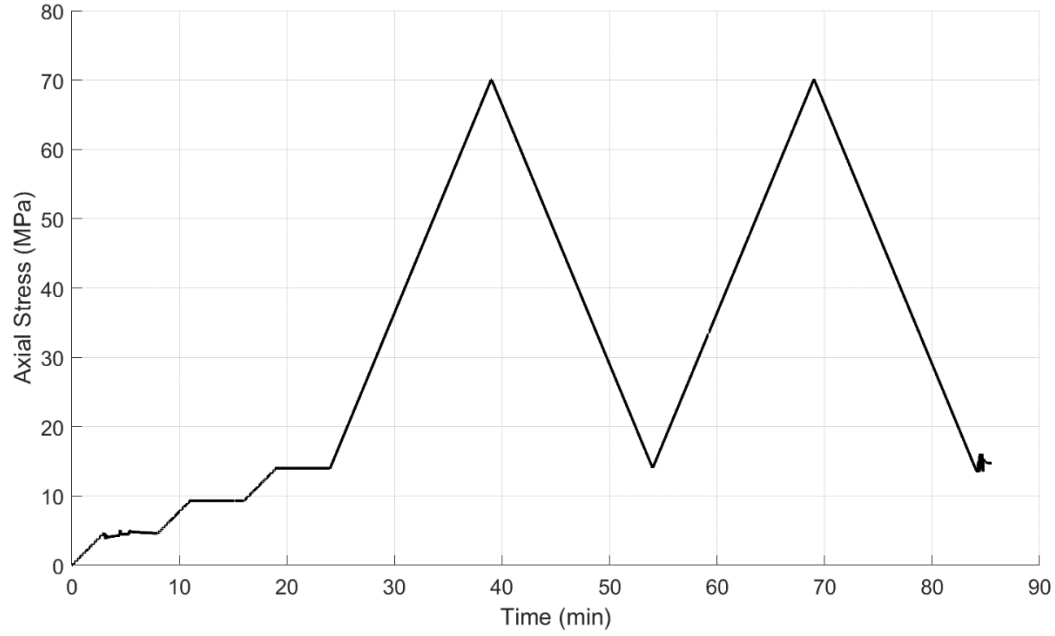

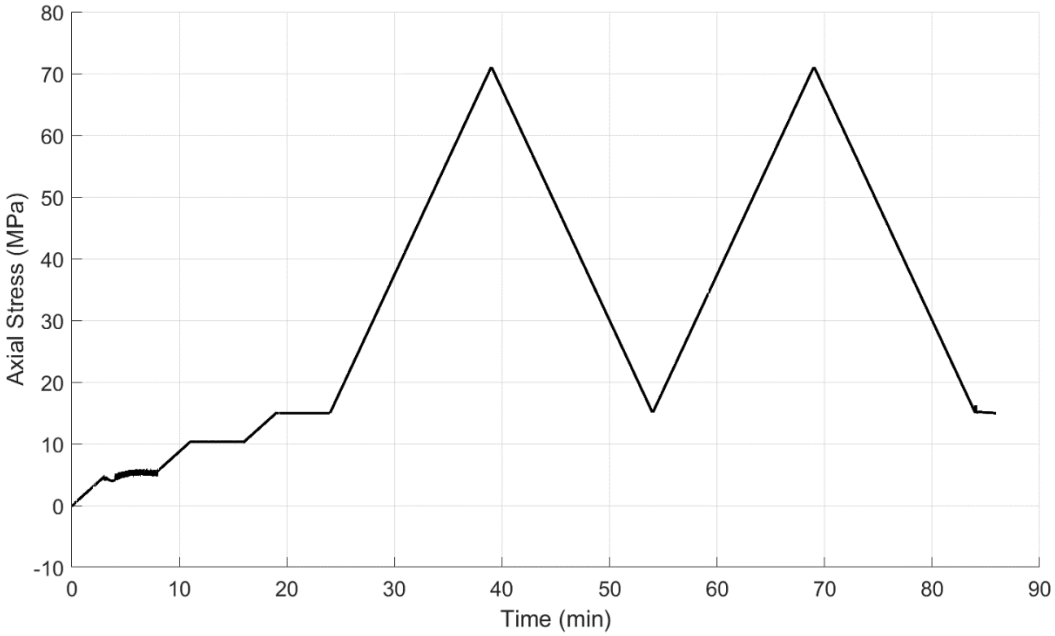

This results in the following displacements, which have been reduced by an amount estimated for deformation of 100mm of tool steel with E=210 GPa (comprising a lower bound on the platen deformation). This gives

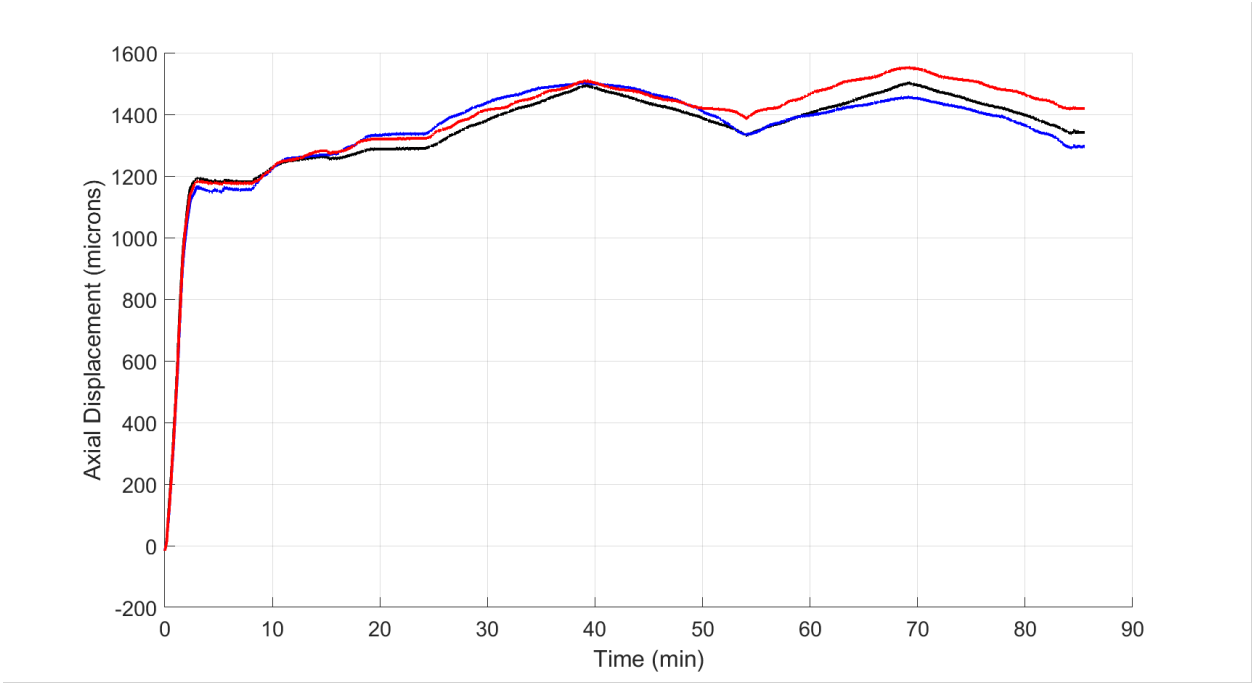

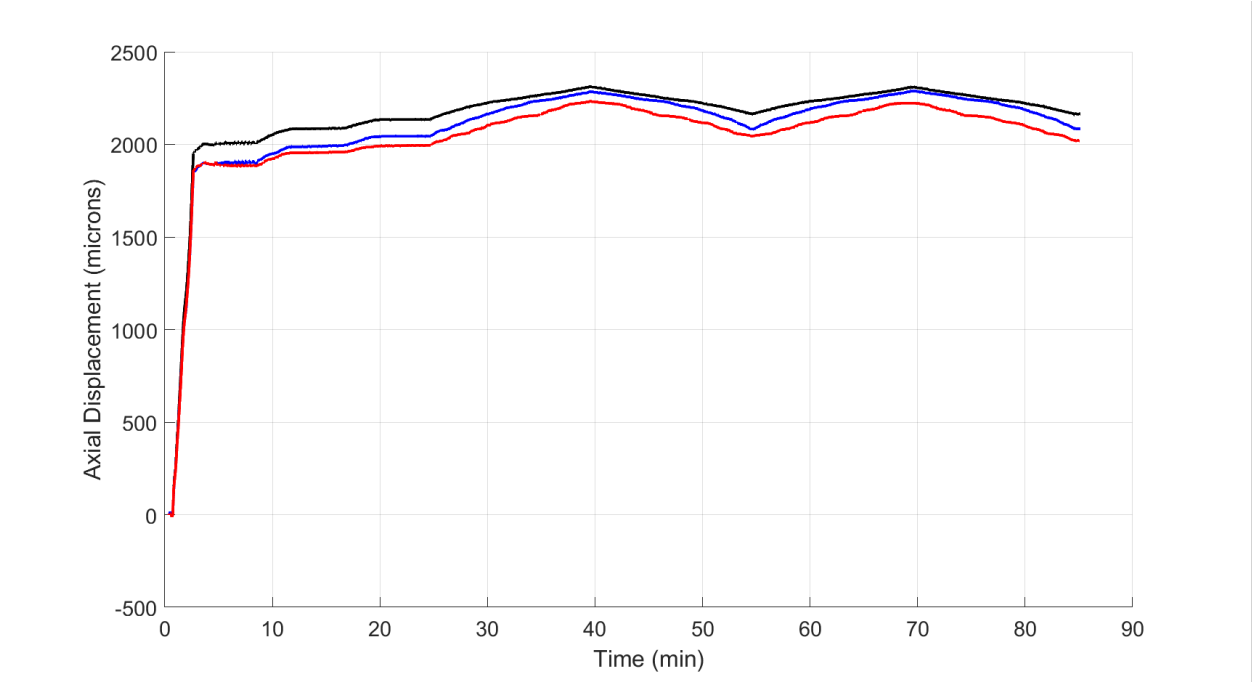

Averaging and plotting stress versus strain relationships for the 2 load/unload cycles, setting zero strain at the beginning of the first load cycle, gives

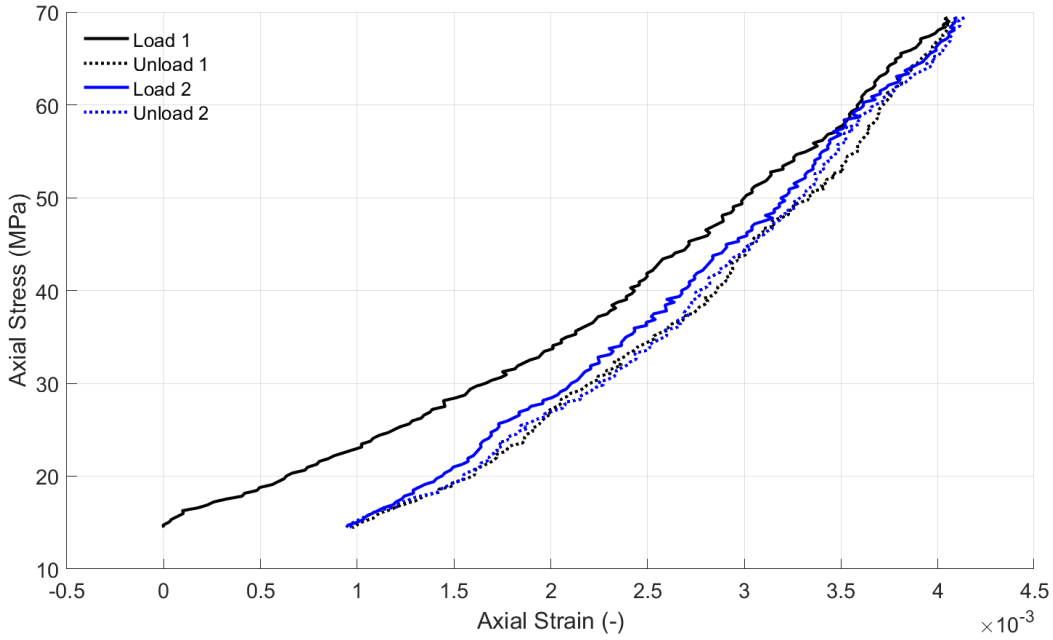

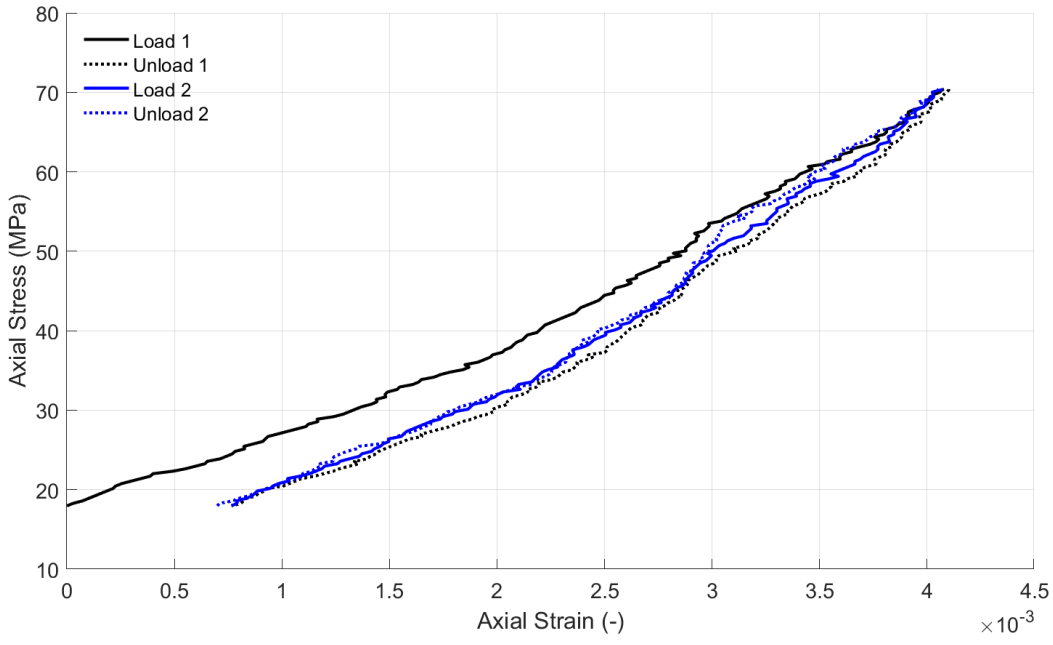

The difference between the strain measurements for the load/unload stages is given by

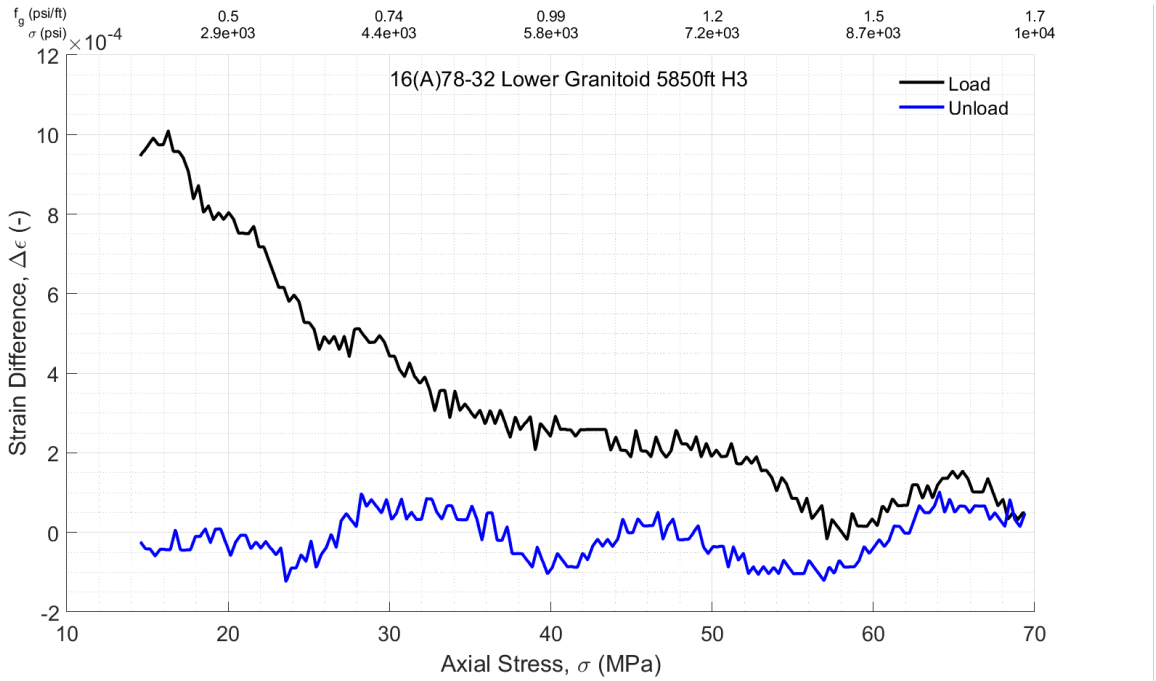

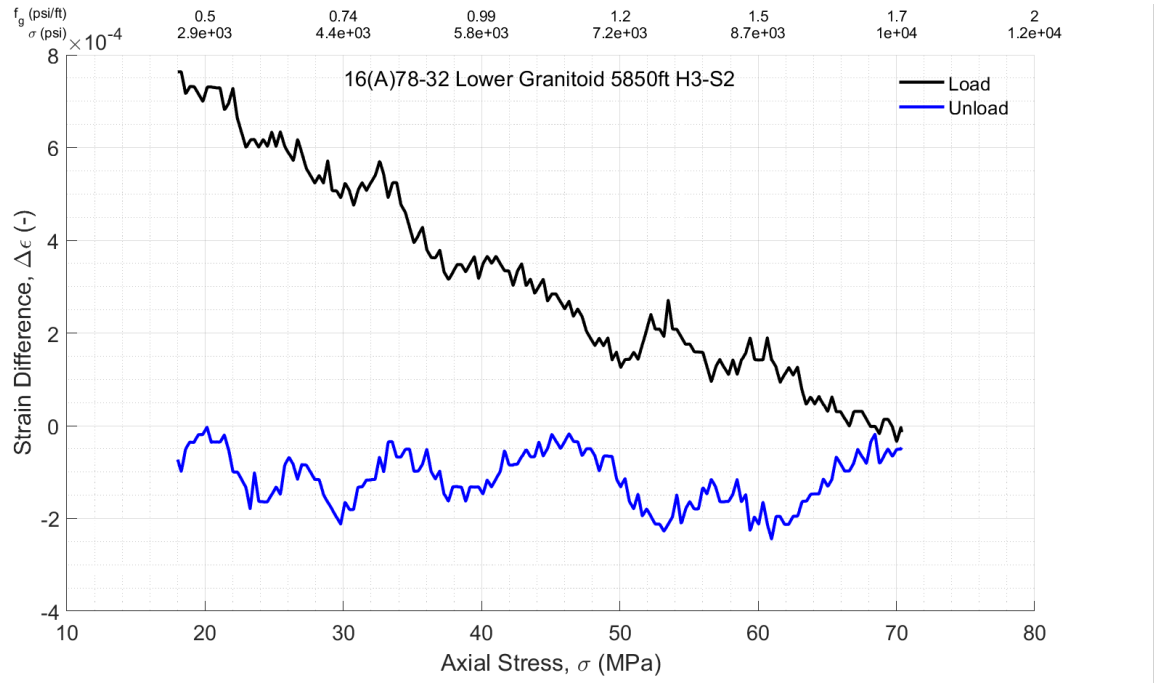

One can observe:

1) Upon the first load/unload cycle, it would interpreted that the hysteresis loop implies plastic strain around 0.001. This is basically the same as H1 and H2.
2) Again, upon reloading, the stiffness of the material is almost exactly compensating the amount of plastic strain, so that by the end of the reloading, the stress-strain curves from the first and second loadings are nearly identical once the stress reaches about 60 MPa. This is also very similar to H2.
3) Both unloading curves are similar to one another, as was the case with H1 and H2.

4) It does not appear that there is the distinctive non-monotonic stiffening.

Bringing DRA and TUV stiffnesses together (by taking derivative of stress with respect to strain for DRA curves) gives (here showing TUV for x-direction, just to have another example that is oblique to fabric, although in the present case we may be closer to 40 degrees to fabric).

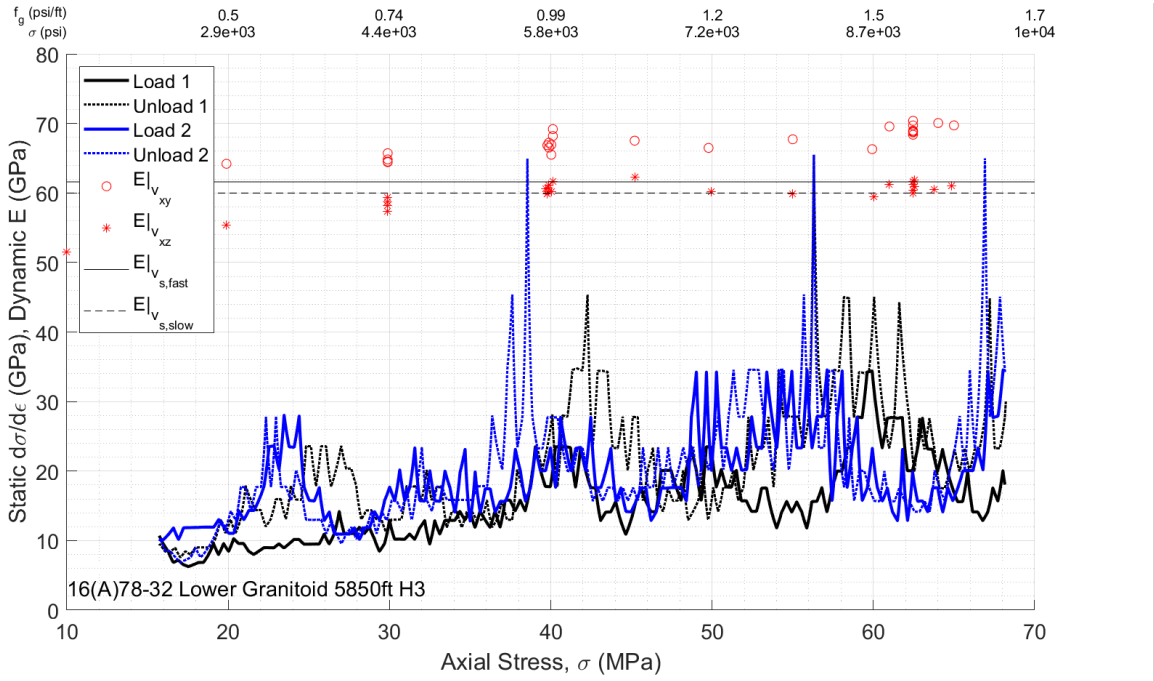

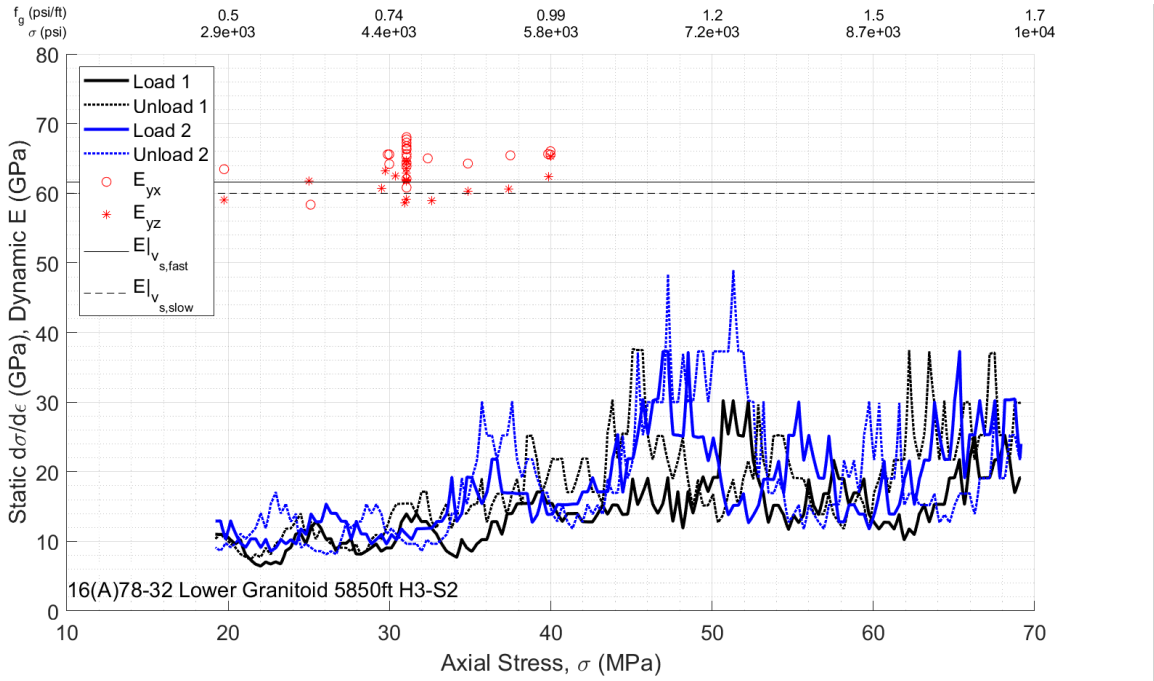

Here we observe:

1) Overall, the static stiffness values are somewhere between the y and x directions

2) There might be some systematic changes – maybe around 38 MPa for example – but it is far less distinct compared to the cases that are better aligned (or only slightly oblique) to the fabric.
3) Both cases are more like a monotonic stiffening with a final plateau or just reduction in rate of increase.

Additionally, we can make a similar plot (though DRA only) but putting strain on the x-axis:

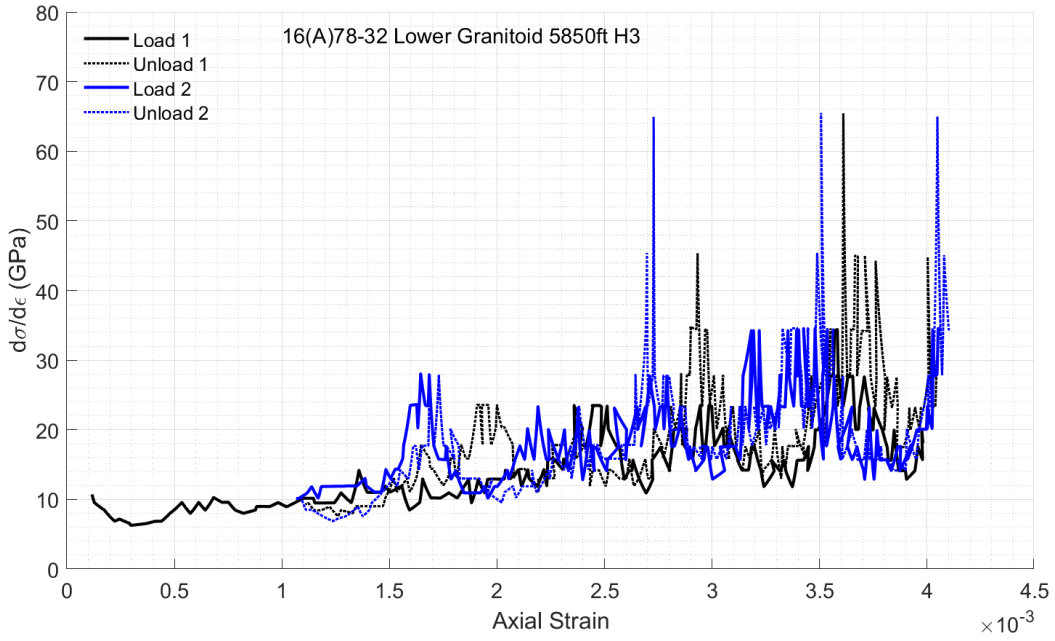

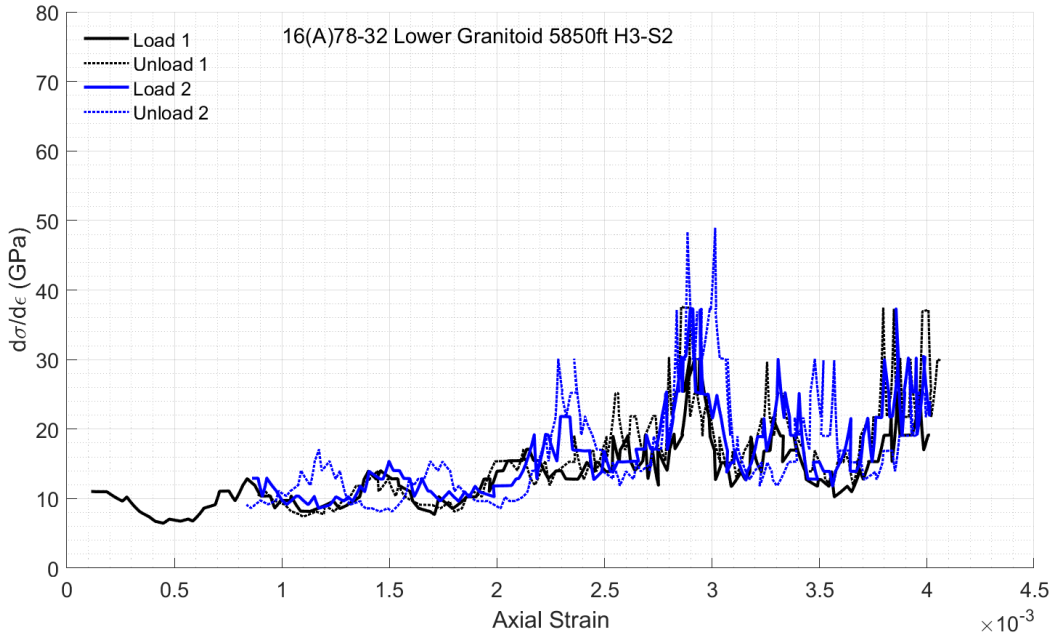

Again, there is not the distinct strain point where the sample stiffens. Perhaps in H3-2 there is something at around a strain of 0.0032, but it is not as striking as in other cases. So, it appears that when the sample is approaching 45 degrees to the fabric, there is a more monotonic behavior.

Z-Direction: Compendium

The 16A Lower Granitoid samples are from 5848-5850 MD and the same TVD because well is vertical to this point. There are needle-like crystals in nearly horizontal orientation and z-direction (vertical) on the TUV sample is therefore nearly perpendicular to these.

Running the TUV experiments, we find

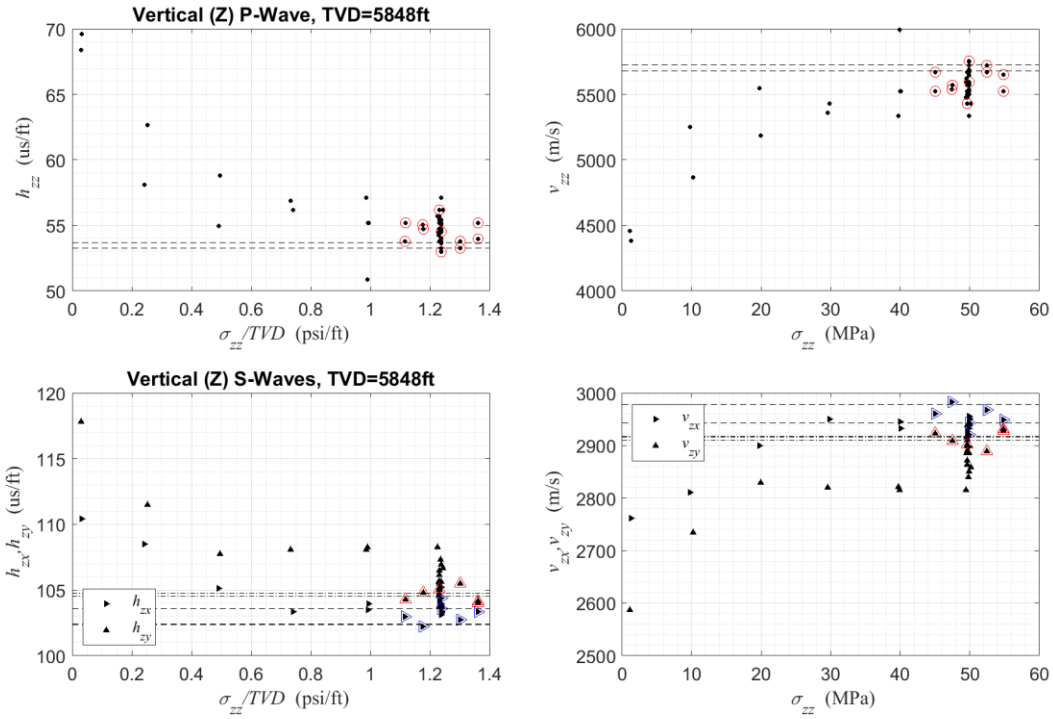

From Eq. (1), the quasi-isotropic elastic moduli are given by

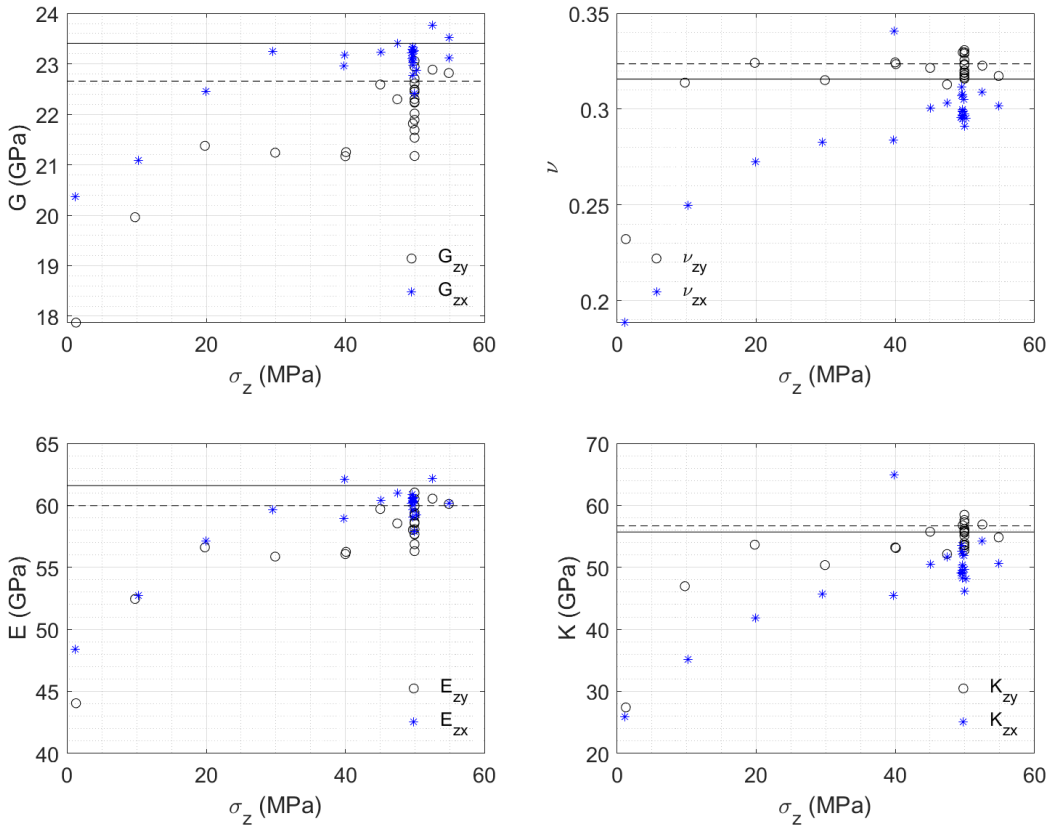

The vertical waves lead to agreement with the well logs (shows in solid and dashed lines). This makes sense because this is the direction of propagation for the sonic logging tool.

From the DRA on the V core, which is oriented vertically and hence perpendicular to the fabric:

Dimensions	
height (mm):	31.32
width (mm):	32.10
Angle retrieved (degrees):	0

The z-direction for TUV is vertical, so there is a 0 degree misalignment between the V core and the y-direction of the TUV. DRA experiments are run with the loading sequence

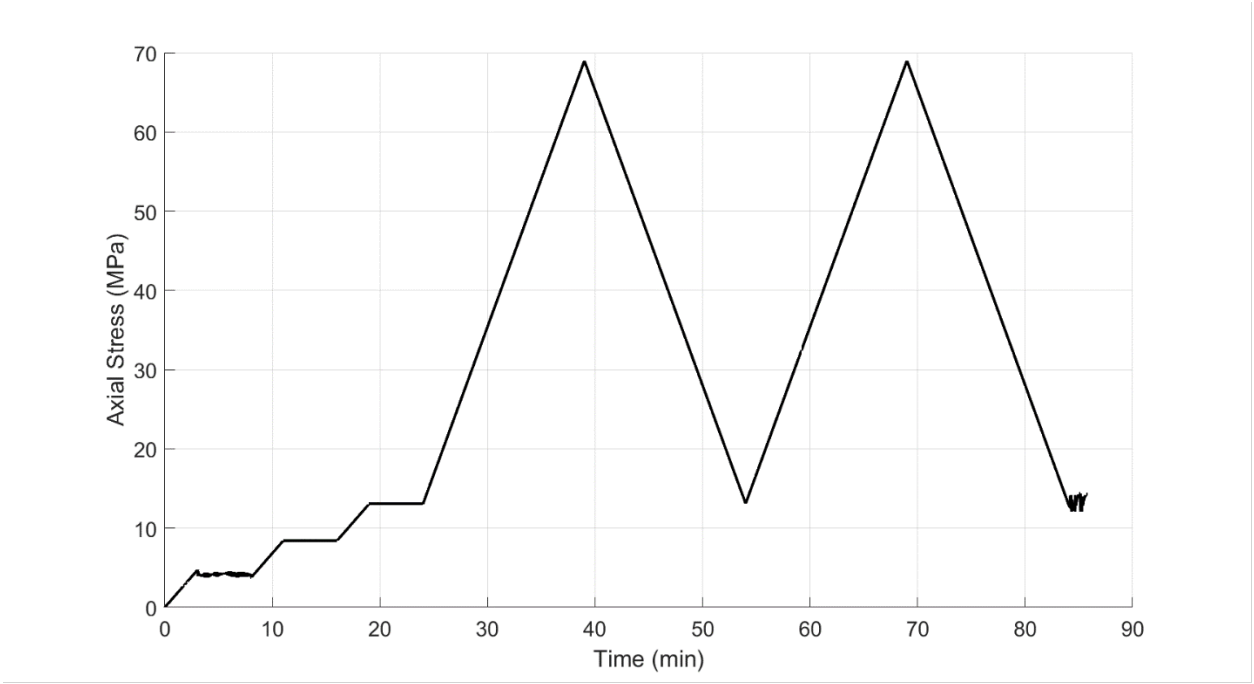

This results in the following displacements, which have been reduced by an amount estimated for deformation of 100mm of tool steel with E=210 GPa (comprising a lower bound on the platen deformation). This gives

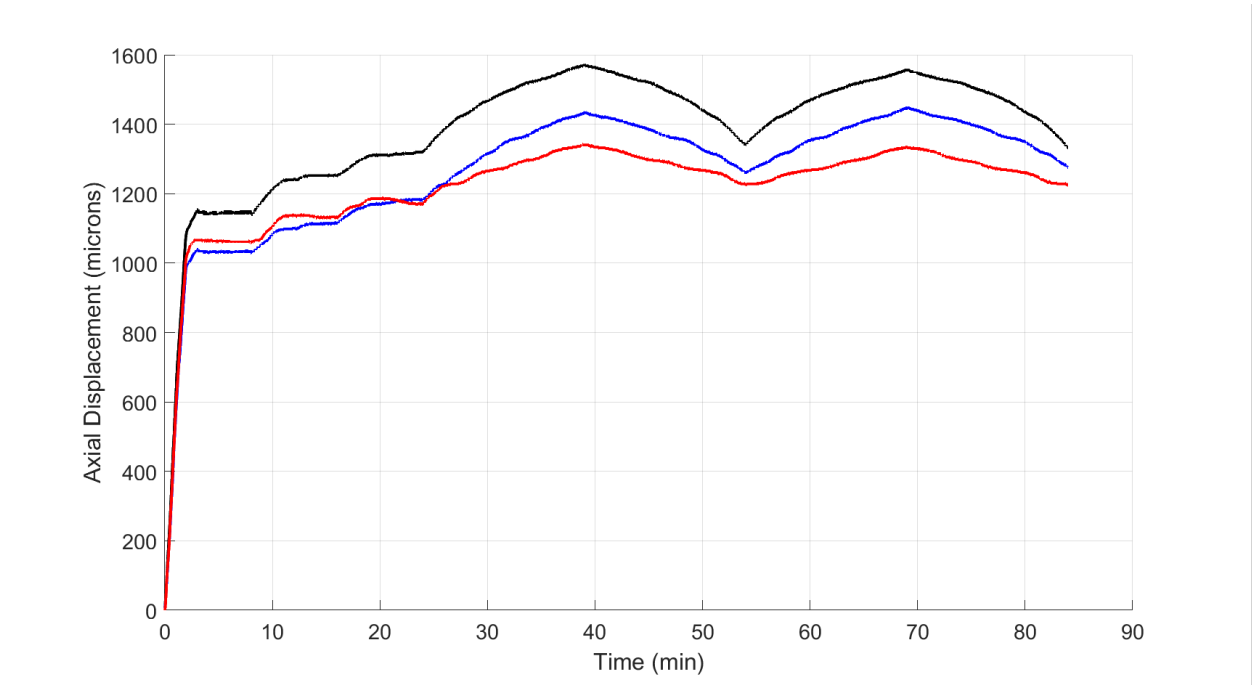

Averaging and plotting stress versus strain relationships for the 2 load/unload cycles, setting zero strain at the beginning of the first load cycle, gives

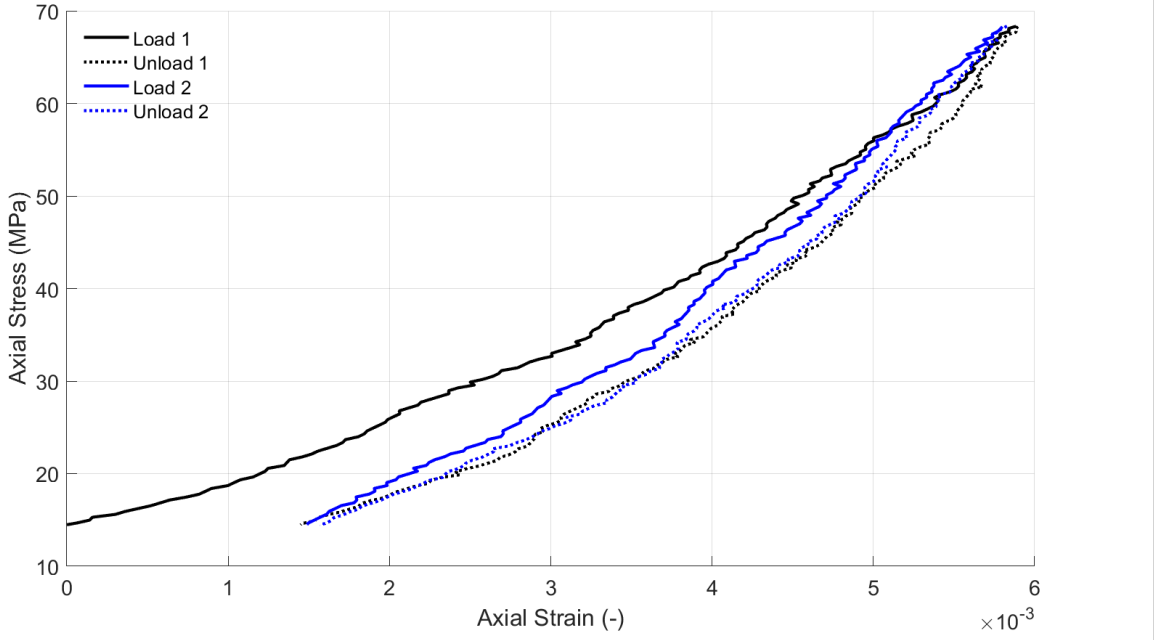

The difference between the strain measurements for the load/unload stages is given by

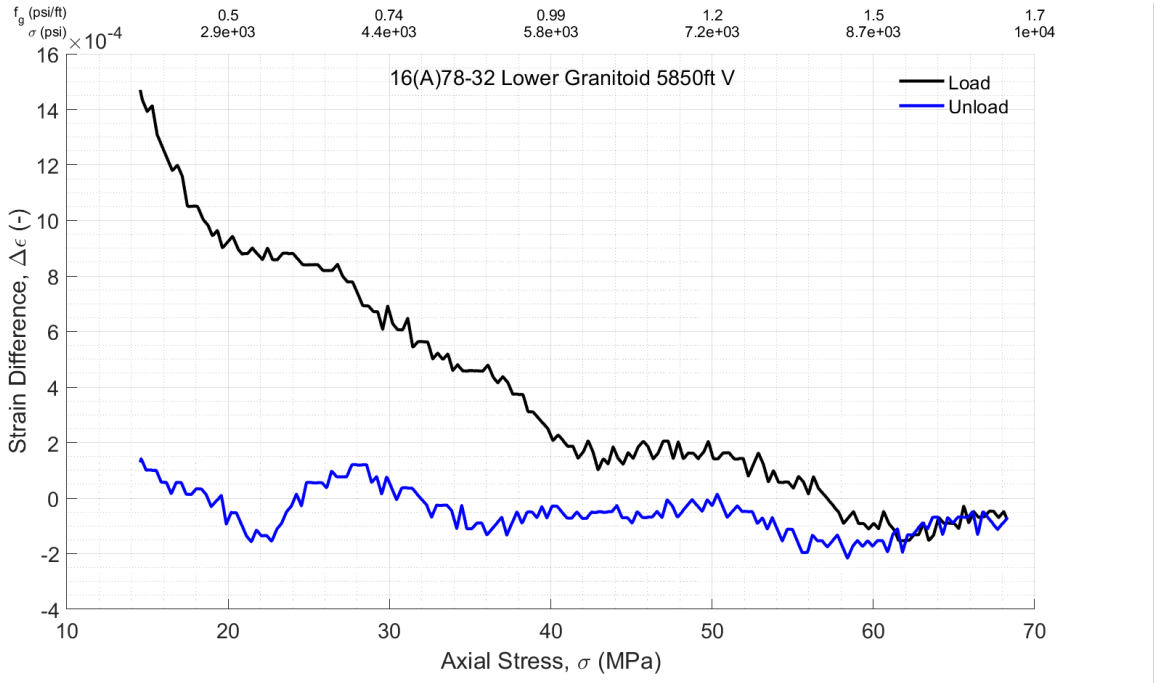

One can observe:

1) Upon the first load/unload cycle, it would interpreted that the hysteresis loop implies plastic strain around 0.0015. This is similar to horizontal cases, just a bit larger in magnitude.

2) Upon reloading, the stiffness of the material is almost exactly compensating the amount of plastic strain, so that by the end of the reloading, the stress-strain curves from the first and second loadings are nearly identical once the stress reaches about 60 MPa. This is very similar to horizontal cases.
3) The unloading curves are very similar. Divergence between them is above 52 MPa.
4) At around 35 MPa of axial stress on the second loading, the specimen slightly stiffens, bringing the curve closer to the first loading and causing a sudden downward deflection of the strain difference.
5) There is another stiffening later, that is harder to see on the stress-strain plot, but the strain different drops at 50 MPa.

Bringing DRA and TUV stiffnesses together (by taking derivative of stress with respect to strain for DRA curves) gives

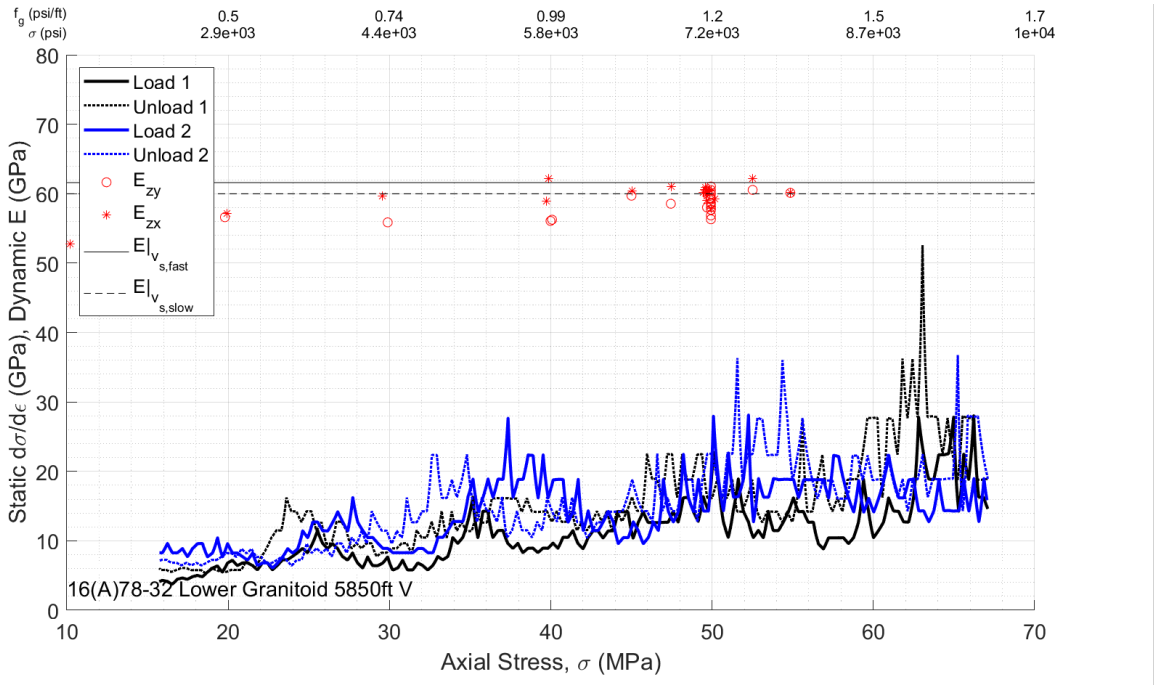

Here we observe:

1) The stiffness is attaining a value ~25 GPa – similar to the y-direction.
2) Stiffening is more subtle than for x- and y- directions, but seems there is some stiffening around 34 MPa and then softening to mid-40s of MPa, and then stiffening again from about 46 MPa.

Additionally, we can make a similar plot (though DRA only) but putting strain on the x-axis:

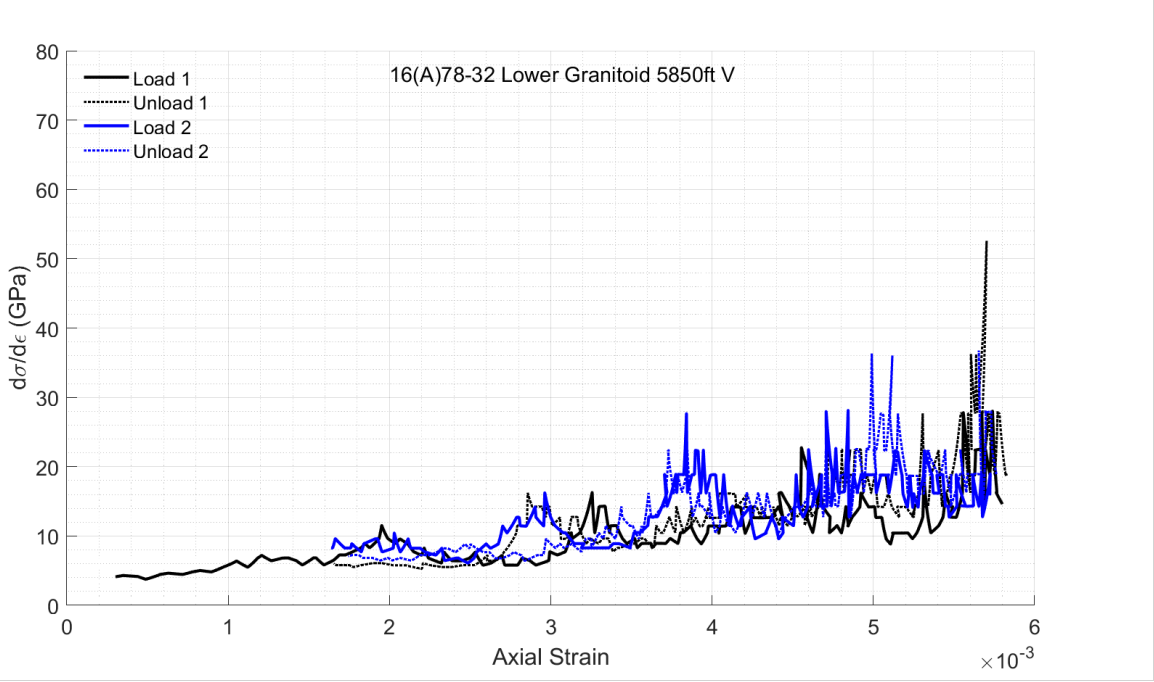

Although a bit more subtle compared to x- and y-directions, there are clear bumps at around 0.003, 0.004, and 0.005 strain.

Lines of Evidence

A summary of the lines of evidence obtained from these experiments is given by:

Series	LoE	s1_val	s1_V	s1_L	s1_C	s1_R	s2_val	s2_V	s2_L	s2_C	s2_R	s3_val	s3_V	s3_L	s3_C	s3_R	s4_val	s4_V	s4_L	s4_C	s4_R	s5_val	s5_V	s5_L	s5_C	s5_R
LrGr_x	hxz	40	2	2	2	0.9	0	0	0	0	0.9	0	0	0	0	0.9	0	0	0	0	0.9	0	0	0	0	0.9
LrGr_x	vxy	40	2	3	3	0.9	62	1.5	0.5	1.5	0.9	0	0	0	0	0.9	0	0	0	0	0.9	0	0	0	0	0.9
LrGr_x	vxz	45	2	3	3	0.9	62	1.5	0.5	1.5	0.9	0	0	0	0	0.9	0	0	0	0	0.9	0	0	0	0	0.9
LrGr_x	Exy	40	2	3	3	0.9	62	1.5	0.5	1.5	0.9	0	0	0	0	0.9	0	0	0	0	0.9	0	0	0	0	0.9
LrGr_x	Exz	45	2	3	3	0.9	62	1.5	0.5	1.5	0.9	0	0	0	0	0.9	0	0	0	0	0.9	0	0	0	0	0.9
LrGr_x	s_e	43	2	2	3	0.9	0	0	0	0	0.9	0	0	0	0	0.9	0	0	0	0	0.9	0	0	0	0	0.9
LrGr_x	s_e	40	2	1.5	3	0.9	58	2	1.5	1.5	0.9	0	0	0	0	0.9	0	0	0	0	0.9	0	0	0	0	0.9
LrGr_x	De	29	2	2.5	3	0.9	42	1.5	3	2.5	0.9	0	0	0	0	0.9	0	0	0	0	0.9	0	0	0	0	0.9
LrGr_x	De	28	2	2.5	3	0.9	39	1.5	1	2.5	0.9	51	1.5	1	1.5	0.9	58	1.5	1	1.5	0.9	0	0	0	0	0.9
LrGr_x	ds_de	40	2	1.5	3	0.9	55	2	1	3	0.9	0	0	0	0	0.9	0	0	0	0	0.9	0	0	0	0	0.9
LrGr_x	ds_de	38	2	1.5	3	0.9	56	2	2	3	0.9	17	1.5	0.5	1.5	0.9	28	1.5	1	1.5	0.9	0	0	0	0	0.9
LrGr_y	hyz	25	2	2	2	0.9	0	0	0	0	0.9	0	0	0	0	0.9	0	0	0	0	0.9	0	0	0	0	0.9
LrGr_y	vyx	32	2	2.5	2	0.9	0	0	0	0	0.9	0	0	0	0	0.9	0	0	0	0	0.9	0	0	0	0	0.9
LrGr_y	vyz	32	2	2	2	0.9	0	0	0	0	0.9	0	0	0	0	0.9	0	0	0	0	0.9	0	0	0	0	0.9
LrGr_y	s_e	33	2	3	1.5	0.9	49	2	2	1.5	0.9	0	0	0	0	0.9	0	0	0	0	0.9	0	0	0	0	0.9
LrGr_y	De	26	2	1	1.5	0.9	47	1.5	3	1.5	0.9	59	1.5	2	1.5	0.9	0	0	0	0	0.9	0	0	0	0	0.9
LrGr_y	ds_de	32	2	2.5	1.5	0.9	48	2	1.5	1.5	0.9	60	2	2	1.5	0.9	0	0	0	0	0.9	0	0	0	0	0.9
LrGr_H3	s_e	22	2	2	1	0.9	29	2	1	2	0.9	46	2	1	3	0.9	0	0	0	0	0.9	0	0	0	0	0.9
LrGr_H3	s_e	33	2	1	2	0.9	45	2	3	3	0.9	0	0	0	0	0.9	0	0	0	0	0.9	0	0	0	0	0.9
LrGr_H3	De	30	2	2	2.5	0.9	54	1.5	1.5	2	0.9	0	0	0	0	0.9	0	0	0	0	0.9	0	0	0	0	0.9
LrGr_H3	De	33	2	2	2.5	0.9	41	1.5	1	1	0.9	54	1.5	1.2	0	0.9	60	1.5	1	1.5	0.9	0	0	0	0	0.9
LrGr_H3	ds_de	20	2	2	1	0.9	34	2	0.5	2	0.9	47	2	0.5	2	0.9	0	0	0	0	0.9	0	0	0	0	0.9
LrGr_H3	ds_de	34	2	1.5	2	0.9	44	2	2	2	0.9	58	2	1	1	0.9	0	0	0	0	0.9	0	0	0	0	0.9
LrGr_z	hzz	45	2	2.5	2.5	0.9	0	0	0	0	0.9	0	0	0	0	0.9	0	0	0	0	0.9	0	0	0	0	0.9
LrGr_z	hzx	30	1.5	2.5	2.5	0.9	0	0	0	0	0.9	0	0	0	0	0.9	0	0	0	0	0.9	0	0	0	0	0.9
LrGr_z	hzy	45	2	2	2.5	0.9	0	0	0	0	0.9	0	0	0	0	0.9	0	0	0	0	0.9	0	0	0	0	0.9
LrGr_z	vzx	30	2	2	2	0.9	47	2	3	2	0.9	0	0	0	0	0.9	0	0	0	0	0.9	0	0	0	0	0.9
LrGr_z	vzy	45	2	1.5	2	0.9	0	0	0	0	0.9	0	0	0	0	0.9	0	0	0	0	0.9	0	0	0	0	0.9
LrGr_z	vzz	50	2	1	2	0.9	0	0	0	0	0.9	0	0	0	0	0.9	0	0	0	0	0.9	0	0	0	0	0.9
LrGr_z	Ezx	40	1.5	2	1.5	0.9	0	0	0	0	0.9	0	0	0	0	0.9	0	0	0	0	0.9	0	0	0	0	0.9
LrGr_z	Ezy	50	1.5	0.5	1.5	0.9	0	0	0	0	0.9	0	0	0	0	0.9	0	0	0	0	0.9	0	0	0	0	0.9
LrGr_z	s_e	24	2	2	1.5	0.9	34	2	2.5	1.5	0.9	47	2	1	1.5	0.9	0	0	0	0	0.9	0	0	0	0	0.9
LrGr_z	De	28	2	2	1.5	0.9	36	2	2	1.5	0.9	50	2	1	1.5	0.9	0	0	0	0	0.9	0	0	0	0	0.9
LrGr_z	ds_de	24	2	2.5	2	0.9	33	2	1.5	2	0.9	45	2	1.5	2	0.9	58	1.5	1	1.5	0.9	0	0	0	0	0.9

To note:

- Each series is named with the direction after an underscore (column 1).
- The source of the line of evidence (LoE) is given in column 2, where v is velocity, E is Young's modulus, s_e is stress-strain curve, De is the change in strain curve, and ds_de is the instantaneous stiffness curve. Subscripts indicate direction of propagation followed by polarity, as usual, such that for example vxy indicates a shear wave velocity propagating in x-direction with y-polarity.
- All stress values (i.e. s1_val, s2_val) are given in MPa.
- Each source can give multiple lines of evidence, thus the table is set up to accept up to 5 lines of evidence for each source. Zeros are filled into the table where there are no additional lines of evidence.
- The weight assigned according to the prescribed rubric is given after an underscore, where V indicates relevance, L indicates reliability, C indicates consistency, and R indicated representivity. All values of representivity are set at 0.9 because there is insufficient data to determine exactly how representative the sample is of the surrounding formation.

Upper Gneiss

Summary

The 16A(78)-32 Upper Gneiss samples are from around 10,956 MD (3340 m). They are in the 65 degree deviated part of the well, and here TVD=8548 ft (2606 m). These are from the toe of the well, and so there

is a slight increase in actual TVD because of the incline of the Earth's surface. However, relative to the collar of 16A(78)-32, the TVD will not be significantly changed due to the sloping surface.

The core has a foliation that is subparallel to the core axis (Figure 21). Because the well is deviated, this observation leaves two choices. Either the core is drilled along the strike of the foliation, or it is drilled along the dip of the foliation. The option that the well deviation serendipitously matches the dip is unlikely. So let us firstly accept the more likely scenario that the deviated well is drilled along the strike of the foliation.

Additionally, if the strike of the foliation is aligned with present-day principal stress orientations, and so also is the well, then colinear well and foliation strike would be expected. Furthermore, because the well is not horizontal but instead deviated at 65 degrees from vertical, if the foliation was not deeply dipping (i.e. subvertical), it would crosscut the core rather than being subparallel to the core axis. Hence, let us accept a second conjecture, that is the foliation orientation is nearly in the vertical plane.

Finally, because the well orientation is intended to strike along the direction of the minimum stress, so also the foliation must be striking nearly in the minimum principal stress direction. The maximum principal stress would therefore be acting perpendicular to foliation, which would be consistent if the foliation of this metamorphic rock was associated with folding or other shortening crustal deformation associated with the maximum principal stress.

If one accepts these core orientation arguments, then the x-direction as defined for the TUV experiments is nearly aligned with the maximum principal stress. The DRA sample H3 is the most closely aligned to maximum principal stress. Meanwhile, the z-direction in the TUV experiments (Vertical core for DRA experiments) is the most closely aligned to the minimum principal stress – although it is dipping at 25 degrees due to the 65 degree well deviation and so will also be expected to have some impact from the vertical stress. Finally, the y-direction in TUV experiments (H1 in DRA experiments) is the most closely aligned to vertical, although it is also expected to be impacted by the minimum horizontal stress.

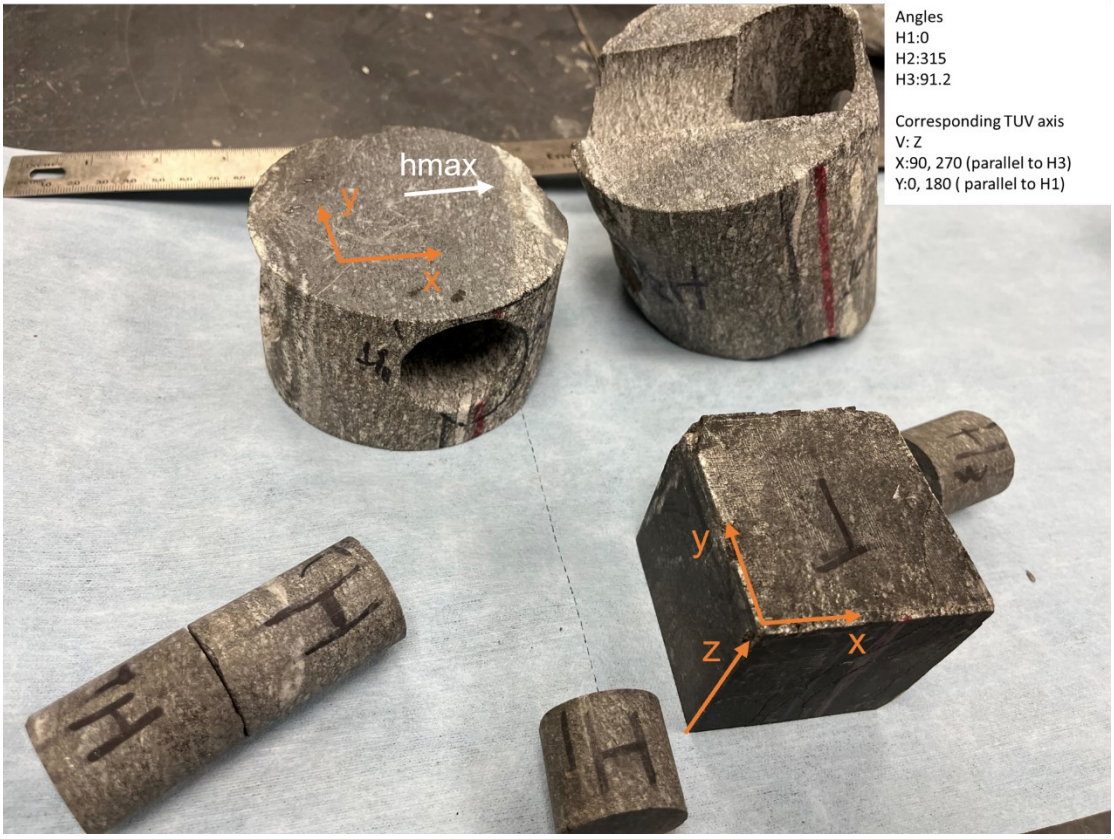

Figure 21: Upper Gneiss sample preparation for TUV sample (cube) with DRA samples (cylinders), showing x, y, z axes on TUV sample and with cylinders laying in approximate directional correspondence to TUV sample. The TUV sample was cut from the top of the image and the foliation that is subparallel to the core axis is visible in this parent core. The proposed orientation of the maximum horizontal stress is indicated on the surface of the top-left parent core.

The main observations begin with alignment of the maximum horizontal stress. If the x-direction is taken as the maximum horizontal stress direction, then Figure 22a shows a rollover of the shear wave velocity at around 78 MPa (~1.33 psi/ft). There are no other signs of inflection that would indicate a maximum stress at a lower level and we also note that the x-direction, across the foliation, is the minimum wavespeed direction.

Turning attention, then, to the y-orientation, there is a striking s-shaped behavior wherein the shear wavespeed decreases around 42 MPa (~0.70 psi/ft), as shown in Figure 22b. It then turns and increases again after 50 MPa. However, the specimen was observed to be damaged in the course of these loading cycles and so additional orientations were unable to be measured.

Before moving on it is useful to pause and reflect on the fact that Granitoid samples showed ostensibly no signs of damage when loaded at levels similar to their candidate in-situ stress levels. On the other hand, the Gneiss sample, cubic in shape, readily failed with at least two observable shear-type failures when the load was similar to candidate in-situ stress levels. This observation could imply that the Gneiss formation is closer to being critically-stressed under field conditions.

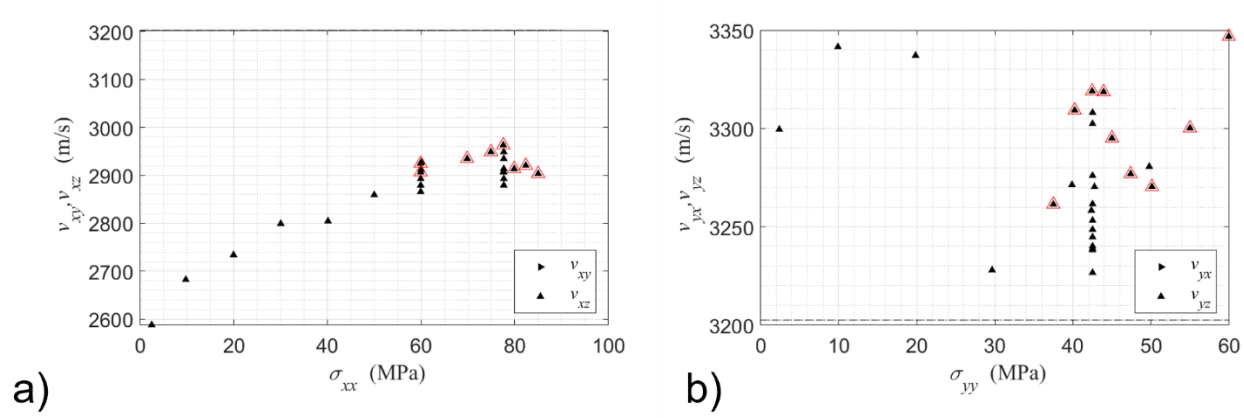

Figure 22: Shear wave velocities versus normal stress applied in the direction of wave propagation for a) x-direction, and b) y-direction. Highlighted points with colored overmarkings in this type of figure indicate results where two of the three applied stresses are fixed while the stress that is plotted on the x-axis is varied, hence experimentally taking a "partial derivative". The dashed lines give a reference to the measured shear wave velocity from well-logging, which was obtained for waves propagating in the slower vertical (z-) direction.

Secondly, the various inflection points from both TUV and DRA approaches provide lines of evidence range from 34-52 MPa (~0.57-0.85 psi/ft), as indicated by Figure 23. These lines of evidence are mainly coming from the z- and y- orientations, which is consistent with the proposal that these are best aligned with minimum stress. If one considers that misalignment with respect to the true minimum stress direction will lead the lines of evidence to be overestimates of the actual minimum horizontal stress, then the best estimate is 40 MPa (~0.67 psi/ft). In this case, it would appear that alignment of minimum stress could be slightly better with the y-axis rather than the z-axis. If true, then the true minimum "horizontal" stress direction is actually somewhat dipping and could lead to hydraulic fracture orientations that are also dipping (see illustration in Figure 24). On the other hand, if we make a conjecture that minimum stress must be horizontal, then we have to give more weight to the data from the z-direction and with this we would conclude that minimum stress is around 46 MPa (~0.77 psi/ft). Lacking a reason to impose horizontal orientation of the minimum stress, the best estimate at this point of our understanding is taken as s_{hmin}~40 MPa (~0.67 psi/ft).

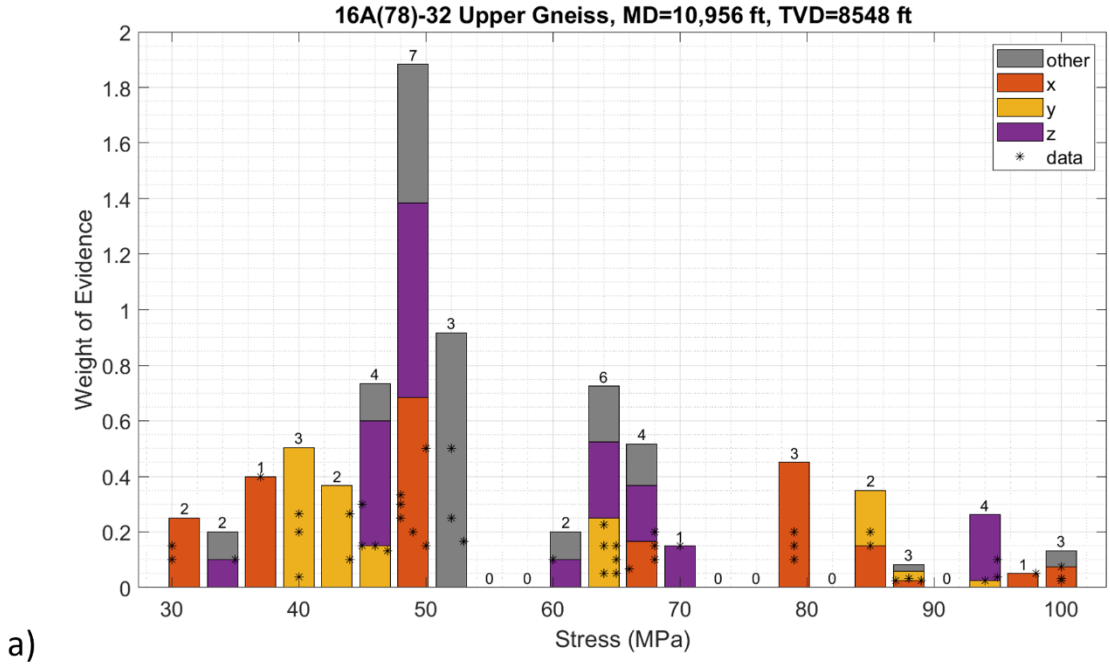

a)

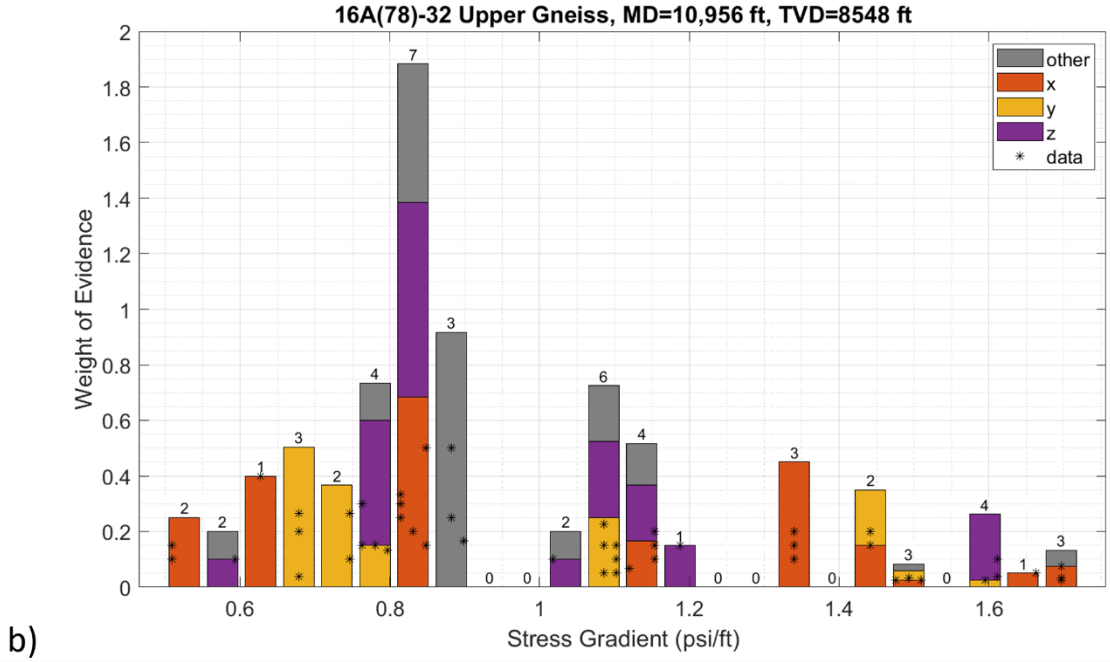

b)

Figure 23: Integrated weight of evidence from TUV and DRA tests versus a) applied stress (axial stress in DRA experiments and normal stress in direction of propagation in TUV tests), b) corresponding implied stress gradient. The stars indicate individual data points, noting some lie directly on top of one another. The number at the top of each bar is the total lines of evidence in that bin. The bars are color coded to indicate the orientation of the sample giving the line(s) of evidence leading to that part of the bar.

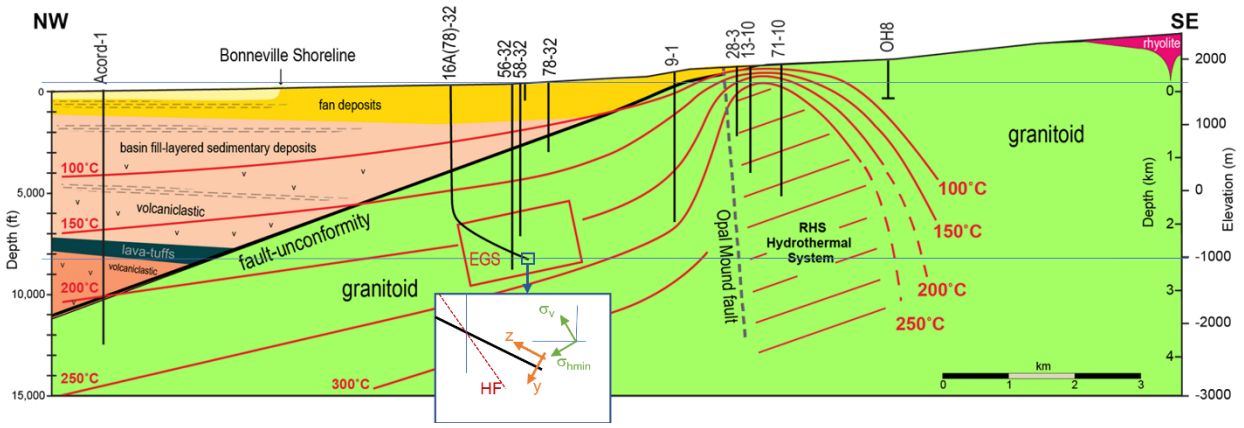

Figure 24: Cross sectional view of FORGE site showing 16A(78)-32 with an illustration of the orientation of core axes z- and y-, along with hypothesized orientations of "vertical" and minimum "horizontal" stress and the correspondingly dipping hydraulic fracture orientation that would result if this inclined principal stress hypothesis were true. Note that if the hypothesis was true, the minimum stress would be dipping so as to align with the fault-unconformity rather than being horizontal. Figure modified from Moore et al. 2020.

Thirdly, there is a collection of lines of evidence around a next-higher stress, with the mode of the distribution at 64 MPa (~1.09 psi/ft), as shown in Figure 23. This value is very close to the expected overburden gradient. Interesting, the strongest lines of evidence come from the z-orientation rather than the (more vertical) y-orientation. This again is consistent with a hypothesis that the principal stresses are rotated in this location and that the intermediate principal stress is not exactly vertical, but is inclined by some angle, as illustrated in Figure 24. While impossible to specify this inclination angle (especially until a rock-physics model that is currently in progress is used for the interpretation), one could infer it would be at least 20 degrees from vertical so that the intermediate stress, associated with overburden, is more closely aligned to the z- rather than the y-axis.

Fourthly, there are not many lines of evidence related to a viable maximum horizontal stress. However, what lines are present are strong as in the breakover of the shear wavespeed shown in Figure 22a. Furthermore, all 3 lines of evidence come from the x-orientation that was previously proposed to be aligned with the maximum stress. The implied value of the maximum stress from these lines of evidence is 79 MPa (~1.34 psi/ft).

With that said, an alternative interpretation is that the substantial collection of lines of evidence around 49 MPa (~0.83 psi/ft) is the maximum principal stress. This is also plausible in that there is a collection of lines of evidence related to the x-direction that comprise this mode of the weight of evidence distribution.

Finally, as with other testing locations it is observed that there are some additional inflections giving several lines of evidence at higher stresses with some convergence of these around 1.45 psi/ft and 1.60 psi/ft. The former of these bears intriguing similarity in its implied stress gradient to high stress lines of evidence from the Lower Granitoid while the latter bears similarity in its implied stress gradient to high stress lines of evidence from the Upper Granitoid. The origin of these responses remains unknown but, again, can be expected to be clarified by application of a micromechanical rock physics model (being developed now) to the interpretation.

To summarize:

1) **Minimum horizontal stress** is likely dipping so as to be somewhat aligned with the nearby fault unconformity and has a magnitude of around 40 MPa (~0.67 psi/ft).
2) **Maximum horizontal stress** is aligned across the foliation and colinear with the minimum wavespeed direction and is most likely around 79 MPa (~1.34 psi/ft). However, an alternative interpretation would involve the maximum stress instead being around 49 MPa (~0.83 psi/ft).
3) **Vertical stress** is probably not actually a principal stress, but the nearest principal stress is the intermediate magnitude, inclined to the vertical at an angle of at least 20 degrees, and with a magnitude of 64 MPa (1.09 psi/ft).
4) **The hypothesis of inclination of principal stresses** is supported by the evidence collected so far and would result in hydraulic fractures dipping at least 20 degrees from vertical, to be closer to perpendicular to the fault-unconformity than they would be to being perpendicular to the well axis of 16A(78)-32.

X-Direction: Compendium

The 16A(78)-32 Upper Gneiss samples are from around 10,956 MD. They are in the 65 degree deviated part of the well, and here TVD=8548 ft. There is a platy foliation and the x-direction is perpendicular to the platy foliation. Running the TUV experiments, we find

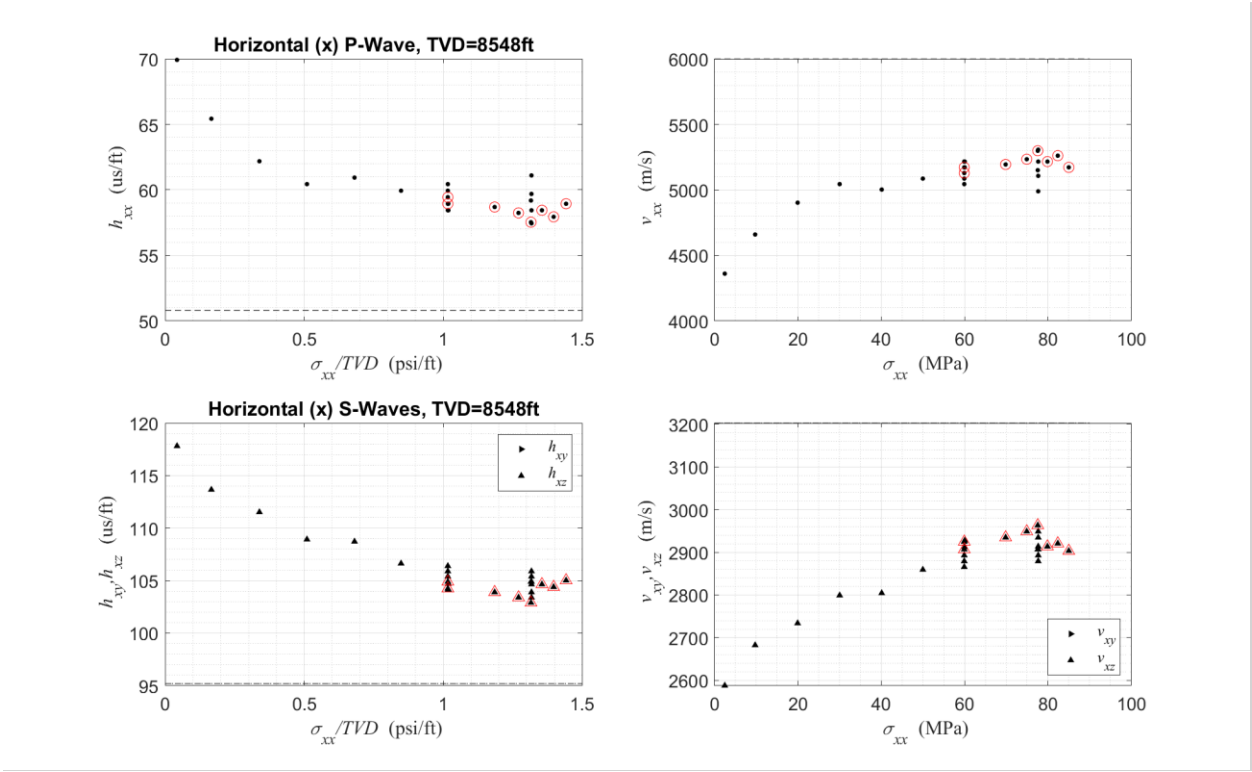

Note that sonic log only goes to 10,940 MD and at this point is clearly broken already. Using Eq. (1), the quasi-isotropic elastic moduli are

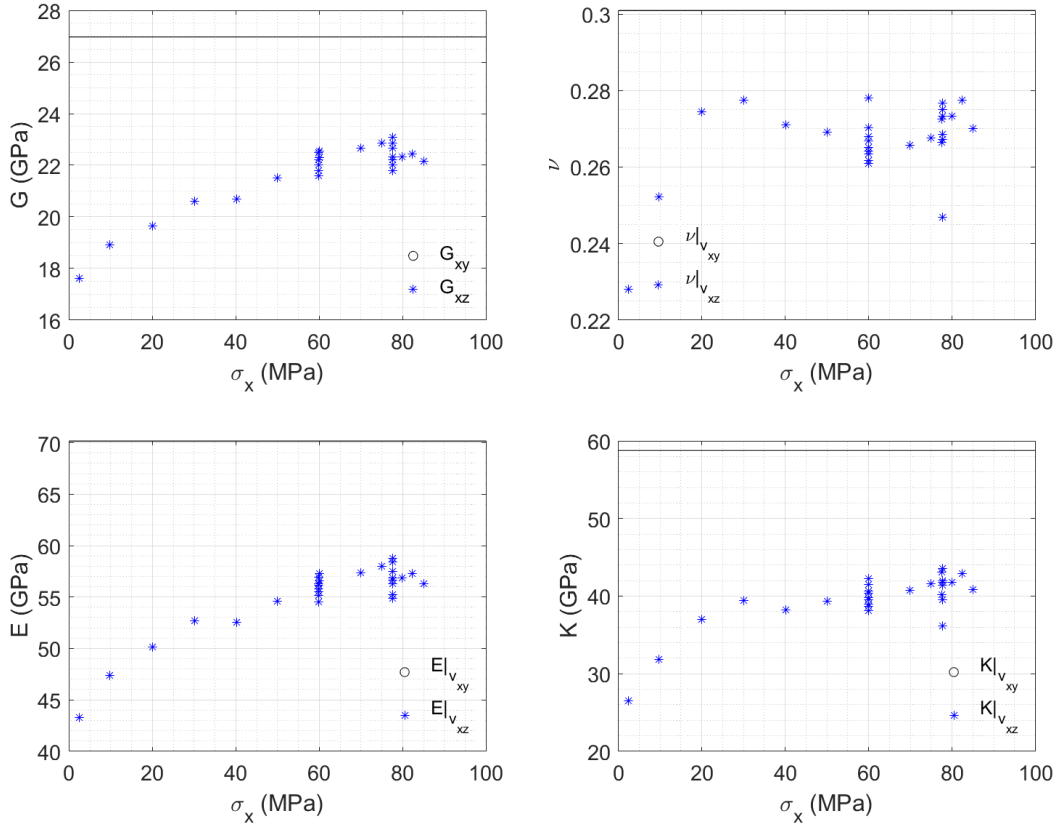

The H3 sample from DRA is aligned the x-direction within 1 degree. Sample dimensions and photograph are as follows:

Dimensions	
height (mm):	51.63
width (mm):	32.05
Angle retrieved (degrees):	91.2

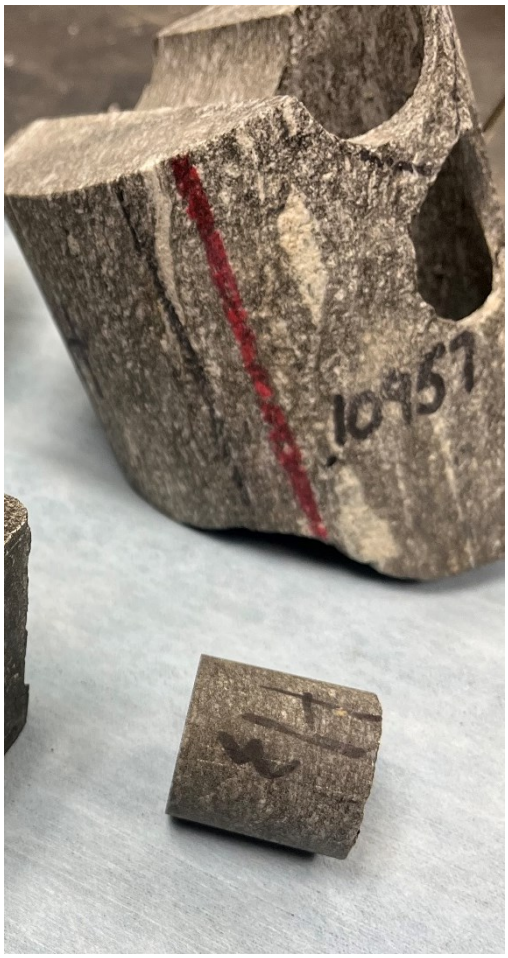

DRA experiments are run with the loading sequence

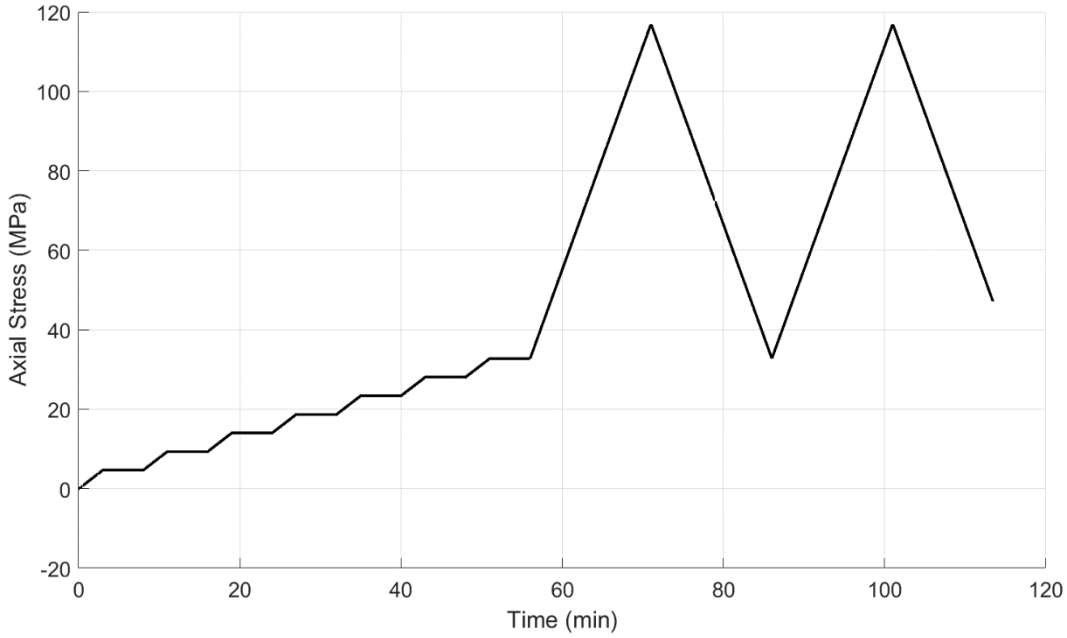

This results in the following displacements, which have been reduced by an amount estimated for deformation of 100mm of tool steel with E=210 GPa (comprising a lower bound on the platen deformation). This gives

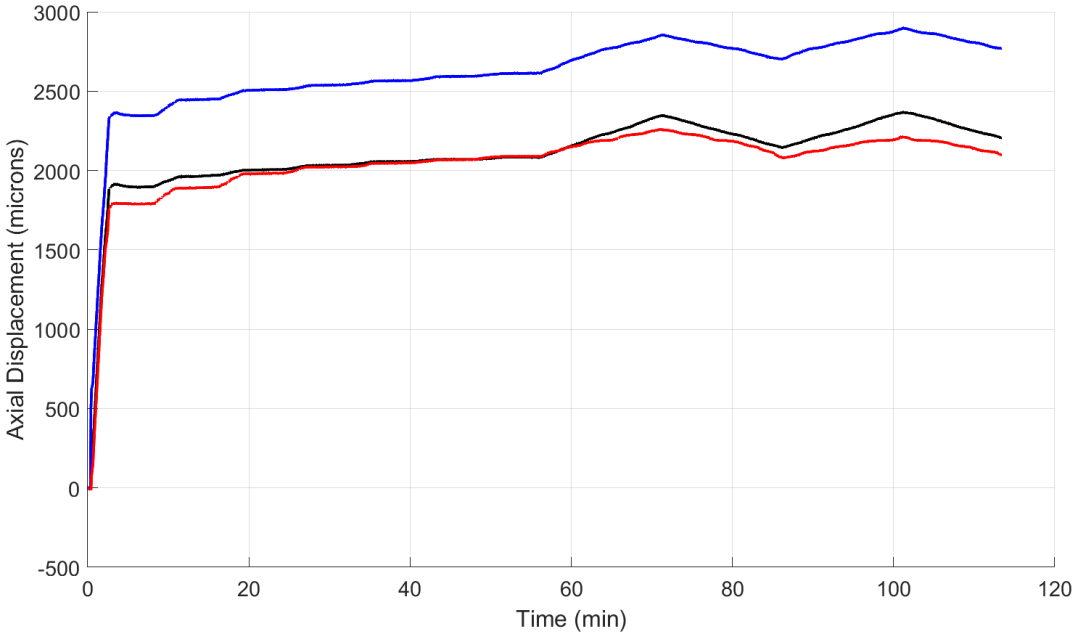

There is very slight tilting of the platens evidenced by larger displacement on one LVDT compared to the other dwo.

Averaging and plotting stress versus strain relationships for the 2 load/unload cycles, setting zero strain at the beginning of the first load cycle, gives

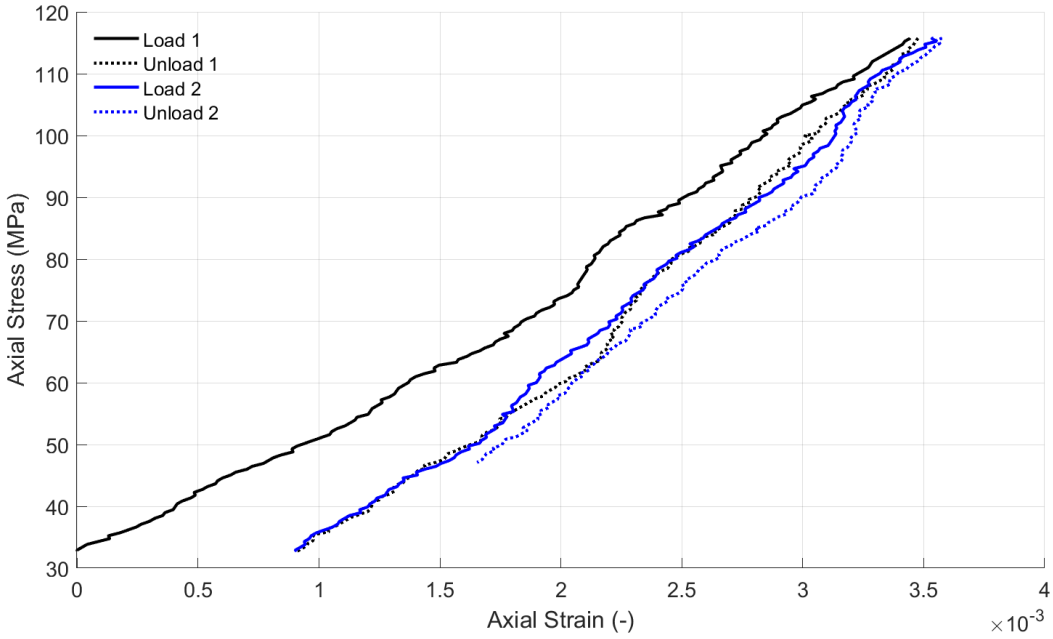

Both cases clearly stiffening around 50 MPa, maybe again around 68 MPa and 98 MPa. There is a small amount of hysteresis evidenced by there being around 0.0001 difference in strain at the end of loading between the first and second cycles.

The difference between the strain measurements for the load/unload stages is given by

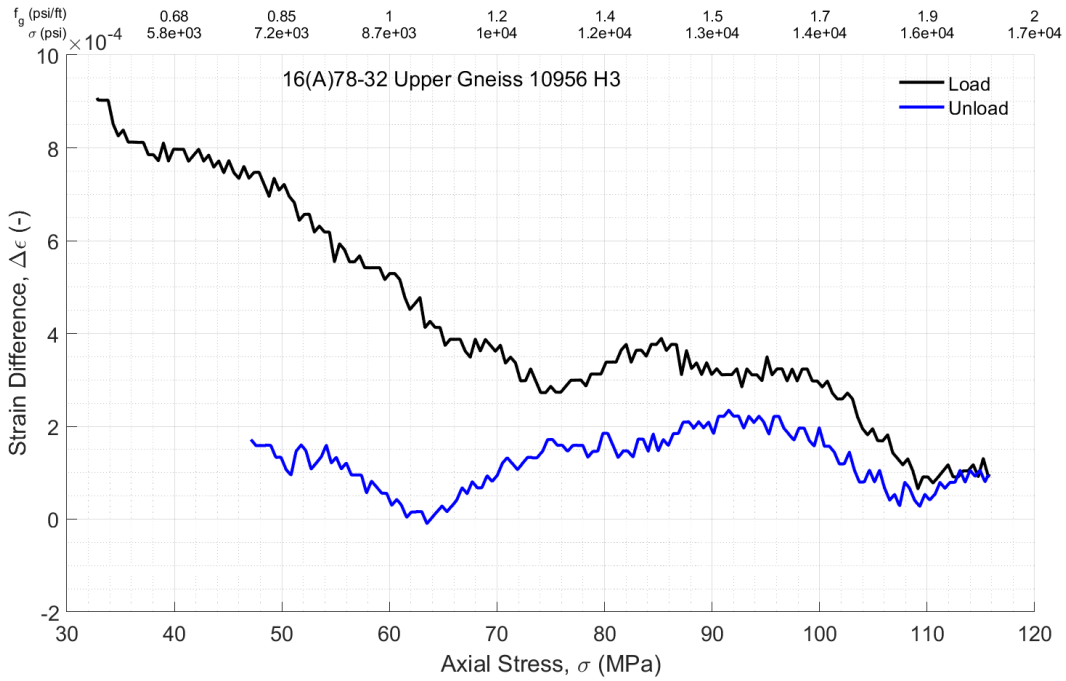

Bringing DRA and TUV stiffnesses together (by taking derivative of stress with respect to strain for DRA curves) gives

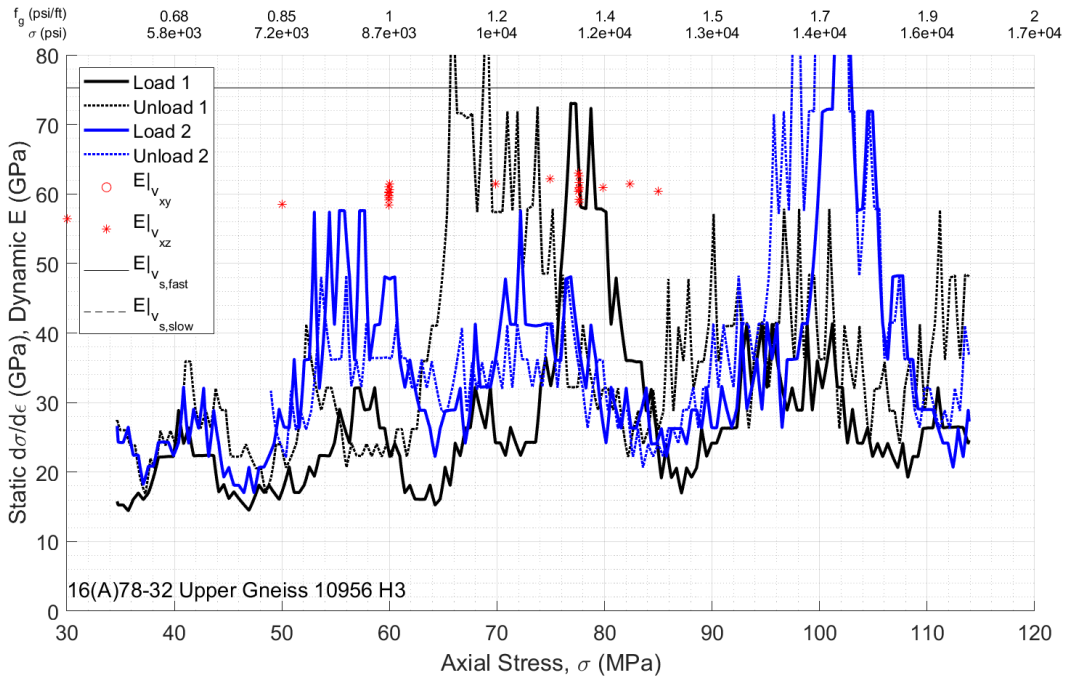

Here we observe at least 4 loading peaks indicative of stress-strain inflections at various stress levels. Additionally, the first two inflections happen consistently at the same strain levels, as can be observed by putting strain on the x-axis:

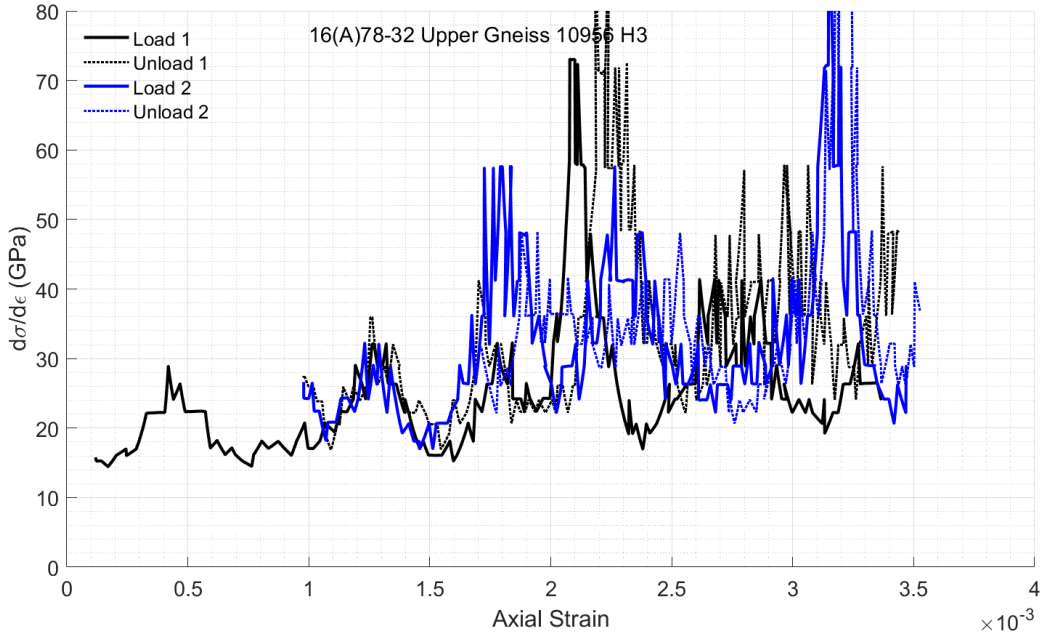

Y-Direction: Compendium

These samples are parallel to bedding and, based on prior arguments about core orientation, are likely to be the most well-aligned with vertical stress but are also striking in the same direction as minimum stress.

Running the TUV experiments gives

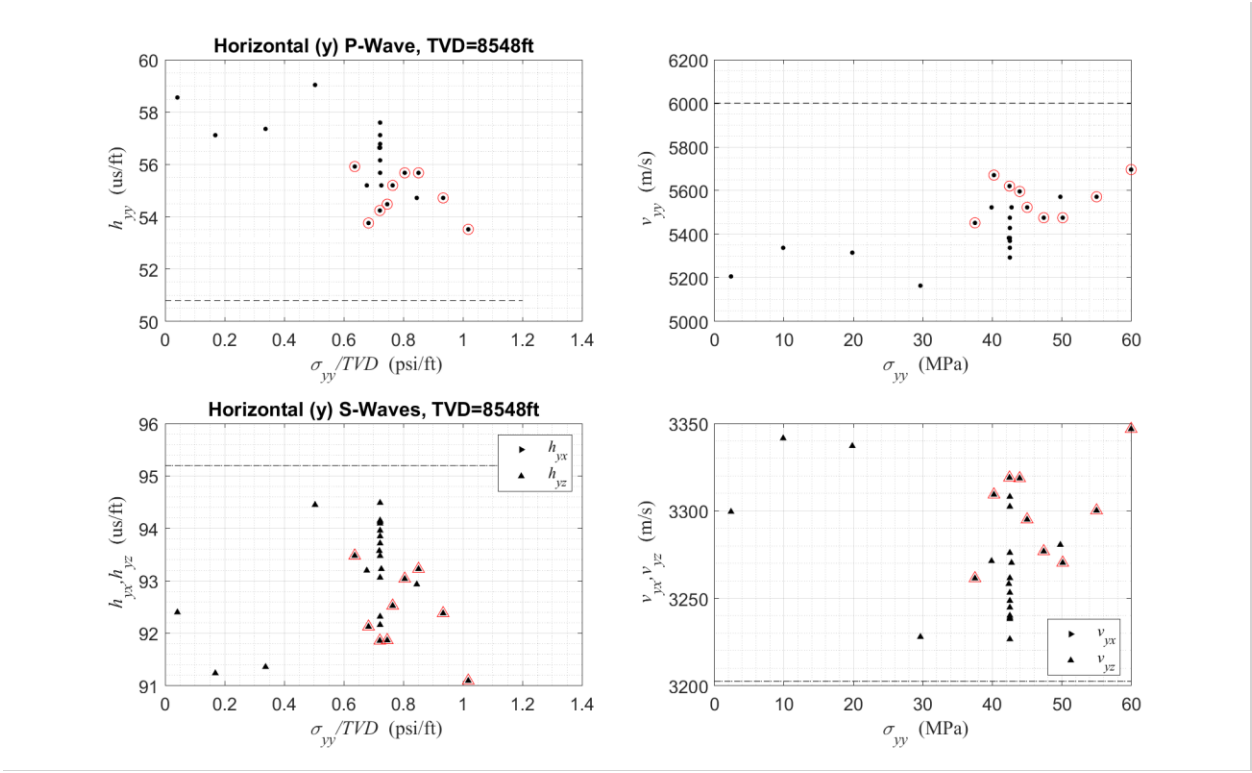

We can see striking rollover at around 40-42 MPa (~0.70 psi/ft). Using Eq. (1), the quasi-isotropic wavespeeds are

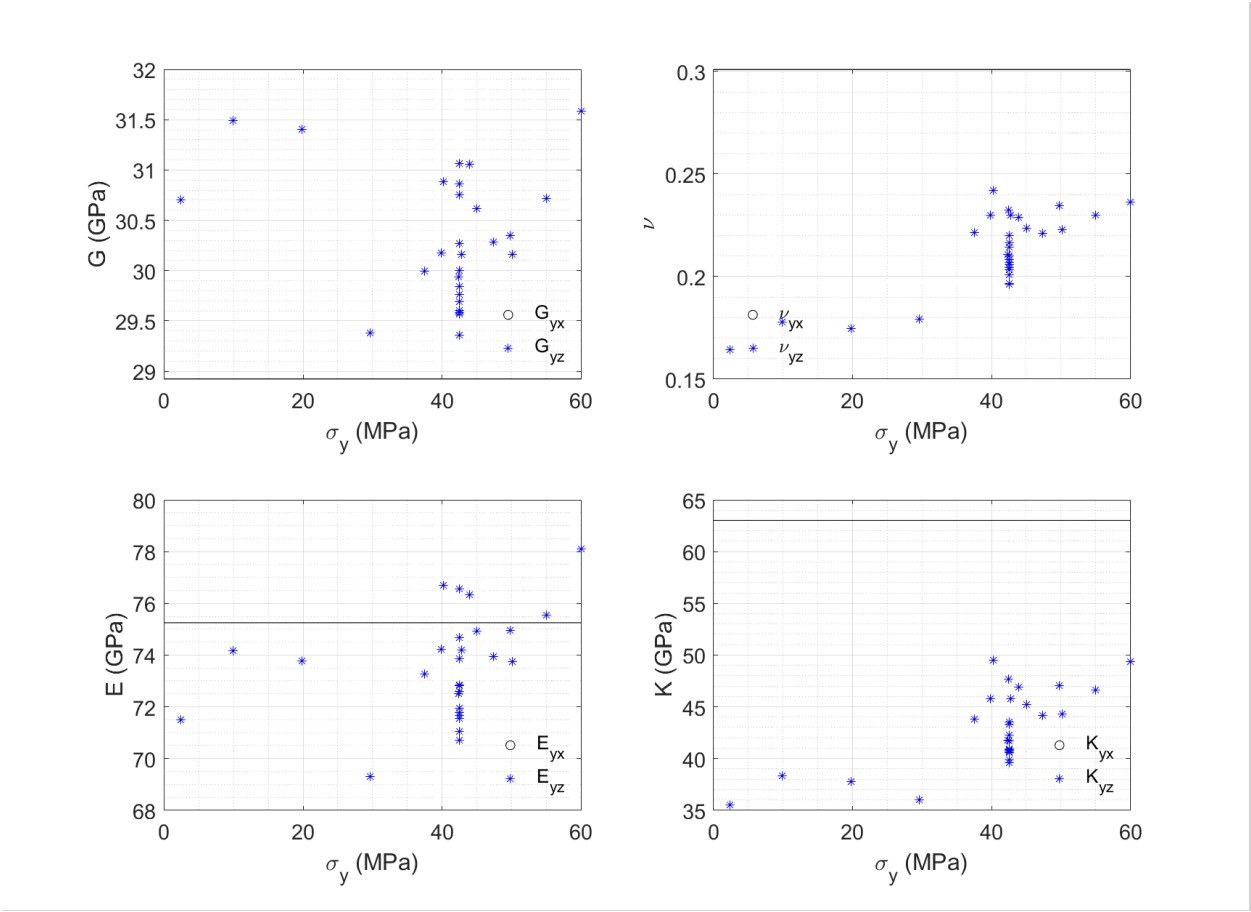

The log-derived values are not as reliable here because the noise level was indicating damage occurring to the logging tool. Also the specimen was undergoing damage during the lab experiments.

Turning attention to the DRA experiments, H1 is the best to compare with the y-direction because they are aligned with one another. The sample dimensions and photographs are as follows:

Dimensions	
height (mm):	28.50
width (mm):	32.04
Angle retrieved (degrees):	0

The DRA experiment was run with the loading sequence

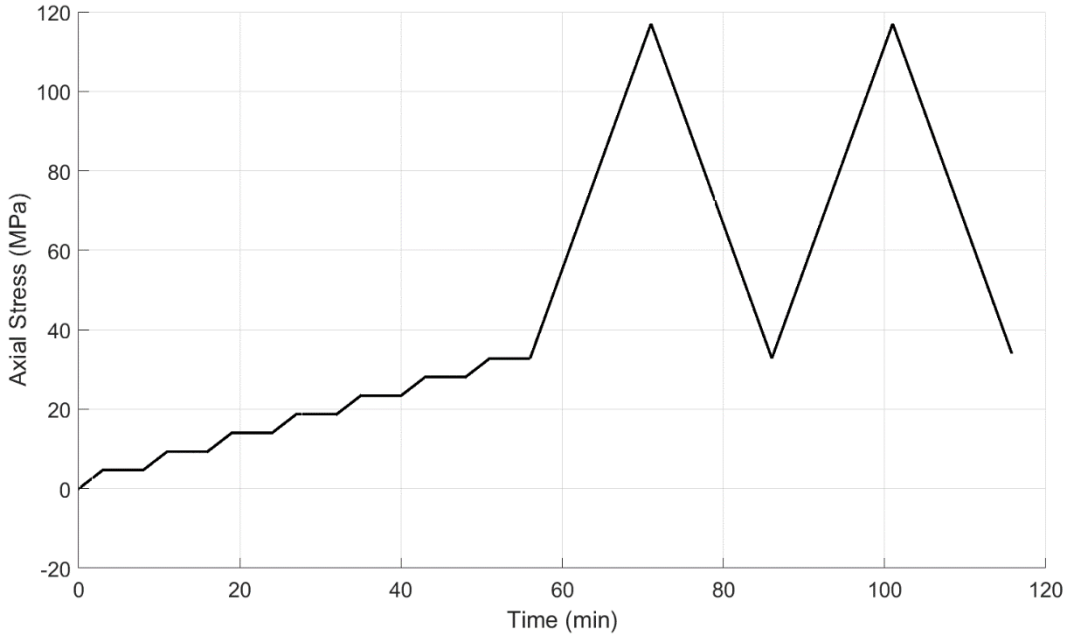

This results in the following displacements, which have been reduced by an amount estimated for deformation of 100mm of tool steel with E=210 GPa (comprising a lower bound on the platen deformation). This gives

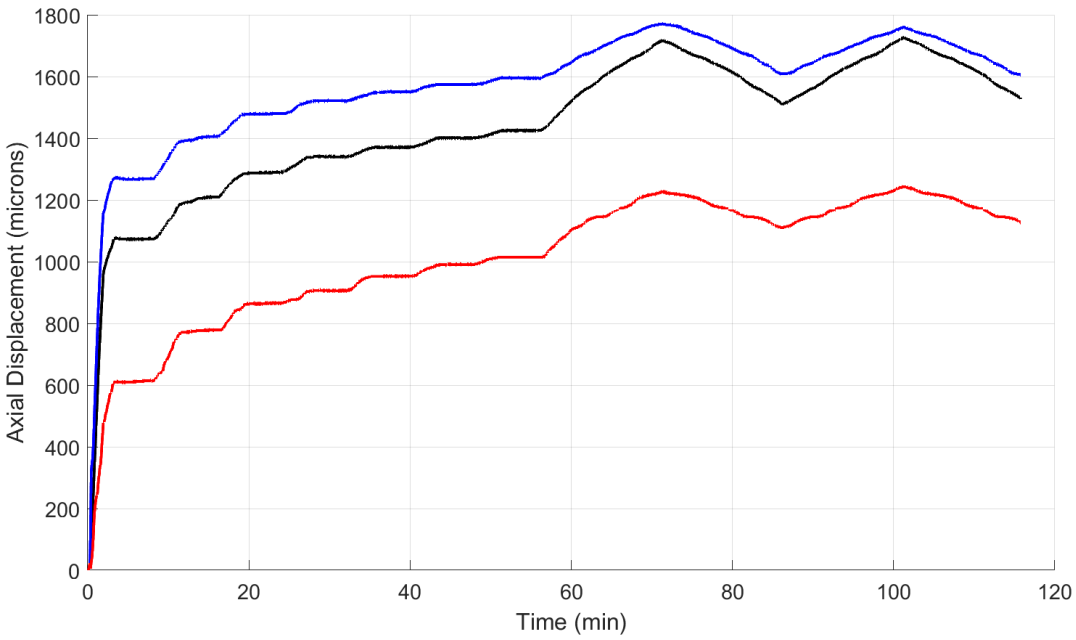

There was some apparent platen tilting. Averaging and plotting stress versus strain relationships for the 2 load/unload cycles, setting zero strain at the beginning of the first load cycle, gives

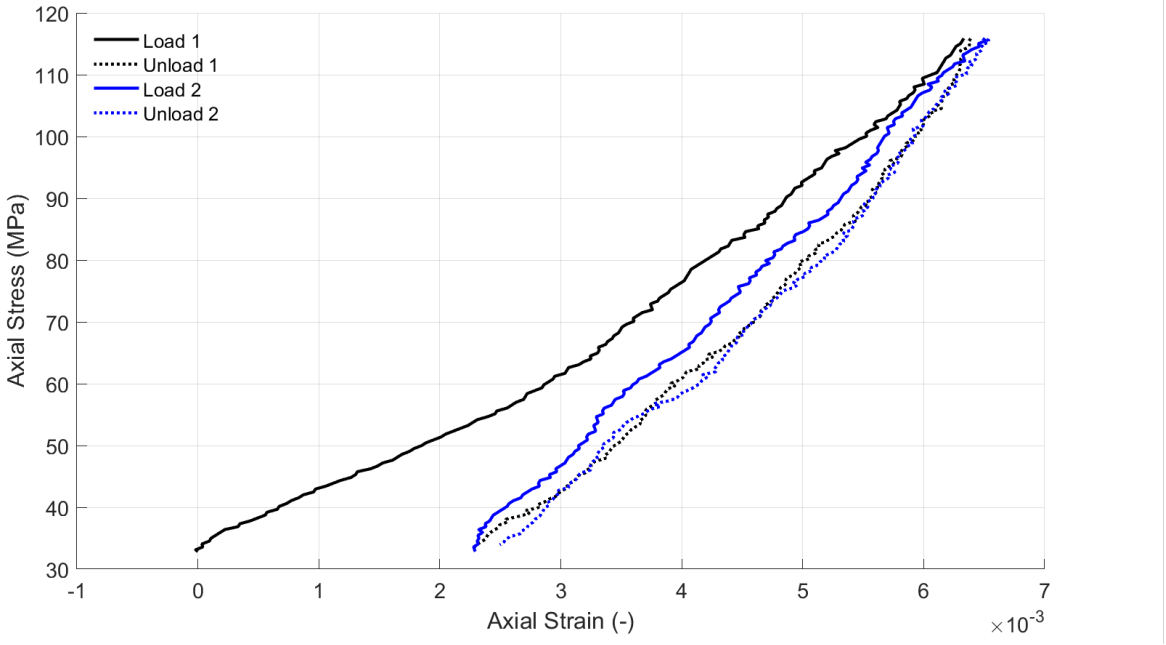

Here we can see stiffening around 45, 65, and 85 MPa. There is hysteresis indicating once again around 0.0001 plastic strain. The difference between the strain measurements for the load/unload stages is given by

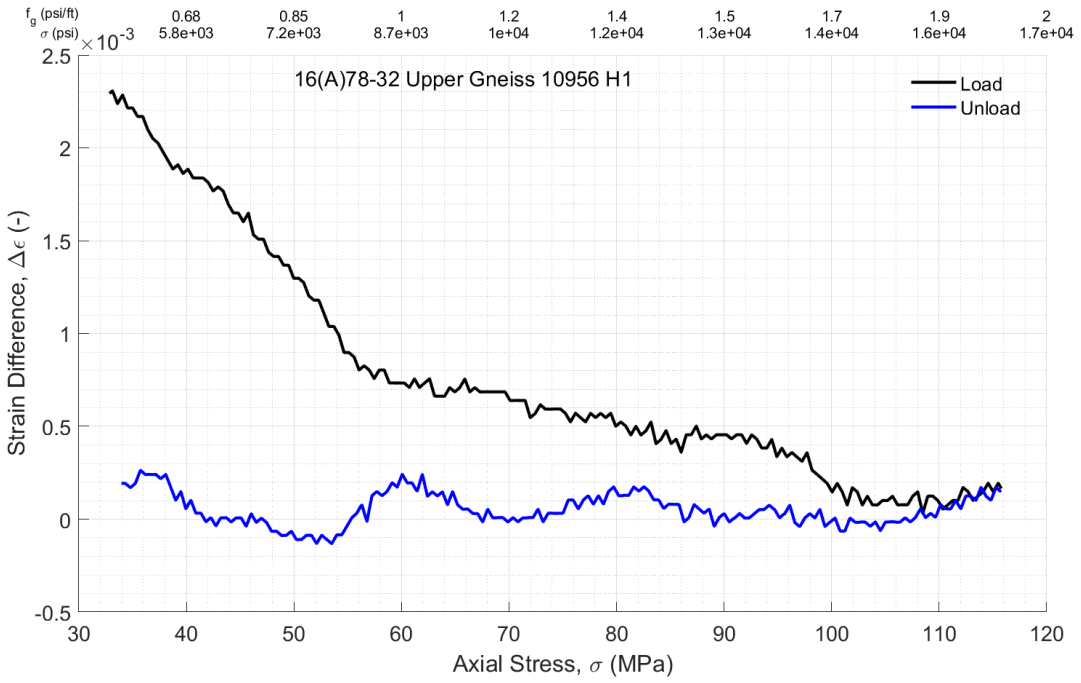

Although somewhat subtle, the first inflection is nonetheless clear at around 44 MPa.

Bringing DRA and TUV stiffnesses together (by taking derivative of stress with respect to strain for DRA curves) gives

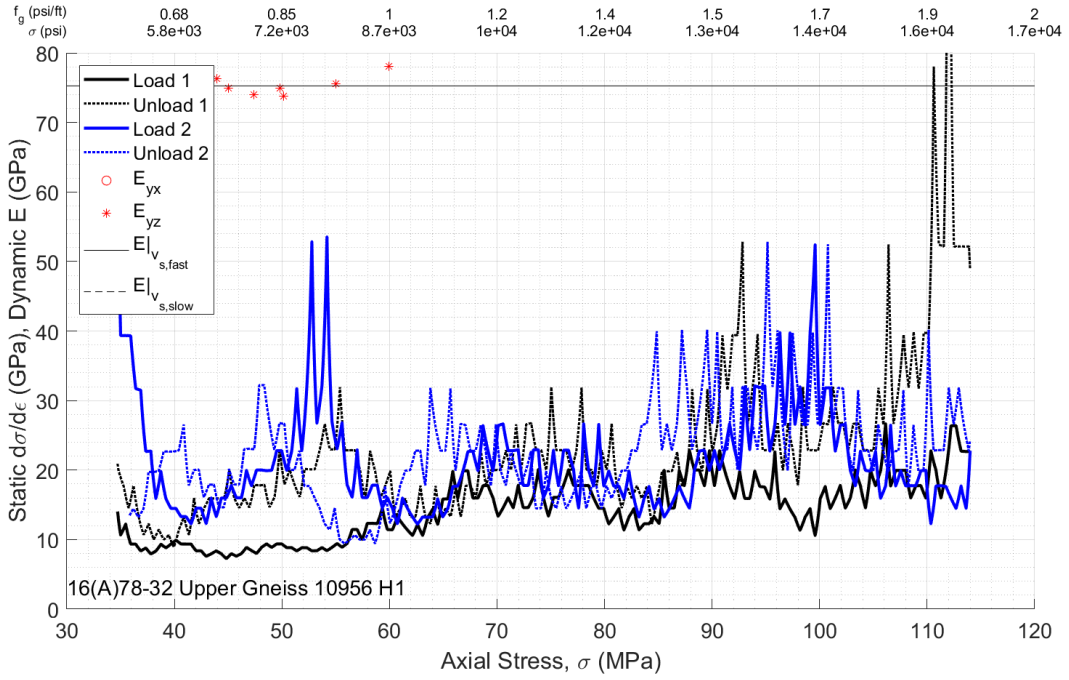

Here we have clear evidence of stiffening at around 42 MPa. There is also something around 62 MPa and 85 MPa. Additionally, we can make a similar plot (though DRA only) but putting strain on the x-axis:

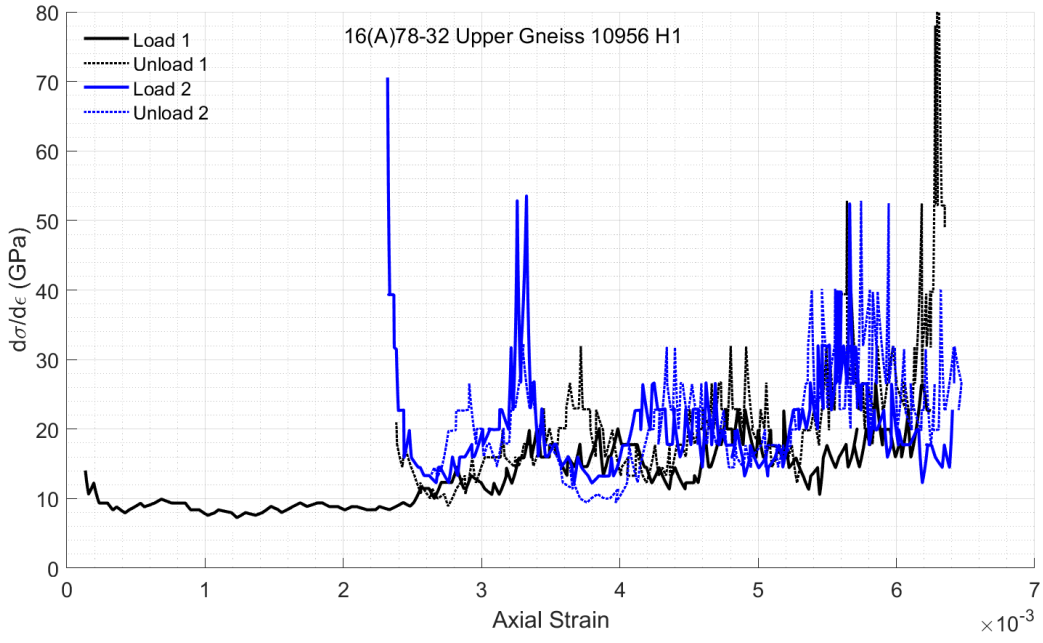

As usual, there appears to be some consistency in the strain level for the stiffening with each cycle, but it is not as striking as in other cases.

H2-Direction: Compendium

The H2 core plug for DRA is oblique to the TUV testing axes. There are two samples:

H2-1

Dimensions	
height (mm):	45.52
width (mm):	32.04
Angle retrieved (degrees):	315

H2-2

Dimensions	
height (mm):	28.46
width (mm):	32.03
Angle retrieved (degrees):	315

DRA experiments are run with the loading sequence

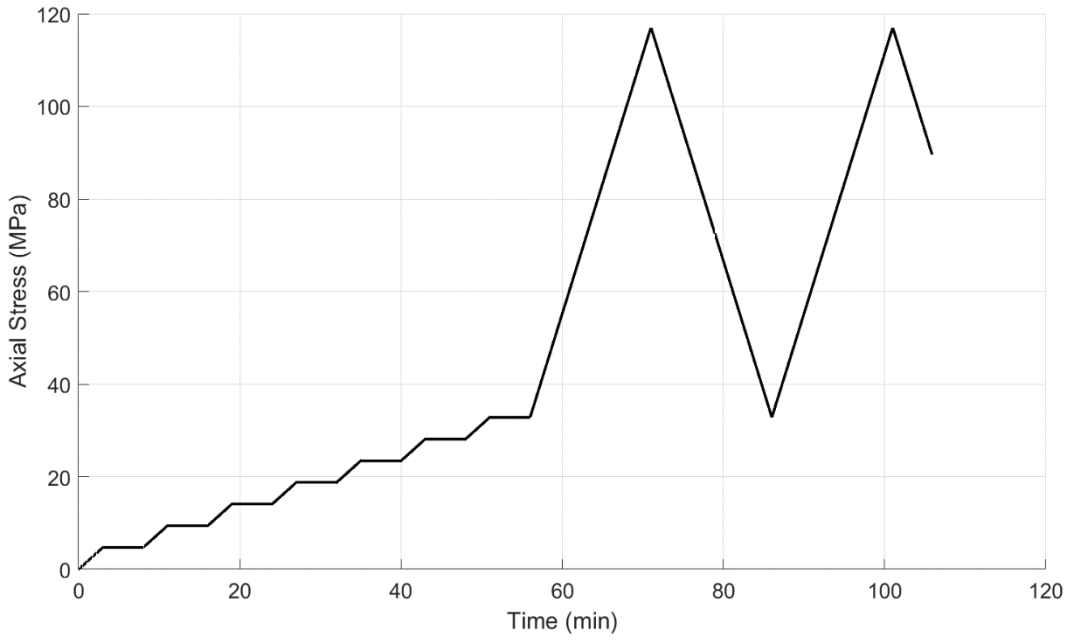

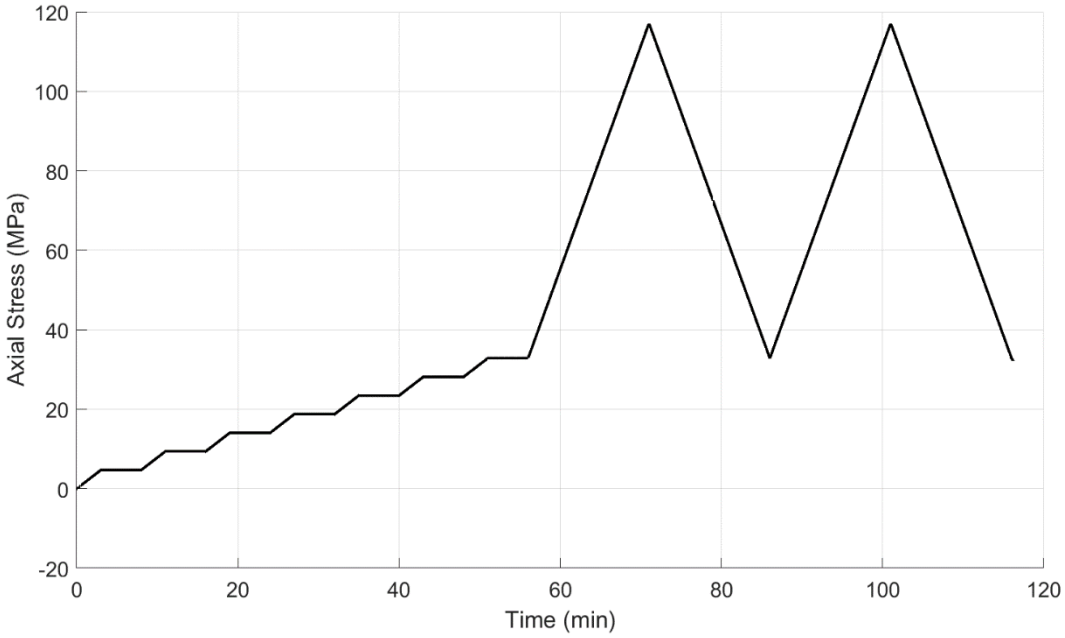

This results in the following displacements, which have been reduced by an amount estimated for deformation of 110mm of tool steel with E=210 GPa (comprising a lower bound on the platen deformation). This gives

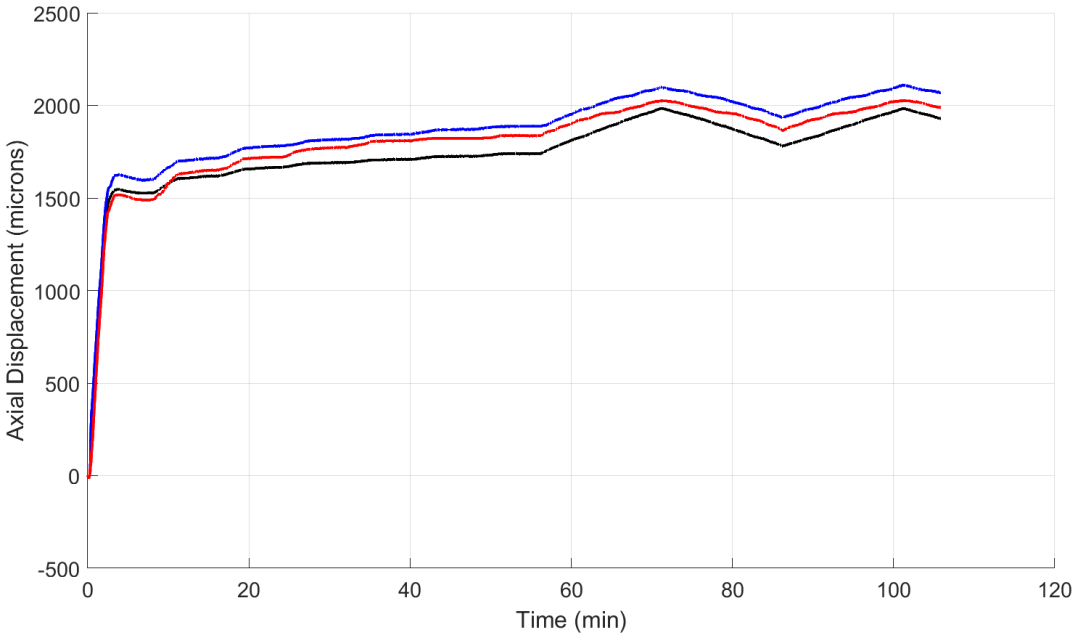

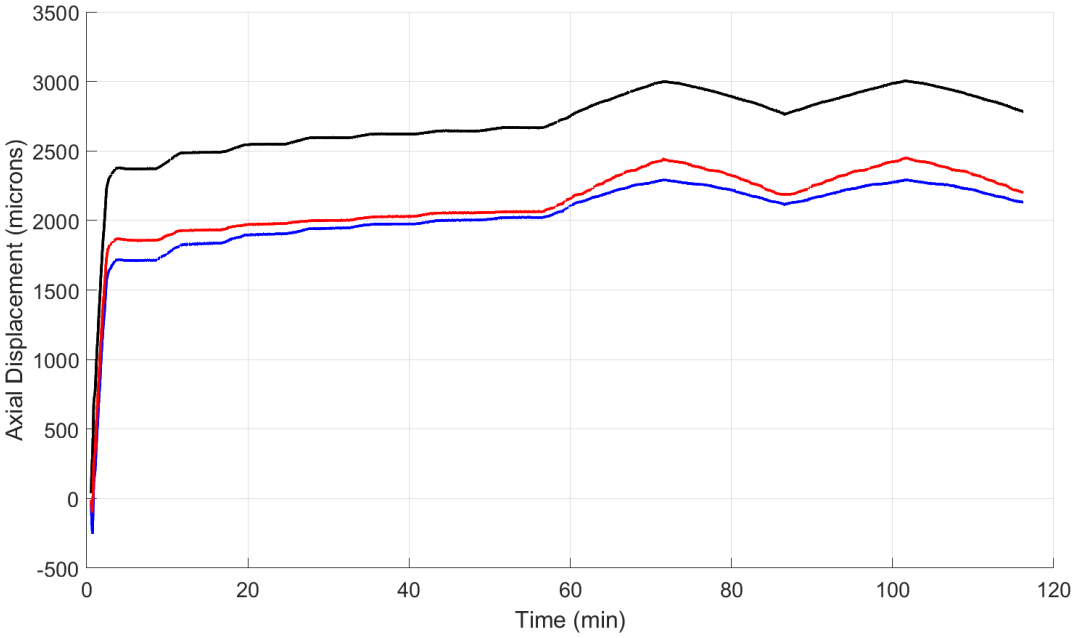

Both are very clean experiments, with the first having a striking absence of platen tilting. Averaging and plotting stress versus strain relationships for the 2 load/unload cycles, setting zero strain at the beginning of the first load cycle, gives

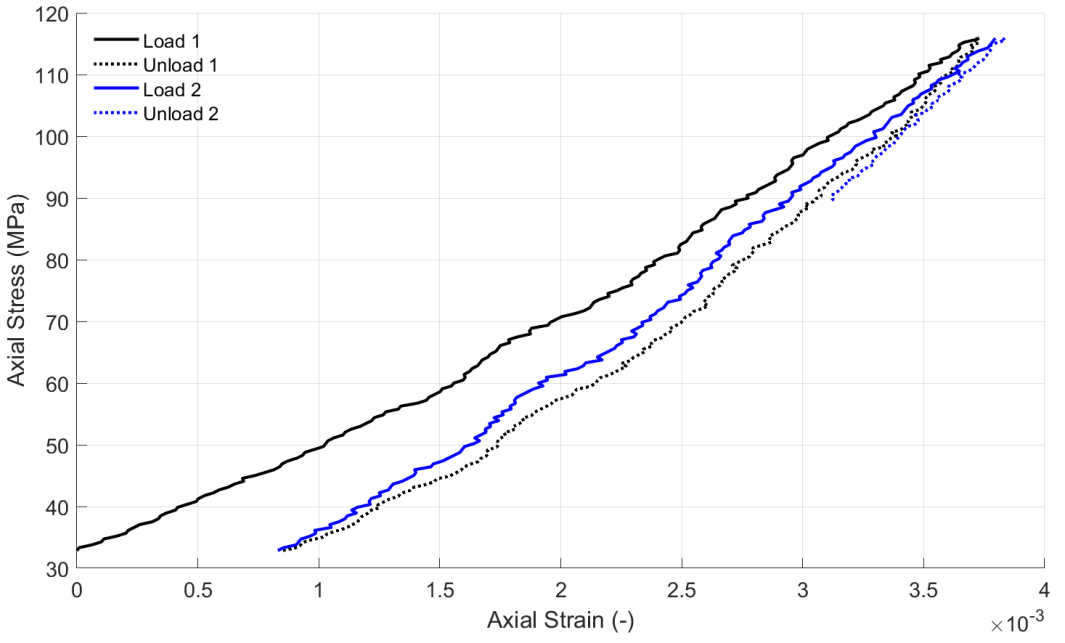

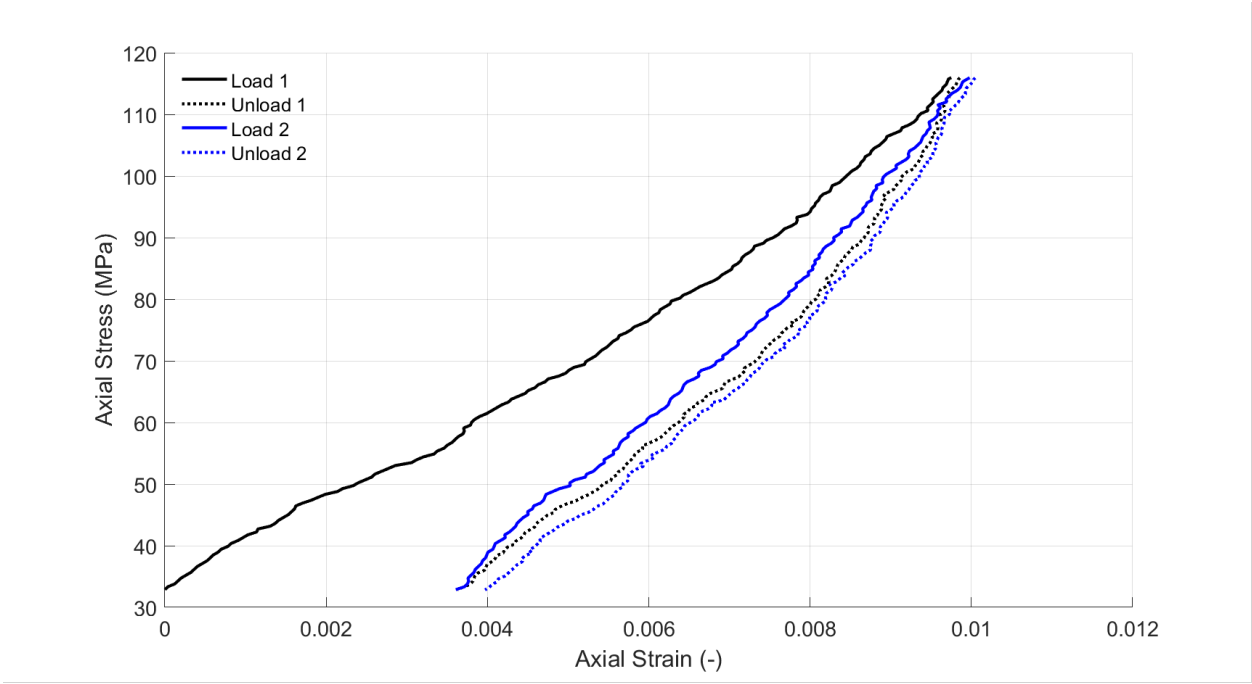

Both show consistent points of stiffening as well as a similar level of hysteresis as the other DRA experiments. The difference between the strain measurements for the load/unload stages is given by

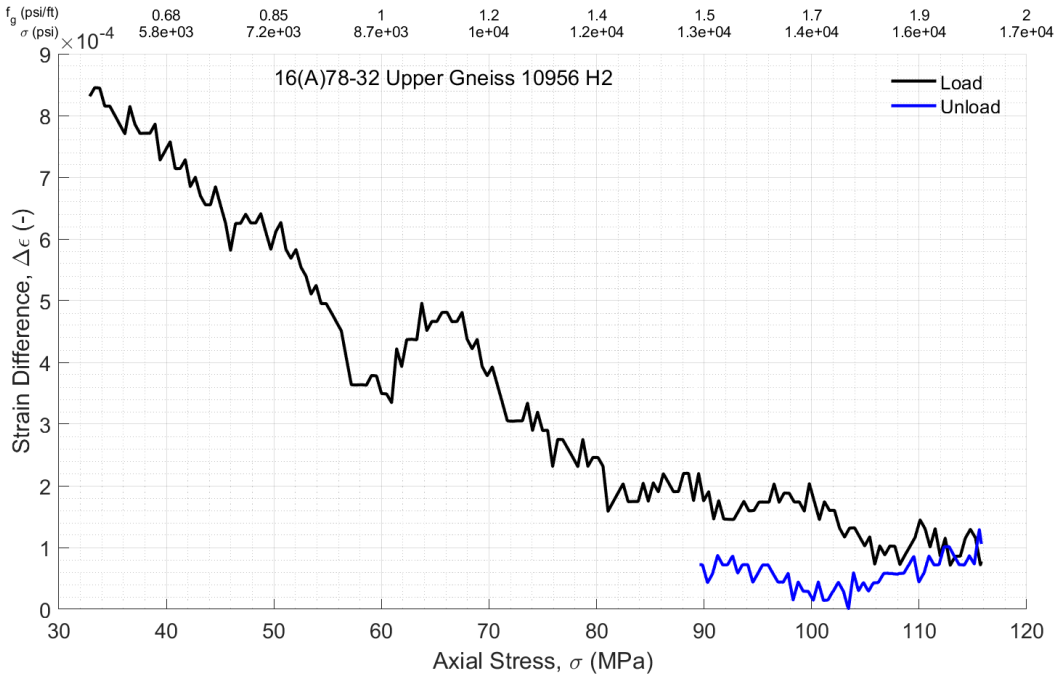

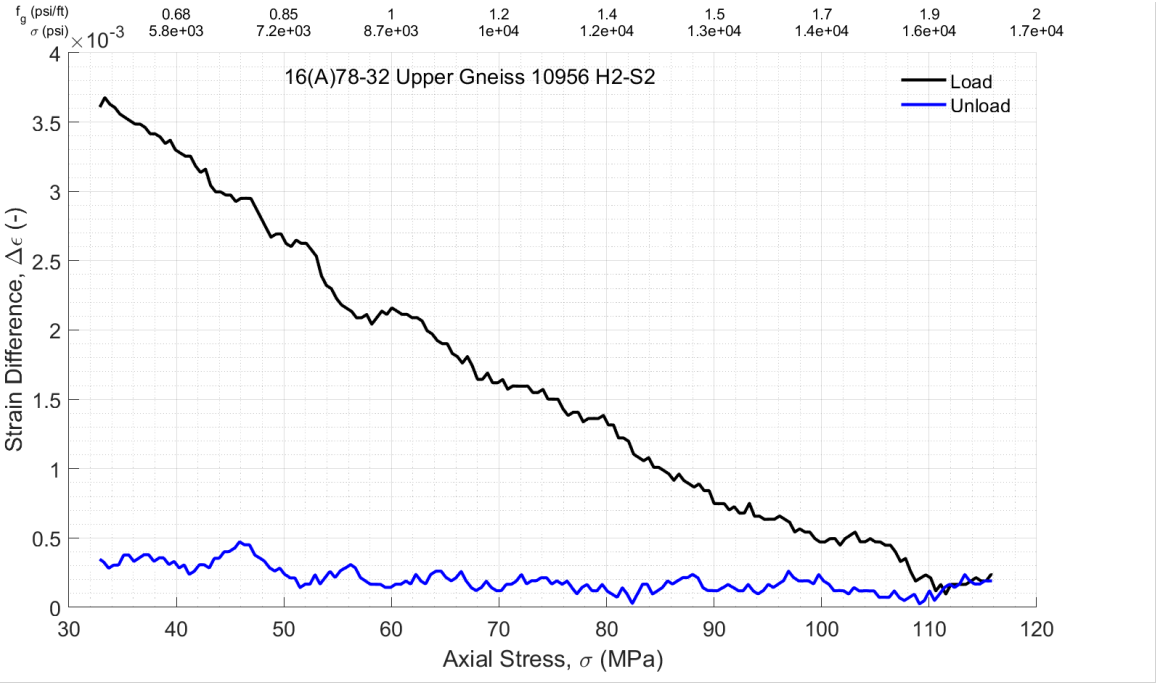

There are not clear inflections, though if anything, there is a first inflection around 52 MPa for both.

Bringing DRA and TUV stiffnesses together (by taking derivative of stress with respect to strain for DRA curves) gives (here showing TUV for y-direction, just for a reference)

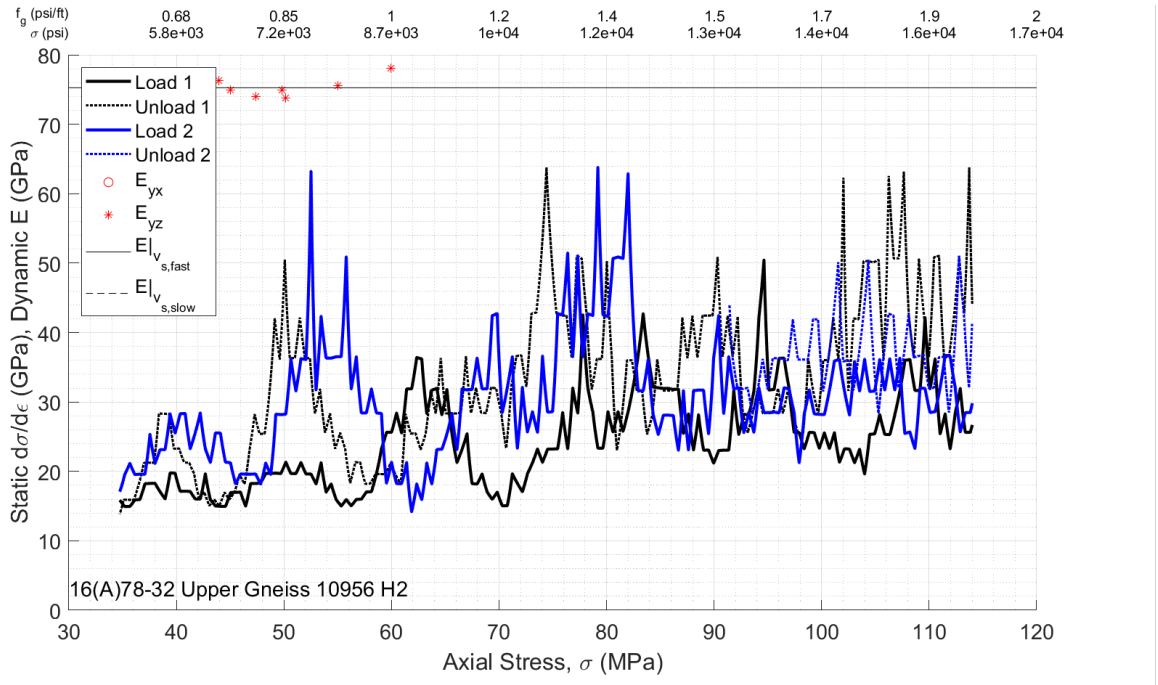

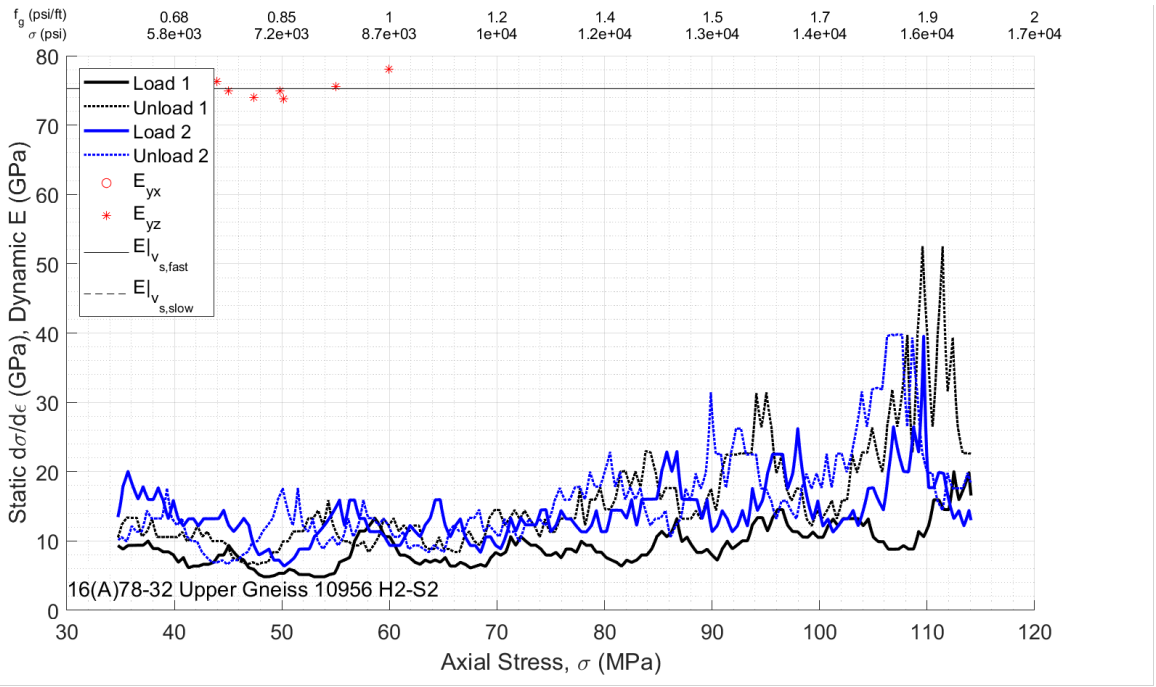

There is considerably less consistency of inflection points compared to other orientations. This could be due to the sample being from around 45 degrees to proposed principal stress orientations, meaning that dominant sets of compliant pores (such as microcracks) could be at an orientation to have less impact compared to H1 and H3.

Additionally, we can make a similar plot (though DRA only) but putting strain on the x-axis:

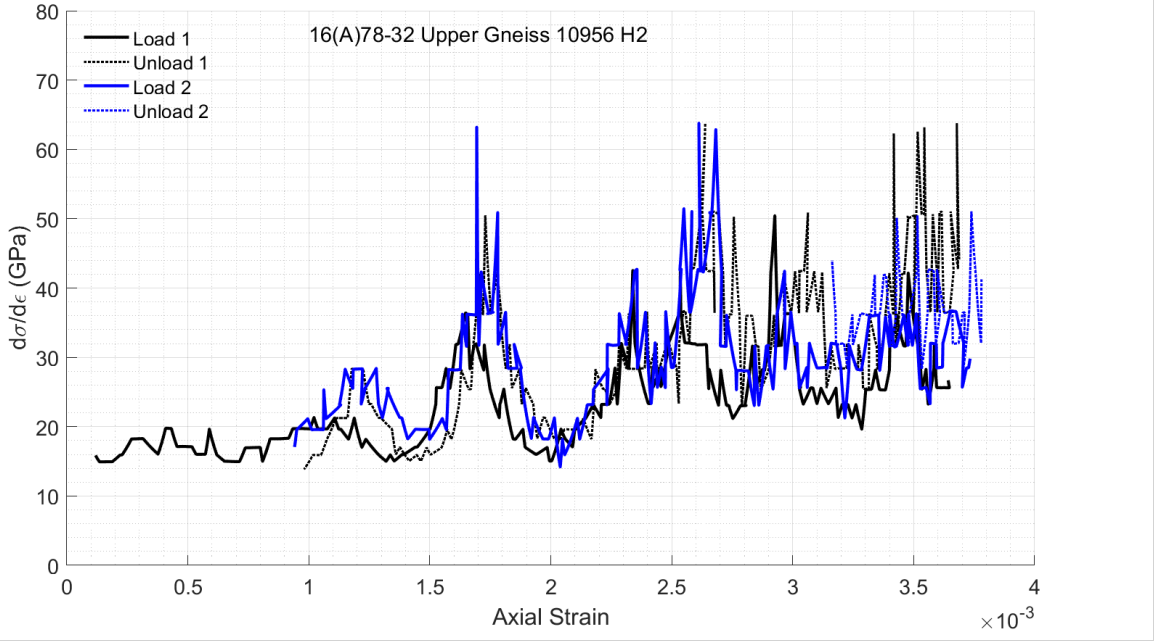

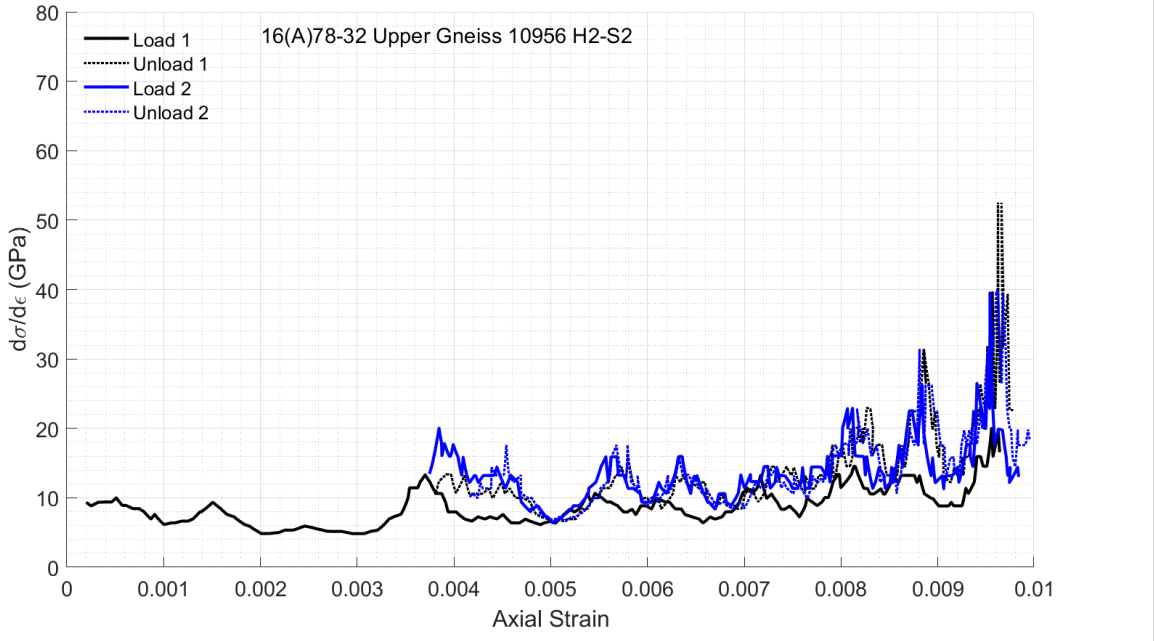

When viewed in this way, the consistency of inflections with certain levels of strain is clear.

Z-Direction: Compendium

Here the z-direction is along the core axis, where the core axis is deviated at 65 degrees from the vertical. Also, because the well is intended to be oriented toward the nominal minimum principal stress direction, it is likely that the z-direction gives the best alignment to minimum stress. Note that by convention this along-axis orientation is called “V” in the DRA tests.

Running the TUV experiments, we find

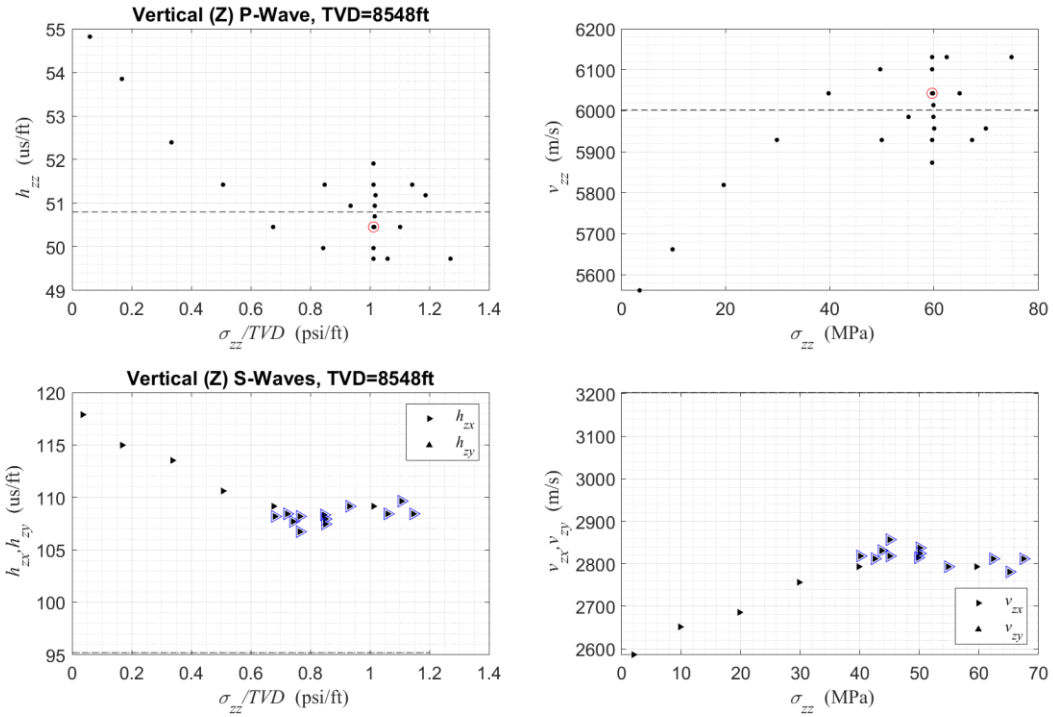

There is a clear rollover around 44 MPa in the shear wave velocity. Using Eq. (1), the quasi-isotropic wavespeeds are

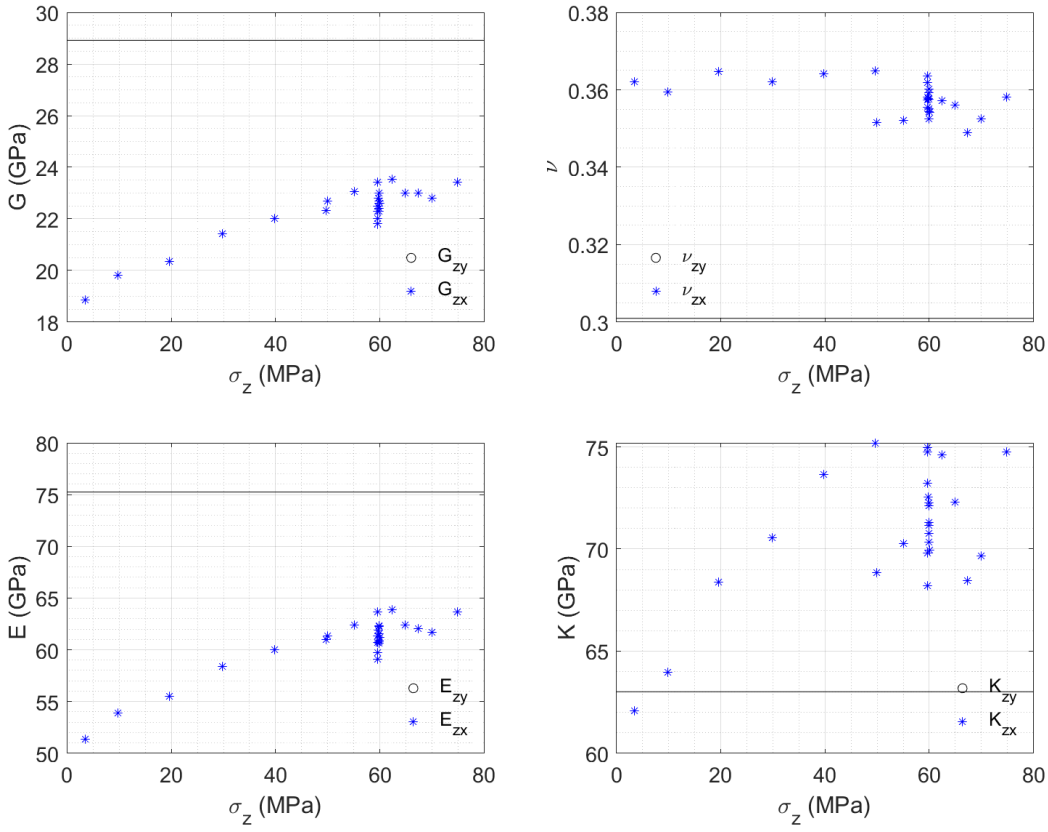

Interestingly, the Young's modulus appears to roll over around 65 MPa. Note that the reference lines from the sonic logs are again not very reliable because the noise level was indicating the sensor was under distress at this point in the logging process.

From the DRA on the V core, which is oriented co-linear to the TUV z-axis, we have one sample:

Dimensions	
height (mm):	50.25
width (mm):	32.05
Angle retrieved (degrees):	NA

DRA experiments are run with the loading sequence

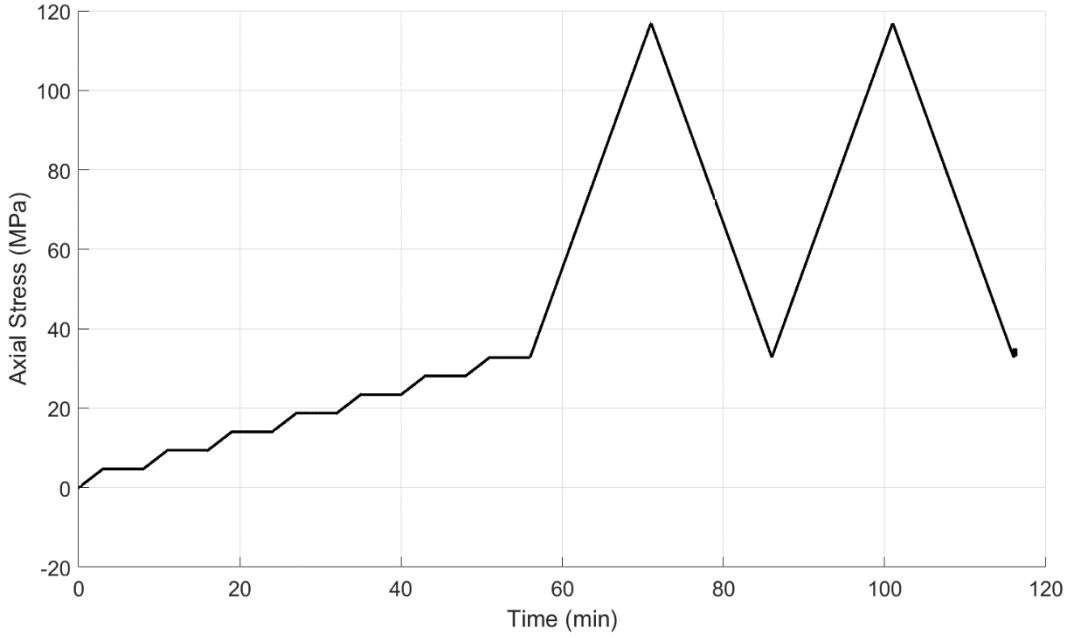

This results in the following displacements, which have been reduced by an amount estimated for deformation of 100mm of tool steel with E=210 GPa (comprising a lower bound on the platen deformation). This gives

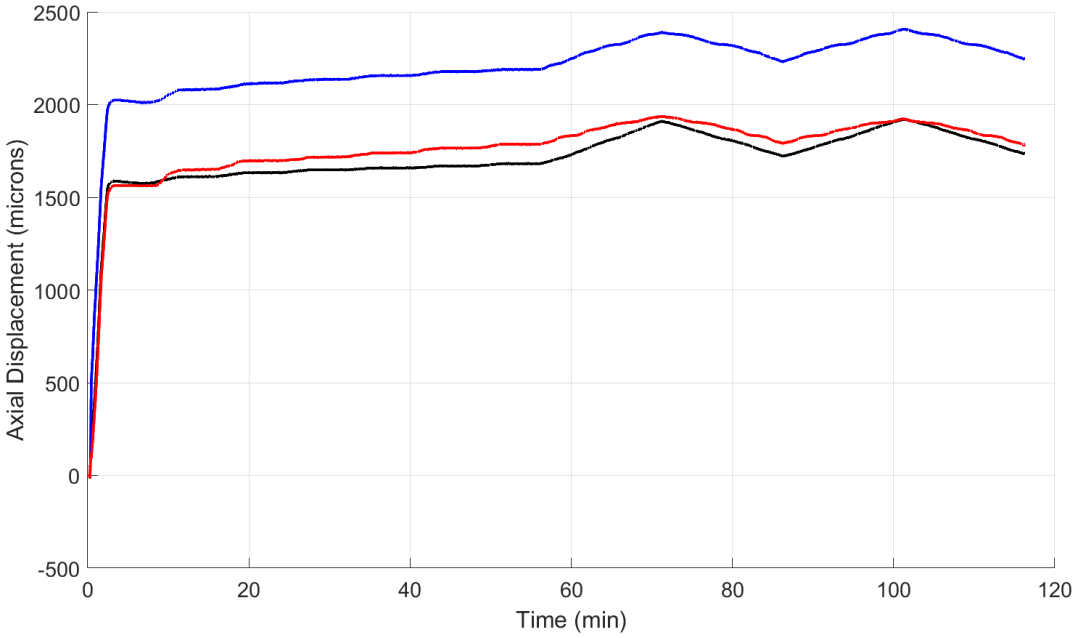

Averaging and plotting stress versus strain relationships for the 2 load/unload cycles, setting zero strain at the beginning of the first load cycle, gives

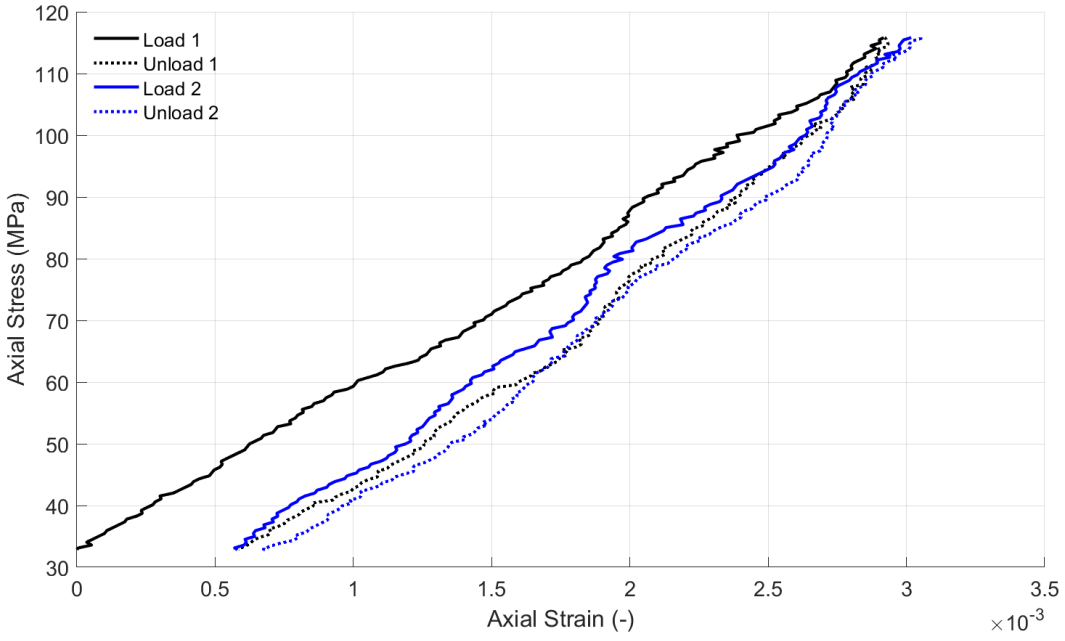

Appears to be stiffening around 50 MPa and 70 MPa. And, again, there is around plastic strain of around 0.0001 evidenced by the difference between the end of first and second loading and unloading stages. The difference between the strain measurements for the load/unload stages is given by

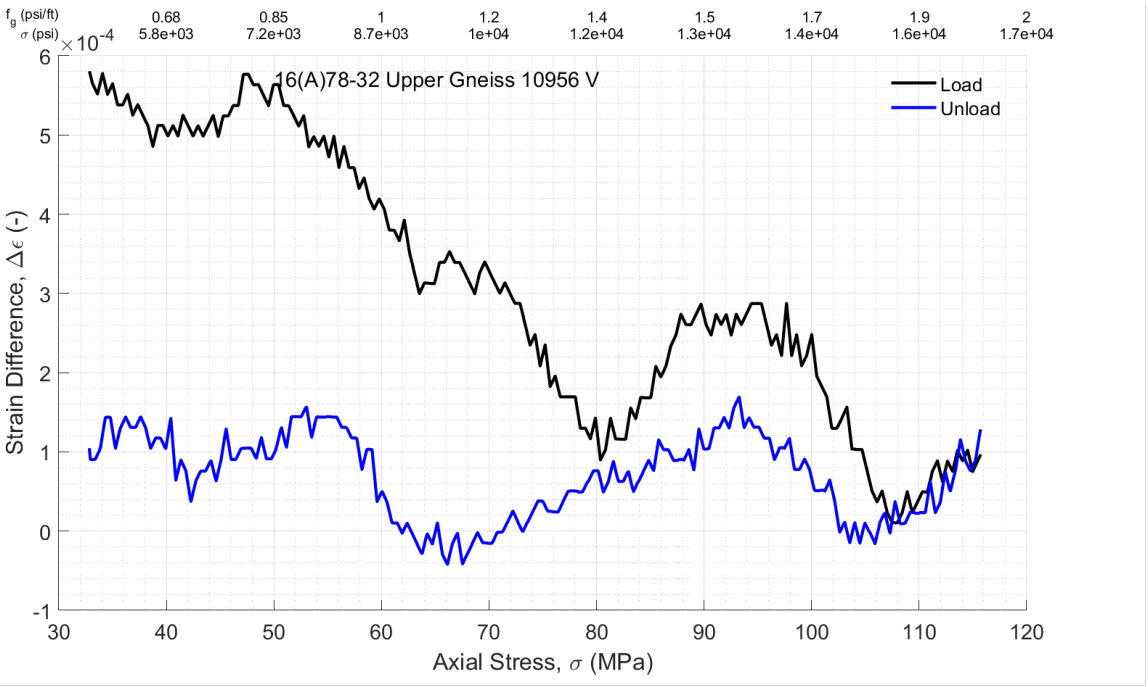

The most striking downward inflection is around 48 MPa. Bringing DRA and TUV stiffnesses together (by taking derivative of stress with respect to strain for DRA curves) gives

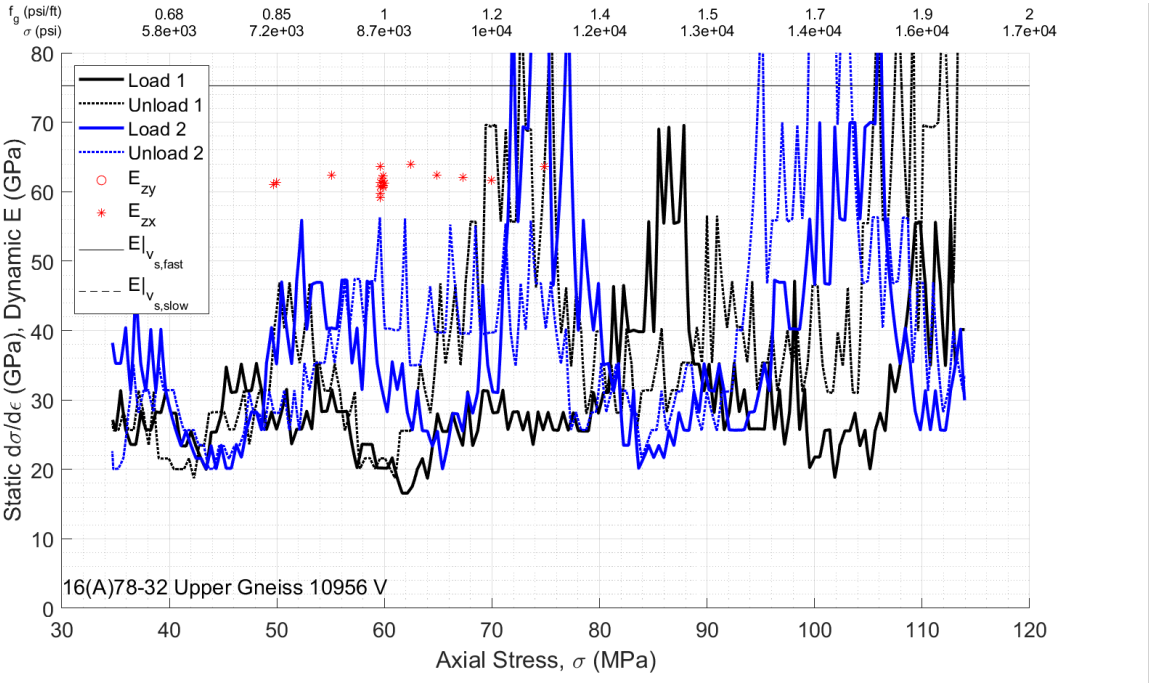

This again shows inflection around 48 MPa. Additionally, we can make a similar plot (though DRA only) but putting strain on the x-axis:

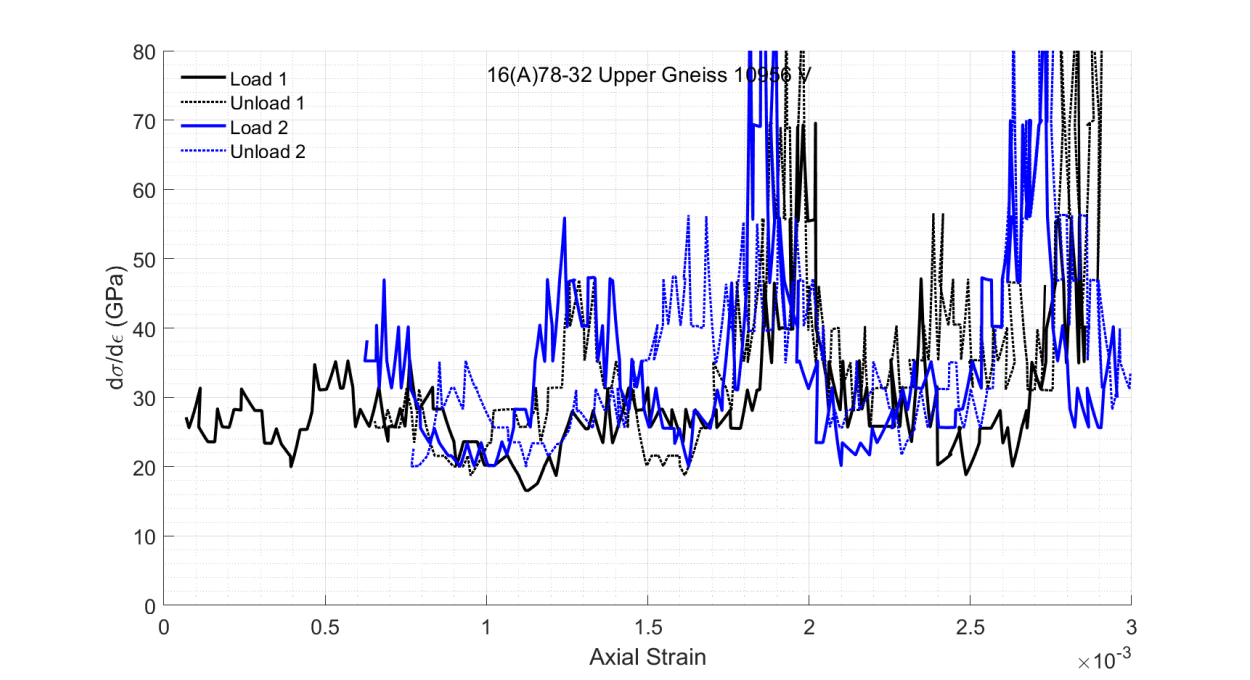

This again shows there to be apparent consistency of the load levels at which stiffening occurs, although the consistency is less by the time of the second unloading, possibly due to accumulation of plastic deformation by this final step in the experiment.

Lines of Evidence

A summary of the lines of evidence obtained from these experiments is given by:

Series	LoE	s1_val	s1_V	s1_L	s1_C	s1_R	s2_val	s2_V	s2_L	s2_C	s2_R	s3_val	s3_V	s3_L	s3_C	s3_R	s4_val	s4_V	s4_L	s4_C	s4_R	s5_val	s5_V	s5_L	s5_C	s5_R
UpGn_x	vxx	30	2	1	1.5	0.9	79	2	1	1.5	0.9	0	0	0	0	0.9	0	0	0	0	0.9	0	0	0	0	0.9
UpGn_x	vxz	79	2	2	1.5	0.9	0	0	0	0	0.9	0	0	0	0	0.9	0	0	0	0	0.9	0	0	0	0	0.9
UpGn_x	Exz	79	1.5	2	1.5	0.9	0	0	0	0	0.9	0	0	0	0	0.9	0	0	0	0	0.9	0	0	0	0	0.9
UpGn_x	Kxz	30	1.5	2	1.5	0.9	0	0	0	0	0.9	0	0	0	0	0.9	0	0	0	0	0.9	0	0	0	0	0.9
UpGn_x	s_e	49	2	2	1.5	0.9	68	2	1	1.5	0.9	98	2	0.5	1.5	0.9	0	0	0	0	0.9	0	0	0	0	0.9
UpGn_x	De	50	2	1.5	1.5	0.9	85	1.5	2	1.5	0.9	100	1.5	1	1.5	0.9	0	0	0	0	0.9	0	0	0	0	0.9
UpGn_x	ds_de	37	2	3	2	0.9	48	2	2.5	2	0.9	66	2	1	1	0.9	87	1.5	0.5	1	0.9	0	0	0	0	0.9
UpGn_y	vyy	40	2	2	2	0.9	0	0	0	0	0.9	0	0	0	0	0.9	0	0	0	0	0.9	0	0	0	0	0.9
UpGn_y	vyz	44	2	2	2	0.9	0	0	0	0	0.9	0	0	0	0	0.9	0	0	0	0	0.9	0	0	0	0	0.9
UpGn_y	Kyz	40	1.5	0.5	1.5	0.9	0	0	0	0	0.9	0	0	0	0	0.9	0	0	0	0	0.9	0	0	0	0	0.9
UpGn_y	De	44	2	1	1.5	0.9	94	1.5	0.5	1	0.9	0	0	0	0	0.9	0	0	0	0	0.9	0	0	0	0	0.9
UpGn_y	s_e	46	2	1.5	1.5	0.9	65	2	1	1.5	0.9	88	2	0.5	1	0.9	0	0	0	0	0.9	0	0	0	0	0.9
UpGn_y	ds_de	40	2	1.5	2	0.9	64	2	1.5	1.5	0.9	85	2	1.5	2	0.9	0	0	0	0	0.9	0	0	0	0	0.9
UpGn_H2	s_e	50	2	2.5	3	0.9	65	2	1.5	1.5	0.9	0	0	0	0	0.9	0	0	0	0	0.9	0	0	0	0	0.9
UpGn_H2	s_e	52	2	2.5	3	0.9	0	0	0	0	0.9	0	0	0	0	0.9	0	0	0	0	0.9	0	0	0	0	0.9
UpGn_H2	De	52	2	1.5	2.5	0.9	68	1.5	3	1	0.9	89	1.5	0.5	1	0.9	100	1.5	0.5	1	0.9	0	0	0	0	0.9
UpGn_H2	De	53	2	1	2.5	0.9	60	1.5	2	1	0.9	0	0	0	0	0.9	0	0	0	0	0.9	0	0	0	0	0.9
UpGn_H2	ds_de	35	2	1.5	1	0.9	47	2	1	2	0.9	64	2	0.5	1.5	0.9	0	0	0	0	0.9	0	0	0	0	0.9
UpGn_H2	ds_de	100	2	0.5	1	0.9	0	0	0	0	0.9	0	0	0	0	0.9	0	0	0	0	0.9	0	0	0	0	0.9
UpGn_z	vzz	60	2	1	1.5	0.9	0	0	0	0	0.9	0	0	0	0	0.9	0	0	0	0	0.9	0	0	0	0	0.9
UpGn_z	vzx	45	2	3	1.5	0.9	0	0	0	0	0.9	0	0	0	0	0.9	0	0	0	0	0.9	0	0	0	0	0.9
UpGn_z	Ezx	64	1.5	3	1.5	0.9	0	0	0	0	0.9	0	0	0	0	0.9	0	0	0	0	0.9	0	0	0	0	0.9
UpGn_z	Kzx	50	1.5	2	1.5	0.9	0	0	0	0	0.9	0	0	0	0	0.9	0	0	0	0	0.9	0	0	0	0	0.9
UpGn_z	s_e	48	2	2.5	1.5	0.9	68	2	2	1.5	0.9	95	2	1	1.5	0.9	0	0	0	0	0.9	0	0	0	0	0.9
UpGn_z	De	48	2	3	1.5	0.9	70	1.5	2	1.5	0.9	95	2	1	1.5	0.9	0	0	0	0	0.9	0	0	0	0	0.9
UpGn_z	ds_de	35	2	1	1.5	0.9	45	2	1.5	1.5	0.9	65	2	0.5	1.5	0.9	95	1.5	0.5	1.5	0.9	0	0	0	0	0.9

To note:

- Each series is named with the direction after an underscore (column 1).

- The source of the line of evidence (LoE) is given in column 2, where v is velocity, E is Young's modulus, s_e is stress-strain curve, De is the change in strain curve, and ds_de is the instantaneous stiffness curve. Subscripts indicate direction of propagation followed by polarity, as usual, such that for example vxy indicates a shear wave velocity propagating in x-direction with y-polarity.
- All stress values (i.e. s1_val, s2_val) are given in MPa.
- Each source can give multiple lines of evidence, thus the table is set up to accept up to 5 lines of evidence for each source. Zeros are filled into the table where there are no additional lines of evidence.
- The weight assigned according to the prescribed rubric is given after an underscore, where V indicates relevance, L indicates reliability, C indicates consistency, and R indicated representivity. All values of representivity are set at 0.9 because there is insufficient data to determine exactly how representative the sample is of the surrounding formation.

Lower Gneiss

Summary

The 16A(78)-32 Lower Gneiss samples are from around 10,979 MD (3347 m). They are therefore from 23 ft (7 m) further along the well than the Upper Gneiss samples. They are in the 65 degree deviated part of the well, and here TVD=8557 ft (2609 m). There is a platy foliation and mineral differentiation into stripes. It is not clear the original orientation (in-situ) because of the deviation of the core axis and the unknown azimuthal orientation of the core. However, similar to the Upper Gneiss, the core has a foliation that is subparallel (although slightly more inclined than Upper Gneiss) to the core axis (Figure 25). Following the same arguments as for the Upper Gneiss, we propose that the foliation is vertical and that the maximum principal stress is acting perpendicular to the foliation.

This section does not have TUV data. However, for convenience, the x-direction will be defined perpendicular to foliation, as in the Upper Gneiss. The y- and z-directions will also be defined the same relative to foliation as in the Upper Gneiss (see Figure 21). In this regard, the H2 core is aligned with foliation and taken as the y-direction. The H3 core is 114 degrees from the H2, and so it is 24 degrees from the actual x-axis. The H1 core is between the two, and the V core is parallel to the z-axis.

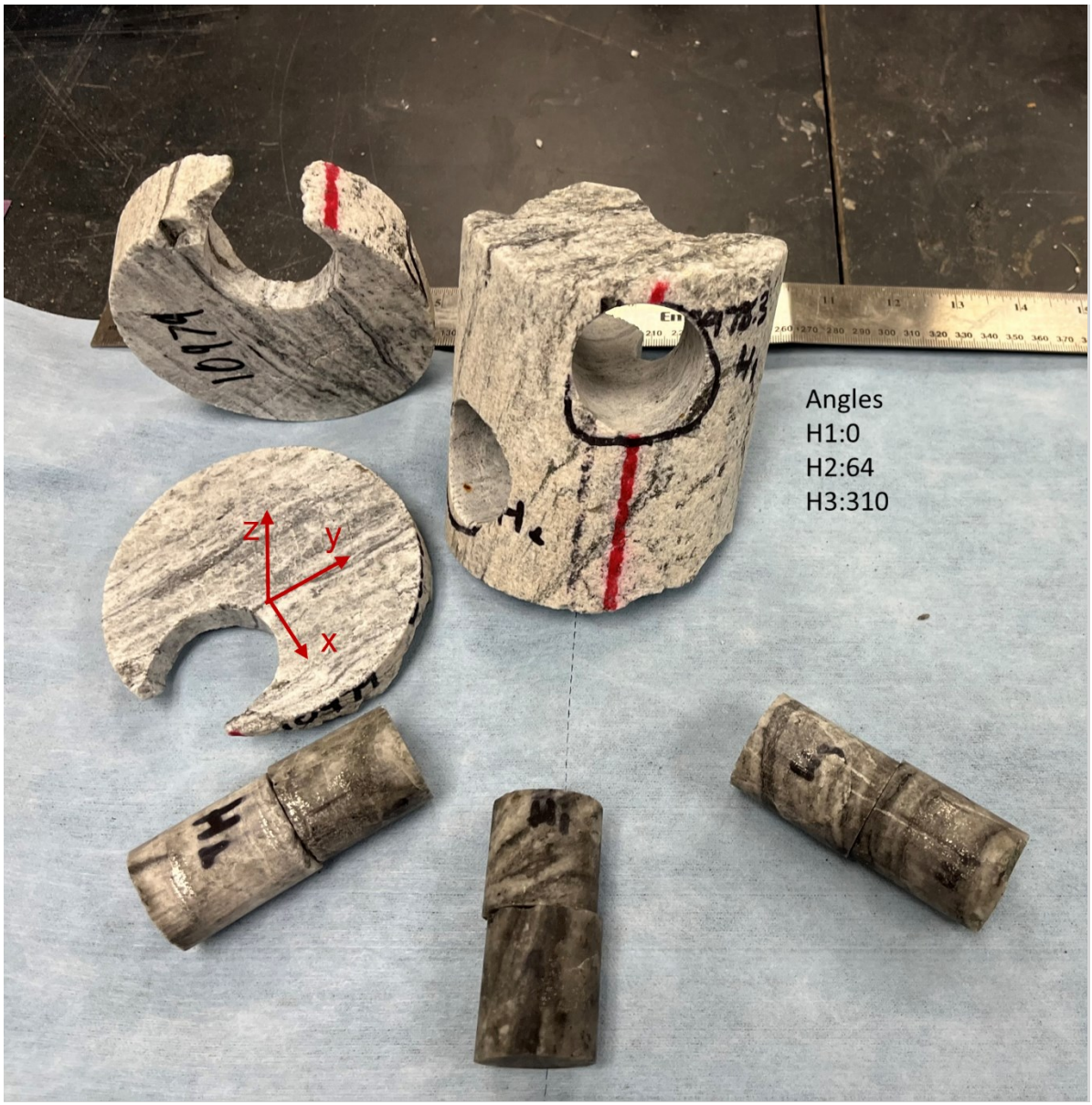

Figure 25: Parent core for Lower Gneiss with DRA samples (cylinders), showing x, y, z axes and with cylinders laying in approximate directional correspondence to TUV sample.

In the absence of the TUV data, which in formations where it is available provides the clearest indication of stress orientation relative to core axes, we will proceed directly to discussion of the lines of evidence implying candidate in-situ stress levels. The lowest value has its mode at around 47 MPa (0.8 psi/ft). It is predominantly implied by lines of evidence from the z-direction, which is dipping at 25 degrees below horizontal, but is nonetheless the best aligned with the minimum horizontal stress direction. Similar to the nearby Upper Gneiss, if one assumes that the misalignment with the actual minimum stress leads this to be an upper estimate, one can then propose that the minimum stress could be as low as 41 MPa (0.69 psi/ft). Interestingly, the lines of evidence that are directly supporting this estimate of minimum stress are from the y-orientation. Potentially this is once again implying that the minimum stress is actually dipping

(as previously discussed and illustrated in Figure 24), and its magnitude is s_{hmin}~41 MPa (~0.69 psi/ft), which is in very close agreement with the results from the Upper Gneiss.

Secondly, there is a collection of lines of evidence around a next-higher stress, with the mode of the distribution at 62 MPa (~1.05 psi/ft), as shown in Figure 26. This value is very close to the expected overburden gradient. Interesting, the strongest lines of evidence come from the z-orientation and x-orientation rather than the (most vertical) y-orientation. While the weight of evidence from the z-orientation could again imply that nominally vertical principal stress is actually inclined by some angle, as illustrated in Figure 24, the lines of evidence from the x-direction could imply that the maximum horizontal stress is very similar to the vertical stress and so the two are getting mixed together in the weight of evidence summary.

Thirdly, once can observe that, other than the lines of evidence from the x-direction at around 62 MPa (1.05 psi/ft), there are not many lines of evidence with clearly arguable relationship to a viable maximum horizontal stress. However, there is a collection of lines of evidence around 77 MPa (~1.30 psi/ft), very similar to the value inferred from the testing in nearby the Upper Gneiss. The strongest of these come from the x-orientation, which supports the idea that it is approximately aligned with the maximum principal stress direction. However, it is very difficult to argue one of these candidates for maximum horizontal stress over the other. With that said, there are no lines of evidence from the Upper Gneiss supporting that maximum principal stress gradient is ~1.05 psi/ft, whereas the option of maximum stress gradient of ~1.30 psi/ft is quite consistent with observation in the Upper Gneiss.

In the nearby Upper Gneiss, there was an alternative interpretation wherein a substantial collection of lines of evidence around 49 MPa (~0.83 psi/ft) was a possible value of the maximum principal stress. However, in the present case, the collection of lines of evidence around that point are most strongly from the z-direction, which is almost certainly much more closely aligned to the minimum stress direction. Hence it seems unlikely that the maximum stress is at this lower value.

Finally, as with other testing locations it is observed that there are some additional inflections giving several lines of evidence at higher stresses with some convergence of these around 1.45 psi/ft and 1.60 psi/ft. These are both completely consistent with observations from the Upper Gneiss. And, the former of these bears intriguing similarity in its implied stress gradient to high stress lines of evidence from the Lower Granitoid while the latter bears similarity in its implied stress gradient to high stress lines of evidence from the Upper Granitoid. The origin of these responses remains unknown but, again, can be expected to be clarified by application of a micromechanical rock physics model (being developed now) to the interpretation.

To summarize:

1) **Minimum horizontal stress** is likely dipping so as to be somewhat aligned with the nearby fault unconformity and has a magnitude of around 41 MPa (~0.69 psi/ft).
2) **Maximum horizontal stress** is aligned across the foliation and colinear with the minimum wavespeed direction and has candidate values around 62 MPa (~1.05 psi/ft) and around 77 MPa (~1.30 psi/ft), noting that the latter option is more consistent with the Upper Gneiss while the former is arguably more consistent with the weight of evidence provided by the Lower Gneiss.

3) **Vertical stress** is probably not actually a principal stress, but the nearest principal stress is the intermediate magnitude, inclined to the vertical at an angle of at least 20 degrees, and with a magnitude of 62 MPa (1.05 psi/ft).
4) **The hypothesis of inclination of principal stresses** is further supported by the evidence collected on this subunit, and would result in hydraulic fractures dipping at least 20 degrees from vertical, to be closer to perpendicular to the fault-unconformity than they would be to being perpendicular to the well axis of 16A(78)-32.

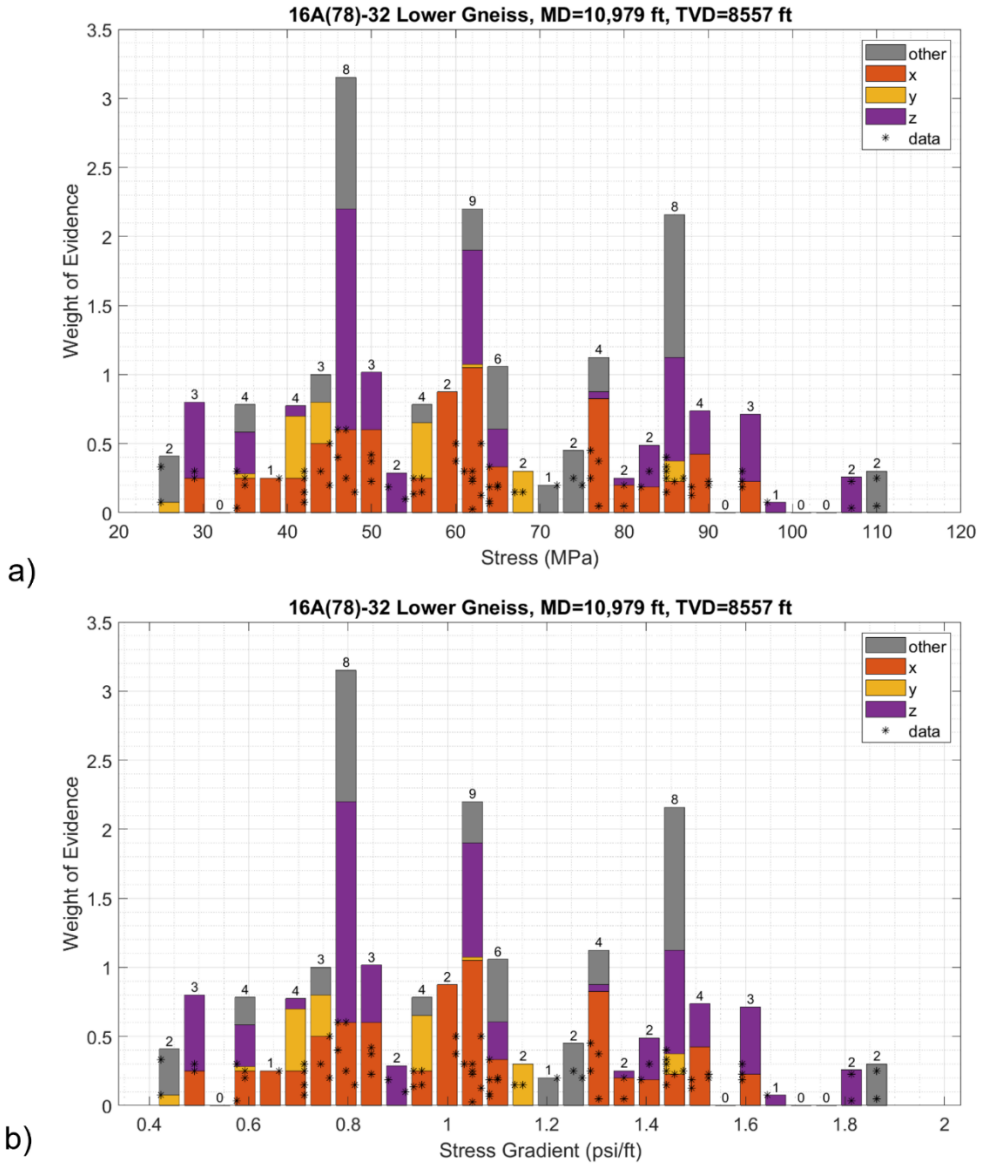

Figure 26: Integrated weight of evidence from DRA tests versus a) applied axial stress for the DRA experiments, b) corresponding implied stress gradient. The stars indicate individual data points, noting some lie directly on top of one another. The number at the top of each bar is the total lines of evidence in that bin. The bars are color coded to indicate the orientation of the sample giving the line(s) of evidence leading to that part of the bar.

H1-Direction: Compendium

The H1 direction is oblique to the x-y-z coordinate system. It generated two samples, with measurements and images as follows:

H1-1

Dimensions	
height (mm):	37.27
width (mm):	32.02
Angle retrieved (degrees):	0

H1-2

Dimensions	
height (mm):	32.16
width (mm):	31.97
Angle retrieved (degrees):	0

DRA experiments are run with the loading sequence

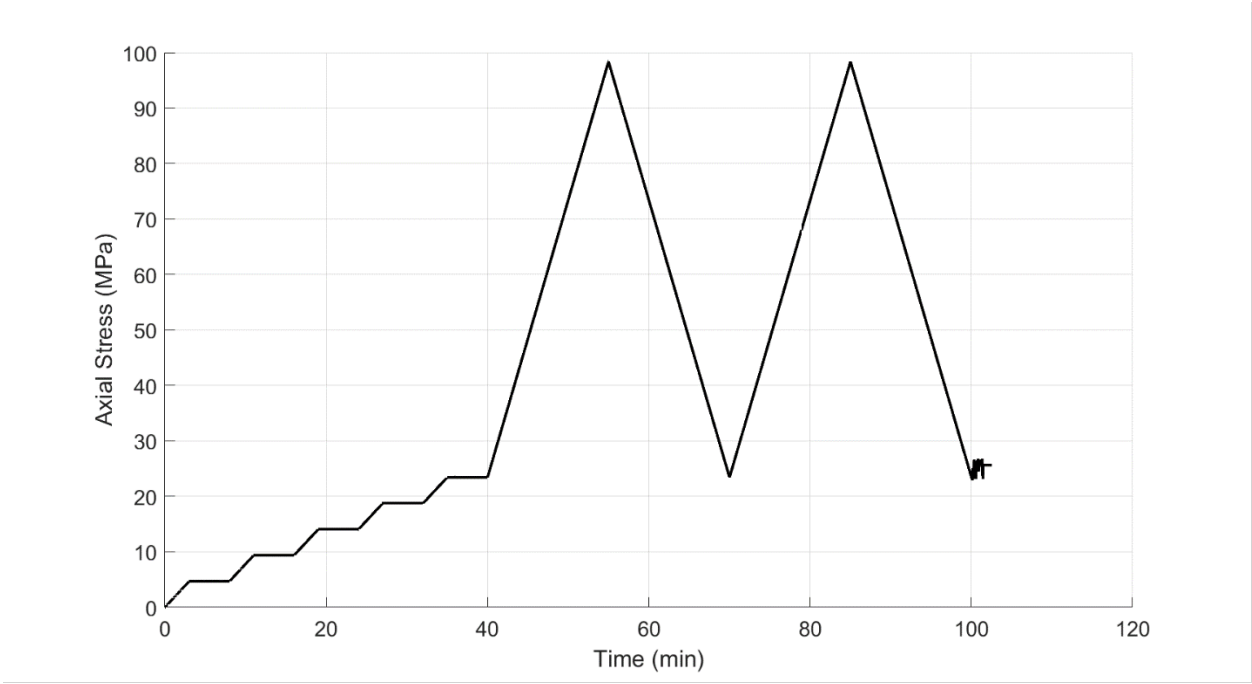

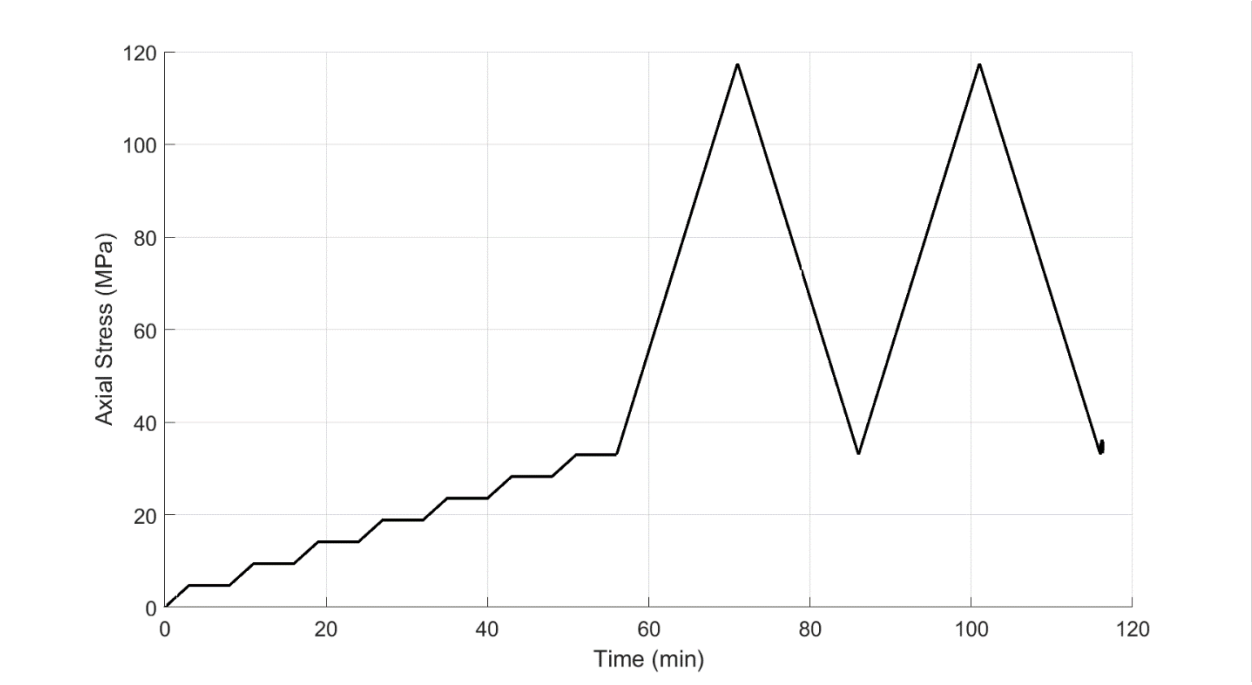

This results in the following displacements, which have been reduced by an amount estimated for deformation of 100mm of tool steel with E=210 GPa (comprising a lower bound on the platen deformation). This gives

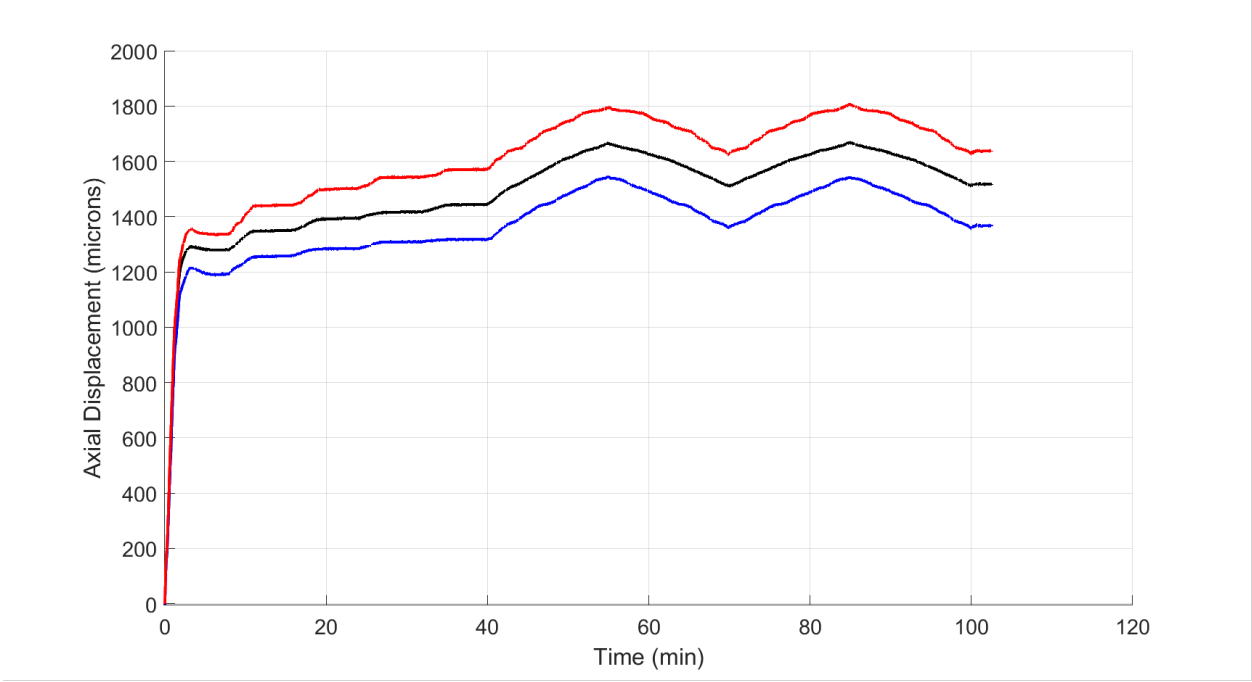

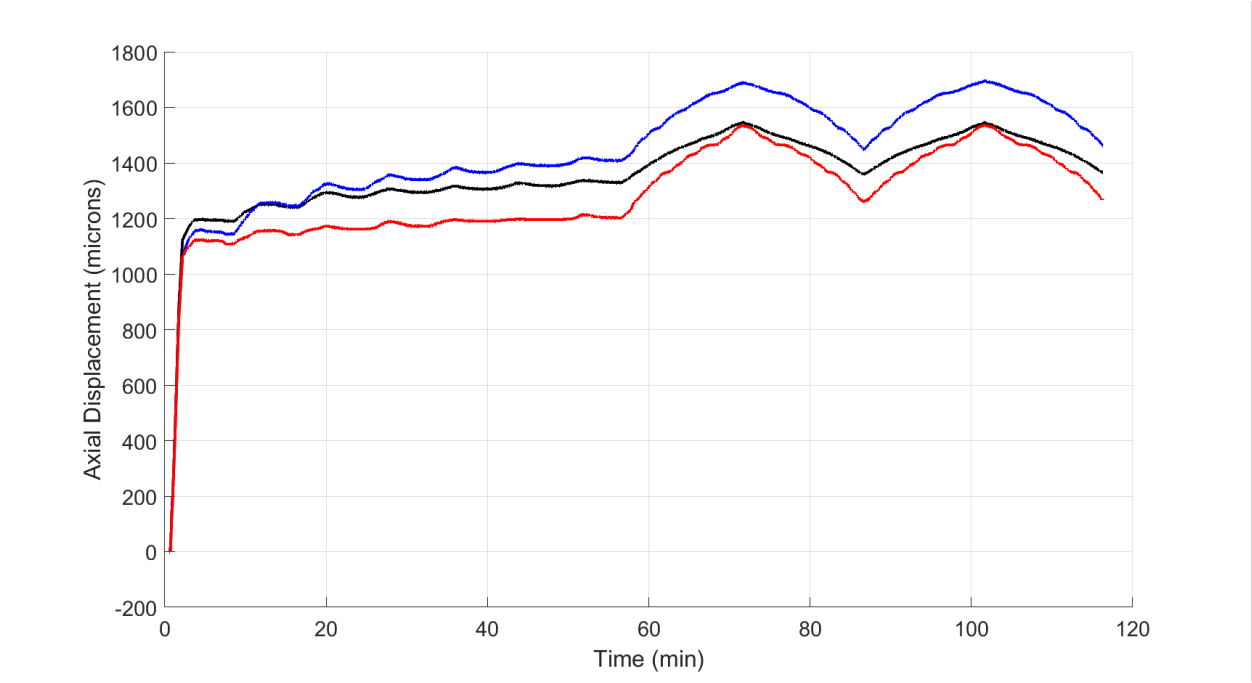

Both of these tests have relatively little tilting of the platens.

Averaging and plotting stress versus strain relationships for the 2 load/unload cycles, setting zero strain at the beginning of the first load cycle, gives

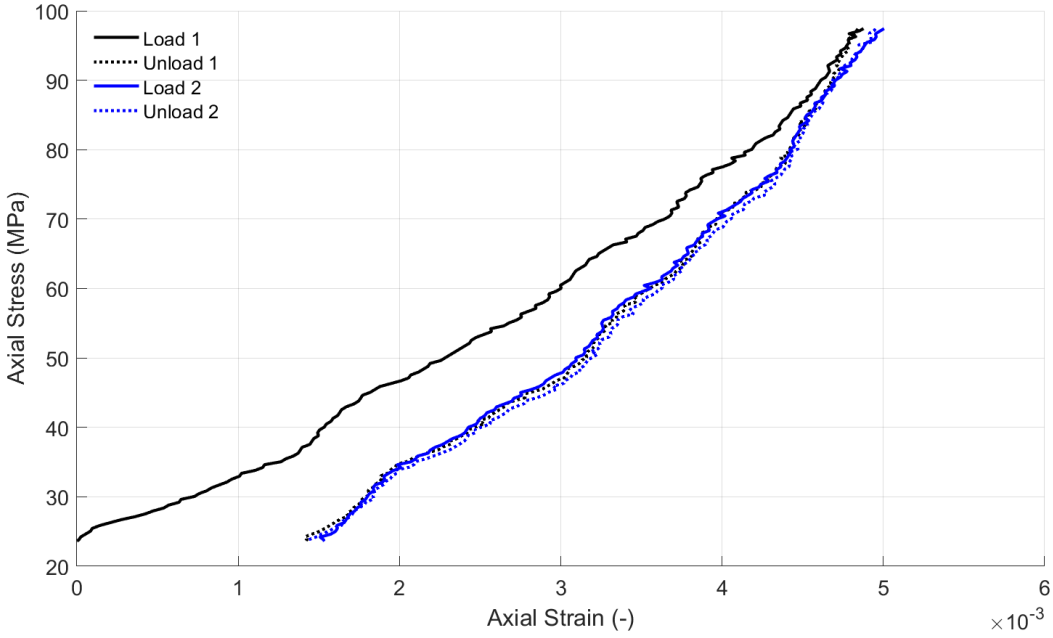

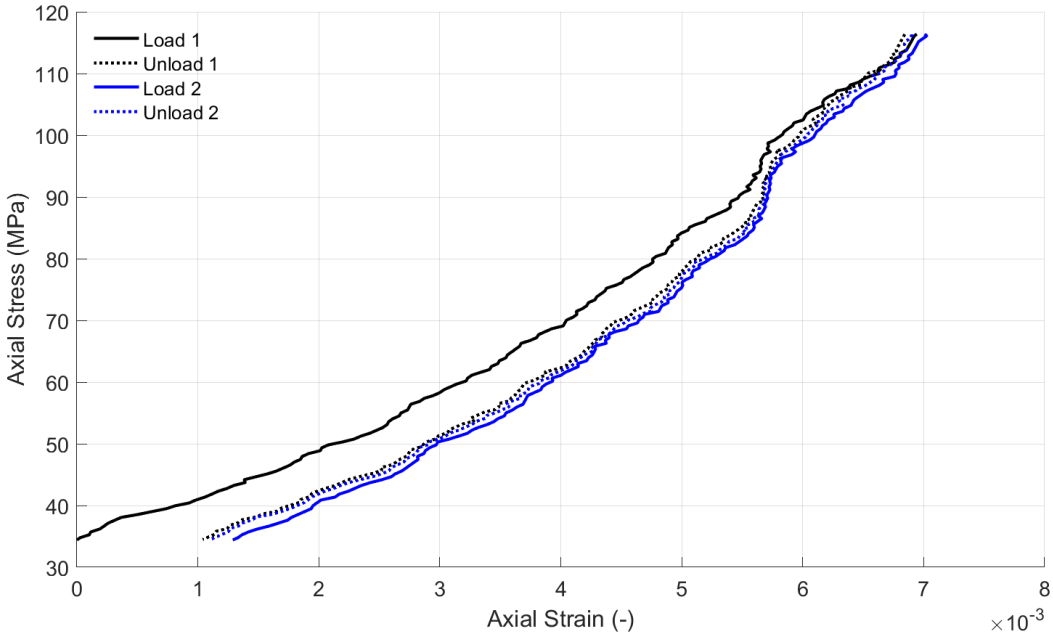

There are multiple stiffening sections in both tests, with the strongest at around 85 MPa in test 2. The strain difference between the first and second load cycles is given by

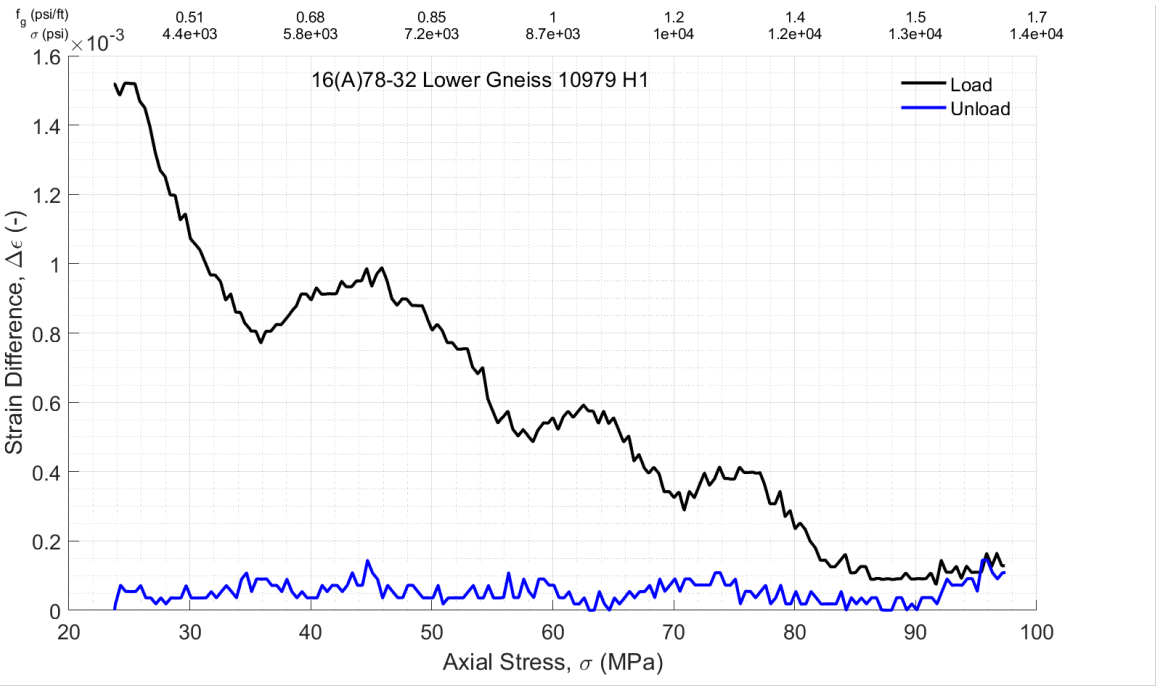

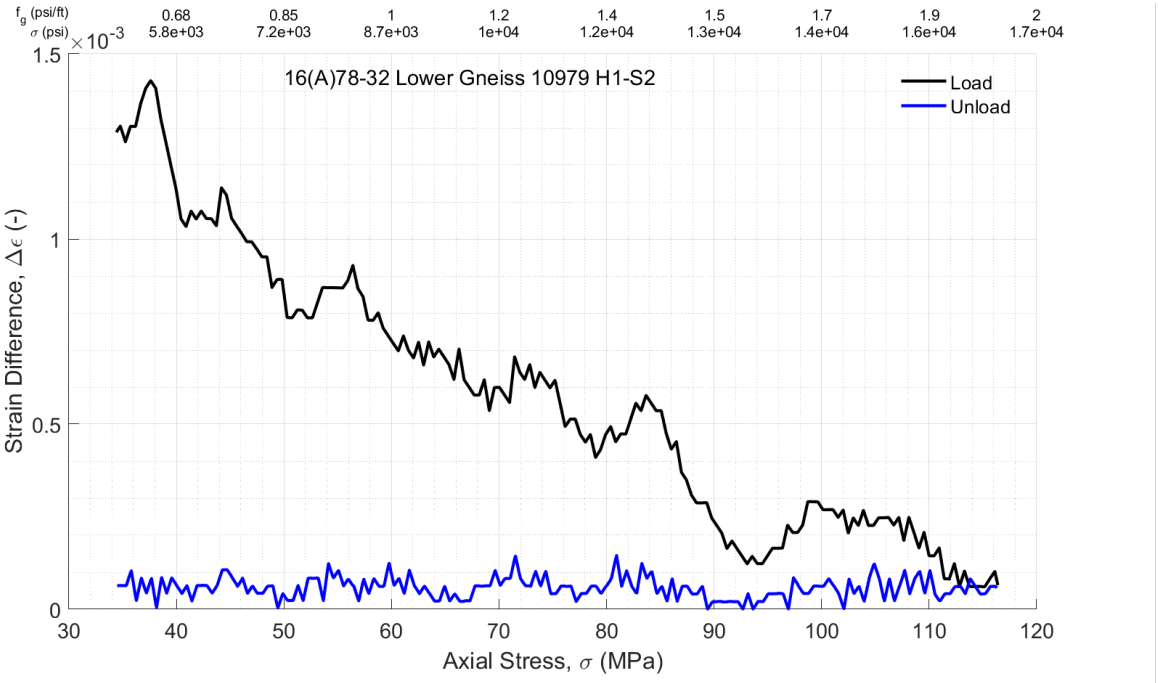

The second test once again has the strongest response at around 85 MPa. The first has multiple inflections. Bringing DRA and TUV stiffnesses together (by taking derivative of stress with respect to strain for DRA curves, and presenting here comparable TUV from Upper Gneiss) gives

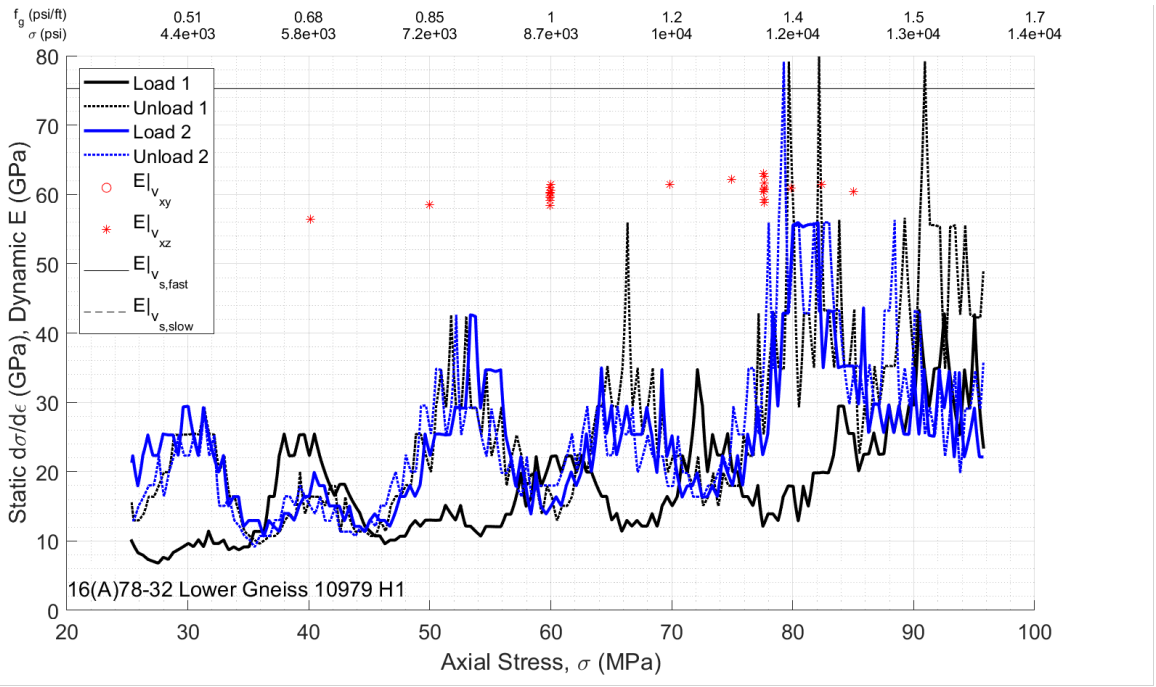

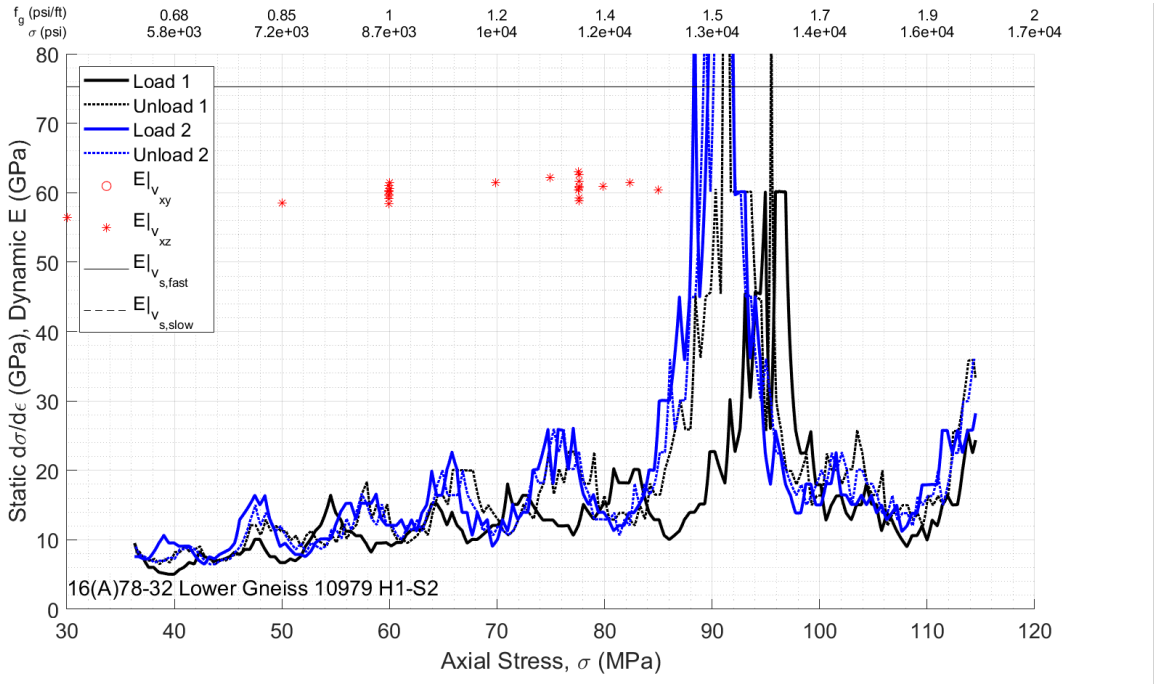

The non-monotonic stiffening is striking in both cases and very consistent in terms of load level. In the second experiment, the static Young's modulus reaches a similar value to the dynamic value (albeit taken from the Upper Gneiss where there were TUV experiments) after the increase at 85 MPa. In the first case, there are multiple inflection, all of which are readily incorporated (like with all lines of evidence) to the weight of evidence approach. Additionally, we can make a similar plot (though DRA only) but putting strain on the x-axis:

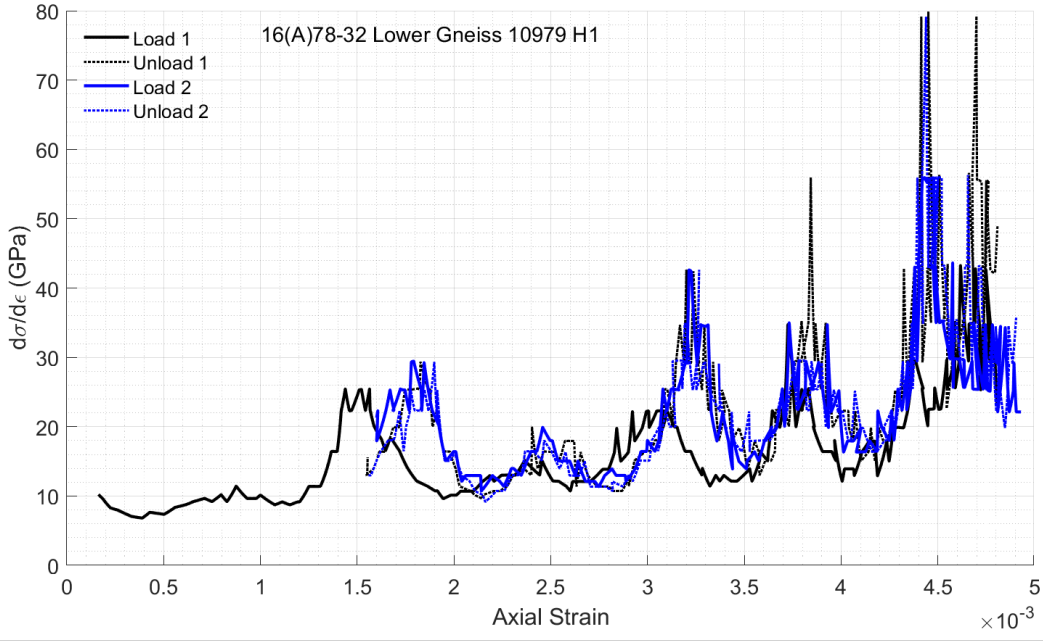

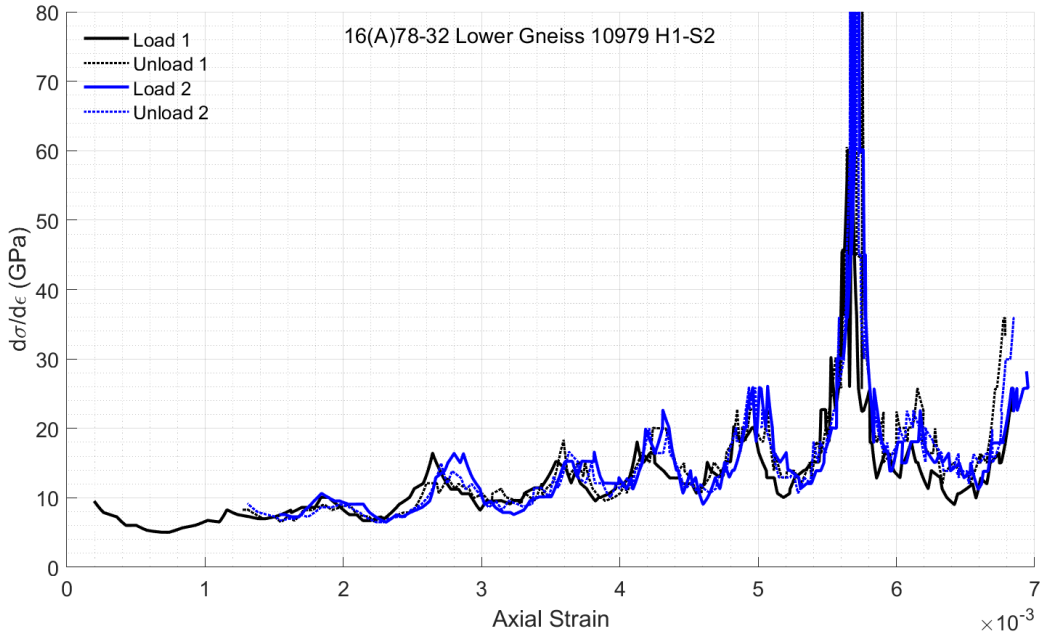

Again there is striking the agreement in stiffening at the strain of the first bump.

H2- (Y-) Direction: Compendium

Only one sample in this orientation, which was aligned with foliation. The dimensions and photograph of the sample are as follows:

Dimensions	
height (mm):	40.69
width (mm):	31.81
Angle retrieved (degrees):	63.8

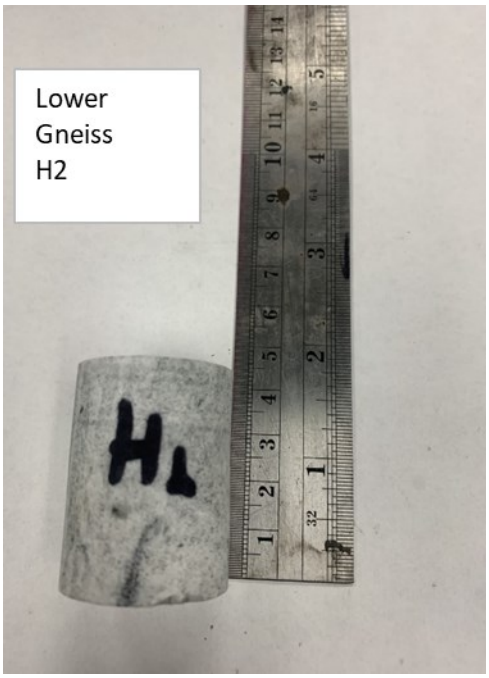

DRA experiments are run with the loading sequence

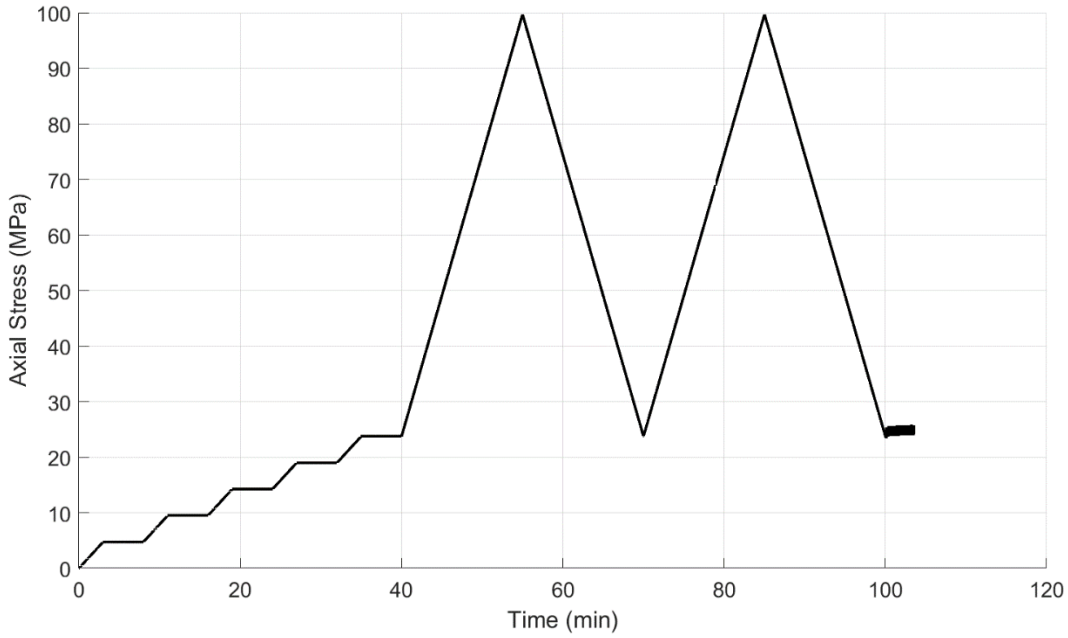

This results in the following displacements, which have been reduced by an amount estimated for deformation of 95mm of tool steel with E=210 GPa (comprising a lower bound on the platen deformation). This gives

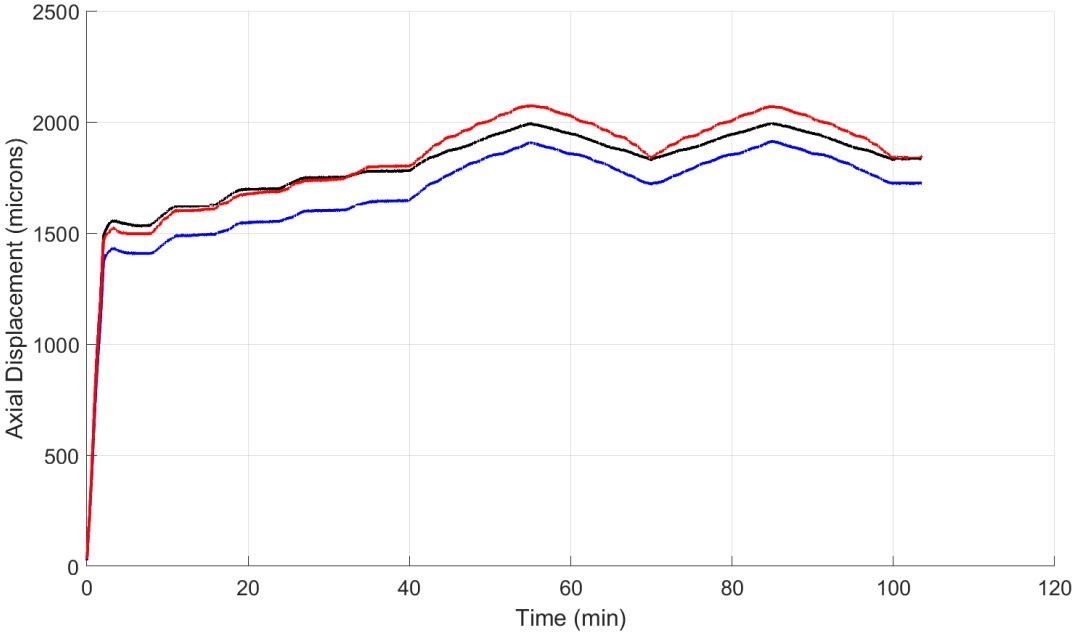

Again there is very little tilting of the platens, evidenced by consistency among the 3 LVDTs.

Averaging and plotting stress versus strain relationships for the 2 load/unload cycles, setting zero strain at the beginning of the first load cycle, gives

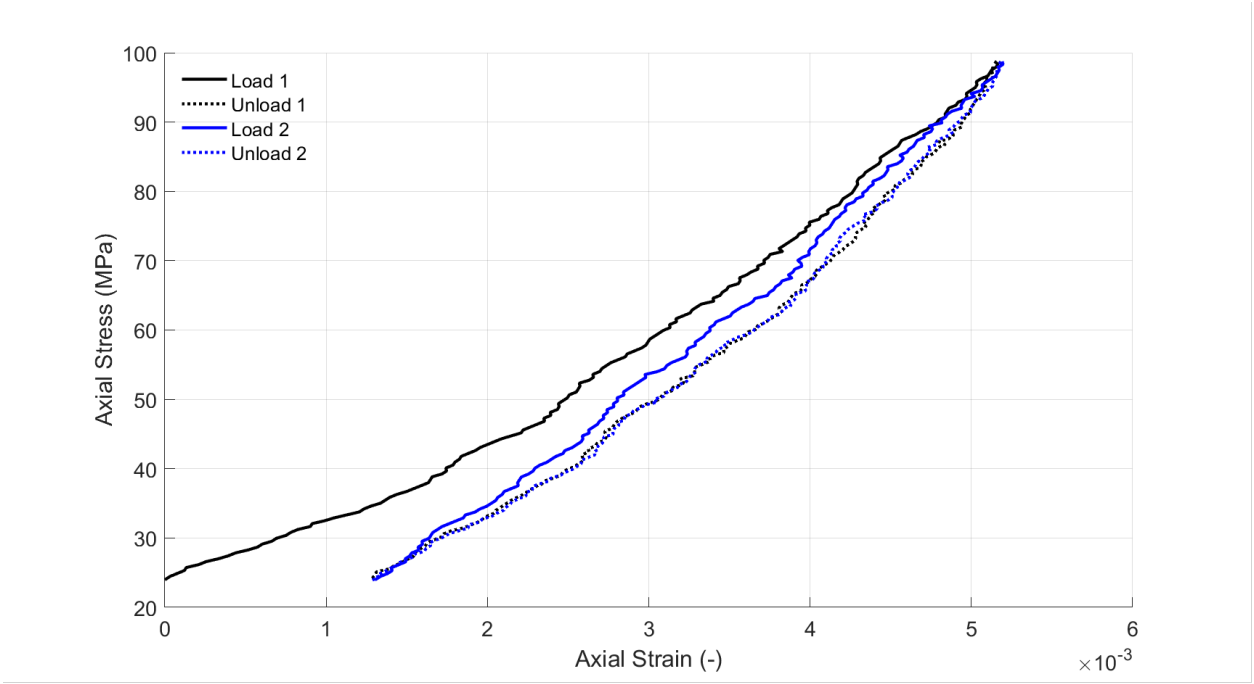

Here we can see several stiffening regions, particularly around 45 MPa and 65 MPa.

The difference between the strain measurements for the load/unload stages is given by

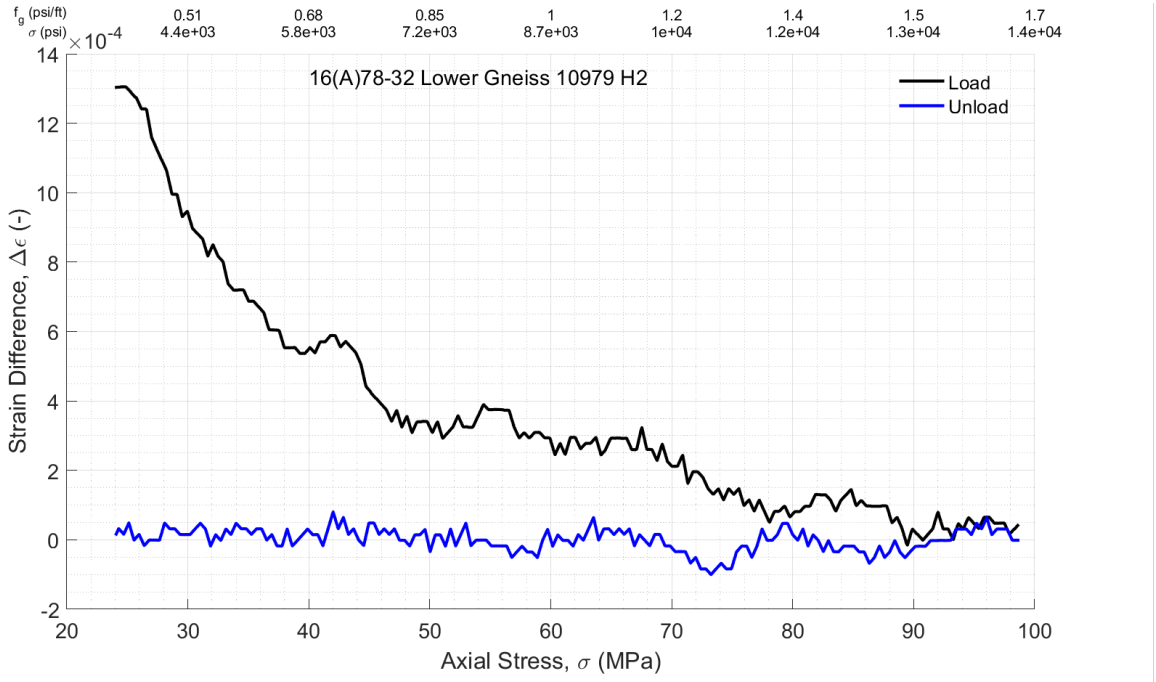

The most striking inflections are around 42 MPa and 68 MPa. Bringing DRA and TUV stiffnesses together (by taking derivative of stress with respect to strain for DRA curves, and presenting here comparable TUV from Upper Gneiss) gives

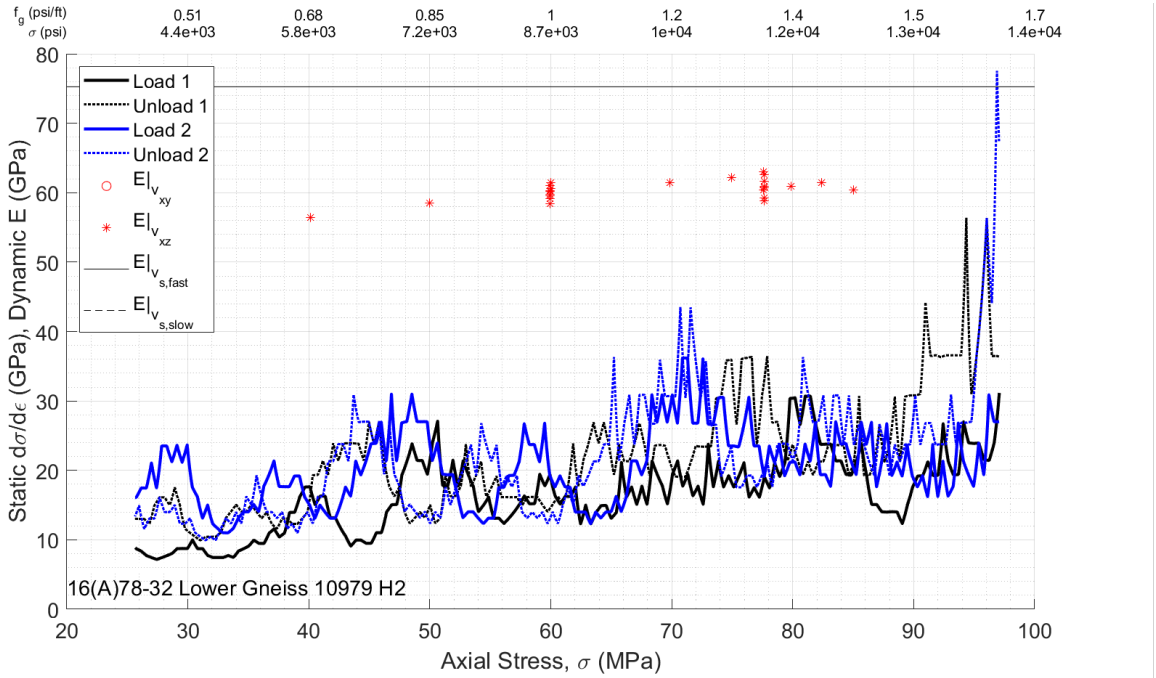

We can only see the consistency of the stiffening by putting strain on the x-axis:

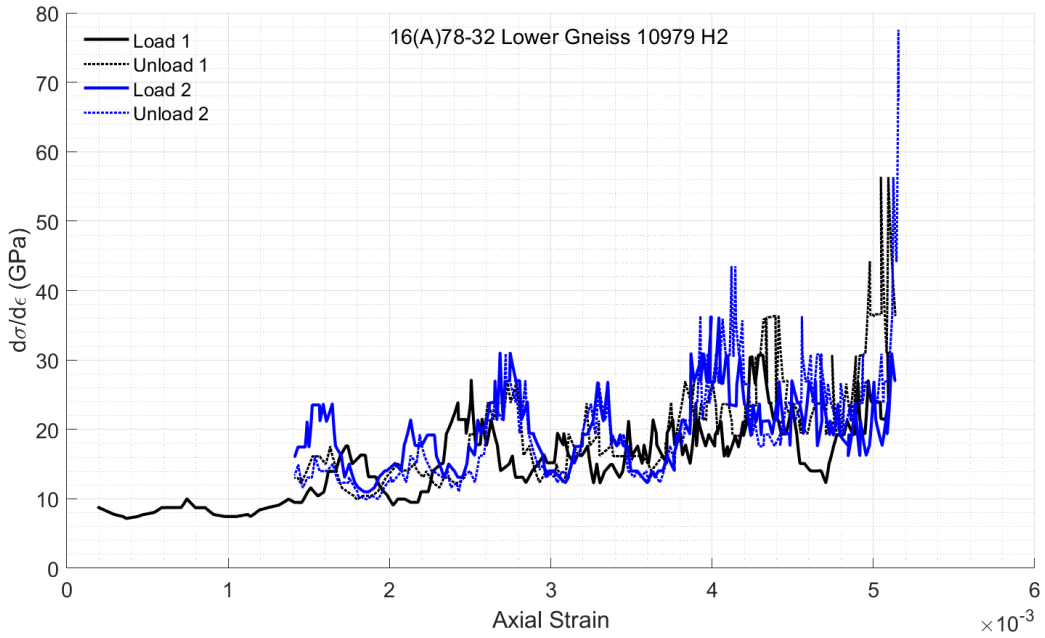

Hence the most notable stiffening zones are observed to be those which appeared at around 45 MPa and 65 MPa, with other, less notable regions of stiffening.

H3-(~ X-) Direction: Compendium

The H3 direction is about 24 degrees from the nominal x-direction, which is argued to be potentially aligned with maximum in-situ stress direction. There are two samples from this orientation, with geometry and photograph given by:

H3-1

Dimensions	
height (mm):	40.73
width (mm):	31.98
Angle retrieved (degrees):	309.9

H3-2

Dimensions	
height (mm):	42.42
width (mm):	32.00
Angle retrieved (degrees):	309.9

DRA experiments are run with the loading sequence

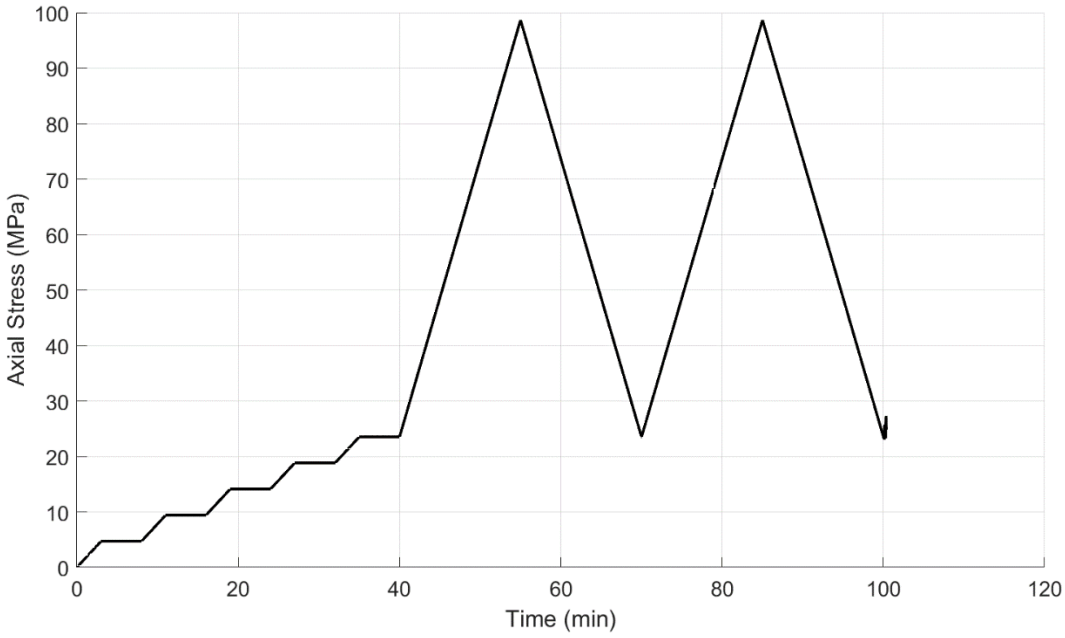

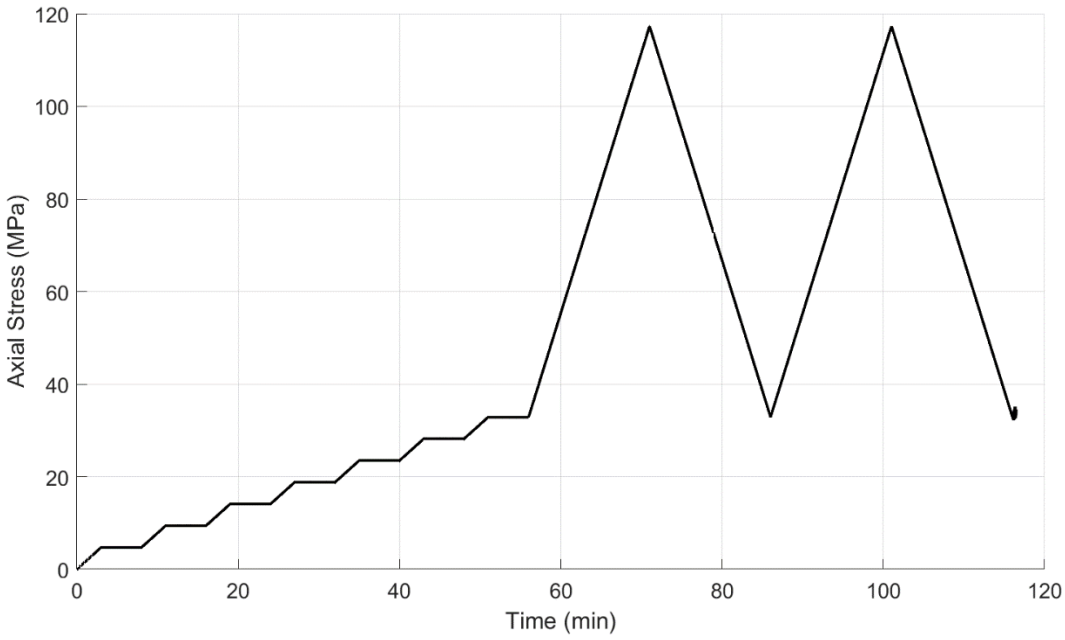

This results in the following displacements, which have been reduced by an amount estimated for deformation of 95mm of tool steel with E=210 GPa (comprising a lower bound on the platen deformation). This gives

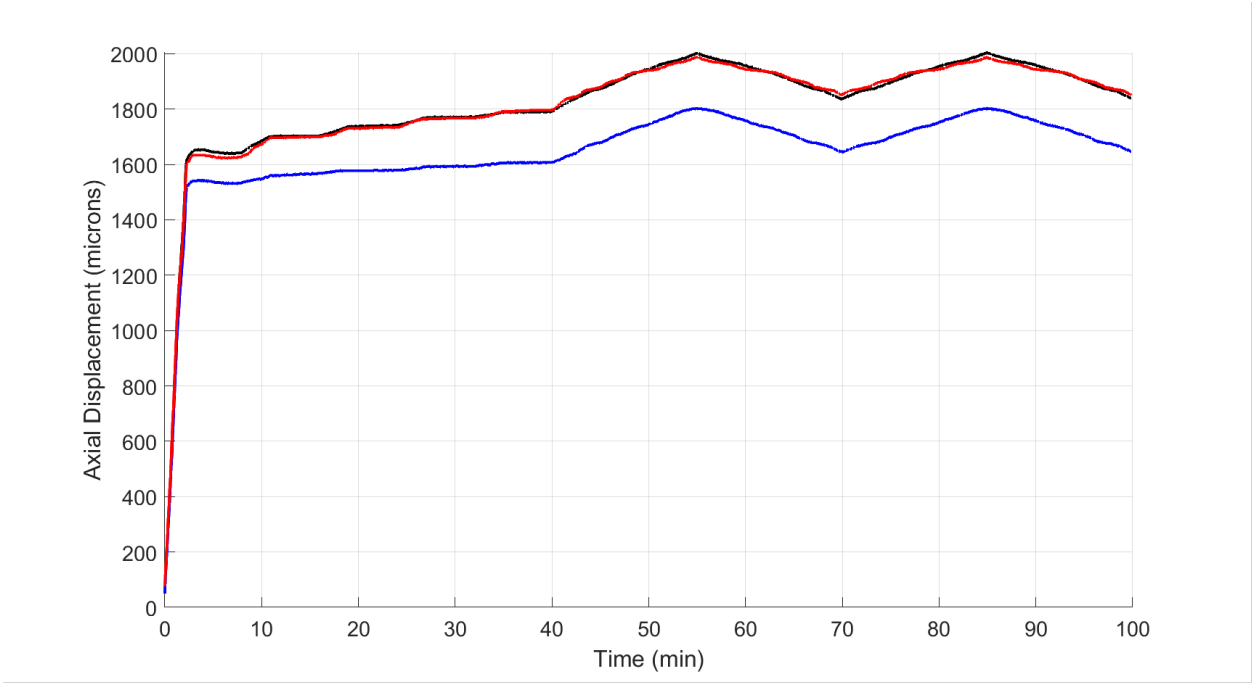

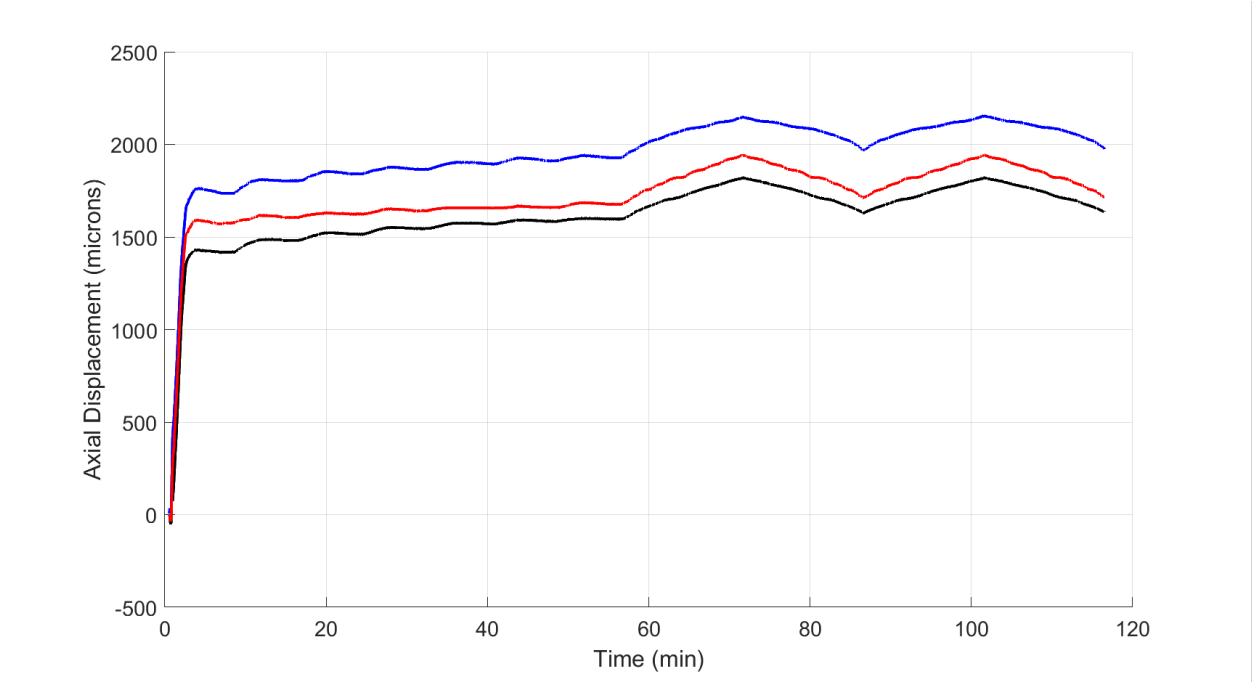

Once again there is little evidence of tilting of the platens. Instead, the displacement from all 3 LVDTs are reasonably consistent with one another. Averaging and plotting stress versus strain relationships for the 2 load/unload cycles, setting zero strain at the beginning of the first load cycle, gives

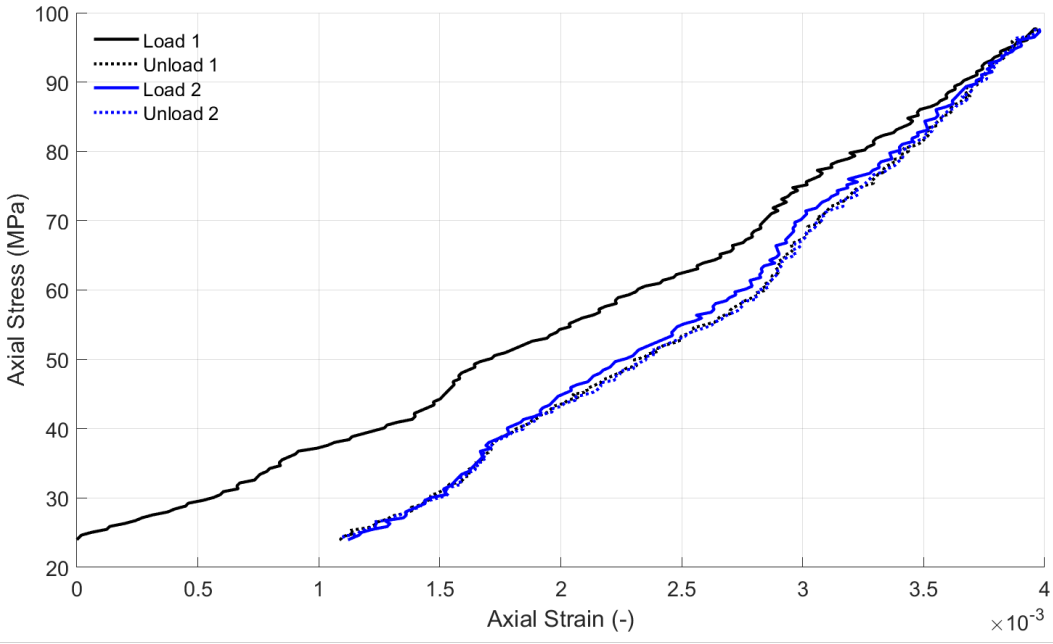

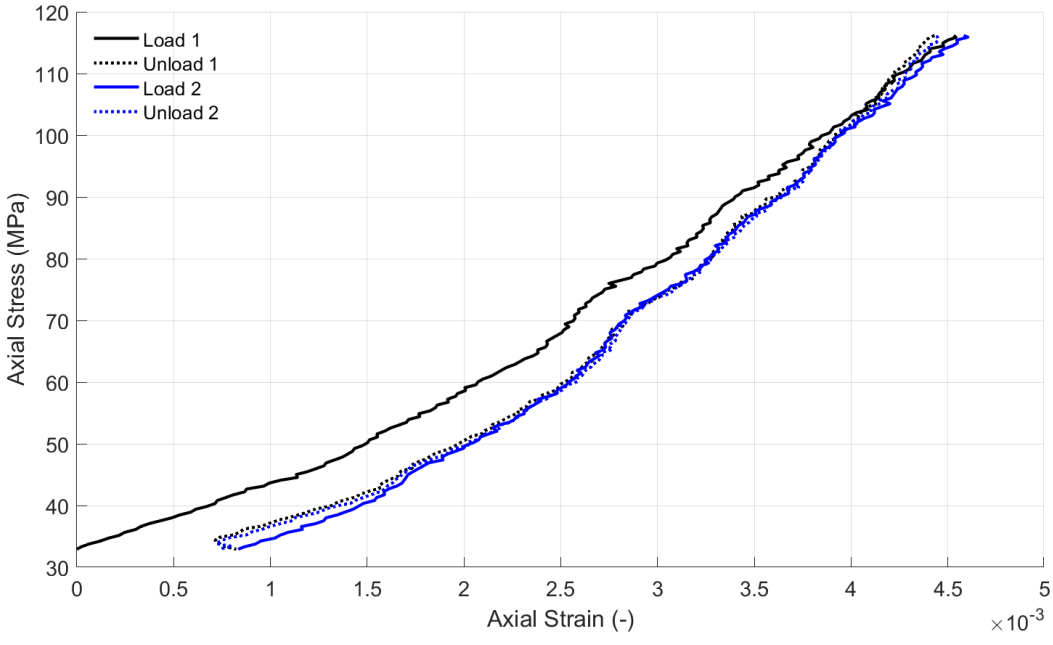

There are several stiffening inflections, perhaps most notably in both at just about 60 MPa.

The difference between the strain measurements for the load/unload stages is given by

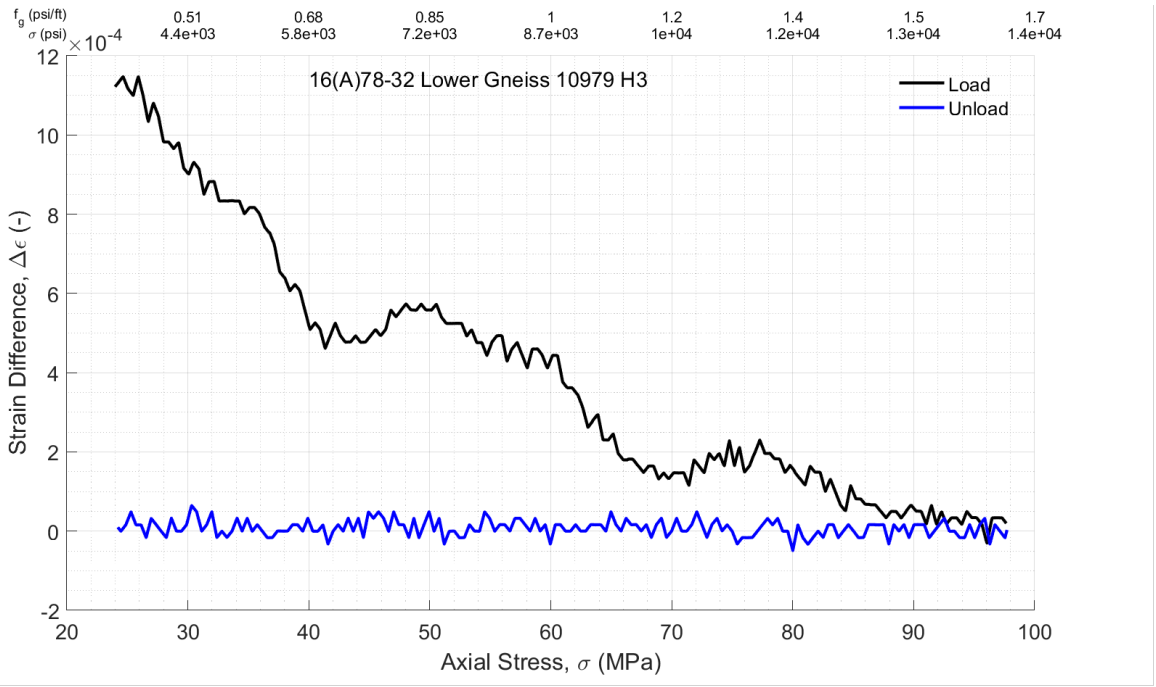

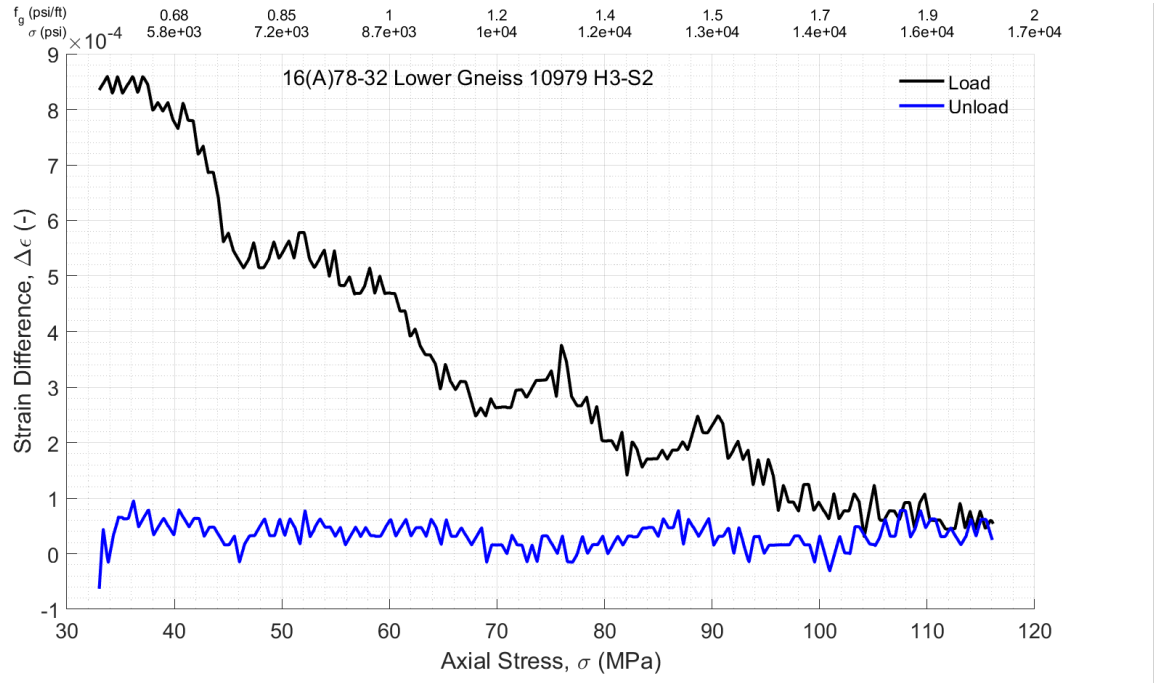

There are multiple inflections here. Both show the first between 35-42 MPa. Both show another at around 52 MPa, another around 60 MPa, another around 76 MPa. The second test shows a final inflection around 90 MPa. As with all inflections, they are accounted for via the weight of evidence approach.

Bringing DRA and TUV stiffnesses together (by taking derivative of stress with respect to strain for DRA curves, and presenting here comparable TUV from Upper Gneiss) gives

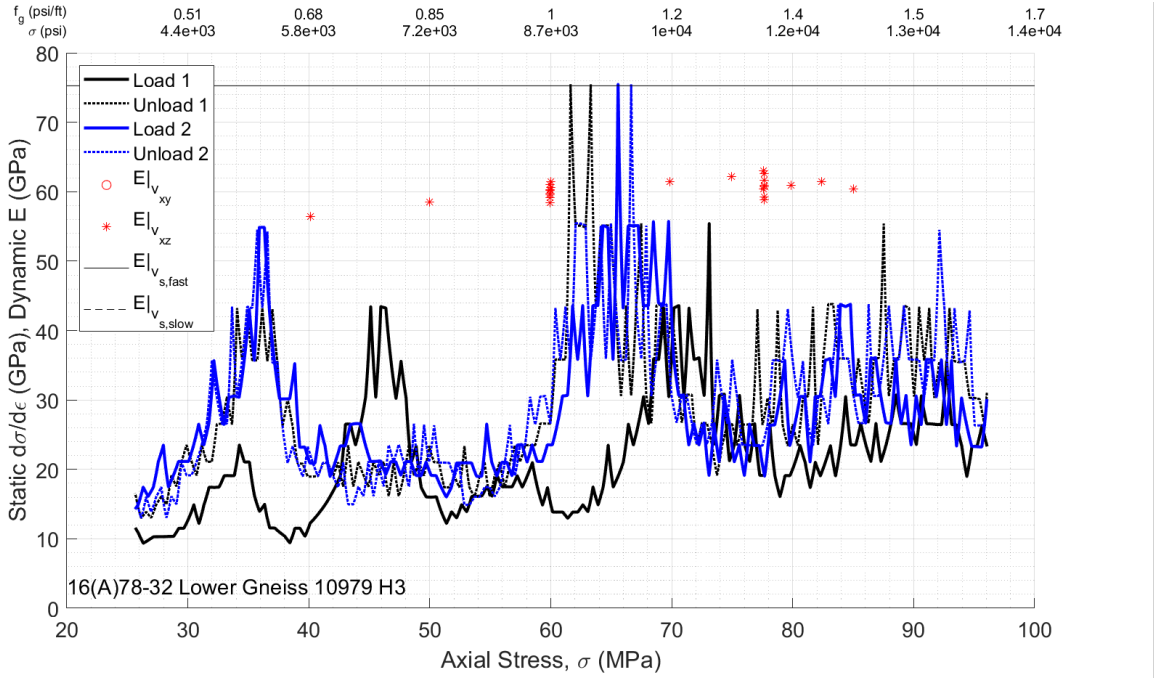

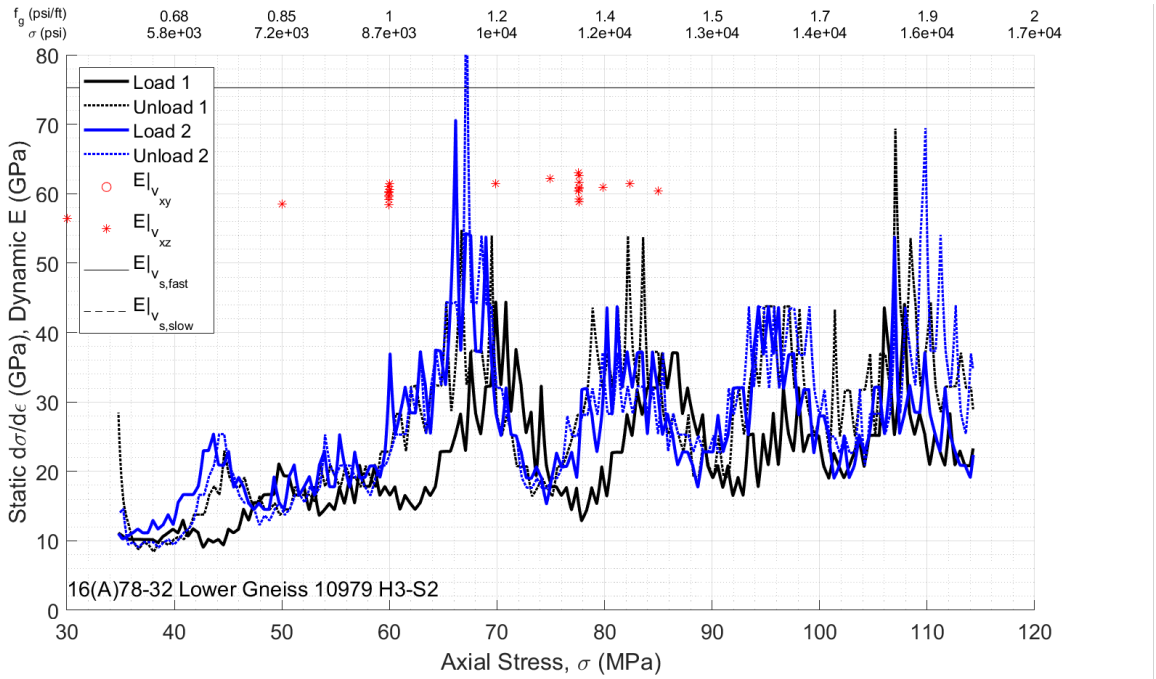

Perhaps the most striking inflection, consistent between the two cases, is at 60 MPa. The second most striking is around 75 MPa. In this regard, it is possible that these could be the most viable options to interpret as maximum horizontal stress. As usual, the inflections take place at a consistent strain level, as seen in

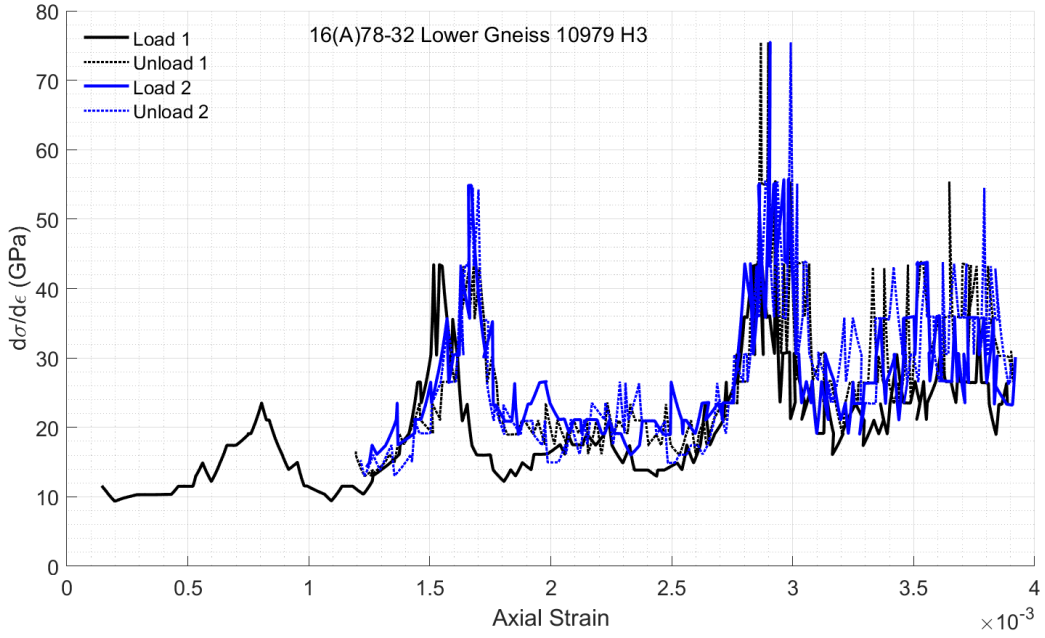

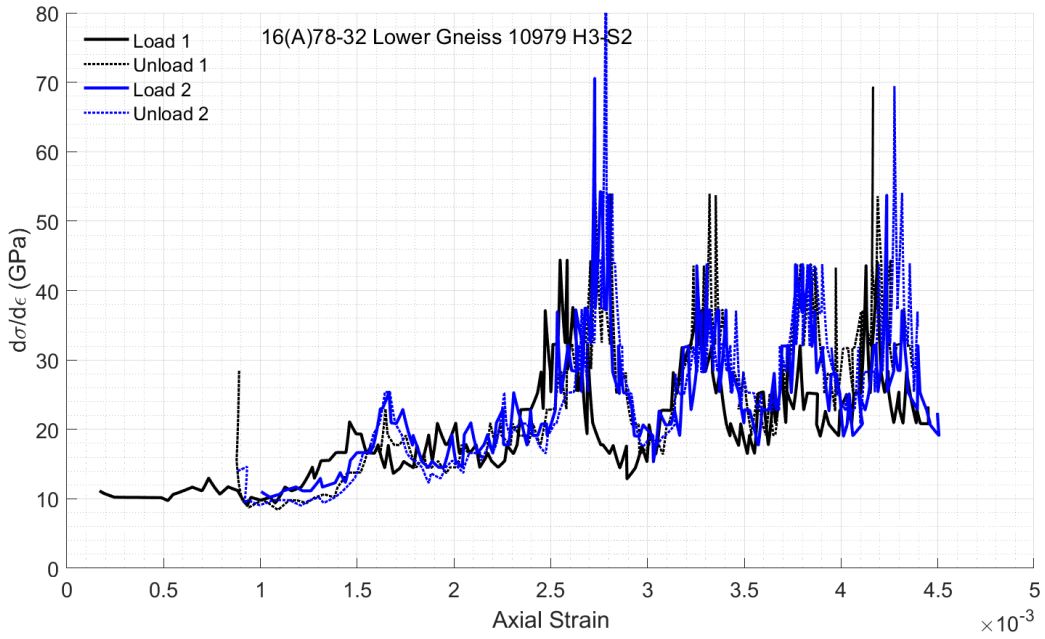

The inflection at around 0.0025 strain in both cases is the ~60 MPa inflection. It is so striking in really should be put forward as an option for maximum horizontal stress.

V-(Z-) Direction: Compendium

This orientation is along the core axis and therefore nearest the nominal minimum stress, owing to the deviation of the well along the expected minimum stress direction. There are two samples:

V-1

Dimensions	
height (mm):	36.4
width (mm):	31.99
Angle retrieved (degrees):	NA

V-2

Dimensions	
height (mm):	36.96
width (mm):	32.01
Angle retrieved (degrees):	NA

DRA experiments are run with the loading sequence

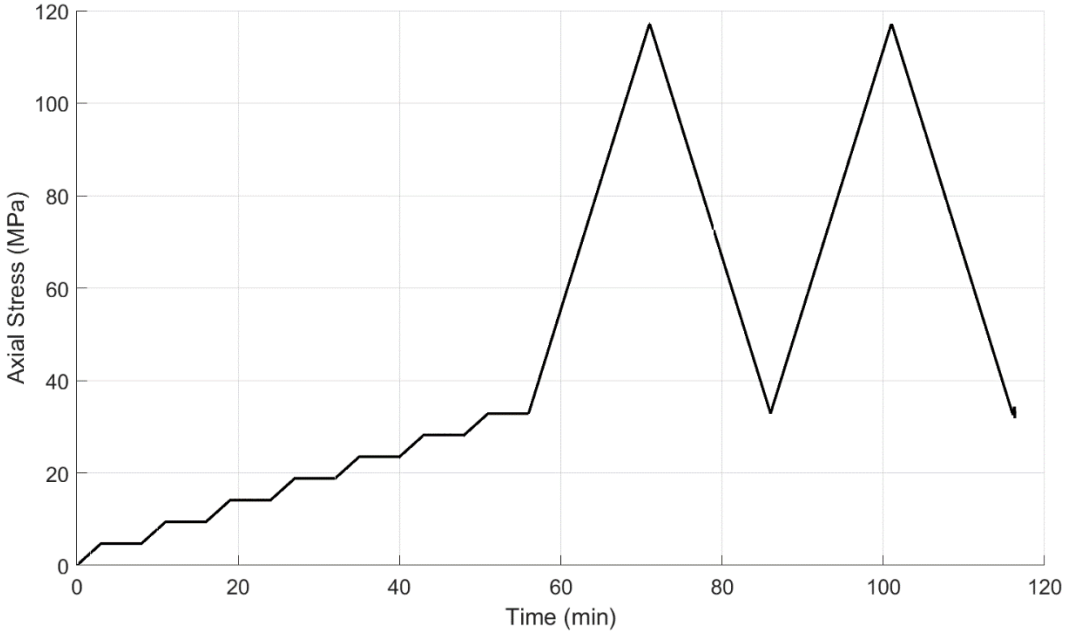

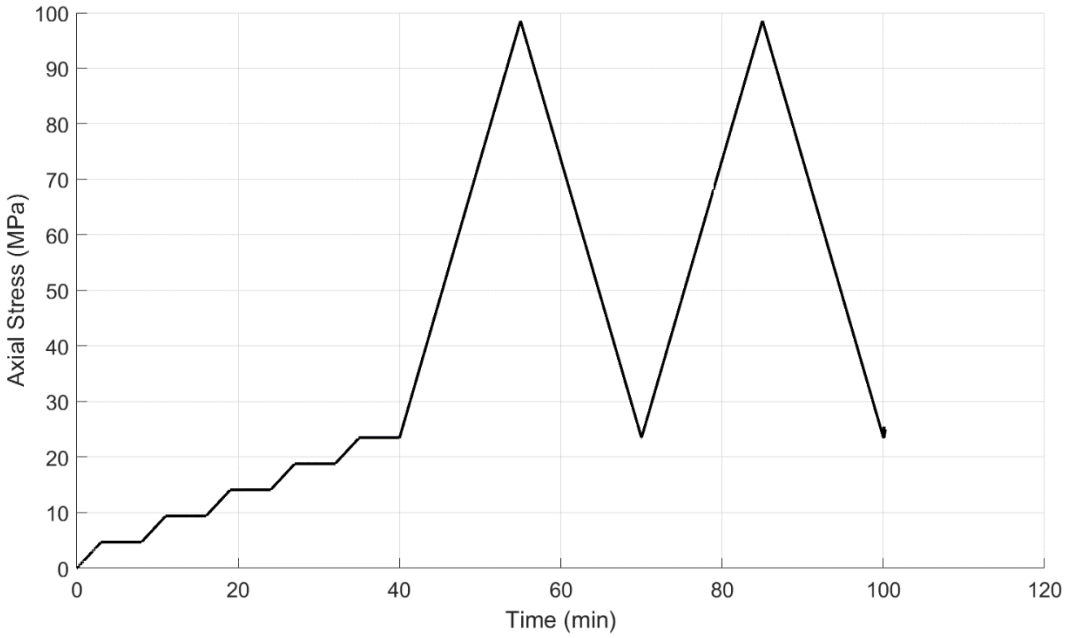

This results in the following displacements, which have been reduced by an amount estimated for deformation of 100mm of tool steel with E=210 GPa (comprising a lower bound on the platen deformation). This gives

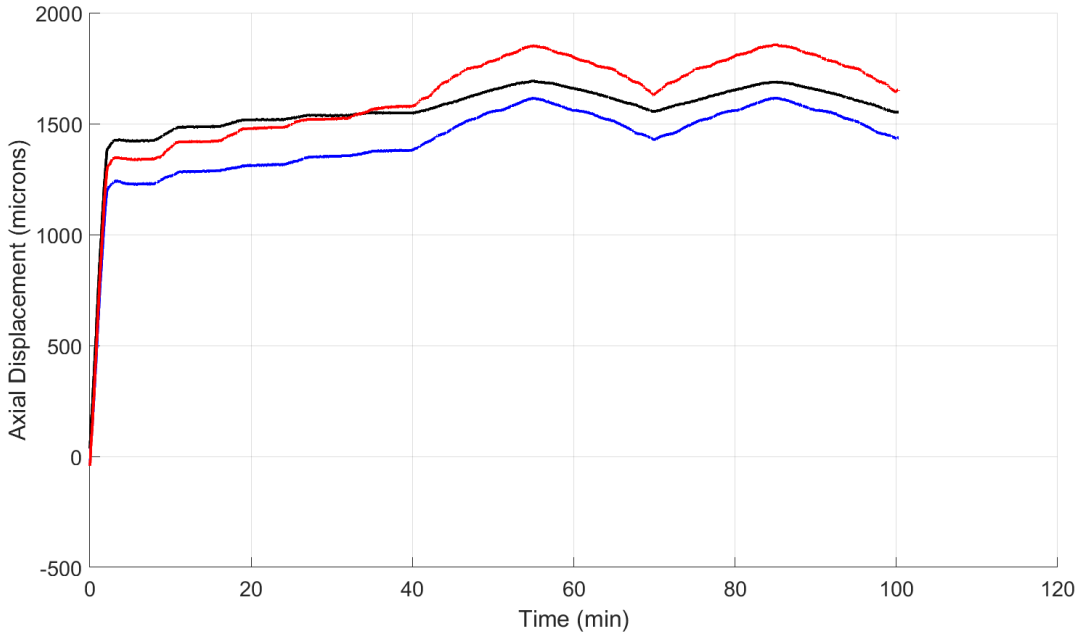

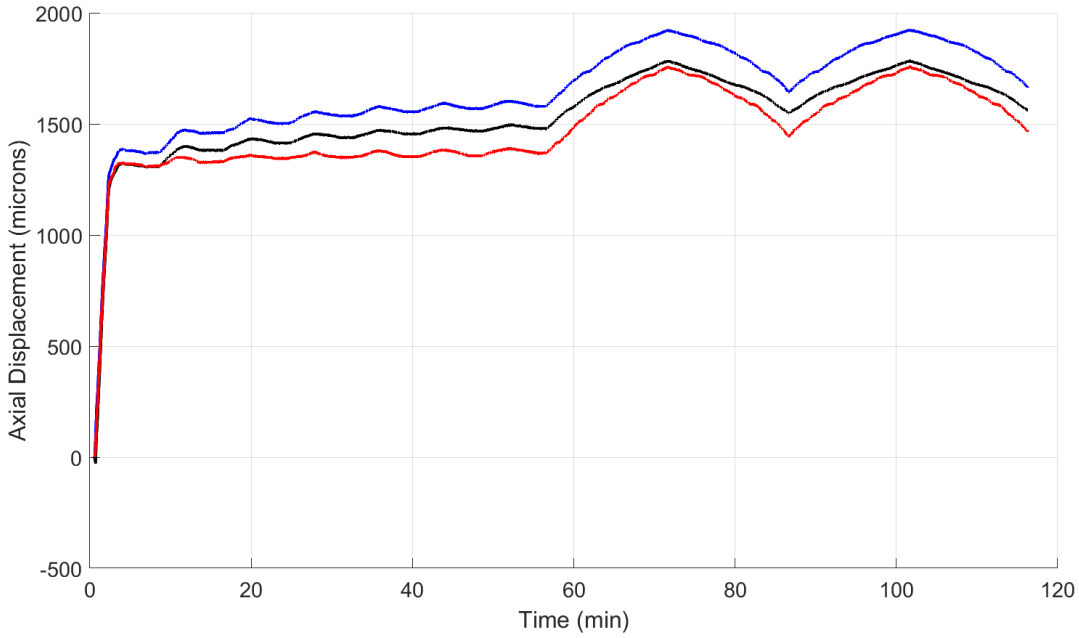

Averaging and plotting stress versus strain relationships for the 2 load/unload cycles, setting zero strain at the beginning of the first load cycle, gives

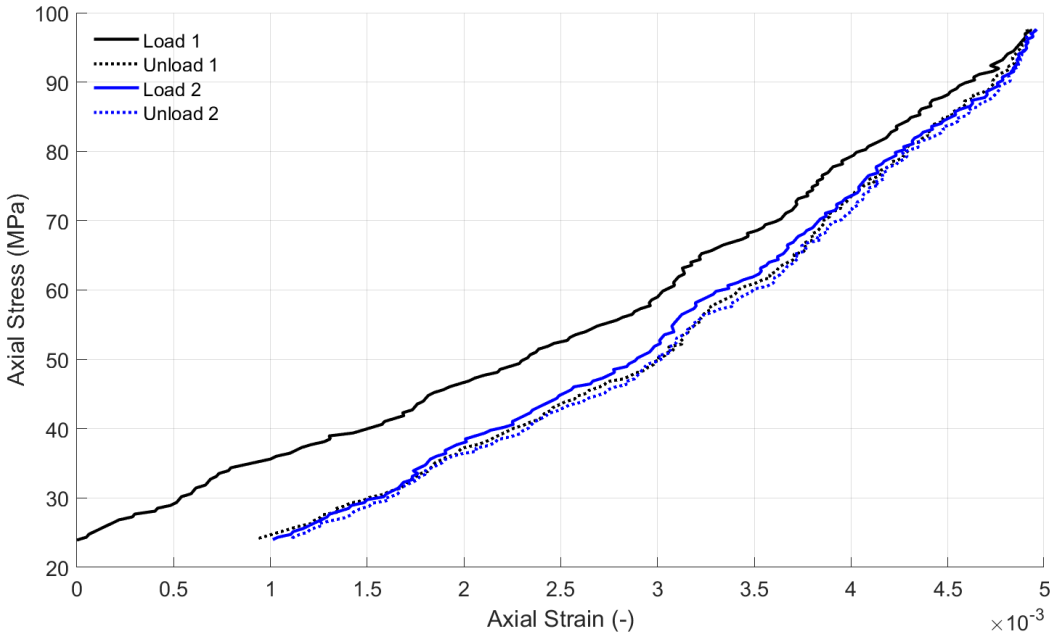

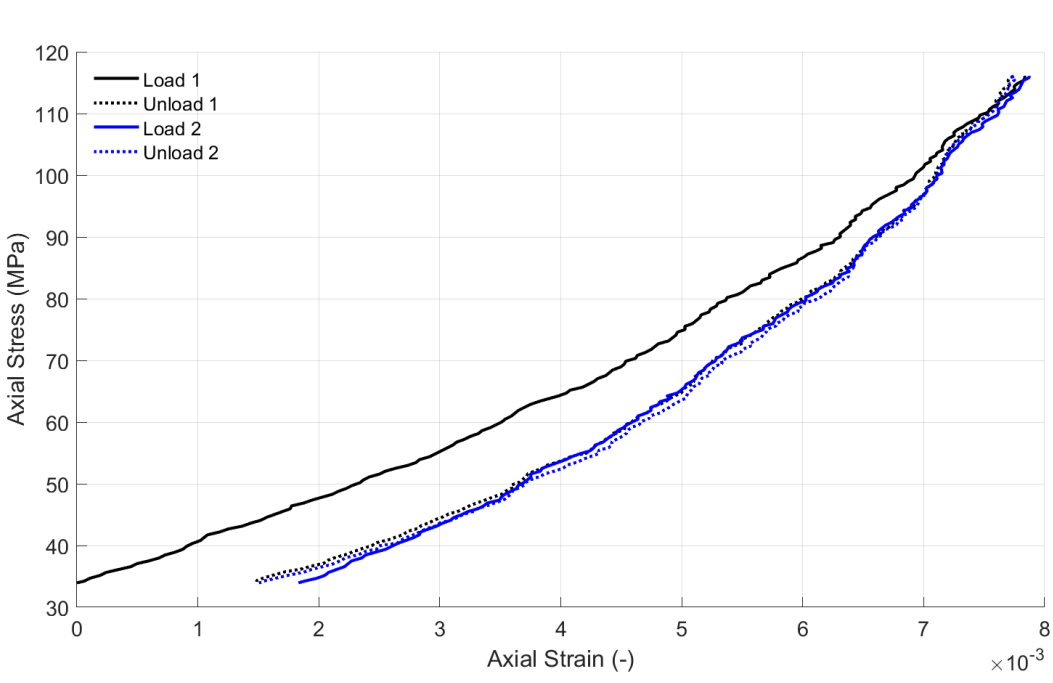

In both cases there are multiple inflections indicating nonmonotonic stiffening, with one of the most notable around 50 MPa.

The difference between the strain measurements for the load/unload stages is given by

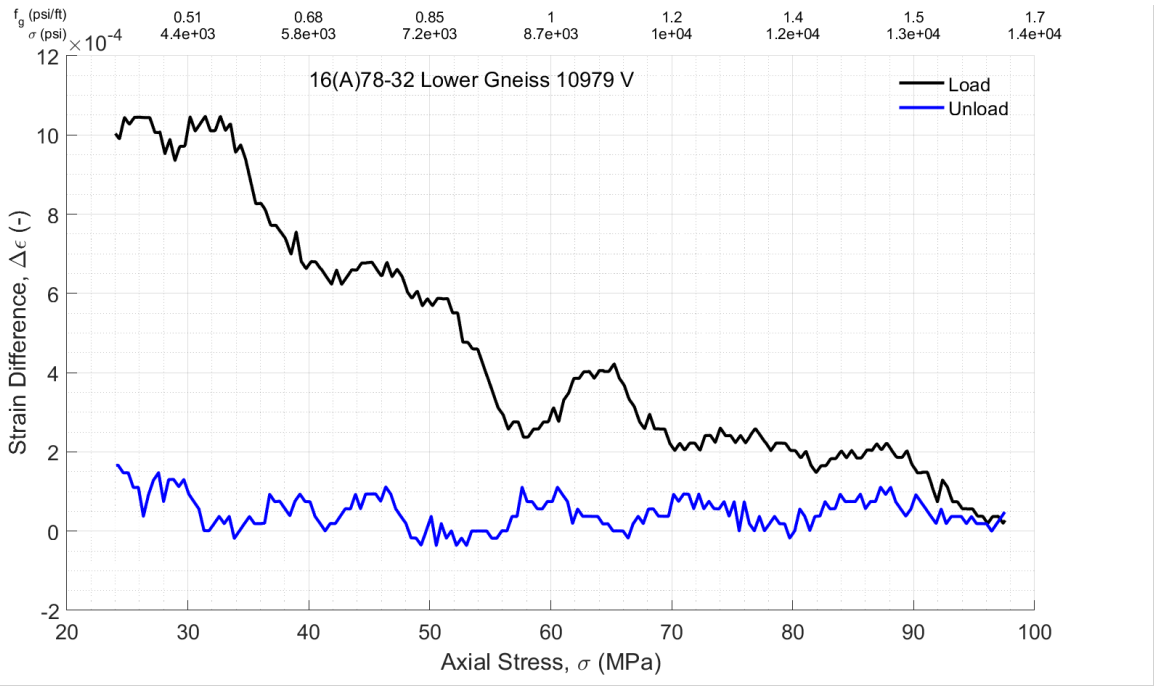

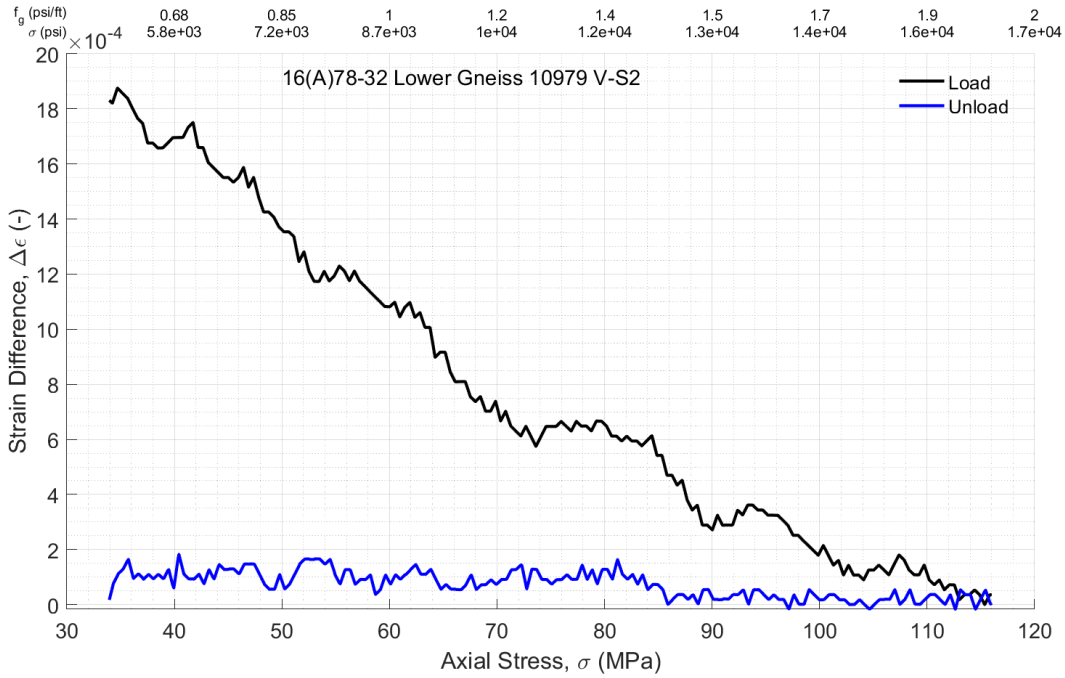

Bringing DRA and TUV stiffnesses together (by taking derivative of stress with respect to strain for DRA curves, and presenting here comparable TUV from Upper Gneiss) gives

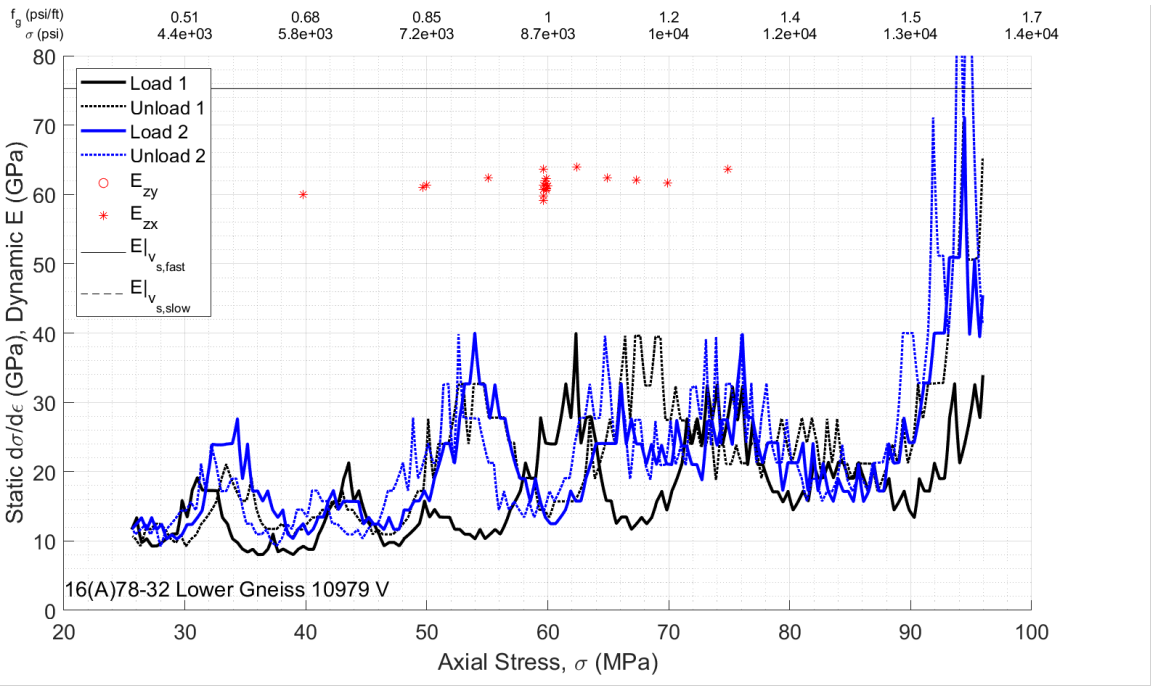

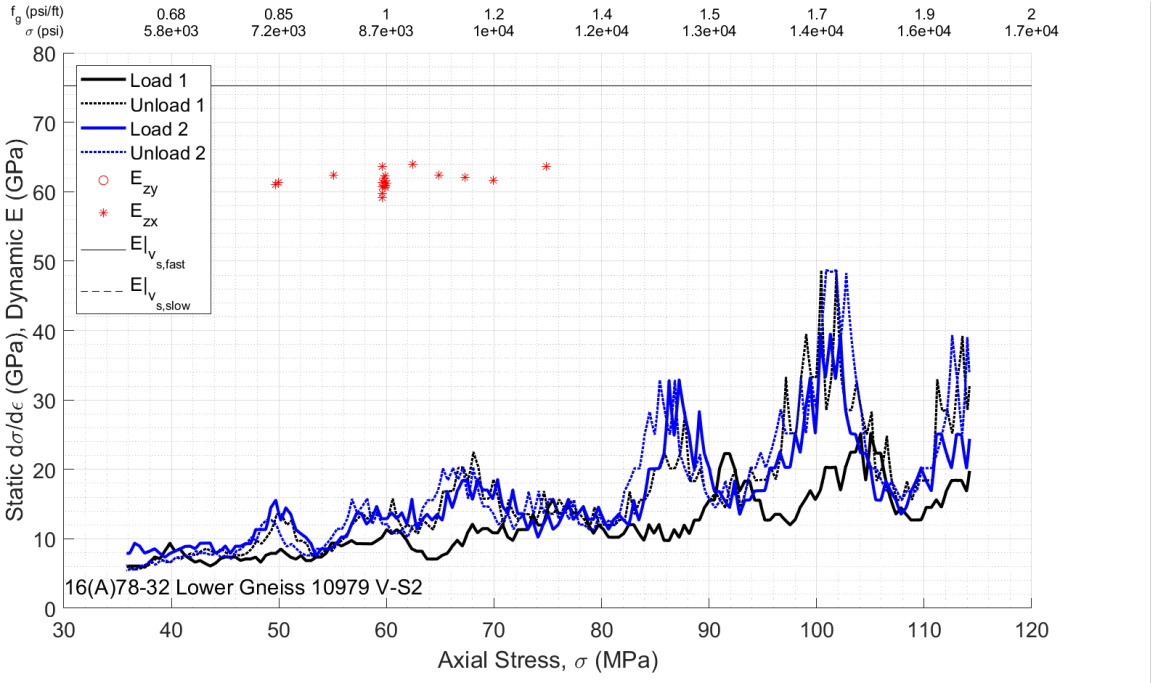

There are multiple inflections, but among the most striking and consistent is between 45-50 MPa. Plotting versus strain, the consistency of the strain level for each inflection is again clear.

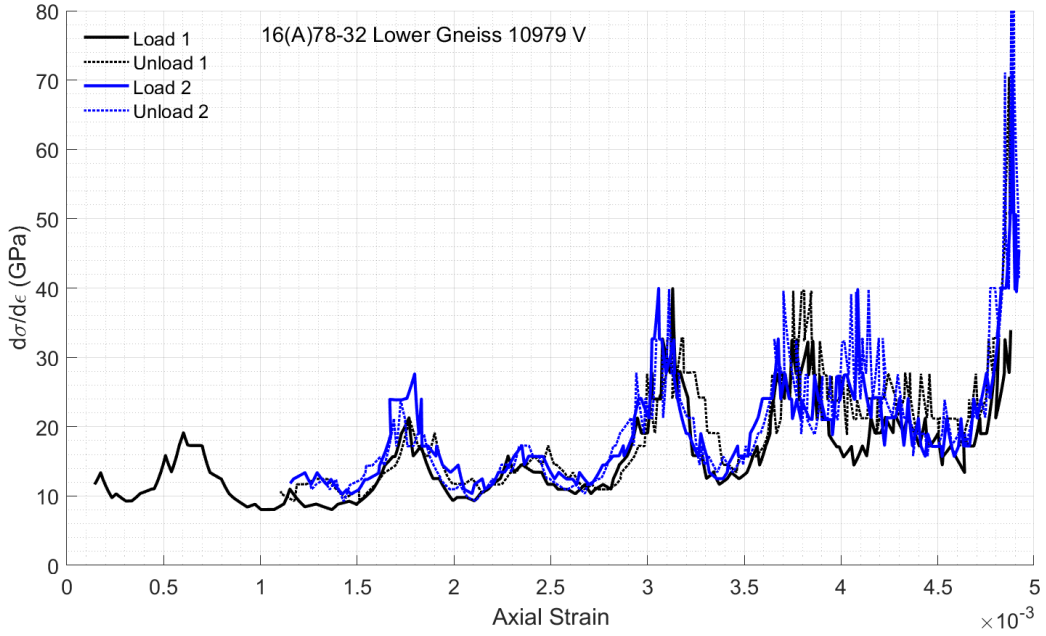

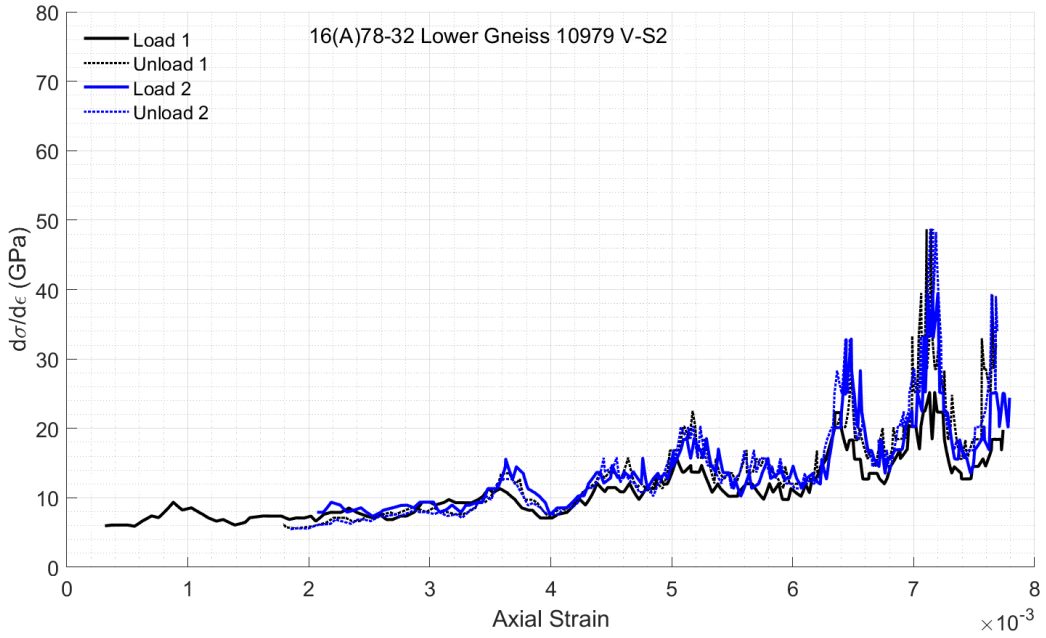

Lines of Evidence

A summary of the lines of evidence obtained from these experiments is given by:

Series	LoE	s1_val	s1_V	s1_L	s1_C	s1_R	s2_val	s2_V	s2_L	s2_C	s2_R	s3_val	s3_V	s3_L	s3_C	s3_R	s4_val	s4_V	s4_L	s4_C	s4_R	s5_val	s5_V	s5_L	s5_C	s5_R
LrGn_H1	s_e	48	2	1.5	1.5	0.9	64	2	1	1	0.9	75	2	2	1.5	0.9	0	0	0	0	0.9	0	0	0	0	0.9
LrGn_H1	s_e	85	2	3	2	0.9	0	0	0	0	0.9	0	0	0	0	0.9	0	0	0	0	0.9	0	0	0	0	0.9
LrGn_H1	De	46	2	3	2	0.9	64	1.5	2.5	1.5	0.9	76	1.5	2.5	2	0.9	0	0	0	0	0.9	0	0	0	0	0.9
LrGn_H1	De	85	2	2.5	2	0.9	110	1.5	1	1	0.9	0	0	0	0	0.9	0	0	0	0	0.9	0	0	0	0	0.9
LrGn_H1	ds_de	25	2	2.5	2	0.9	35	2	1.5	2	0.9	46	2	3	2	0.9	62	1.5	3	2	0.9	74	1.5	2.5	2	0.9
LrGn_H1	ds_de	45	2	1.5	2	0.9	55	2	1	2	0.9	65	2	1.5	2	0.9	72	1.5	2	2	0.9	85	1.5	3	2	0.9
LrGn_H1	ds_de	110	1.5	2.5	2	0.9	0	0	0	0	0.9	0	0	0	0	0.9	0	0	0	0	0.9	0	0	0	0	0.9
LrGn_y	s_e	44	2	3	1.5	0.9	56	2	2.5	1.5	0.9	67	2	1.5	1.5	0.9	0	0	0	0	0.9	0	0	0	0	0.9
LrGn_y	De	42	2	3	1.5	0.9	56	1.5	2	1.5	0.9	68	1.5	2	1.5	0.9	85	1.5	2	1.5	0.9	0	0	0	0	0.9
LrGn_y	ds_de	25	1.5	1	1.5	0.9	34	2	0.5	1	0.9	42	2	1.5	1.5	0.9	62	1.5	0.5	1	0.9	0	0	0	0	0.9
LrGn_x	s_e	60	2	2.5	3	0.9	0	0	0	0	0.9	0	0	0	0	0.9	0	0	0	0	0.9	0	0	0	0	0.9
LrGn_x	s_e	63	2	2.5	3	0.9	80	2	2	1.5	0.9	90	2	2	1.5	0.9	0	0	0	0	0.9	0	0	0	0	0.9
LrGn_x	De	35	2	2.5	1.5	0.9	50	1.5	2.5	3	0.9	61	1.5	2	3	0.9	77	1.5	2.5	3	0.9	0	0	0	0	0.9
LrGn_x	De	42	2	2.5	1.5	0.9	50	1.5	1.5	3	0.9	60	1.5	2.5	3	0.9	76	1.5	3	3	0.9	90	1.5	3	1.5	0.9
LrGn_x	ds_de	29	2	2.5	1.5	0.9	39	2	2.5	1.5	0.9	46	2	3	3	0.9	62	1.5	2	2.5	0.9	86	1.5	3	1.5	0.9
LrGn_x	ds_de	45	2	2.5	3	0.9	55	2	2.5	1.5	0.9	64	2	2	2.5	0.9	82	1.5	2.5	1.5	0.9	94	1.5	3	1.5	0.9
LrGn_z	s_e	29	2	2.5	1.5	0.9	50	2	2.5	2.5	0.9	62	2	1.5	2.5	0.9	88	1.5	1	2.5	0.9	0	0	0	0	0.9
LrGn_z	s_e	47	2	1.5	2.5	0.9	64	2	0.5	2.5	0.9	85	2	1.5	2.5	0.9	97	1.5	1	1.5	0.9	0	0	0	0	0.9
LrGn_z	De	34	2	3	1.5	0.9	48	1.5	1	3	0.9	52	1.5	1.5	2.5	0.9	65	1.5	2.5	1.5	0.9	77	1.5	0.5	2	0.9
LrGn_z	De	88	1.5	1.5	2.5	0.9	0	0	0	0	0.9	0	0	0	0	0.9	0	0	0	0	0.9	0	0	0	0	0.9
LrGn_z	De	63	1.5	1	2.5	0.9	80	1.5	1	1	0.9	85	1.5	2	2.5	0.9	94	1.5	2.5	1.5	0.9	107	1	1	1	0.9
LrGn_z	ds_de	29	2	3	1.5	0.9	42	1.5	1.5	1	0.9	47	2	3	3	0.9	62	1.5	1.5	3	0.9	87	1.5	2.5	2	0.9
LrGn_z	ds_de	47	2	3	3	0.9	54	1.5	2	1	0.9	62	1.5	1.5	3	0.9	83	1.5	3	2	0.9	94	1.5	3	2	0.9
LrGn_z	ds_de	107	1.5	3	1.5	0.9	0	0	0	0	0.9	0	0	0	0	0.9	0	0	0	0	0.9	0	0	0	0	0.9

To note:

- Each series is named with the direction after an underscore (column 1).
- The source of the line of evidence (LoE) is given in column 2, where v is velocity, E is Young's modulus, s_e is stress-strain curve, De is the change in strain curve, and ds_de is the instantaneous stiffness curve. Subscripts indicate direction of propagation followed by polarity, as usual, such that for example vxy indicates a shear wave velocity propagating in x-direction with y-polarity.
- All stress values (i.e. s1_val, s2_val) are given in MPa.
- Each source can give multiple lines of evidence, thus the table is set up to accept up to 5 lines of evidence for each source. Zeros are filled into the table where there are no additional lines of evidence.
- The weight assigned according to the prescribed rubric is given after an underscore, where V indicates relevance, L indicates reliability, C indicates consistency, and R indicated representivity. All values of representivity are set at 0.9 because there is insufficient data to determine exactly how representative the sample is of the surrounding formation.

Acknowledgment

This work was performed at the University of Pittsburgh with support via Subcontract No. 845391 to Battelle Memorial Institute for Utah FORGE Project 2439, Prime Contract No. DE_EE0007080. Additional support for APB is provided by the RK Mellon Faculty Fellowship in Energy. We wish to acknowledge the technical contributions of Charles "Scooter" Hager. We also wish to acknowledge the contributions of past postdoctoral researcher Dr Navid Zolfaghari, who developed aspects of the TUV method and who authored project reports from which photographs and sketches of the TUV experimental setup are modified. Current Pitt research group members Margaret Benge and Yunxing Lu assisted with supervision and training of JH and YH on the DRA and TUV equipment. All of these contributions are gratefully acknowledged.

References

Dight, P. (2006). Determination of In Situ Stress from Oriented Core. Proceedings International Symposium on In-Situ Rock Stress, Trondheim, Norway, pp. 167-175.

Dolinar, D. R. (2003). Variation of horizontal stresses and strains in mines in bedded deposits in the eastern and midwestern United States. Proceedings of the 22nd International Conference on Ground Control in Mining, August 5-7, 2003, Morgantown, West Virginia. Peng SS, Mark C, Khair AW, Heasley KA, eds., Morgantown, WV: West Virginia University, 2003 Aug; :178-185.

Higgins, J., Lu, Y., Benge, M., Gunaydin, D., Bunger, A. P., & Kelley, M. (2022). Triaxial Deformation Rate Analysis for Stress Estimation in the Sedimentary and Basement Rocks from the FutureGen Carbon Sequestration Project. Proceedings 56th US Rock Mechanics Symposium, Santa Fe, New Mexico, USA, 26-29 June 2022, Paper 458.

Economides, M. J., & Nolte, K. G. (Eds.). (2000). *Reservoir Stimulation*. John Wiley & Sons, Chichester, UK.

EFSA Scientific Committee: Hardy, A., Benford, D., Halldorsson, T., Jeger, M. J., Knutsen, H. K., ... & Younes, M. (2017). Guidance on the use of the weight of evidence approach in scientific assessments. *Efsa Journal*, *15*(8), e04971.

Moore, J., McLennan, J., Pankow, K., Simmons, S., Podgorney, R., Wannamaker, P., Jones, C., Rickard, W., & Xing, P. (2020). The Utah Frontier Observatory for Research in Geothermal Energy (FORGE): a laboratory for characterizing, creating, and sustaining enhanced Geothermal systems. In *Proceedings of the 45th Workshop on Geothermal Reservoir Engineering*. 10-12 February 2020, Stanford University, Stanford, California, USA. Paper SGP-TR-216.

Regmi, N. R., Giardino, J. R., & Vitek, J. D. (2010). Modeling susceptibility to landslides using the weight of evidence approach: Western Colorado, USA. *Geomorphology*, *115*(1-2), 172-187.

Yamamoto, K., Kuwahara, Y., Kato, N. and Hirasawa, T. (1990). Deformation rate analysis: a new method for in situ stress examination from inelastic deformation of rock samples under uni-axial compressions. *Tohoku Geophysical Journal.* 33, 127–147.

Weed, D. L. (2005). Weight of evidence: a review of concept and methods. *Risk Analysis: An International Journal*, *25*(6), 1545-1557.